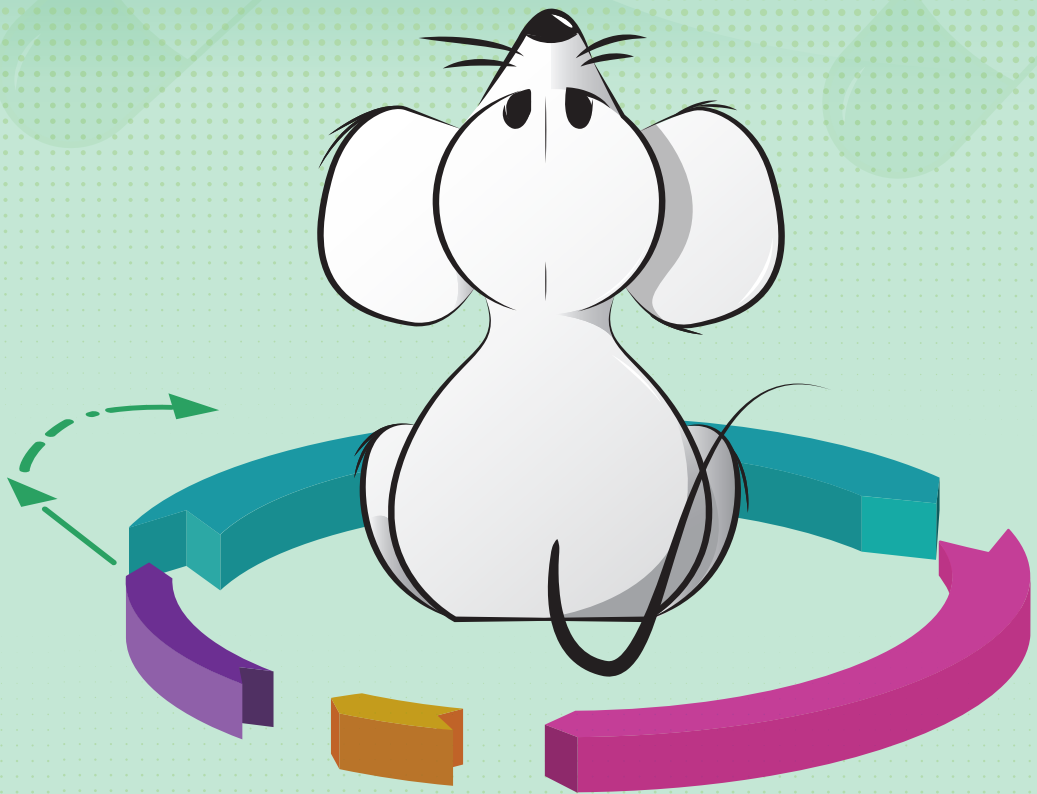


# Cyclin-dependent kinase inhibitors in cancer: bioanalysis and pharmacokinetics



Alejandra Martínez Chávez



**Cyclin-dependent kinase inhibitors in cancer:  
bioanalysis and pharmacokinetics**

**Alejandra Martínez Chávez**

## **Cyclin-dependent kinase inhibitors in cancer: bioanalysis and pharmacokinetics**

© Diana Alejandra Martínez Chávez, Utrecht 2021

ISBN: 978-94-6423-458-9

Cover design: Sergio Morales Serrato, [www.behance.net/envysin](http://www.behance.net/envysin)

Layout: Wendy Schoneveld, [www.wenziD.nl](http://www.wenziD.nl)

Print: ProefschriftMaken

The research in this thesis was performed at the Pharmacology Division and the Laboratory of the Pharmacy of the Netherlands Cancer Institute – Antoni van Leeuwenhoek hospital, Amsterdam, the Netherlands

Printing of this thesis was financially supported by:  
The Netherlands Cancer Institute



# **Cyclin-dependent kinase inhibitors in cancer: bioanalysis and pharmacokinetics**

**Cycline-afhankelijke kinase remmers in kanker:  
bioanalyse en farmacokinetiek**  
(met een samenvatting in het Nederlands)

## **Proefschrift**

ter verkrijging van de graad van doctor aan de  
Universiteit Utrecht  
op gezag van de  
rector magnificus, prof.dr. H.R.B.M. Kummeling,  
ingevolge het besluit van het college voor promoties  
in het openbaar te verdedigen op

woensdag 10 november 2021 des middags te 2.15 uur

door

**Diana Alejandra Martínez Chávez**

geboren op 16 mei 1988  
te Mexico Stad, Mexico

**Promotor:**

Prof. dr. J.H. Beijnen

**Copromotor:**

Dr. A.H. Schinkel

This dissertation was accomplished in part with financial support from the Mexican National Council for Science and Technology (CONACyT), which granted D.A. Martínez Chávez the scholarship No. 440476.

*A mi Tita, mi ángel más grande en el cielo*

## Table of contents

<b>Preface</b>	8
<b>Part I. Bioanalysis of cyclin-dependent kinase inhibitors</b>	
<b>Chapter 1.</b> Development and validation of a bioanalytical method for the quantification of the CDK4/6 inhibitors abemaciclib, palbociclib and ribociclib in human and mouse matrices using liquid chromatography-tandem mass spectrometry <i>Anal Bioanal Chem.</i> 2019, 411 (20): 5531-5345	15
<b>Chapter 2.</b> Simultaneous quantification of abemaciclib and its active metabolites in human and mouse plasma by UHPLC/MSMS <i>J Pharm Biom Anal.</i> 2021, 203: 114225	45
<b>Chapter 3.</b> Development and validation of an LC-MS/MS method for the quantitative analysis of milciclib in human and mouse plasma, mouse tissue homogenates and tissue culture medium <i>J Pharm Biom Anal.</i> 2020, 190: 113516	71
<b>Chapter 4.</b> Bioanalytical method for the simultaneous quantification of irinotecan and its active metabolite SN-38 in mouse plasma and tissue homogenates using HPLC-fluorescence <i>J Chrom B.</i> 2020, 1149: 122177	93
<b>Part II. The impact of drug transporters and drug-metabolizing enzymes on the pharmacokinetics of the cyclin-dependent kinase inhibitors</b>	
<b>Chapter 5.</b> P-glycoprotein limits ribociclib brain exposure and CYP3A4 restricts its oral bioavailability <i>Mol Pharm.</i> 2019, 16 (9, 3): 3842-3852	109
<b>Chapter 6.</b> ABCB1 and ABCG2 limit brain penetration and, together with CYP3A4, total plasma exposure of abemaciclib and its active metabolites <i>Submitted</i>	137

<b>Chapter 7.</b> The role of drug efflux and uptake transporters ABCB1 (P-gp), ABCG2 (BCRP) and OATP1A/1B and of CYP3A4 in the pharmacokinetics of the CDK inhibitor milliclib <i>Eur J Pharm Sci. 2021, 190: 113516</i>	183
<b>Part III. Clinical pharmacokinetics and pharmacodynamics of the cyclin-dependent kinase inhibitors</b>	
<b>Chapter 8.</b> Clinical pharmacokinetics and pharmacodynamics of the cyclin-dependent kinase 4 and 6 inhibitors palbociclib, ribociclib, and abemaciclib <i>Clin Pharmacokinet. 2020, 59 (12): 1501-1520</i>	213
<b>Conclusions and perspectives</b>	249
<b>Summary</b>	257
<b>Nederlandse samenvatting</b>	263
<b>Resumen en español</b>	271
<b>Appendices</b>	
List of publications	280
Acknowledgements	282
Curriculum vitae	285

## **Preface**

Cancer remains a leading global health problem with expected increases in incidence and mortality for the coming years [1]. The rapid advances in molecular techniques and understanding of cancer biology have led to the development of compounds that target specific molecular abnormalities related to tumor growth and cancer progression [2]. Compared to unspecific cytotoxic compounds, targeted anticancer drugs have been demonstrated to have higher efficacy and reduced toxicity, improving the quality of life of patients. Recently, the development of small-molecule targeted anticancer drugs has been rapidly accelerating, focusing mostly on the inhibition of the kinase proteins involved in various signaling pathways. Hitherto, more than 50 small-molecule targeted anticancer drugs have been approved for cancer treatments [3].

Cyclin-dependent kinases (CDKs) have been regarded as promising targets for cancer treatment, since they can control critical checkpoints in the cell cycle when activated by cyclins: the cell cycle entry, the DNA replication and the initiation of mitosis [4,5]. CDKs, cyclins and the endogenous (protein) CDK inhibitors are frequently dysregulated in cancer cells, favoring aberrant cell proliferation. This has led to the development of small molecules that inhibit CDKs. The first generation of CDK inhibitors failed in clinical development, because of their unspecific pan-CDK inhibition, which led to non-cancer cell toxicity [5]. Therefore, the development of new CDK inhibitors successfully focused on selectively targeting CDKs. To date, three CDK inhibitors selective for CDK4 and CDK6 have been approved by health authorities, including the U.S. Food and Drug Administration (FDA) and the European Medicines Agency (EMA): palbociclib (2016), ribociclib (2017) and abemaciclib (2017 - 2018). These drugs are used for the treatment of metastatic or advanced breast cancer, and their efficacy against other cancer types is currently being investigated. In addition, clinical studies of many other CDK inhibitors with different CDK subclass specificities are ongoing [6].

The disposition of small-molecule drugs can be affected by efflux and uptake transporters and drug-metabolizing enzymes, often with clinically relevant (pharmacodynamic) consequences. Within the ATP-binding cassette (ABC) efflux transporter family, P-glycoprotein (ABCB1, P-gp, MDR1) and the Breast Cancer Resistance Protein (ABCG2, BCRP) are the most relevant transporters, due to their wide substrate specificity and influence on the disposition of many drugs [7,8]. ABCB1 and ABCG2 can control the net absorption from the gut, facilitate the elimination and limit the brain penetration of substrate drugs [7,9]. In addition, ABCB1 and ABCG2, when overexpressed in tumor cells, can confer resistance to anticancer drugs [10,11]. Similarly, within the organic anion-transporting polypeptides (OATPs) family, which are primarily uptake transporters, the subtypes OATP1A and OATP1B have been demonstrated to impact the pharmacokinetics of several drugs [12,13]. On the other hand, the cytochrome P450 (CYP) 3A enzyme family participates in the metabolism of

numerous clinically used drugs, causing drug inactivation, either directly or by facilitating its excretion from the body, or bioactivation to form active and/or toxic compounds. CYP3A4 and CYP3A5 are the most abundant isoforms in liver, and due to genetic polymorphisms, high inter-individual variation in activity can occur [14,15]. Additionally, activity of these enzymes can be markedly induced or inhibited by dietary compounds or other drugs. This, together with their broad substrate specificity, can lead to several drug-drug and drug-food interactions [14]. For these reasons, it is important to characterize the function of CYP3A in the metabolism of drugs.

This thesis therefore addresses several pharmacological aspects of the CDK inhibitors, from bioanalysis (Part I) to preclinical (Part II) and clinical pharmacokinetics (Part III).

First, as reliable bioanalytical methods are pivotal for supporting clinical and preclinical studies of drugs. Part I of this thesis describes the development and validation of bioanalytical methods for the quantitative analysis of CDKs in several biological matrices, mainly to support the studies described in Part II. **Chapter 1** provides a liquid chromatography-tandem mass spectrometry (LC-MS/MS) method for the combined analysis of the three approved CDK4/6 inhibitors (abemaciclib, palbociclib and ribociclib) in human and mouse plasma and tissue homogenates. As three active metabolites of abemaciclib are encountered in patients, **Chapter 2** examines the simultaneous quantification of abemaciclib and its active metabolites (M2, M20 and M18) in human and mouse plasma by ultrahigh performance liquid chromatography-tandem mass spectrometry (UHPLC-MS/MS). Furthermore, this chapter elaborates on some differences encountered in mouse and human samples in the course of the analysis of these molecules. **Chapter 3** focuses on the development, validation and applicability of a quantitative LC-MS/MS method for miliciclib, a promising CDK2 inhibitor that is being investigated in phase II clinical studies. Finally, **Chapter 4** reports a quantitative high performance liquid chromatography-fluorescence (HPLC-FL) method for simultaneous analysis of the prodrug irinotecan and its active metabolite SN-38 in several mouse matrices. This method was established to support preclinical investigation on the metabolic conversion of irinotecan into SN-38 by carboxylesterases using several genetically modified mouse models.

Part II of this thesis focuses on the impact of efflux and uptake transporters and the drug-metabolizing enzyme CYP3A on the preclinical pharmacokinetics of the CDK inhibitors using *in vitro* and *in vivo* models. **Chapter 5** presents the impact of ABCB1, ABCG2 and CYP3A on the pharmacokinetics and brain penetration of ribociclib. Additionally, this chapter examines the effects on brain accumulation of the coadministration of the dual (ABCB1 and ABCG2) inhibitor elacridar with ribociclib. **Chapter 6** describes the influence of ABCB1, ABCG2 and CYP3A4 on the plasma exposure and tissue distribution of abemaciclib and its active metabolites (M2, M20 and M18). Since OATP transporters can influence the pharmacokinetics of substrate

drugs, **Chapter 7** explores the role of the efflux (ABCB1 and ABCG2) and uptake (OATP1) transporters on the plasma pharmacokinetics and tissue distribution of the investigational CDK2 inhibitor milciclib. Additionally, the impact of CYP3A on the metabolism of milciclib is described in this chapter.

Finally, in Part III, **Chapter 8** reviews the clinical pharmacokinetics and pharmacodynamics of the three approved CDK4/6 inhibitors: palbociclib, ribociclib and abemaciclib. Furthermore, it summarizes the known drug-drug and food-drug interactions, and the exposure-response analyses of the reviewed CDK4/6 inhibitors.



## References

- [1] H. Sung, J. Ferlay, R.L. Siegel, M. Laversanne, I. Soerjomataram, A. Jemal, F. Bray, Global cancer statistics 2020: GLOBOCAN estimates of incidence and mortality worldwide for 36 cancers in 185 countries, *CA. Cancer J. Clin.* 0 (2021) 1–41. <https://doi.org/10.3322/caac.21660>.
- [2] M. Huang, A. Shen, J. Ding, M. Geng, Molecularly targeted cancer therapy: Some lessons from the past decade, *Trends Pharmacol. Sci.* 35 (2014) 41–50. <https://doi.org/10.1016/j.tips.2013.11.004>.
- [3] W.A. Liu, L. Yu, P.N. Morcos, F. Mercier, B.J. Brennan, Assessing the translational value of pre-clinical studies for clinical response rate in oncology: an exploratory investigation of 42 FDA-approved small-molecule targeted anticancer drugs, *Cancer Chemother. Pharmacol.* (2020) 1015–1027. <https://doi.org/10.1007/s00280-020-04076-2>.
- [4] Malínková, J. Vylíčil, V. Kryštof, Cyclin-dependent kinase inhibitors for cancer therapy: a patent review (2009 – 2014), *Expert Opin. Ther. Pat.* 25 (2015) 953–970. <https://doi.org/10.1517/13543776.2015.1045414>.
- [5] B. O’Leary, R.S. Finn, N.C. Turner, Treating cancer with selective CDK4/6 inhibitors, *Nat. Rev. Clin. Oncol.* 13 (2016) 417–430. <https://doi.org/10.1038/nrclinonc.2016.26>.
- [6] C. Sánchez-Martínez, M.J. Lallena, S.G. Sanfeliciano, A. de Dios, Cyclin dependent kinase (CDK) inhibitors as anticancer drugs: Recent advances (2015–2019), *Bioorganic Med. Chem. Lett.* 29 (2019) 126637. <https://doi.org/10.1016/j.bmcl.2019.126637>.
- [7] A.H. Schinkel, J.W. Jonker, Mammalian drug efflux transporters of the ATP binding cassette (ABC) family: An overview, *Adv. Drug Deliv. Rev.* 64 (2012) 138–153. <https://doi.org/10.1016/j.addr.2012.09.027>.
- [8] G. Szakács, A. Váradi, C. Özvegy-Laczka, B. Sarkadi, The role of ABC transporters in drug absorption, distribution, metabolism, excretion and toxicity (ADME-Tox), *Drug Discov. Today.* 13 (2008) 379–393. <https://doi.org/10.1016/j.drudis.2007.12.010>.
- [9] K.M. Giacomini, S.-M. Huang, D.J. Tweedie, L.Z. Benet, K.L.R. Brouwer, X. Chu, A. Dahlin, R. Evers, V. Fischer, K.M. Hillgren, K.A. Hoffmaster, T. Ishikawa, D. Keppler, R.B. Kim, C.A. Lee, M. Niemi, J.W. Polli, Y. Sugiyama, P.W. Swaan, J.A. Ware, S.H. Wright, S. Wah Yee, M.J. Zamek-Gliszczynski, L. Zhang, Membrane transporters in drug development, *Nat. Rev. Drug Discov.* 9 (2010) 215–236. <https://doi.org/10.1038/nrd3028>.
- [10] J.H. Lin, M. Yamazaki, Clinical Relevance of P-Glycoprotein in Drug Therapy, *Drug Metab. Rev.* 35 (2003) 417–454. <https://doi.org/10.1081/DMR-120026871>.
- [11] K. Natarajan, Y. Xie, M.R. Baer, D.D. Ross, Role of breast cancer resistance protein (BCRP/ABCG2) in cancer drug resistance, *Biochem. Pharmacol.* 83 (2012) 1084–1103. <https://doi.org/10.1016/j.bcp.2012.01.002>.
- [12] D. Kovacsics, I. Patik, C. Özvegy-Laczka, The role of organic anion transporting polypeptides in drug absorption, distribution, excretion and drug-drug interactions, *Expert Opin. Drug Metab. Toxicol.* 13 (2017) 409–424. <https://doi.org/10.1080/17425255.2017.1253679>.
- [13] D. Iusuf, E. Van De Steeg, A.H. Schinkel, Functions of OATP1A and 1B transporters in vivo: insights from mouse models, *Trends Pharmacol. Sci.* 33 (2012) 100–108. <https://doi.org/10.1016/j.tips.2011.10.005>.
- [14] B. Rochat, Role of Cytochrome P450 Activity in the Fate of Anticancer Agents and in Drug Resistance, *Clin. Pharmacokinet.* 44 (2005) 349–366. <https://doi.org/10.2165/00003088-200544040-00002>.
- [15] L. Elens, T. Van Gelder, D.A. Hesselink, V. Haufroid, R.H.N. Van Schaik, CYP3A4\*22: Promising newly identified CYP3A4 variant allele for personalizing pharmacotherapy, *Pharmacogenomics.* 14 (2013) 47–62. <https://doi.org/10.2217/pgs.12.187>.



## **PART I**

# Bioanalysis of cyclin-dependent kinase inhibitors



# 1

## Development and validation of a bioanalytical method for the quantification of the CDK4/6 inhibitors abemaciclib, palbociclib and ribociclib in human and mouse matrices using liquid chromatography-tandem mass spectrometry

Analytical and Bioanalytical Chemistry 2019, 411: 5331-5345

Alejandra Martínez-Chávez  
Hilde Rosing  
Michel Hillebrand  
Matthijs M. Tibben  
Alfred H. Schinkel  
Jos H. Beijnen

## Abstract

A novel method was developed and validated for the quantification of the three approved CDK4/6 inhibitors (abemaciclib, palbociclib and ribociclib) in both human and mouse plasma and mouse tissue homogenates (liver, kidney, spleen, brain and small intestine) using liquid chromatography coupled to tandem mass spectrometry (LC-MS/MS). For all matrices, pre-treatment was performed using 50  $\mu$ L of sample by protein precipitation with acetonitrile, followed by dilution of the supernatant. Chromatographic separation of the analytes was done on a C18 column using gradient elution. A full validation was performed for human plasma, while a partial validation was executed for mouse plasma and mouse tissue homogenates. The method was linear in the calibration range from 2 to 200 ng/mL, with a correlation coefficient ( $r$ )  $\geq$  0.996 for each analyte. For both human and mouse plasma, the accuracy and precision were within  $\pm$  15% and  $\leq$  15%, respectively, for all concentrations, except for the lower limit of quantification, where they were within  $\pm$  20% and  $\leq$  20%, respectively. A fit-for-purpose strategy was followed for tissue homogenates, and the accuracy and precision were within  $\pm$  20% and  $\leq$  20%, respectively, for all concentrations. Stability of all analytes in all matrices at different processing and storage conditions was tested; ribociclib and palbociclib were unstable in most tissue homogenates and conditions were modified to increase the stability. The method was successfully applied for the analysis of mouse samples from preclinical studies. A new ribociclib metabolite was detected in mouse plasma samples with the same  $m/z$  transition as the parent drug.

## Introduction

The development of new small molecules for targeted therapy in cancer has been accelerated over the past years with the progress of high-resolution molecular techniques [1]. Since cancer cells present a dysregulated cell cycle, the cyclin-dependent kinases (CDKs), enzymes that play a key role in cell cycle control, have been regarded as promising targets for new anticancer molecules [2,3]. The first generation of CDK inhibitors failed in clinical studies because they were found to be toxic to non-cancerous cells due to their lack of selectivity. In contrast, the second generation of this class of compounds, which is selective for CDK4/6, has shown efficacy in the clinic [2]. So far, three molecules within this class have been approved by the U.S. Food and Drug Administration (FDA): palbociclib in 2015, and ribociclib and abemaciclib both in 2017. These drugs specifically inhibit the CDK 4/6-cyclin D complex, thereby preventing the inactivation of the retinoblastoma (Rb) tumor suppressor protein, and arresting the cell cycle between G-phase and S-phase [3]. Despite these drugs interacting with their targets through the same 2-aminopyrimidine group, they differ in selectivity and potency [4]. Palbociclib and ribociclib are highly selective for CDK4/6 compared to other CDKs, and abemaciclib shows the highest potency with an  $IC_{50}$  for CDK4/CDK6 of 2/5 nM, compared to 9-11/15 and 10/39 nM for palbociclib and ribociclib, respectively [4,5]. This is related to differences in their molecular structures and drug-target binding. Abemaciclib presents two fluorine atoms around the ATP-binding pocket, whereas ribociclib and palbociclib contain much larger substituents (a dimethylamino group, and methylketone and adjacent methyl groups, respectively) which might influence their increase in selectivity. Furthermore, the lipophilicity (cLogP) of each compound correlates with their potency, the cLogP of abemaciclib (5.5) is significantly higher than that of palbociclib (2.7) or ribociclib (2.3) [4]. These molecules are currently indicated to treat certain types of breast cancer in combination with hormone therapy. Furthermore, the efficacy of each compound to treat other cancer types is still under investigation in preclinical models and clinical trials, either as single agents or in combination with other drugs [6,7].

Validated bioanalytical methods are needed to support these investigations. To date, some bioanalytical methods have been reported for the quantification of palbociclib in biological matrices. Nguyen *et al.* reported a validated quantitative analysis for palbociclib in breast tumor homogenates using LC-MS/MS [8]. Smith *et al.* introduced the use of an automated micro-sample processing for the pretreatment of mouse plasma samples prior to LC-MS/MS analysis of palbociclib; however, the availability of this system is restricted in many laboratories [9]. Recently, Paul *et al.* described two bioanalytical methods for the quantification of palbociclib in rat plasma using an LC-MS method using a high resolution quadrupole time of flight (Q-TOF) mass spectrometer, which is more convenient for qualitative rather than quantitative assays; therefore, the instrumentation is restricted in most bioanalytical laboratories [10,11]. For ribociclib,

two bioanalytical assays have been published. A method for the quantification of ribociclib in mouse plasma and Ringer's solution for a cerebral microdialysis study was first described [12]. Recently, Bao *et al.* reported a method for the quantification of ribociclib in human plasma, brain tumor, and CSF samples [13]. Finally, Raub *et al.* reported the use of LC-MS/MS for the quantification of palbociclib and abemaciclib in biological matrices, but no further details of the methods and their performance were described [14]. Since our particular interest is to characterize the function of transporters and metabolic enzymes in drug pharmacokinetics and tissue distribution, a validated assay is needed for the quantification of these compounds in mouse plasma and tissue homogenates. Previously published assays for the determination of abemaciclib, palbociclib and ribociclib do not include all the matrices needed for our study. Since these compounds show similar molecular structures, one versatile method could be used to optimize bioanalytical measurements of samples from different preclinical studies or patients, using one single method and thus simplifying the logistics of the bioanalytical laboratory.

Therefore, the objective of this study was to develop and validate the first LC-MS/MS method for the quantitative analysis of the three approved CDK4/6 inhibitors abemaciclib, palbociclib and ribociclib in human and mouse plasma and mouse tissue homogenates, including the liver, kidney, spleen, brain, and small intestine. A full validation was performed in human plasma, while for mouse plasma and tissue homogenates, a partial validation was executed. Calibration standards in a surrogate matrix (human plasma) were used for the quantification in these matrices. This method was set up to support pharmacokinetics and tissue distribution studies in mice.

## Materials and methods

### Chemicals

Abemaciclib, palbociclib and ribociclib, as well as their internal standards (IS)  $^2\text{H}_8$ -abemaciclib,  $^2\text{H}_8$ -palbociclib and  $^2\text{H}_6$ -ribociclib (100.0% purity for all compounds), were purchased from Alsachim (Illkirch-Graffenstaden, France). The isotopic enrichment of the internal standards was 98.0%, 98.3% and 99.9% for  $^2\text{H}_8$ -abemaciclib,  $^2\text{H}_8$ -palbociclib and  $^2\text{H}_6$ -ribociclib, respectively. Methanol (MeOH), acetonitrile (ACN), formic acid and water (all supragradient grade) were supplied by Biosolve Ltd (Valkenswaard, The Netherlands). Dimethylsulfoxide (DMSO, SeccoSolv  $\geq 99.9\%$  purity) was obtained from Merck (Darmstadt, Germany), and ammonium bicarbonate (LC-MS grade) was from Sigma Aldrich (Darmstadt, Germany).

### Blank matrices

Control human  $\text{K}_2\text{EDTA}$  plasma originated from Bioreclamations LLC (Hicksville, NY, USA). Mouse sodium heparin plasma and mouse organs (including the brain, kidneys,



liver, small intestine and spleen) were obtained from the animal laboratory of the Netherlands Cancer Institute (Amsterdam, The Netherlands). All blanks were stored at  $-20^{\circ}\text{C}$  prior to use.

#### *Tissue homogenate preparation*

Blank tissue homogenates were prepared using 6.5 mm ceramic beads and a Fast Prep-24™ 5G (MP Biomedicals Inc, Santa Ana, CA, USA). Bovine serum albumin (BSA, Fraction V), obtained from Roche Diagnostics GmbH (Mannheim, Germany) was dissolved in distilled water (B Braun Medical, Melsungen, Germany), at a concentration of 4% (w/v). After weighing the complete organ, a volume of 3 mL of this solution was added to liver and small intestine, 2 mL to kidneys and 1 mL to brain and spleen. The tissue/BSA ratio (w/v) of the homogenates were approximately 0.4:1 for brain and liver, 0.1:1 for spleen, 0.2:1 for kidneys and 0.25:1 for small intestine. All samples were shaken in the Fast Prep at 6.0 m/s during 60 s.

#### **Stock and working solutions**

Two independent stock solutions (one for calibration standards and the other for quality control (QC) samples) of each analyte were prepared at 1 mg/mL in DMSO for abemaciclib and ribociclib, and in 0.1% formic acid in water for palbociclib. All stock solutions for the analytes were stable for at least 12 months. Individual stock solutions of each IS were prepared at 1 mg/mL in the same solvents as their corresponding analyte.

From the stock solutions, six working solutions were prepared for calibration standards adding all analytes at a concentration of 40, 200, 1000, 2000, 3000 and 4000 ng/mL in MeOH. For the QC samples, four working solutions were prepared at 40, 100, 2000 and 3000 ng/mL. The IS-working solution was prepared by mixing and diluting all the IS stock to obtain 250 ng/mL in MeOH. Stock and working solutions were stored at  $-20^{\circ}\text{C}$ .

#### **Calibration standards and QC samples**

Analyte working solutions were diluted 1:20 (v/v) with blank human plasma to obtain six calibration standards with final concentrations of 2, 10, 50, 100, 150 and 200 ng/mL for all analytes.

The same dilution was used to prepare QC samples in human plasma, mouse plasma and mouse tissue homogenates at concentrations of 2 (lower limit of quantification (LLOQ)), 5 (QC L), 50 (QC M) and 150 ng/mL (QC H) for each analyte.

#### **Sample pretreatment**

50  $\mu\text{L}$  of sample (either from a preclinical study, calibration standard or QC) was mixed with 25  $\mu\text{L}$  of IS-working solution, followed by 150  $\mu\text{L}$  of ACN for protein precipitation.

Samples were vortex mixed and centrifuged at 23,100 g for 10 min at 20 °C. An aliquot of 80 µL of supernatant was diluted with 120 µL of 10 mM ammonium bicarbonate in water:MeOH (1:1 v/v). The final extract was transferred to a glass vial with insert, and 10 µL was injected to the LC-MS/MS system for analysis.

### LC-MS/MS system and method

The chromatographic system consisted of an Agilent 1100 chromatograph (Palo Alto, CA, USA) equipped with a binary pump (Model G1312A), a degasser (Model G1379A), an autosampler (Model G1367A) and a column oven (Model G1316A). The analytes were separated using a Gemini C18 column (50 x 2.0 mm ID, 5µm) coupled to a Gemini C18 (4 x 2 mm) guard column (Phenomenex, Torrance, CA, USA), and a mobile phase composed of 10 mM ammonium bicarbonate in water (eluent A) and 10 mM ammonium bicarbonate in water-methanol (1:9, v/v; eluent B). Gradient elution was applied and the eluent composition and flow rate are described in Table 1. The temperature of the autosampler and column oven was set at 6 °C and 40 °C, respectively.

**Table 1.** Gradient and flowrate settings

Time (min)	B%	Flow Rate (µL/min)
Initial	55	250
1.0	100	400
2.0	100	400
2.5	55	400
3.0	55	400
4.0	100	500
4.5	100	500
5.5	55	500
6.5	55	250
7.0	55	250

For detection, an API 3000 triple quadrupole with electrospray ionization (ESI) mass spectrometer (Sciex, Foster City, CA, USA) was operated in a positive ion mode. Samples were acquired via multiple reaction monitoring (MRM) and analyzed using the Analyst software version 1.6.2 (Sciex). The following general settings were used to detect all the compounds: the ion spray voltage was set at 5000 V, the temperature for the solvent evaporation was established at 350 °C, and the nebulizer, curtain and collision gases were set at 3, 9 and 11 (arbitrary units), respectively. The entrance and focusing potentials were 10 and 350 V, respectively, and the scan/dwell time was 100 ms. The analyte-specific settings are described in Table 2. The chromatographic system was coupled to the mass spectrometer by a divert valve, which directed the flow to the detector from 1 to 3.5 min and the rest to the waste container.

**Table 2.** MS compound specific parameters

	<b>Abemaciclib</b>	<b>Palbociclib</b>	<b>Ribociclib</b>
Analyte parent to product transition ( <i>m/z</i> )	507 → 393	448 → 380	435 → 322
IS parent to product transition ( <i>m/z</i> )	515 → 393	456 → 388	441 → 322
Declustering Potential (V)	56	71	71
Collision energy (V)	29	39	47
Collision Cell Exit Potential (V)	26	24	30

### Method validation

A full method validation was performed in human plasma, and was based on the US FDA and European Medicine Agency (EMA) guidelines for bioanalytical method validation [15,16]. A partial validation was executed for mouse plasma and the following performance characteristics were tested: accuracy and precision, selectivity, dilution integrity and stability. Finally, for tissue homogenates a fit-for-purpose strategy was followed according to Xue *et al.* [17], where accuracy and precision, selectivity, dilution integrity and stability were evaluated using the acceptance criteria for method qualification.

#### *Calibration model*

Human plasma calibration standards (6 non-zero standards with duplicate points at each concentration in the range 2 to 200 ng/mL for each analyte), including a blank and a zero calibration standard (blank spiked with IS), were freshly prepared in duplicate and analyzed at the beginning and the end of each analytical run. A linear model with a  $1/x^2$  weighting factor was used to describe the concentration-response relationship for all analytes, where  $x$  is the analyte concentration. At least 75% of non-zero calibration standards should meet the following criteria: their calculated concentrations should be within  $\pm 15\%$  of the nominal concentrations, except at LLOQ where the calculated concentration should be  $\pm 20\%$  of the nominal concentration in a minimum of three validation runs.

#### *Selectivity and specificity*

The selectivity of the method was established by the analysis of LLOQ and blank samples from 6 different batches of control human  $K_2EDTA$  and mouse plasma. For each tissue homogenate one batch was evaluated. LC-MS/MS chromatograms of the blanks and LLOQ samples were monitored and compared for chromatographic integrity and potential interferences.

Furthermore, the cross analyte/internal standard interferences were determined by separately spiking abemaciclib, palbociclib and ribociclib to control human plasma at the upper limit of quantification (ULOQ). Independently, blank human plasma was spiked also with each internal standard at the concentration used in the assay. For each sample, any interference at the retention times of the analytes and internal standard was evaluated.

In at least 4 of 6 batches, the response of the interfering peaks at the retention times of the analytes should be  $\leq 20\%$  of the LLOQ response at the LLOQ, and for the interfering peaks at the retention time of the internal standard, their response should be  $\leq 5\%$  of the response of the internal standard. LLOQ samples should be within  $\pm 20\%$  of the nominal concentration.

#### *Lower limit of quantification*

This parameter was evaluated comparing the response of the zero calibrator and the LLOQ in three validation runs. To meet the acceptance criteria, the response at the LLOQ should be at least 5 times the response compared with the zero calibrator response for each CDK4/6 inhibitor.

#### *Carryover*

Carryover was tested in three analytical runs by injecting two blank matrix samples after the ULOQ. The percentage of response compared to the LLOQ obtained for each analyte in the blank matrix samples was calculated. Carryover should not exceed 20% of LLOQ.

#### *Accuracy and precision*

QC samples were prepared in human and mouse plasma, and mouse tissue homogenates at the concentrations described in "Calibration standards and QC samples" section. Five replicates of each level were analyzed in three analytical runs for human plasma. For the remaining matrices, five replicates of each level were tested in one analytical run. The intra-assay coefficient of variation (CV) and bias (between the nominal and measured concentrations) were calculated for the precision and the accuracy, respectively. Furthermore, for human plasma, the inter-assay CV (calculated by ANOVA) and bias were determined. For plasma matrices, the accuracy should be within  $\pm 15\%$  of nominal concentrations and for the precision, the CV should be  $\leq 15\%$  for all concentration levels, except at LLOQ, where  $\pm 20\%$  and  $\leq 20\%$ , respectively are accepted. For the accuracy and precision in tissue homogenates,  $\pm 20\%$  and  $\leq 20\%$  were accepted at all concentration levels, respectively.

#### *Matrix factor and recovery*

Matrix effects were investigated in 6 different batches of human plasma at QC L and QC H concentrations. Each concentration level was prepared in the presence of matrix

(each blank plasma batch was processed until final extract and spiked with the corresponding QC working solution) and in the absence of matrix (QC working solutions diluted with organic solvents). The matrix factor (MF) was determined for each lot of matrix by calculating the ratio of the peak area in the presence of matrix to the peak area in the absence of matrix. Furthermore, the IS-normalized MF was calculated dividing the MF of the analyte by the MF of the IS.

For the recovery, the processed QC L and QC H samples were compared with the matrix-absent samples (previously described) and the percentage of recovery was calculated as well as the CV for each concentration level. The CV for the matrix factor and the recovery should be < 15%.

#### *Dilution integrity*

The integrity of mouse plasma and tissue homogenate samples diluted with control human plasma was investigated. Five replicates of each homogenate at around 5 times the ULOQ (1000 ng/mL) were prepared and diluted 10 times with control human plasma. For mouse plasma dilution integrity, two samples were prepared in 5-fold at 25 and 1000 ng/mL and separately diluted 5 times in control human plasma. The accuracy and precision for these samples were calculated, and for the acceptance criteria they should be within  $\pm 15\%$  of the nominal concentration and the CV should be  $\leq 15\%$ , respectively.

#### *Stability*

The stability of each analyte was investigated in all the previously mentioned matrices. For plasma (both human and mouse) the stability was determined in triplicate at two concentration levels, QC L and QC H, whereas for mouse tissue homogenates only at QC M (except the brain in one stability condition). For all matrices, the following stability conditions were assessed: short-term at room temperature (RT), long-term at  $-20\text{ }^{\circ}\text{C}$  and after 3 freeze-thaw (F/T) cycles at  $-20\text{ }^{\circ}\text{C}/\text{RT}$ . Furthermore, for tissue homogenates, the short-term stability in ice-water, long-term stability at  $-70\text{ }^{\circ}\text{C}$  and F/T stability at  $-70\text{ }^{\circ}\text{C}/\text{ice water}$  were also evaluated. Additionally, the stability in the final extract was tested. For this, the QC L and QC H final extracts from plasma, brain and spleen, and the QC M final extract from liver, kidney and small intestine were stored at  $4\text{-}8\text{ }^{\circ}\text{C}$  up to 3 days. Lastly, the stability of the stock solutions at  $-20\text{ }^{\circ}\text{C}$  was investigated. Analytes were considered stable if the accuracy was  $\pm 15\%$  and  $\pm 20\%$  of nominal concentration for plasma and tissue homogenates, respectively.

#### **Preclinical application of the method**

This method was developed to support pharmacokinetic and tissue distribution studies of the CDK4/6 inhibitors in mice (FVB background). These studies were done separately for each drug. Animal housing and studies were conducted according to institutional guidelines complying with Dutch and European Union legislation (approval number

from The Dutch Central Animal Testing Committee: AVD301002016595). After a minimum of 2 h fasting, the drug solution was orally administered at doses of 10 mg/kg for abemaciclib (n = 6) and palbociclib (n = 4), and at 20 mg/kg for ribociclib (n = 6). Approximately 50 µL of blood was collected from the tip of the tail at several time points, except at the last one, when 500-1000 µL of blood was collected by cardiac puncture under isoflurane anesthesia. For the ribociclib pharmacokinetic study the sampling time points were 0.25, 0.5, 1, 3, 8 and 24 h. Mice were sacrificed by cervical dislocation and the organs were collected and weighed. Plasma was obtained using sodium heparin as anticoagulant after centrifugation at 9000g, 4 °C, for 6 min. When necessary, 10 µL of mouse plasma was diluted with 40 µL of human plasma. The tissue homogenates were prepared according to the procedure described in the "Tissue homogenate preparation" section. Plasma and tissue homogenate samples were stored at -20 and -70 °C, respectively, until the LC-MS/MS analysis was performed.

### **Qualitative analysis using HR-MS**

High resolution mass spectrometry (HR-MS) measurements were performed in an LC (Shimadzu, Kyoto, Japan) composed by an LC-20AD pump, a CTO-LOAC column oven and a SIL-HTC autosampler, and coupled to an LTQ Orbitrap Discovery (Thermo Fisher Scientific, Waltham, MA, USA). A mouse plasma sample obtained after the pharmacokinetics study was injected into the system using the same chromatographic settings as described above, except for the gradient. In the initial conditions, the flow rate and the eluent B were set at 0.25 mL/min and 55%, respectively. These conditions were maintained for 2.5 min, % B increased up to 100% in 1 min, and it was held during 2.5 min. The gradient reverted back to the initial condition at 55% B in 0.1 min and held up to 8.0 min of the total run time.

## **Results and discussion**

### **Method development**

#### *Mass spectrometry and chromatography*

To establish the analyte-dependent parameter settings of the mass spectrometer, each compound (dissolved in MeOH:water (80:20 v/v) 1% formic acid) was directly infused into the MS at a concentration of 100 ng/mL for abemaciclib and palbociclib, and 1000 ng/mL for ribociclib. The most abundant fragment ion of each analyte was chosen for quantification (Figure 1). A compound optimization was performed for each analyte and those values that produced the highest intensity in the parent ion response from each parameter were selected. The general settings were chosen by a flow injection analysis of ribociclib, to enhance the response intensity, since this compound showed the lowest intensity compared with palbociclib and abemaciclib.

Similarly to previous publications [8,12], carryover post-injection was observed for all the CDK4/6 inhibitors. In general, the more hydrophobic the compound, the higher percentage of carryover was detected. Thus, abemaciclib was the compound that showed the highest carryover, followed by palbociclib and then ribociclib. In order to decrease the percentage of carryover, a washing step in the solvent gradient was included after the elution of all the analytes, and a narrow concentration range was chosen, from 2 to 200 ng/mL.

### Sample pre-treatment

Two different precipitation agents (MeOH-ACN (1:1, v/v) and ACN) and three different dilution solvents for the supernatant (acidic (formic acid 0.1% v/v), alkaline (10 mM ammonium bicarbonate in water:MeOH (1:1, v/v)), and water) were tested. The analyte responses were evaluated using all combinations of precipitation agents with dilution solvents. ACN showed the highest response for abemaciclib, whereas for the other two analytes, no difference was observed between both precipitation agents. The alkaline solvent was chosen to dilute the supernatant before injection, since it was observed that the percentage of carryover decreased for all analytes.

### Method validation

#### *Calibration curve*

A linear model with a  $1/x^2$  weighting factor properly described the concentration-response relationship for all the analytes. Representative chromatograms of each CDK 4/6 inhibitor and of their internal standards at the LLOQ and ULOQ are shown in Figure 2. The correlation coefficients obtained ( $n = 3$ ) were  $>0.998$ ,  $>0.996$ , and  $>0.997$  for abemaciclib, palbociclib, and ribociclib, respectively. The regression equations were  $y = (0.0115 \pm 0.0004)x + (0.001 \pm 0.001)$  for abemaciclib,  $y = (0.0116 \pm 0.0006)x + (0.004 \pm 0.001)$  for palbociclib, and  $y = (0.0099 \pm 0.0009)x + (0.0009 \pm 0.0019)$  for ribociclib, where  $y$  is the ratio of the analyte and IS response and  $x$  is the analyte concentration in ng/mL. All back-calculated concentrations from non-zero calibrators were within  $\pm 15\%$  of the nominal concentrations. Thus, the method was linear in the concentration range of 2-200 ng/mL for each analyte.

#### *Selectivity and specificity*

All batches of both human and mouse plasma were free of interferences for the analytes and IS at their corresponding mass transitions. Furthermore, the spiked LLOQ human and mouse plasma samples were within  $\pm 20\%$  of the nominal concentration, for at least 4 out of 6 tested batches for all analytes. For tissue homogenates, none of the blanks evaluated showed any interference, and the bias obtained for the LLOQ was within the acceptance criteria.

Moreover, cross-analyte and IS did not show any interference, except for ribociclib-IS (RBC-IS) which interfered with ribociclib response. However, the peak response of RBC-IS was 16.1% of the ribociclib LLOQ area. Since this value is  $\leq 20\%$ , it was found to be acceptable.

### Lower limit of quantification

The peak height at the LLOQ was more than 13 times the noise obtained with the blank response in three validation runs for all analytes. Furthermore, the accuracy and precision for each analyte in human plasma were within  $\pm 20\%$  and  $\leq 20\%$ , respectively, in three analytical runs (Table 3). For the other matrices, the LLOQ met these acceptance criteria as well (Table 4).

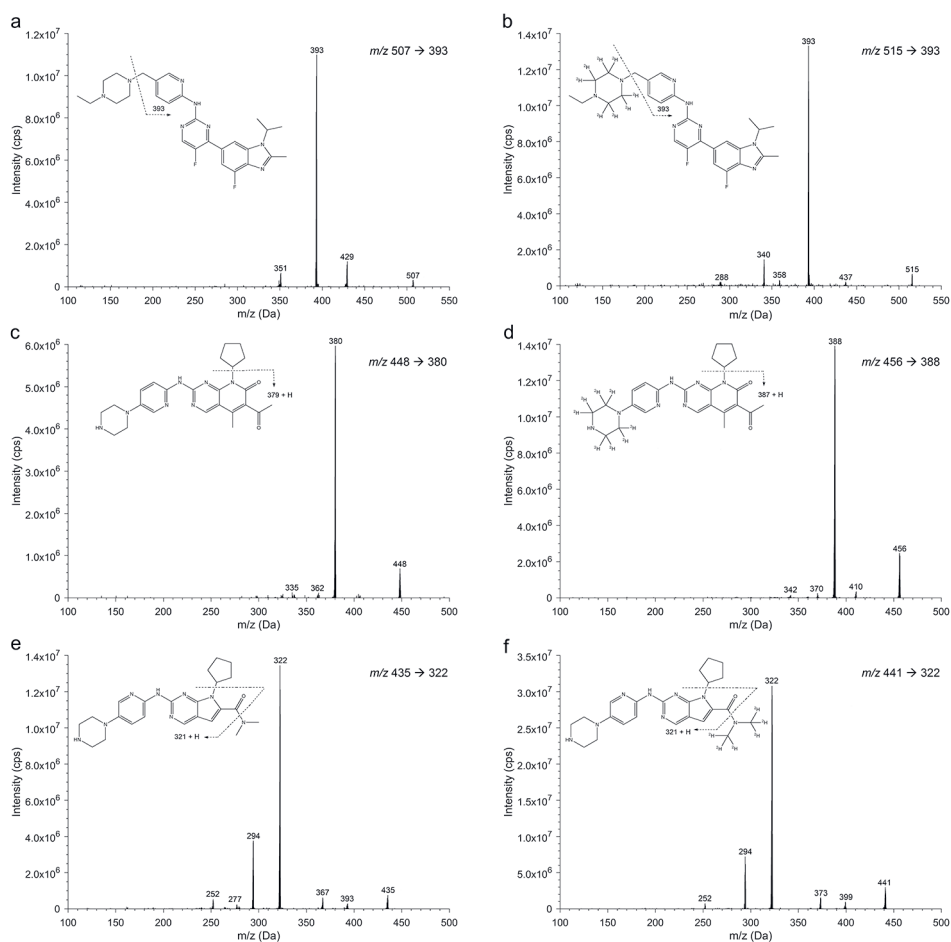


**Figure 1.** Mass spectra with the molecular structure and proposed MS fragmentation pattern of abemaciclib (a), palbociclib (c), ribociclib (e) and their stable isotopically labeled internal standards (b, d, f, respectively).



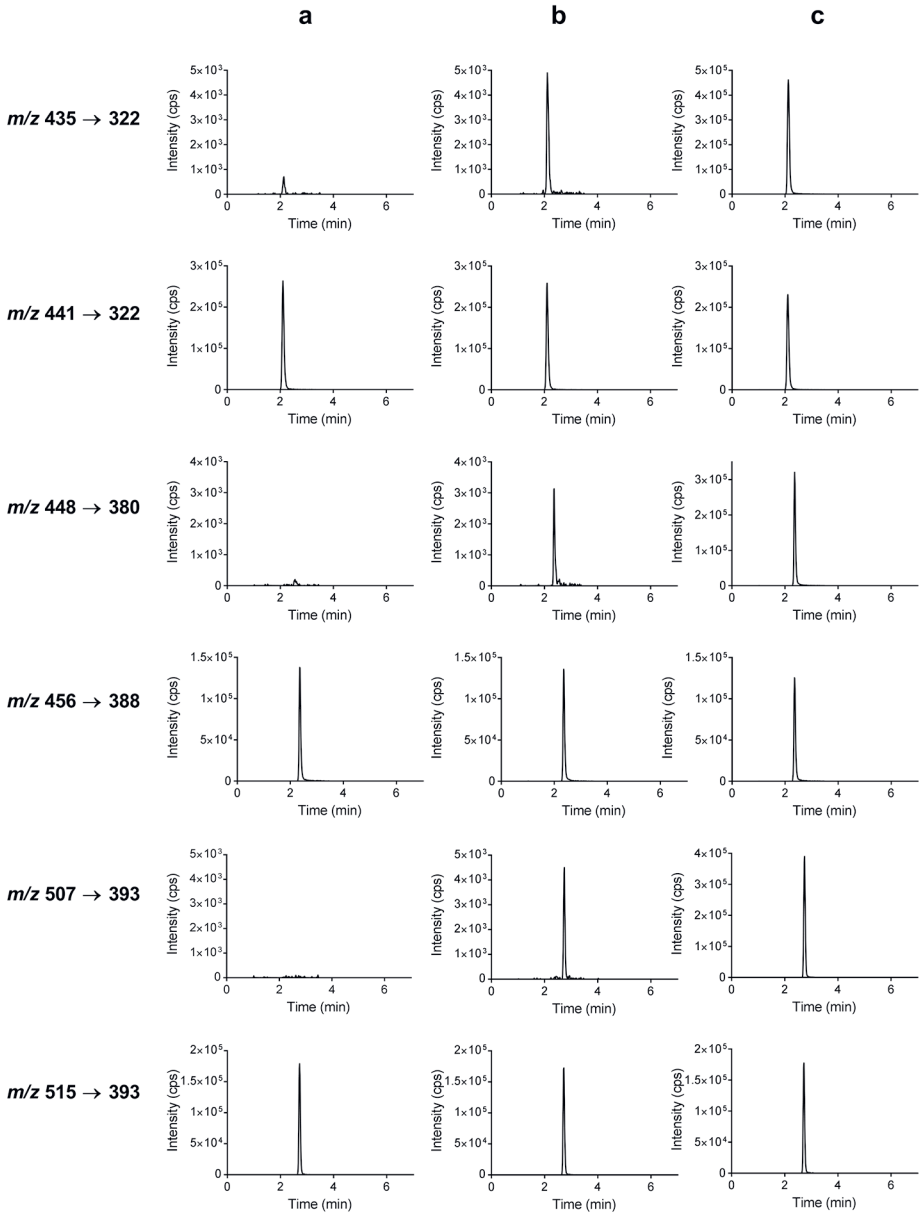


**Figure 2.** Representative chromatograms of control human plasma spiked with internal standards (a), spiked at the LLOQ (b) and spiked at the ULOQ (c) at the mass transitions of ribociclib ( $m/z$  435 $\rightarrow$ 322), ribociclib-IS ( $m/z$  441 $\rightarrow$ 322), palbociclib ( $m/z$  448 $\rightarrow$ 380), palbociclib-IS ( $m/z$  456 $\rightarrow$ 388), abemaciclib ( $m/z$  507 $\rightarrow$ 393), and abemaciclib-IS ( $m/z$  515 $\rightarrow$ 393). Y-axis in chromatograms of a and b series for the analyte mass transitions ( $m/z$  435 $\rightarrow$ 322,  $m/z$  448 $\rightarrow$ 380 and  $m/z$  507 $\rightarrow$ 393) have the same scale, but Y-axis scale in chromatograms from c are adjusted to the highest response.

### Carryover

The carryover was evaluated in three analytical runs and the percentage obtained was  $\leq 14.0\%$ ,  $14.5\%$  and  $6.4\%$  of the LLOQ for abemaciclib, palbociclib and ribociclib, respectively. The internal standards showed a negligible carryover since it was  $\leq 0.4\%$  compared with the mean response of each internal standard.

### Accuracy and precision

In Table 3, the intra- and inter-assay accuracy and precision results for the quantification of the CDK4/6 inhibitors in human plasma are presented. The bias and CV were within  $\pm 20\%$  and  $\leq 20\%$  at the LLOQ, and within  $\pm 15\%$  and  $\leq 15\%$  for the other QC samples for all analytes. These results meet the acceptance criteria established in the official FDA and EMA guidelines [15,16]. For the other matrices, intra-assay accuracy and precision were assessed and the results are shown in Table 4. For mouse plasma all the data meet the criteria previously mentioned. For the tissue homogenates, the bias was within  $\pm 20\%$  at all concentration levels, and the CV was  $\leq 15\%$ . These results meet the criteria for a qualified method according to Xue *et al.* [17]. Since the QC samples meet the acceptance criteria, the quantification of the three CDK4/6 inhibitors in mouse plasma and tissue homogenates using human plasma as a surrogate matrix is accepted. This involves the use of calibration standards prepared in human plasma to quantify the analytes in the tested matrices.

**Table 3.** Accuracy and precision of abemaciclib, palbociclib and ribociclib in human plasma

	Nominal concentration (ng/mL)	Intra-assay		Inter-assay	
		Bias (%)	CV (%)	Bias (%)	CV (%)
Abemaciclib	2	$\pm 11.4$	$\leq 11.0$	-7.6	1.8
	5	$\pm 7.2$	$\leq 5.0$	-5.4	1.1
	50	$\pm 4.6$	$\leq 4.3$	3.7	*
	150	$\pm 3.1$	$\leq 2.7$	2.0	0.4
Palbociclib	2	$\pm 18.5$	$\leq 10.9$	-9.9	10.9
	5	$\pm 9.6$	$\leq 8.9$	-8.1	*
	50	$\pm 2.5$	$\leq 4.8$	-2.0	*
	150	$\pm 6.4$	$\leq 3.0$	-3.0	3.2
Ribociclib	2	$\pm 18.5$	$\leq 10.0$	-13.3	4.0
	5	$\pm 13.5$	$\leq 4.8$	-9.7	4.4
	50	$\pm 6.2$	$\leq 3.9$	-4.6	2.5
	150	$\pm 5.2$	$\leq 4.4$	-5.2	3.6

\*The inter-run precision cannot be calculated, because the mean square between groups is lower than the mean square within groups (calculated with analysis of variances, ANOVA). This means that there is no significant additional variation that can be assigned to the analysis in different runs.

**Table 4.** Accuracy and precision of abemaciclib, palbociclib and ribociclib inhibitors in mouse plasma and tissue homogenates

Matrix	Nominal concentration (ng/mL)	Abemaciclib		Palbociclib		Ribociclib	
		Bias (%)	CV (%)	Bias (%)	CV (%)	Bias (%)	CV (%)
Plasma	2	-3.4	4.6	-4.2	7.0	-11.2	4.7
	5	-0.5	4.7	-8.6	5.2	-8.7	8.6
	50	3.3	2.0	-7.5	3.6	-4.8	3.0
	150	0.5	2.3	-7.1	2.1	-8.3	2.6
Liver homogenate	2	14.1	13.2	11.1	9.6	5.0	9.3
	5	10.3	2.8	14.1	7.7	10.0	7.7
	50	14	3.3	14.2	3.5	8.2	2.7
	150	10.7	2.3	18.4	1.9	6.4	1.9
Kidney homogenate	2	12.3	6.5	12.4	2.3	8.9	8.0
	5	8.2	6.6	7.6	7.5	1.2	4.7
	50	9.7	1.8	12.8	1.7	0.4	1.8
	150	9.1	3.4	10.5	3.6	0.3	3.8
Spleen homogenate	2	3.9	8.8	16.4	9.8	4.1	12.6
	5	5.7	5.3	10.3	3.5	0.2	1.1
	50	13.9	2.3	12.4	2.6	6.4	4.1
	150	13.5	2.6	12.7	1.3	8.1	3.0
Brain homogenate	2	6.3	10.4	11.5	7.8	1.6	11.7
	5	8.1	2.6	9.4	2.8	-3.8	4.5
	50	11.6	3.4	4.6	3.8	6.4	4.1
	150	13.6	1.8	4.5	2.5	1.7	1.4
Small intestine homogenate	2	10.2	6.3	11.9	7.4	18.4	3.7
	5	15.4	6.8	7.7	9.1	12.5	7.2
	50	6.6	2.1	12.2	4.4	8.7	3.8
	150	-0.1	2.3	8.0	3.7	0.1	2.4

#### Matrix factor and recovery

The CV of the normalized matrix factor at both concentration levels was  $\leq 7.4\%$  for all analytes. The mean normalized matrix factor was between 1.05 and 1.08, between 1.09 and 1.19, and between 1.11 and 1.20, for abemaciclib, palbociclib and ribociclib, respectively. The matrix showed no significant effect on the analyte responses, since the normalized MF values are close to 1. The absolute matrix factor for each analyte and internal standard are described in the Supplementary Material Table S1.

Furthermore, the normalized recovery after the extraction process was consistent at low and high concentrations for each analyte, 82.8% (CV = 1.6%) for abemaciclib, 79.9% (CV = 5.6%) for palbociclib and 83.4% (CV = 4.1%) for ribociclib. Absolute recoveries are shown in the Supplementary Material Table S2.

### *Dilution integrity*

A 1:5 dilution of mouse plasma samples in human plasma was investigated during the validation, since the volume of plasma obtained from a pharmacokinetics experiment in mice is low (10-20  $\mu\text{L}$ ). To reach a sample volume of 50  $\mu\text{L}$  necessary for the sample pretreatment, 10  $\mu\text{L}$  of mouse plasma with high concentration of the analytes was diluted with 40  $\mu\text{L}$  of control human plasma. The bias and CV values obtained were within  $\pm 3.7\%$  and  $\leq 3.5\%$  for abemaciclib,  $\pm 4.5\%$  and  $\leq 7.5\%$  for palbociclib, and  $\pm 9.4\%$  and  $\leq 12.9\%$  for ribociclib, complying with the acceptance criteria.

On the other hand, the bias and CV obtained for 10-fold diluted tissue samples with human plasma were  $\pm 7.6\%$  and  $\leq 5.4\%$  for abemaciclib,  $\pm 4.0\%$  and  $\leq 4.6\%$  for palbociclib, and  $\pm 5.5\%$  and  $\leq 4.6\%$  for ribociclib, respectively. All these results meet the acceptance criteria ( $\pm 20\%$  and  $\leq 20\%$ ) for method qualification.

### *Stability*

Stock solutions of abemaciclib, palbociclib and ribociclib were stable at  $-20\text{ }^{\circ}\text{C}$  after at least 12 months of storage. Plasma stability, in both mouse and human matrices, is presented in Table 5. In summary, all the analytes were stable in plasma at all stability conditions tested, except for QC L ribociclib after 3 F/T cycles and QC H abemaciclib in mouse plasma samples after 3 months storage at  $-20\text{ }^{\circ}\text{C}$ . Ribociclib QC L showed a mean bias slightly higher than  $\pm 15\%$ , where only one of three samples was outside the acceptance criteria. However, after the second F/T cycle the mean bias of ribociclib was  $-5.4\%$  and the CV was  $5.4\%$ , demonstrating that ribociclib is stable in human plasma after 2 F/T cycles. Abemaciclib QC H sample was stable in human plasma for 12 months, but it was not in mouse plasma after 3 months of storage since the bias was  $>15\%$ , although there is no indication of degradation since the bias is positive.

The stability in tissue homogenates is reported in Table 6. It shows that abemaciclib is stable in all matrices at all conditions. In contrast, palbociclib and ribociclib showed instability in tissues. For example, palbociclib or ribociclib were not stable in liver, kidney and small intestine when stored at  $-20\text{ }^{\circ}\text{C}$  for 1 month; therefore, the long-term stability was tested at  $-70\text{ }^{\circ}\text{C}$  where both compounds were stable in all matrices. After 24 h at room temperature, palbociclib and ribociclib showed significant degradation in kidney and spleen homogenates, however, they were stable for at least 3h at room temperature and in an ice/water bath. Thus, the instability of these two analytes in kidneys after freeze/thaw cycles from  $-20\text{ }^{\circ}\text{C}$  to room temperature is likely a consequence of their instability at the previously described conditions. Therefore, the stability after 3 freeze/thaw cycles from  $-70\text{ }^{\circ}\text{C}$  to ice/water bath was tested, and at these conditions, the analytes were found to be stable. In spite of the instability of palbociclib and ribociclib in some tissue homogenates, appropriate conditions for samples storage and processing have been found.

**Table 5.** Stability of abemaciclib, palbociclib and ribociclib in mouse and human plasma

Analyte	Matrix	Stability conditions	Nominal concentration (ng/mL)	Mean concentration (ng/mL)	Accuracy (% Bias)	Precision (% CV)		
Abemaciclib	Human plasma	RT, 3 d	5	4.8	-4.5	6.1		
			150	159.3	6.2	1.4		
		3 F/T (-20 °C/RT)	5	4.7	-6.5	5.2		
			150	144.3	-3.8	1.1		
		-20 °C, 12 m	5	4.8	-4.7	0.8		
			150	141.7	-5.6	3.5		
	Final extract	4-8 °C, 4 d	5	5.2	4.5	2.6		
			150	160.7	7.1	1.8		
	Mouse plasma	RT, 3 d		5	4.8	-4.6	4.7	
				150	159.3	6.2	1.6	
			3 F/T (-20 °C/RT)	5	5.2	4.3	2.6	
				150	161.3	7.6	3.6	
-20 °C, 3 m			5	5.1	1.0	10.1		
		150	182.7	21.8	0.3			
Final extract		4-8 °C, 4 d	5	5.4	8.1	3.2		
			150	157.7	5.1	6.4		
Palbociclib		Human plasma	RT, 3 d	5	4.8	-3.8	2.8	
				150	142.7	-4.9	2.1	
	3 F/T (-20 °C/RT)		5	4.3	-14.5	0.4		
			150	137.7	-8.2	1.1		
	-20 °C, 12 m		5	4.4	-12.8	1.5		
			150	137.0	-8.7	3.2		
	Final extract		4-8 °C, 4 d	5	4.7	-6.9	5.2	
				150	148.7	-0.9	0.8	
	Mouse plasma		RT, 3 d		5	4.5	-10.1	1.3
					150	141.3	-5.8	3.2
				3 F/T (-20 °C/RT)	5	4.6	-8.8	6.1
			-20 °C, 3 m		150	149.7	-0.2	2.7
				5	5.1	1.4	7.3	
			150	166.7	11.1	3.0		
	Final extract	4-8 °C, 4 d		5	5.0	-0.8	5.9	
				150	142.7	-4.9	5.3	

see next page for the continuation of this table.

**Table 5.** Continued

Analyte	Matrix	Stability conditions	Nominal concentration (ng/mL)	Mean concentration (ng/mL)	Accuracy (% Bias)	Precision (% CV)
Ribociclib	Human plasma	RT, 3 d	5	4.6	-8.9	2.4
			150	144.3	-3.8	3.3
		3 F/T (-20 °C/RT)	5	4.3	-16.3	9.3
			150	136.3	-9.1	1.8
		2 F/T (-20 °C/RT)	5	4.7	-5.4	5.4
			-20 °C, 12 m	5	4.9	-2.7
	150	134.3	-10.4	0.9		
		Final extract	4-8 °C, 4 d	5	4.6	-7.5
	150			142.7	-4.9	4.8
	Mouse plasma	RT, 3 d	5	4.5	-9.9	2.8
				150	144.0	-4.0
			3 F/T (-20 °C/RT)	5	5.0	-0.3
150				147.7	-1.6	1.4
-20 °C, 3 m		5	4.8	-3.7	5.5	
		150	157.0	4.7	0.6	
Final extract		4-8 °C, 4 d	5	4.8	-4.5	3.8
			150	141.0	-6.0	3.5

RT=Room Temperature, F/T=Freeze-Thaw cycles, d=days, m=months.

**Table 6.** Stability of abemaciclib, palbociclib and ribociclib in tissue homogenates

Analyte	Matrix	Stability conditions	Nominal concentration (ng/mL)	Mean concentration (ng/mL)	Accuracy (% Bias)	Precision (% CV)
Abemaciclib	Liver homogenate	RT, 1 d	50	47.9	-4.1	1.4
		Ice/water bath, 3 h	50	51.9	3.8	3.0
		3 F/T (-20 °C, RT)	50	52.5	5.0	5.8
		3 F/T (-70 °C, ice/water bath)	50	50.0	0.1	1.3
		LT -20 °C, 1 m	50	50.7	1.4	5.3
		LT -70 °C, 1 m	50	50.6	1.2	3.4
	Final extract	4-8 °C, 2 d	50	47.9	-4.1	8.0
	Spleen homogenate	RT, 1 d	50	46.5	-6.9	2.9
		RT, 3 h	50	51.7	3.4	4.7
		Ice/water bath, 3 h	50	52.4	4.9	9.3
		3 F/T (-20 °C, RT)	50	48.7	-2.6	4.7
		3 F/T (-70 °C, ice/water bath)	50	56.1	12.1	3.5
		LT -20 °C, 1 m	50	48.6	-2.7	3.0
	Final extract	LT -70 °C, 1 m	50	51.8	3.5	2.3
		4-8 °C, 3 d	5	5.5	10.7	4.2
			150	156.3	4.2	10.7
	Kidney homogenate	RT, 1 d	50	43.3	-13.5	6.7
		RT, 3 h	50	50.9	1.7	0.6
		Ice/water bath, 3 h	50	49.3	-1.3	1.4
		3 F/T (-20 °C, RT)	50	49.5	-1.1	12.1
		3 F/T (-70 °C, ice/water bath)	50	51.8	3.6	6.3
		LT -20 °C, 1 m	50	49.0	-1.9	3.9
	Final extract	LT -70 °C, 1 m	50	52.7	5.5	0.8
		4-8 °C, 2 d	50	48.8	-2.3	1.4
Brain homogenate		RT, 1 d	5	5.3	6.2	3.0
	150		167	11.3	9.4	
	Ice/water bath, 3 h	50	55.2	10.4	1.6	
	3 F/T (-20 °C, RT)	50	53.4	6.9	3.0	
	3 F/T (-70 °C, ice/water bath)	50	51.1	2.2	6.2	
	LT -20 °C, 1 m	50	52.0	3.9	4.7	
Final extract	LT -70 °C, 1 m	50	52.1	4.3	5.8	
	4-8 °C, 3 d	5	4.9	-1.5	8.0	
		150	163	8.7	2.2	

see next page for the continuation of this table.

Table 6. Continued

Analyte	Matrix	Stability conditions	Nominal concentration (ng/mL)	Mean concentration (ng/mL)	Accuracy (% Bias)	Precision (% CV)	
Abemaciclib	Small intestine homogenate	RT, 1 d	50	46.4	-7.1	1.3	
		RT, 3 h	50	56.4	12.3	1.5	
		Ice/water bath, 3 h	50	51.6	3.1	3.5	
		3 F/T (-20 °C, RT)	50	49.0	-2.0	4.2	
		3 F/T (-70 °C, ice/water bath)	50	50.7	1.5	5.3	
		LT -20 °C, 1 m	50	48.2	-3.7	2.2	
	LT -70 °C, 1 m	50	48.3	-3.4	4.0		
	Final extract	4-8 °C, 2 d	50	52.4	4.7	6.1	
Palbociclib	Liver homogenate	RT, 1 d	50	44.9	-10.2	4.8	
		Ice/water bath, 3 h	50	49.8	-0.5	5.2	
		3 F/T (-20 °C, RT)	50	43.6	-12.7	2.7	
		3 F/T (-70 °C, ice/water bath)	50	50.6	1.2	1.5	
		LT -20 °C, 1 m	50	34.3	-31.5	6.7	
		LT -70 °C, 1 m	50	47.1	-1.9	5.8	
		Final extract	4-8 °C, 2 d	50	41.3	-17.4	4.2
	Spleen homogenate	RT, 1 d	50	30.7	-38.5	6.0	
			50	47.2	-5.7	8.4	
		Ice/water bath, 3 h	50	46.0	-8.1	5.8	
			50	42.1	-15.8	3.8	
		3 F/T (-20 °C, RT)	50	47.9	-4.2	1.3	
			50	42.6	-14.9	3.8	
		3 F/T (-70 °C, ice/water bath)	50	46.9	-6.1	4.1	
			50	46.9	-6.1	4.1	
Final extract	4-8 °C, 3 d	5	4.9	-1.3	5.7		
		150	157	4.7	6.3		
Kidney homogenate	RT, 1 d	50	2.91	-94.2	11.8		
		50	45.3	-9.4	13.6		
	Ice/water bath, 3 h	50	43.4	-13.3	6.6		
		50	19.3	-61.5	19.5		
	3 F/T (-20 °C, RT)	50	52.0	4.1	0.7		
		50	52.0	4.1	0.7		
	3 F/T (-70 °C, ice/water bath)	50	33.2	-33.6	7.9		
50		47.9	-4.1	3.3			
	Final extract	4-8 °C, 2 d	50	46.5	-7.1	2.6	



Table 6. Continued

Analyte	Matrix	Stability conditions	Nominal concentration (ng/mL)	Mean concentration (ng/mL)	Accuracy (% Bias)	Precision (% CV)	
Palbociclib	Brain homogenate	RT, 1 d	5	4.7	-6.5	8.4	
			150	149.3	-0.4	7.2	
		Final extract	Ice/water bath, 3 h	50	49.4	-1.2	3.1
			3 F/T (-20 °C, RT)	50	47.3	-5.3	5.8
			3 F/T (-70 °C, ice/water bath)	50	51.0	2.1	1.9
			LT -20 °C, 1 m	50	46.7	-6.6	2.1
	LT -70 °C, 1 m	50	52.1	4.2	1.4		
	Small intestine	4-8 °C, 3 d	5	5.4	7.5	0.9	
			150	168.3	12.2	2.4	
		Final extract	RT, 1 d	50	43.8	12.5	1.5
			RT, 3 d	50	48.5	-3.0	7.0
			Ice/water bath, 3 h	50	49.0	-2.0	9.6
			3 F/T (-20 °C, RT)	50	44.6	-10.7	3.5
			3 F/T (-70 °C, ice/water bath)	50	49.9	-0.3	3.6
LT -20 °C, 1 m			50	42.2	-15.5	7.2	
LT -70 °C, 1 m	50	48.8	-2.3	3.7			
4-8 °C, 2 d	50	45.9	-8.2	5.9			
Ribociclib	Liver homogenate	RT, 1 d	50	41.9	-16.2	7.3	
			50	45.4	-9.3	4.7	
		Final extract	3 F/T (-20 °C, RT)	50	47.7	-4.7	2.7
			3 F/T (-70 °C, ice/water bath)	50	50.0	0.1	1.7
			LT -20 °C, 1 m	50	32.4	-35.1	13.9
			LT -70 °C, 1 m	50	49.1	-1.9	7.2
	4-8 °C, 2 d	50	42.6	-14.9	6.6		
	Spleen homogenate	RT, 1 d	50	21.8	-56.4	6.4	
			50	44.3	-11.5	5.8	
		Final extract	RT, 3 h	50	46.2	-7.5	2.3
			Ice/water bath, 3 h	50	46.2	-7.5	2.3
			3 F/T (-20 °C, RT)	50	42.9	-14.1	1.2
			3 F/T (-70 °C, ice/water bath)	50	49.9	-0.1	1.4
			LT -20 °C, 1 m	50	40.5	-19.1	4.3
LT -70 °C, 1 m			50	45.0	-9.9	1.2	
4-8 °C, 3 d	5	5.16	3.2	4.1			
	150	148.7	-0.9	0.8			

see next page for the continuation of this table.

**Table 6.** Continued

Analyte	Matrix	Stability conditions	Nominal concentration (ng/mL)	Mean concentration (ng/mL)	Accuracy (% Bias)	Precision (% CV)
Ribociclib	Kidney homogenate	RT, 1 d	50	0.91	-98.2	24.4
		RT, 3 h	50	43.4	-13.2	1.2
		Ice/water bath, 3 h	50	42.7	-14.6	1.5
		3 F/T (-20 °C, RT)	50	15.7	-68.6	30.1
		3 F/T (-70 °C, ice/water bath)	50	49.1	-1.7	3.4
		LT -20 °C, 1 m	50	31.5	-37.1	4.1
		LT -70 °C, 1 m	50	50.2	0.5	3.6
	Final extract	4-8 °C, 2 d	50	43.2	-13.5	6.7
	Brain homogenate	RT, 1 d	5	4.6	-7.9	1.8
			150	129.7	-13.6	5.1
		Ice/water bath, 3 h	50	49.4	-1.3	4.3
		3 F/T (-20 °C, RT)	50	48.8	-2.3	5.8
		3 F/T (-70 °C, ice/water bath)	50	50.0	0.1	2.1
		LT -20 °C, 1 m	50	49.1	-1.7	2.0
		LT -70 °C, 1 m	50	52.3	4.6	4.7
	Final extract	4-8 °C, 3 d	5	5.1	2.7	5.1
			150	154.7	3.1	1.9
	Small intestine homogenate	RT, 1 day	50	41.9	-16.3	3.2
			50	50.6	1.3	3.5
		Ice/water bath, 3 h	50	48.4	-3.2	5.3
		3 F/T (-20 °C, RT)	50	45.6	-8.9	0.3
		3 F/T (-70 °C, ice/water bath)	50	50.0	0.1	3.6
		LT -20 °C, 1 m	50	38.9	-22.2	10.5
LT -70 °C, 1 m		50	48.9	-2.1	2.6	
Final extract	4-8 °C, 2 d	50	44.2	-11.5	7.3	

RT=room temperature, F/T=freeze-thaw cycles, LT=long term, d=days, m=months.

### Preclinical application of the method

This method was successfully used for the analysis of samples from preclinical studies of the CDK4/6 inhibitors. Figure 3 depicts a representative chromatogram from a preclinical study in mice for each drug. As shown in panel d, the chromatogram from a mouse plasma sample contains an extra peak eluting prior to ribociclib. This unknown peak was only present in mouse plasma samples and not in spiked samples or tissue homogenates, which indicates it is a potential ribociclib metabolite. In order to obtain the HR-MS spectra from each peak, the gradient was modified to increase the resolution between ribociclib and the potential metabolite (Figure 3, additional figure in panel d). The analysis generated a mass spectrum of both peaks, and the accurate mass of ribociclib was 435.26489 Da (mass difference of 5.58 ppm from the theoretical accurate monoisotopic mass) and for the compound eluting just before ribociclib a mass of 435.22830 Da was found (Supplementary Material Figure S1). The MS spectrum of the unknown peak was analyzed with the software Compound Discoverer 2.1.0 401 (Thermo Fisher Scientific) and the proposed molecular formula is  $C_{22}H_{26}N_8O_2$ . When the molecular formula of this potential metabolite is compared with the parent drug ( $C_{23}H_{30}N_8O$ ), N-desmethylation, oxidation and reduction of the ribociclib molecule are suggested as metabolic conversions. To identify the metabolite further research is needed. A semi quantification was performed using ribociclib calibration standards and the metabolite concentration was less than 10% of ribociclib concentration in each sample. For this reason, it was not considered as a major metabolite.

As an example of the preclinical pharmacokinetics and tissue distribution study, the plasma concentration-time plasma curve of ribociclib is shown in Figure 4a. The calculated pharmacokinetic parameters of ribociclib were the  $AUC_{0-24h}$  of  $6885 \pm 1215$   $ngmL^{-1}h$ , the half-life is  $3.1 \pm 0.2$  h, the  $T_{max}$  range is from 0.5 - 1 h, in which the mean  $C_{max}$  is  $1036 \pm 352$   $ng/mL$ . Ribociclib was quantified in tissue homogenates and their concentration in each organ was calculated considering the weight of each organ. Ribociclib was highly distributed in spleen and kidney, followed by liver and small intestine, in brain the concentration of ribociclib was much lower compared with the other tissues (Fig 5b). In this analysis, 95% of the samples were within the validated range showing the applicability of the method to preclinical studies.

### Conclusions

The first validated multi-assay of the first three approved CDK4/6 inhibitors (abemaciclib, palbociclib and ribociclib) in plasma and tissue homogenates has been described. Human plasma can be used as a surrogate matrix for the quantification of these compounds in mouse plasma and tissue homogenates. As palbociclib and ribociclib showed instability in some tissue homogenates, it is recommended to store these samples at  $-70$  °C and process them within 3 h when these samples are kept at room

temperature. This method can be used for both preclinical and clinical studies. In this article, this method was successfully applied to a preclinical study of ribociclib in mice. A ribociclib metabolite was detected in mouse plasma samples with the same  $m/z$  transition as the parent drug, which was not previously described.

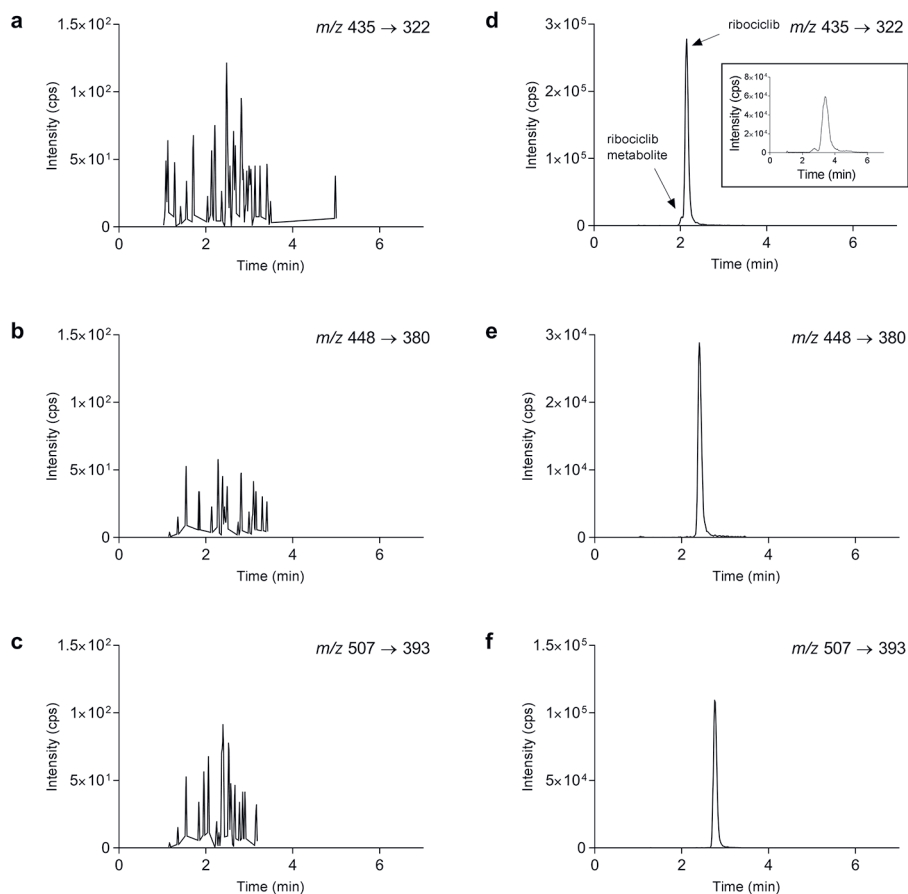


**Figure 3.** Chromatograms of blank mouse plasma at the mass transitions of ribociclib (a), palbociclib (b) and abemaciclib (c), and representative chromatograms of samples from preclinical studies of ribociclib (d, 20 mg/kg orally administered,  $t = 8$  h, 625 ng/mL), palbociclib (e, 10 mg/kg orally administered,  $t = 2$  h, 311 ng/mL) and abemaciclib (f, 10 mg/kg orally administered,  $t = 24$  h, 74.3 ng/mL). The additional figure included in d shows the same acquired with different gradient to increase the resolution between the two peaks.

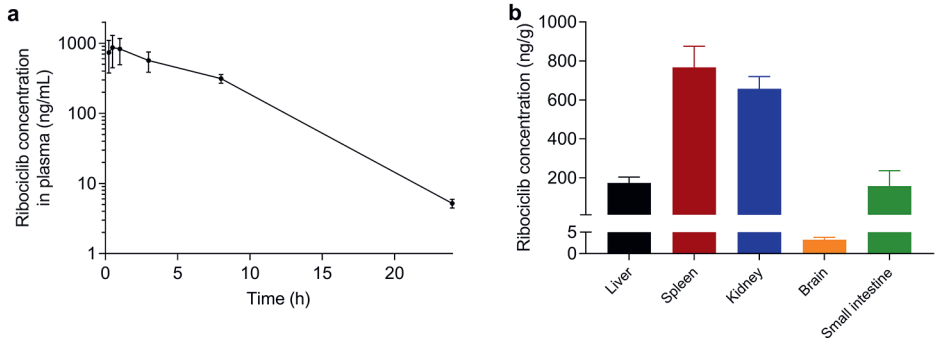


**Figure 4.** Plasma concentration-time curve (a) and tissue concentration (b) of ribociclib over 24 h in female FVB mice after oral administration at 20 mg/kg. Data are presented as mean  $\pm$  SD (n = 6).

## References

- [1] S. Santhosh, K. Prasanna, V. Ramprasad, A. Chaudhurri, Evolution of targeted therapies in cancer: Opportunities and challenges in the clinic, *Futur. Oncol.* 11 (2015) 279–293. doi:10.2217/fon.14.198.
- [2] Malínková, J. Vylíčil, V. Kryštof, Cyclin-dependent kinase inhibitors for cancer therapy : a patent review ( 2009 – 2014 ), *Expert Opin. Ther. Pat.* 25 (2015) 953–970. doi:10.1517/13543776.2015.1045414.
- [3] B. O'Leary, R.S. Finn, N.C. Turner, Treating cancer with selective CDK4/6 inhibitors, *Nat. Rev. Clin. Oncol.* 13 (2016) 417–430. doi:10.1038/nrclinonc.2016.26.
- [4] P. Chen, N. V Lee, W. Hu, M. Xu, R.A. Ferre, H. Lam, S. Bergqvist, J. Solowiej, W. Diehl, Y.-A. He, X. Yu, A. Nagata, T. VanArsdale, B.W. Murray, Spectrum and Degree of CDK Drug Interactions Predicts Clinical Performance, *Mol. Cancer Ther.* 15 (2016) 2273–2281. doi:10.1158/1535-7163.MCT-16-0300.
- [5] D. Kwapisz, Cyclin-dependent kinase 4/6 inhibitors in breast cancer: palbociclib, ribociclib, and abemaciclib, *Breast Cancer Res. Treat.* 166 (2017) 41–54. doi:10.1007/s10549-017-4385-3.
- [6] M.E. Klein, M. Kovatcheva, L.E. Davis, W.D. Tap, A. Koff, CDK4/6 Inhibitors: The Mechanism of Action May Not Be as Simple as Once Thought, *Cancer Cell.* 34 (2018) 9–20. doi:10.1016/j.ccell.2018.03.023.
- [7] N. Vidula, H.S. Rugo, Treatment of Breast Cancer : A Review of Preclinical and Clinical Data, *Clin. Breast Cancer.* 16 (2016) 8–17. doi:10.1016/j.clbc.2015.07.005.
- [8] L. Nguyen, W.Z. Zhong, C.L. Painter, C. Zhang, S. V Rahavendran, Z. Shen, Quantitative analysis of PD 0332991 in xenograft mouse tumor tissue by a 96-well supported liquid extraction format and liquid chromatography/mass spectrometry, *J. Pharm. Biomed. Anal.* 53 (2010) 228–234. doi:10.1016/j.jpba.2010.02.031.
- [9] D. Smith, M. Tella, S. V Rahavendran, Z. Shen, Quantitative analysis of PD 0332991 in mouse plasma using automated micro-sample processing and microbore liquid chromatography coupled with tandem mass spectrometry, *J. Chromatogr. B Anal. Technol. Biomed. Life Sci.* 879 (2011) 2860–2865. doi:10.1016/j.jchromb.2011.08.009.
- [10] D. Paul, S. Surendran, P. Chandrakala, N. Satheeshkumar, An assessment of the impact of green tea extract on palbociclib pharmacokinetics using a validated UHPLC–QTOF–MS method, *Biomed. Chromatogr.* (2019) 1–9. doi:10.1002/bmc.4469.
- [11] D. Paul, P. Chandrakala, S. Surendran, P. Bitla, N. Satheeshkumar, Pharmacokinetic interaction study of novel combination of palbociclib and sorafenib for hepatocellular carcinoma in SD rats, *J. Chromatogr. B Anal. Technol. Biomed. Life Sci.* 1108 (2019) 25–31. doi:10.1016/j.jchromb.2019.01.003.
- [12] A. Kala, Y.T. Patel, A. Davis, C.F. Stewart, Development and validation of LC–MS/MS methods for the measurement of ribociclib, a CDK4/6 inhibitor, in mouse plasma and Ringer's solution and its application to a cerebral microdialysis study, *J. Chromatogr. B Anal. Technol. Biomed. Life Sci.* 1057 (2017) 110–117. doi:10.1016/j.jchromb.2017.05.002.
- [13] X. Bao, J. Wu, N. Sanai, J. Li, Journal of Pharmaceutical and Biomedical Analysis Determination of total and unbound ribociclib in human plasma and brain tumor tissues using liquid chromatography coupled with tandem mass spectrometry, *J. Pharm. Biomed. Anal.* 166 (2019) 197–204. doi:10.1016/j.jpba.2019.01.017.
- [14] T.J. Raub, G.N. Wishart, P. Kulanthaivel, B.A. Staton, R.T. Ajamie, G.A. Sawada, L.M. Gelbert, H.E. Shannon, C. Sanchez-Martinez, A. De Dios, Brain exposure of two selective dual CDK4 and CDK6 inhibitors and the antitumor activity of CDK4 and CDK6 inhibition in combination with temozolomide in an intracranial glioblastoma xenograft, *Drug Metab. Dispos.* 43 (2015) 1360–1371. doi:10.1124/dmd.114.062745.
- [15] US Food and Drug Administration, Guidance for Industry Bioanalytical Method Validation, (2018) 1–22. <https://www.fda.gov/files/drugs/published/Bioanalytical-Method-Validation-Guidance-for-Industry.pdf>.
- [16] European Medicines Agency, Guideline on bioanalytical method validation, (2012) 1–23. [https://www.ema.europa.eu/documents/scientific-guideline/guideline-bioanalytical-method-validation\\_en.pdf](https://www.ema.europa.eu/documents/scientific-guideline/guideline-bioanalytical-method-validation_en.pdf).
- [17] Y.-J. Xue, H. Gao, Q.C. Ji, Z. Lam, X. Fang, Z. Lin, M. Hoffman, D. Schulz-Jander, N. Weng, Bioanalysis of drug in tissue: current status and challenges, *Bioanalysis.* 4 (2012) 2637–2653. doi:10.4155/bio.12.252.

## Supplementary material

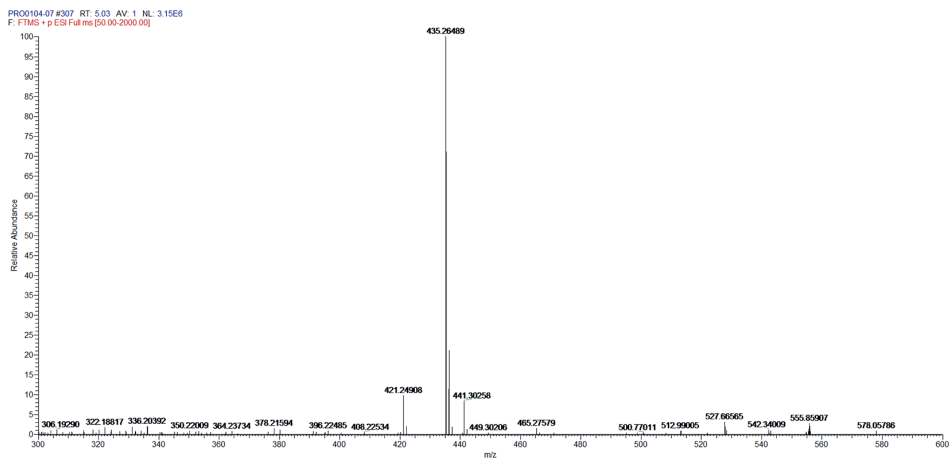
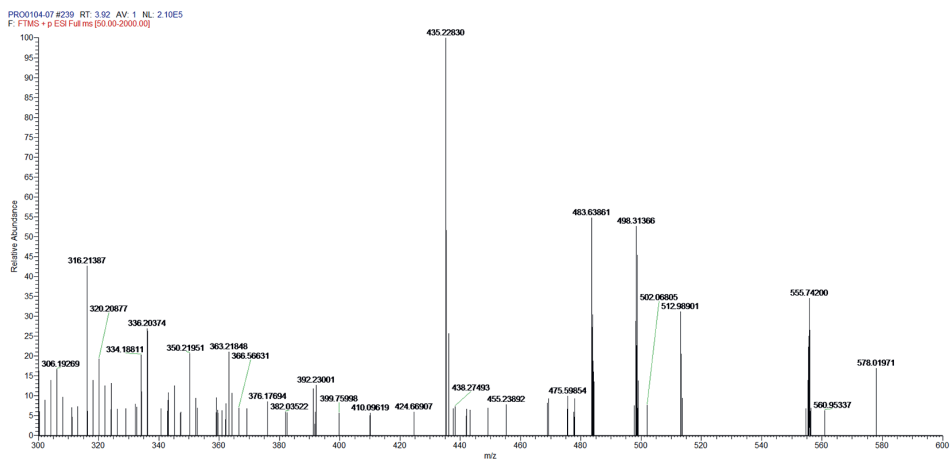
**Supplementary Table S1.** Absolute and normalized matrix factor of abemaciclib, palbociclib and ribociclib at high and low concentrations

	Concentration level	Analyte	IS	Normalized
Abemaciclib	Low	1.022 ± 0.026	0.976 ± 0.059	1.052 ± 0.077
	High	1.107 ± 0.027	1.025 ± 0.028	1.081 ± 0.030
Palbociclib	Low	1.071 ± 0.053	0.903 ± 0.042	1.188 ± 0.071
	High	1.034 ± 0.027	0.940 ± 0.020	1.100 ± 0.024
Ribociclib	Low	1.195 ± 0.082	0.993 ± 0.020	1.203 ± 0.072
	High	1.078 ± 0.017	0.972 ± 0.034	1.110 ± 0.031

Data are presented as mean ± SD (n = 6)

**Supplementary Table S2.** Absolute and normalized recovery (%) of abemaciclib, palbociclib and ribociclib at high and low concentrations

	Concentration level	Analyte	IS	Normalized	Mean recovery (%CV)
Abemaciclib	Low	63.2	77.0	81.9	82.8 (1.6)
	High	60.0	71.7	83.7	
Palbociclib	Low	75.1	97.6	76.8	79.9 (5.6)
	High	81.9	98.9	83.0	
Ribociclib	Low	76.5	94.4	80.9	83.4 (4.1)
	High	77.7	90.3	85.8	

**A****B**

**Supplementary Figure S1.** Mass spectrum of the parent ion of ribociclib (a) and potential ribociclib metabolite (b)







# 2

## Simultaneous quantification of abemaciclib and its active metabolites in human and mouse plasma by UHPLC-MS/MS

Journal of Pharmaceutical and Biomedical Analysis, 2021, 203: 114225

Alejandra Martínez-Chávez  
Matthijs M. Tibben  
Karen A. M. de Jong  
Hilde Rosing  
Alfred H. Schinkel  
Jos H. Beijnen

## Abstract

Abemaciclib is the third cyclin-dependent kinase 4 and 6 inhibitor approved for the treatment of advanced or metastatic breast cancer. In humans, abemaciclib is extensively metabolized by CYP3A4 with the formation of three active metabolites: N-desethylabemaciclib (M2), hydroxyabemaciclib (M20) and hydroxy-N-desethylabemaciclib (M18). These metabolites showed similar potency compared to the parent drug and were significantly abundant in plasma circulation. Thus, M2, M20, and M18 may contribute to the clinical activity of abemaciclib. For this reason, an UHPLC-MS/MS method for the simultaneous quantification of abemaciclib and its active metabolites in human and mouse plasma was developed and validated to support further clinical or preclinical investigations on this drug. Samples were processed by protein precipitation with acetonitrile, followed by supernatant dilution and filtration. Chromatographic separation was performed on a Kinetex C<sub>18</sub> column (150 x 2.1 mm ID, 2.6 µm) using gradient elution with 10 mM ammonium bicarbonate in water (eluent A) and in methanol-water (9:1, v/v, eluent B). This method was selective, linear, accurate and precise within the range of 1-600 ng/mL for abemaciclib, 0.5-300 ng/mL for M2 and M20, and 0.2-120 ng/mL for M18. Furthermore, stability of the analytes in human and mouse plasma samples in several conditions was demonstrated. Finally, this assay was successfully used in a preclinical pharmacokinetic study, where abemaciclib and its active metabolites were identified and quantified. Inter-species differences between human and mouse samples were encountered, especially in the formation of M20, where isomers of this compound were detected in mouse plasma, but not in human plasma. This was confirmed by high resolution-mass spectrometry (HR-MS) measurements.

## Introduction

Abemaciclib (*N*-(5-((4-ethylpiperazin-1-yl)methyl)pyridin-2-yl)-5-fluoro-4-(4-fluoro-1-isopropyl-2-methyl-1*H*-benzo[*d*]imidazol-6-yl)pyrimidin-2-amine) is a reversible and potent ATP-competitive inhibitor of the cyclin-dependent kinases 4 and 6 (CDK4/6) [1]. It was the third compound in this class approved by the US Food and Drug Administration (FDA) and European Medicines Agency (EMA) (2017-2018) for treatment of advanced or metastatic breast cancer in both combination therapy or monotherapy. Abemaciclib is the only CDK4/6 inhibitor that can also be used as a single agent. CDK4/6 inhibitors lead to cell cycle arrest from G1 to S phase, by preventing, first, the phosphorylation of the retinoblastoma protein, and consequently, the activation of the E2F transcription factor [2]. Apart from in breast cancer, molecular aberrations of this pathway have been encountered in other types of cancer, which could expand the use of CDK4/6 inhibitors. Abemaciclib is currently being investigated for other cancer treatments with more than 40 clinical trials ongoing [3].

In humans, abemaciclib is extensively metabolized by CYP3A4 with the formation of three active metabolites: N-desethylabemaciclib (M2), hydroxyabemaciclib (M20), and hydroxy-N-desethylabemaciclib (M18) (Figure 1). These metabolites have a similar potency (described in Figure 1) and protein binding compared to abemaciclib, namely between 93.4 and 97.8% for the metabolites, and 96.3% for abemaciclib. Additionally, the abundance of M2, M20 and M18 in plasma circulation is substantial, since their areas under the plasma concentration-time curve (AUCs) accounted respectively for 25%, 26%, and 13% of the total abemaciclib-derived radioactivity, *versus* 34% for abemaciclib [4,5]. Thus, M2, M20 and M18 may influence the clinical efficacy and safety of abemaciclib. FDA guidelines on safety testing of drug metabolites recommend that metabolites with an exposure greater than 10% of total related drug exposure should be further characterized [6]. Consequently, accurate quantification of M2, M20 and M18 is pivotal for an appropriate conduct of research involving abemaciclib. For this, reliable methods to quantitatively determine abemaciclib and its active metabolites are needed to support these investigations.

Some methods have been described for the bioanalysis of abemaciclib [7–9]. We first developed and validated a liquid chromatography-tandem mass spectrometry (LC-MS/MS) method for the bioanalysis of abemaciclib and the other two approved CDK4/6 inhibitors [7]. Subsequently, other methods involving abemaciclib quantification in plasma or serum have been published [8,9]. Nevertheless, the active metabolites have not been included in any of these bioanalytical methods hitherto. Other LC-MS/MS methods for abemaciclib metabolite identification and/or profiling have been also described, but these are limited to qualitative analyses [10,11].

Thus, the aim of this study is to provide a validated UHPLC-MS/MS method for the simultaneous quantification of abemaciclib, M2, M20, and M18 in human and mouse plasma, to support both clinical and preclinical studies, and also to optimize treatment of patients dosed with abemaciclib. Finally, the applicability of this method for both human and mouse samples is demonstrated. Additionally, since isomers of M20 were detected in mouse plasma, these compounds were further analyzed by high resolution-mass spectrometry.

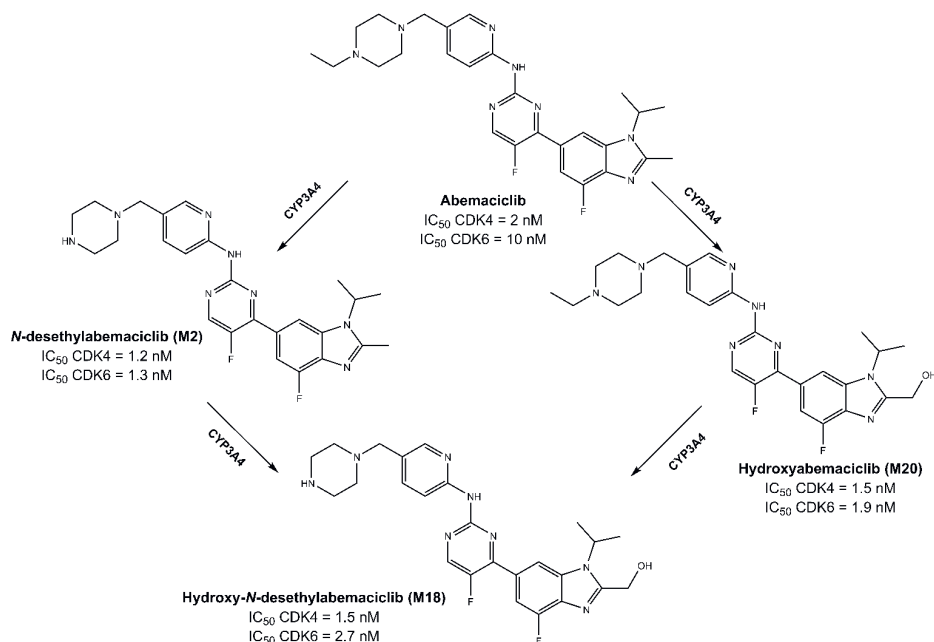


**Figure 1.** Abemaciclib metabolism by CYP3A4 into its active metabolites forming primarily N-desethylabemaciclib (M2) and hydroxyabemaciclib (M20). From these metabolites, hydroxy-N-desethylabemaciclib (M18) is formed. Half-maximal inhibitory concentrations ( $IC_{50}$ ) for CDK4 and CDK6 of each compound are included.

## Materials and methods

### Chemicals

Abemaciclib and  $^2H_8$ -abemaciclib were obtained from Alsachim (Illkirch-Graffenstaden, France), hydroxyabemaciclib (M20) and hydroxy-N-desethylabemaciclib hydrochloride (M18) from MedChemExpress LLC (Monmouth Junction, NJ, USA), and N-desethylabemaciclib from Clearsynth (Mumbai, India). Dimethylsulfoxide (DMSO, seccosolv) and ammonium bicarbonate (LC-MS grade) were supplied by Merck (Darmstadt, Germany). Methanol, water (both ULC-MS grade), and acetonitrile (Supra gradient grade) were purchased from Biosolve Ltd (Valkenswaard, The Netherlands).

K<sub>2</sub>EDTA control human plasma originated from BioIVT (Westbury, NY, USA) and lithium-heparinized mouse plasma was obtained from the animal laboratory of the Netherlands Cancer Institute (Amsterdam, The Netherlands).

### Stock and working solutions

Independent stock solutions of abemaciclib, M2, M20 and M18 were prepared in DMSO at 1 mg/mL in duplicate. Working solutions containing all the analytes were prepared by diluting the stock solutions in methanol-water (1:1, v/v). One set of stock solutions was used to prepare the working solutions for calibration standards and the other one for the working solutions of the quality control samples (QC).

### Calibration standards and quality control samples

Working solutions were 20-fold diluted with control plasma to prepare 8 calibration standards at concentrations of 1, 2, 6, 12, 60, 120, 480, and 600 ng/mL for abemaciclib, 0.5, 1, 3, 6, 30, 60, 240, and 300 ng/mL for M2 and M20, and 0.2, 0.4, 1.2, 2.4, 12, 24, 96, and 120 ng/mL for M18. In addition, blanks (no analyte spiked, but processed with internal standard) and double blanks (no analyte spiked and no internal standard) were prepared.

QC samples containing all analytes were prepared by diluting the working solutions 20-fold in control plasma at the following concentration levels: the lower limit of quantification (LLOQ), low (QC L), mid (QC M) and high (QC H). The final concentrations of abemaciclib, M2, M20, and M18 were respectively 1, 0.5, 0.5 and 0.2 ng/mL for the LLOQ, 3, 1.5, 1.5, and 0.6 ng/mL for the QC L, 45, 22.5, 22.5, and 9 ng/mL for the QC M, and 450, 225, 225, and 90 ng/mL for the QC H.

### Internal standard

For stock solution, <sup>2</sup>H<sub>8</sub>-abemaciclib was dissolved in DMSO at 1 mg/mL. This solution was further diluted with methanol to reach a concentration of 250 ng/mL, and was used as IS-working solution for the sample pre-treatment.

### Sample pre-treatment

An aliquot of 50 µL of sample was used for the pre-treatment, where 20 µL of IS-working solution was added, followed by 150 µL of acetonitrile. Samples were vortex-mixed for 10 s and centrifuged at 32,100g and 4 °C for 10 min. A volume of 80 µL of supernatant was added to a centrifuge tube filter (nylon filter, 0.2 µm pore size, 2 mL tube, Merck, Darmstadt, Germany) containing 120 µL of 10 mM ammonium bicarbonate in methanol-water (1:1, v/v). After vortex-mixing for 10 s, samples were filtered by centrifuging these tubes for 5 min at the conditions previously mentioned. Final extract was transferred to a glass vial for LC-MS/MS analysis, where 5 µL was injected into the UHPLC-MS/MS system.

### **Analytical instrumentation and conditions of the quantitative method**

An ultra-high performance liquid chromatograph (UHPLC) Nexera X2 (Shimadzu, Kyoto, Japan) was used. It was equipped with two binary pumps (LC-30AD model), an autosampler (SIL-30AC<sub>MP</sub>) and a column oven (CTO-20AC). Chromatographic separation was achieved using a Kinetex C<sub>18</sub> column (150 x 2.1 mm ID, 2.6 µm particle size, Phenomenex, Torrance, CA) protected by a guard column (Phenomenex). A gradient elution of 10 mM ammonium bicarbonate in water (A) and water-methanol (1:9 v/v, B) was used at a flow rate of 0.4 mL/min. At the initial conditions the percentage of B was 60%, and it was linearly increased to 100% from 0 to 4 min, and this was maintained for 0.5 min. Then, B decreased to 60% in 0.1 min and maintained for 0.4 min. From 5 to 5.5 min, B increased again to 100% and this proportion was kept for 0.5 min. Finally, in 0.1 min, B decreased to the initial conditions (60%) and this was maintained until 7.0 min. The increase of 100% B from 5.5 to 6.0 min was used to decrease the abemaciclib memory-effects, as we previously described [7]. The autosampler and column oven temperatures were kept at 20 and 40°C, respectively.

For detection, a Triple Quad 6500+ mass spectrometer (Sciex, Foster City, CA) with a turbo ion spray was used in positive ion mode. The flow from the UHPLC was directed from 3 to 6 min to the detector by a divert valve, and the remainder was directed to the waste. Chromatograms were acquired via multiple reaction monitoring (MRM) using the optimized general and analyte-specific settings described in Table 1. The Analyst software version 1.6.3 (Sciex) was used for data acquisition and processing.

### **Method validation**

The bioanalytical method for the quantification of abemaciclib and its active metabolites was fully validated in human plasma following to the US Food and Drug Administration (FDA) and European Medicines Agency (EMA) guidelines on bioanalytical method validation [12,13]. For mouse plasma, a partial validation was performed, in which the accuracy, precision, selectivity, dilution integrity, and sample stability were evaluated. The acceptance criteria for abemaciclib were based on these guidelines, however, for the metabolites, a deviation of nominal concentration of  $\pm 20\%$  and a relative standard deviation (RSD)  $\leq 20\%$  were accepted, because no stable isotopically labeled internal standards were available for the quantification.

#### *Calibration curve*

For each analyte, this parameter was evaluated by processing and analyzing calibration standards in duplicate in at least 3 separate runs. The calibration curves of all analytes were fitted by linear regression of the response (area ratio between the analyte and internal standard) versus the analyte concentration, with a weighting factor of  $1/x^2$ , where  $x$  is the analyte concentration. The calculated concentration of at least 75% of non-zero calibration standards should be within  $\pm 15\%$  of the nominal concentration (or  $\pm 20\%$  for the LLOQ) and at least 50% of the calibration standards at each concentration level should be within these criteria.



**Table 1.** MS/MS settings for analyte-specific and general parameters for the quantification of abemaciclib, M2, M20 and M18

Analyte-specific parameters		Settings			
	Abemaciclib	<sup>2</sup> H <sub>8</sub> -abemaciclib (IS)	M2	M20	M18
Mass transition ( <i>m/z</i> )	507 → 393	515 → 393	479 → 393	523 → 409	495 → 409
Declustering Potential (V)	86	86	111	101	111
Collision energy (V)	29	29	33	31	31
Collision Cell Exit Potential (V)	32	32	42	24	26
General parameters	Settings	General parameters	Settings		
Curtain gas (CUR)	30 au	Ion spray voltage (IS)	5500 V		
Gas 1 (NEB)	30 au	Temperature (TEM)	600 °C		
Gas 2 (Turbo)	60 au	Entrance potential	10 V		
Collision gas (CAD)	9 au	Dwell time	100 msec		

### Accuracy and precision

For human plasma, intra-assay accuracy and precision were determined using 5 replicates of QC samples at 4 concentration levels (including LLOQ, QC L, QC M and QC H) in 3 analytical runs, while for mouse plasma this was investigated in a single analytical run. Accuracy was expressed as the % bias between measured and nominal concentrations, and precision as the relative standard deviation (%RSD). For human plasma, also the inter-assay accuracy was determined by calculating the bias between the overall mean measured concentration, as well as the inter-assay precision by estimating the between-run variability using one-way ANOVA. A bias of  $\pm 15\%$  and a variation  $\leq 15\%$  were accepted for abemaciclib, except at the LLOQ, where  $\pm 20\%$  and  $\leq 20\%$  were respectively accepted. For all metabolites the last acceptance criteria was used at all concentration levels.

### Selectivity

Selectivity was investigated in six different batches of control human and mouse plasma, where double blanks and QC samples at the LLOQ were prepared from each batch and analyzed. The peak area of the interfering peaks should not be greater than 20% of the analyte peak area and 5% of the internal standard to establish absence of interfering peaks. Also, the bias of the QC samples should be within  $\pm 20\%$  in at least 4 out of 6 samples.

### *Lower limit of quantification*

This was determined for each analyte by calculating the signal-to-noise ratio using the responses of the LLOQ and the double blank in at least 3 analytical runs. For the acceptance criteria, the analyte peak height should be at least 5 times higher than the noise obtained with the double blank. Also, for an acceptable precision and accuracy at this concentration level, the RSD should be  $\leq 20\%$  and the bias within  $\pm 20\%$ , respectively.

### *Carry-over*

The impact of the carry-over on the accuracy was assessed in every analytical run by the injection of double blank samples after the upper limit of quantification (ULOQ), where the response obtained at the analyte retention time was compared to the analyte response in the LLOQ sample. Carry-over should not exceed 20% of the LLOQ response.

### *Matrix effect and recovery*

Matrix effect was investigated at low and high concentration levels in six different batches of human and mouse plasma. To evaluate this parameter, the matrix factor was calculated by comparing the analyte or IS peak area of the matrix present sample (MPS) with the respective ones of the matrix absent sample (MAS). Consequently, the IS-normalized matrix factor for each analyte was determined by dividing the matrix factor of the analyte by the matrix factor of the internal standard. For the preparation of MPS's, each plasma batch was processed until final extract and spiked with the corresponding QC working solution. MAS's were prepared by diluting the QC working solution with 10 mM ammonium bicarbonate in water-MeOH (1:1, v/v), reaching the same concentration as the MPS. The RSD of the IS-normalized matrix factor should be  $\leq 15\%$ . In addition, recovery was calculated at the same concentration levels by comparing the response of normally processed low and high QC samples with the equivalent MPS's.

### *Dilution integrity*

The integrity of sample dilution in both matrices was assessed with five replicates of samples spiked 5 times above the ULOQ, that were diluted 10-fold with control human plasma, prior to sample pre-treatment. For accuracy and precision, a bias of  $\pm 15\%$  and a variation  $\leq 15\%$  were, respectively, accepted for abemaciclib, and  $\pm 20\%$  and  $\leq 20\%$  for the metabolites.

### *Stability*

Analytes stability in both matrices, human and mouse plasma, was evaluated in triplicate at two concentration levels (low and high) at room temperature (RT) for short-term stability, at  $-20\text{ }^{\circ}\text{C}$  for long-term stability, and after 3 freeze and thaw (F/T) cycles. Final extract stability from both matrices was also evaluated at  $2-8\text{ }^{\circ}\text{C}$ . Stability was

considered acceptable when measured concentrations were within  $\pm 15\%$  of nominal concentrations for abemaciclib or  $\pm 20\%$  for the metabolites.

#### *Applicability of the method*

The applicability of this method was demonstrated by the measurement of mouse samples from a pharmacokinetic study. For this, female mice (FVB background) were single dosed with abemaciclib at 10 mg/kg after at least 2 h of fasting. Approximately 50  $\mu\text{L}$  of blood was collected from the tip of the tail at 0.125, 0.25, 0.5, 1, 2 in heparin-coated microvette tubes (Starstedt, Nümbrecht, Germany), and at the terminal time point (4 h) blood was collected by cardiac puncture under isoflurane anesthesia. Thereafter, mice were sacrificed by cervical dislocation. Animal housing and studies were conducted according to institutional guidelines complying with Dutch and European Union legislation (approval number from The Dutch Central Animal Testing Committee: AVD301002016595). After centrifugation for 6 min, at 9000g and 4 °C, plasma was obtained from blood. Samples were stored at -20 °C until analysis. Prior the pre-treatment and when necessary, 10  $\mu\text{L}$  of sample was diluted with 40  $\mu\text{L}$  of control human plasma to complete the volume needed for the sample pre-treatment. In addition, the applicability of this method in human plasma was assessed by measuring plasma samples from a patient treated with 50 mg abemaciclib daily in our hospital. Whole venous blood samples were collected at steady state conditions, and centrifuged for 5 min at 2000g. Plasma was separated and stored at -20 °C until analysis. Mouse and human samples were processed and analyzed according to sections 2.5 and 2.6.

#### *HR-MS measurements for the identification of M20 isomers in mouse samples*

To confirm the mass of M20 isomers, high resolution-mass spectrometry (HR-MS) measurements were performed in a Quadrupole-Time of flight mass spectrometer (TripleTOF 6600, Sciex) coupled to a Shimadzu UHPLC chromatograph (Kyoto, Japan) composed by the modules described in the “Analytical instrumentation and conditions of the quantitative method” section. The chromatographic conditions described in this section were also used, except for the column, where a Kinetex EVO C<sub>18</sub> (100 x 2.1 mm, 1.6  $\mu\text{m}$ ) was used (Phenomenex). For the MS general settings, the nebulizer (Gas 1), turbo (Gas 2) and curtain gases were set at 30 (a.u.), the temperature at 450 °C and the ion spray voltage at 5000 V for detection of both parent and product ions of M20 isomers. Parent ions of M20 were detected using a declustering potential of 80 V and a collision energy of 10 V, while for the product ions, these parameters were set at 86 and 29 V, respectively. A mouse liver sample collected during the pharmacokinetics study described in the “applicability of the method” section was used for the HR-MS measurements, since the response of the peaks was higher in this matrix. For this, the mouse liver was homogenized with 4% bovine serum albumin and 50  $\mu\text{L}$  of sample was processed according to the “sample pre-treatment” section. Then, this sample was injected into the system and the accurate  $m/z$  ratios of the parent and product ions of each peak were compared to the theoretical ones.

## Results and discussion

### Method development

Analyte-dependent settings of the mass spectrometer were optimized by direct infusion of each analyte. For each compound, the most abundant product ion was selected together with the parameter values in which the highest signal was produced (Table 1, Figure 2). By flow injection analysis, the general settings of the mass spectrometer were optimized to boost the response of M18, since higher sensitivity was needed to quantify this analyte in the study samples. Therefore, those values that enhanced the response of M18 were chosen. The calibration ranges for quantification were selected based on the reported abundance of each compound in human plasma [14], with abemaciclib the most abundant compound, followed by M2 and M20, and finally M18. As stable isotopically labeled abemaciclib metabolites were not commercially available,  $^2\text{H}_8$ -abemaciclib was used as internal standard for all analytes.

The chromatographic method and sample pre-treatment were based on a bioanalytical method we previously described [7]. This method was further optimized to perform the simultaneous quantification of abemaciclib and its active metabolites. As additional peaks were detected at the M20 and M18 mass transitions in mouse plasma samples, chromatographic separation of these isomers was required for an appropriate identification and quantification of M18 and M20. Therefore, analytical columns with different characteristics including particle sizes lower than 5  $\mu\text{m}$  were tested together with different gradient programs using 10 mM ammonium bicarbonate in water and in methanol-water as mobile phase. Peaks detected at the M20 and M18 mass transitions were completely separated from each other using the Kinetex EVO  $\text{C}_{18}$  (100 x 2.1 mm, 1.6  $\mu\text{m}$ ) (Figure 7), however peak shape was deteriorated soon after using the column. For this reason, the Kinetex  $\text{C}_{18}$  column (150 x 2.1 mm ID, 2.6  $\mu\text{m}$ ) was selected for the quantitative analysis. Although no base resolution was achieved among all the peaks with the 2.6  $\mu\text{m}$  particle size column, M18 and M20 peaks were sufficiently separated from their isomers, which permitted an appropriate quantification of these analytes in mouse plasma samples. Moreover, the robustness of this column was superior compared to the 1.6  $\mu\text{m}$  column. In addition, a final extract filtration was implemented in the sample pre-treatment to improve the sample cleaning and to prolong the column life.

### Method validation

Although  $^2\text{H}_8$ -abemaciclib was used as internal standard for all analytes, it was observed that the response variations of the mass spectrometer were occasionally not properly corrected for the metabolites. This led to variability in the method performance for the metabolites, and could not be solved due to the lack of a stable isotopically labeled M2, M20 and M18 to use as internal standard. Roughly, it was observed that the less difference in retention time between the metabolites and the IS, the better the

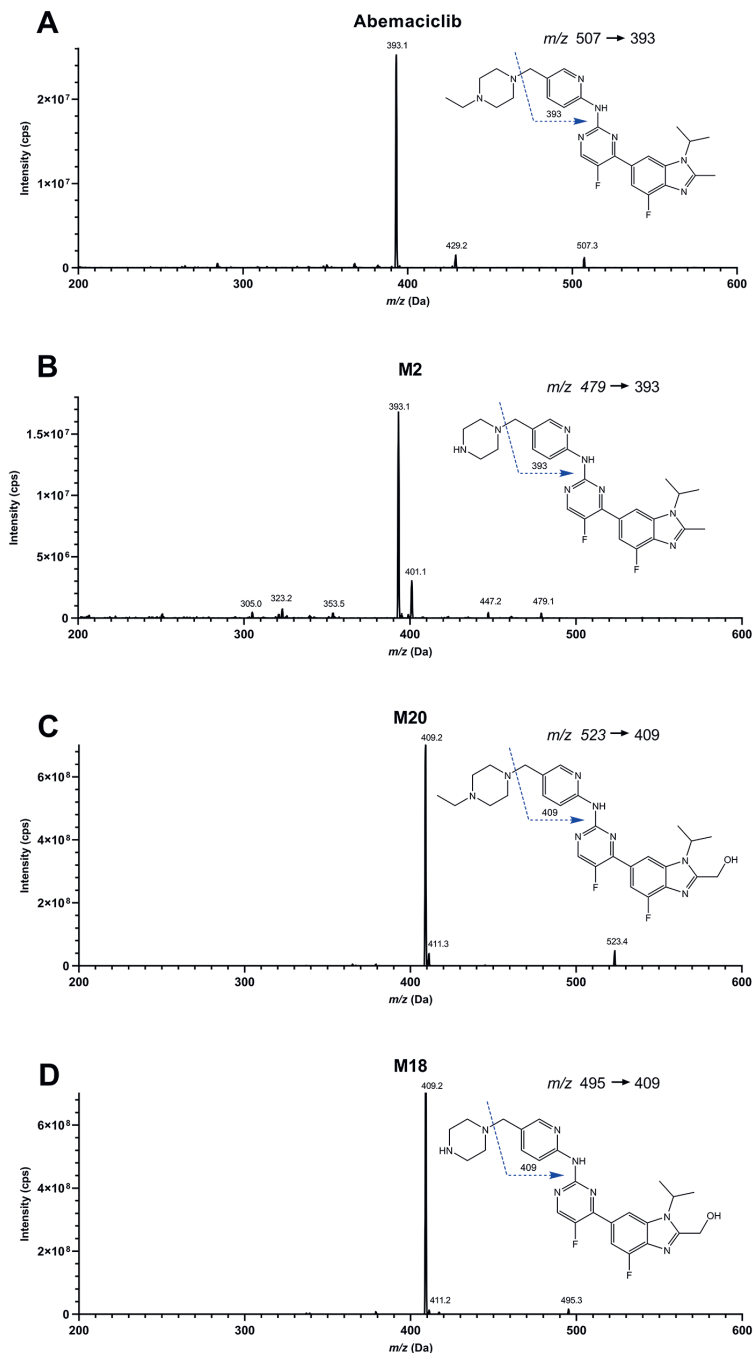


**Figure 2.** Product ion mass spectra and proposed MS fragmentation of abemaciclib (A), M2 (B), M20 (C) and M18 (D). The proposed MS fragment selected for detection and quantification is indicated with the blue dotted line.

correction by the IS. For this reason, a wider acceptance criteria for the accuracy and precision in the metabolites quantification was accepted. However, the method performance of the metabolites analysis is expected to improve when stable isotopically labeled metabolites become available to use as internal standards.

#### *Calibration curve*

The relationship between the analyte concentration and the response (determined by ratio between the analyte and IS area) was linear in the range of 1-600 ng/mL for abemaciclib, 0.5-300 ng/mL for M2 and M20, and 0.2-120 ng/mL for M18, using the regression model previously described. Mean correlation coefficients of 0.999, 0.998, 0.997 and 0.996 were obtained for abemaciclib, M2, M20 and M18, respectively. Representative chromatograms of each compound at the lowest and highest concentration levels are depicted in Figure 3. Furthermore, the back-calculated concentrations of the calibration standards of each analyte complied with the acceptance criteria, where at least 75% were within  $\pm 15\%$  (or  $\pm 20\%$  at the LLOQ) of the nominal concentrations and at least 50% of the calibration standards of each concentration level met these criteria.

#### *Accuracy and precision*

Intra-assay and inter-assay accuracy and precision results are presented in Table 2, where the % bias and RSD obtained were consistent with the acceptance criteria. Since control mouse plasma is generally more difficult to obtain, we tested the use of human plasma as a surrogate matrix for the quantification of mouse plasma samples. Thus, the good accuracy obtained for QC mouse samples quantified with calibration standards in human plasma, validates the use of this as a surrogate matrix.

#### *Selectivity*

Selectivity of the method was proved in six batches of human and mouse plasma, where no interfering peaks were detected at the retention time and mass transition of each compound, including the IS. Representative chromatograms of the control matrix and spiked samples at the LLOQ for all analytes and the IS are depicted in Figures 3 and 4 for human and mouse plasma, respectively. In the chromatograms obtained at M2 mass transition ( $m/z$  479  $\rightarrow$  393), prior M2 peak elution, two peaks were detected in both matrices (Figures 3 and 4, panels B1 and B2). These peaks are probably due to endogenous compounds in the matrices, since they were detected only in matrix processed samples and not in matrix absent samples. In addition, the accuracy of the LLOQ samples was evaluated, where the calculated concentrations were within  $\pm 20\%$  of nominal concentrations in all matrix sources for abemaciclib and in 5 matrix batches for the metabolites. Therefore, this method was selective for the quantification of abemaciclib and its active metabolites in the presence of endogenous interferences.

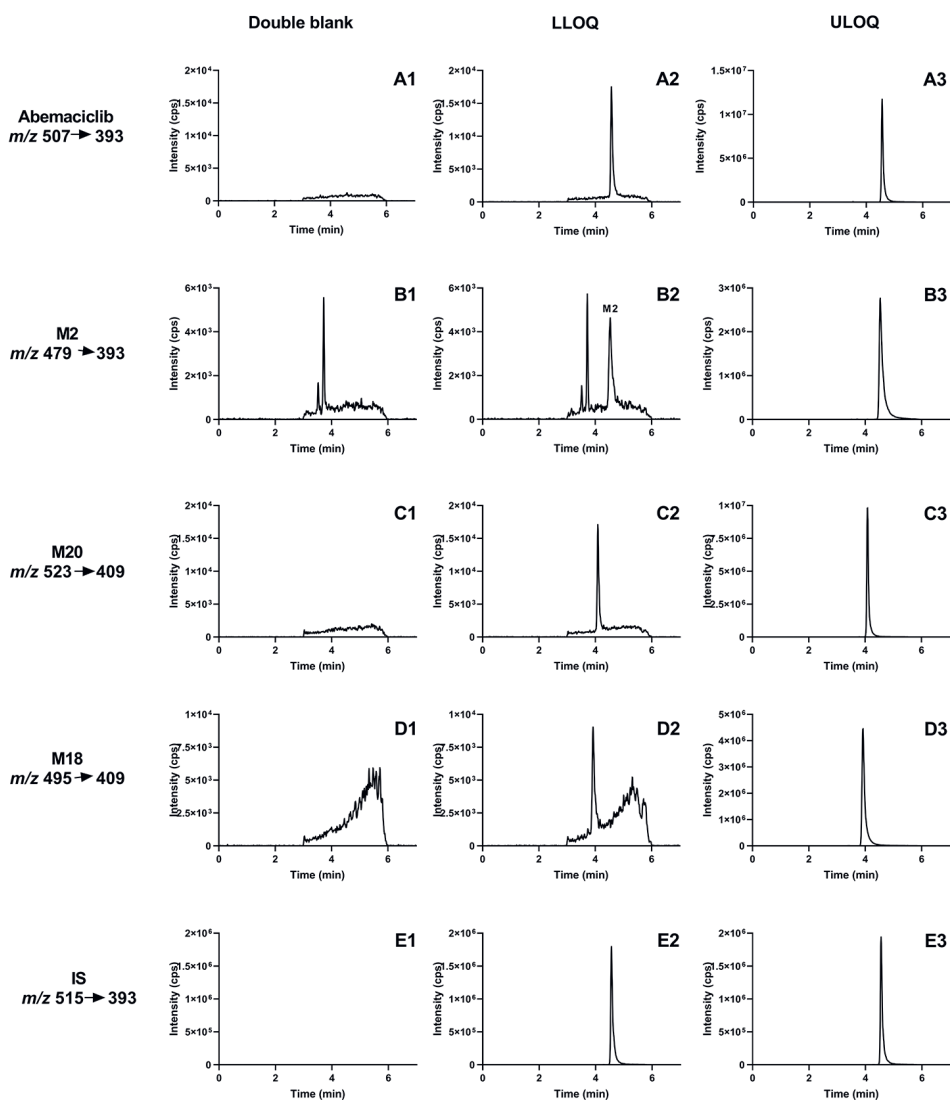


**Figure 3.** Representative chromatograms of control human plasma unspiked (double blank), spiked at the LLOQ (LLOQ) and at the ULOQ (ULOQ) at the mass transition of abemaciclib (A series), M2 (B series), M20 (C series), M18 (D series) and the internal standard (E series). Y axis of chromatograms from double blank and LLOQ columns are presented in the same scale for each analyte, but chromatograms from the ULOQ column are adjusted to the highest response.

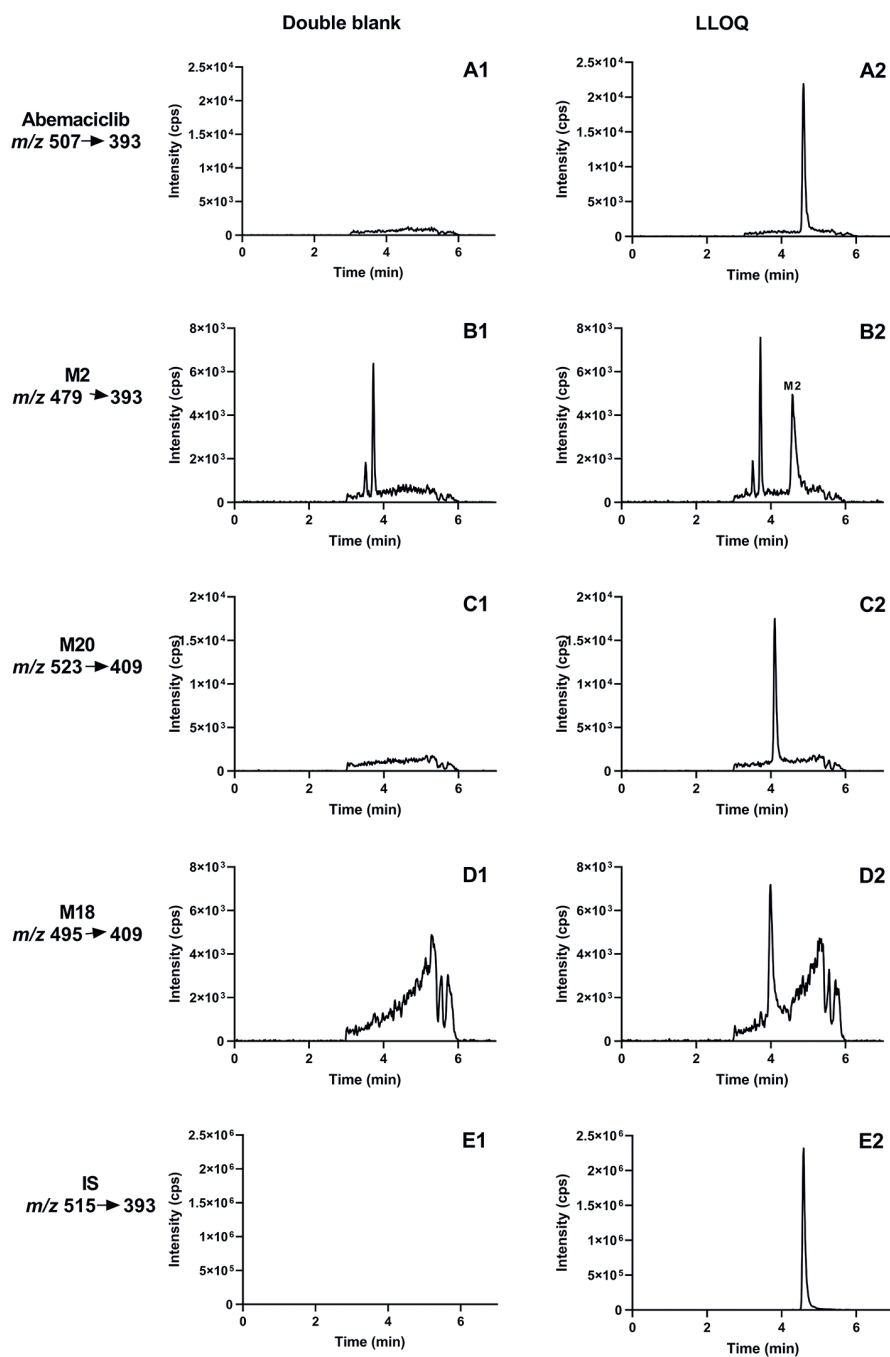


**Figure 4.** Representative chromatograms of control mouse plasma unspiked (double blank) and spiked at the LLOQ (LLOQ) at the mass transition of abemaciclib (A series), M2 (B series), M20 (C series), M18 (D series) and the internal standard (E series).



**Table 2.** Accuracy and precision of abemaciclib, M2, M20 and M18

Analyte	Matrix	Nominal concentration (ng/mL)	Intra-assay		Inter-assay	
			Bias (%)	RSD (%)	Bias (%)	RSD (%)
Abemaciclib	Human plasma	1	±5.5	≤6.5	2.2	1.7
		3	±1.7	≤6.6	0.7	*
		45	±2.4	≤4.6	1.6	*
		450	±1.7	≤3.2	-0.7	*
	Mouse plasma	1	4.4	7.5		
		3	3.0	5.6		
		45	2.1	3.3		
		450	4.6	3.5		
M2	Human plasma	0.5	±6.5	≤9.0	3.6	2.1
		1.5	±3.1	≤9.7	-2.1	*
		22.5	±7.6	≤6.1	-6.5	*
		225	±6.0	≤4.4	-4.2	2.1
	Mouse plasma	0.5	-6.8	7.8		
		1.5	-2.9	8.4		
		22.5	-8.0	6.4		
		225	-11.4	4.4		
M20	Human plasma	0.5	±13.1	≤6.7	10.7	1.5
		1.5	±9.6	≤8.2	7.1	*
		22.5	±9.0	≤7.6	5.6	2.5
		225	±10.2	≤5.5	8.1	0.3
	Mouse plasma	0.5	1.7	3.1		
		1.5	7.5	5.0		
		22.5	-2.0	8.4		
		225	-7.7	7.3		
M18	Human plasma	0.2	±11.9	≤9.2	8.3	*
		0.6	±8.3	≤7.6	2.1	4.6
		9	±7.7	≤3.6	-3.8	3.8
		90	±5.8	≤5.6	-2.6	3.8
	Mouse plasma	0.2	3.3	3.0		
		0.6	7.1	6.0		
		9	-11.4	1.8		
		90	-12	5.3		

\*No significant additional variation due to the analysis in different runs was detected.

*Lower limit of quantification*

The described method exhibited good sensitivity, obtaining signal-to-noise ratios of at least 36 for abemaciclib, 10 for M2, 15 for M20 and 13 for M18 in three analytical runs. Moreover, the accuracy and precision results at the LLOQ, which are described in table 2, met the acceptance criteria (RSD  $\leq$  20% and bias within  $\pm$  20%) for all analytes.

*Carry-over*

Carry-over higher than 20% of the LLOQ was detected for all analytes, where the greatest value was obtained for the least polar analyte (abemaciclib, with 104% carry-over), and the lowest for the most polar analyte (M18, with 50% carry-over). To insure integrity of the results, some strategies were followed during the analysis, for instance, samples were injected in ascendent (expected) concentration order or blanks were injected between high- and low-concentration samples. Furthermore, the calculation of the carry-over factor (CF) was implemented post-analysis, according to the formula:

$$CF = \frac{\frac{Response_x \times Mean\ response_{blank}}{Mean\ response_{ULOQ}}}{Response_{x+1}} \times 100$$

where x symbolizes any sample and x+1 is the consecutive injected sample. When CF  $\leq$  5%, the result of the sample x+1 is not affected by sample x. Nevertheless, when CF  $>$  5%, sample x+1 was re-injected, since the response could have been affected by sample x. By applying this procedure, the validity of the data generated during analysis was assured, despite the carry-over of the method.

*Matrix effect and recovery*

Matrix effect and recovery results are summarized in Table 3, in which the RSD of the mean normalized matrix factor was  $\leq$  15% for all analytes in both concentration levels, meeting the established acceptance criteria. Overall, the method showed a good recovery for all analytes, which was  $>$  90% in all cases.

*Dilution integrity*

QC samples spiked at concentrations higher than the ULOQ were accurately and precisely quantified after dilution, where for human plasma the bias and the RSD (%) were, -0.7 and 3.7 for abemaciclib, -10.1 and 8.3 for M2, 12 and 4.9 for M20, and 10.3 and 7.3 for M18. Similarly, diluted mouse plasma QC samples showed a bias and RSD (%) of -2.9 and 3.4 for abemaciclib, -10.3 and 3.5 for M2, 3.5 and 5.9 for M20, and -1.4 and 5.9 for M18. Therefore, all results met the established acceptance criteria.

*Stability*

Prior to the stability tests described in the methodology section for this validation parameter, biomatrix stability was independently assessed for each single analyte in both human and mouse plasma, with QC samples spiked with a single analyte at mid-level. These samples were maintained at room temperature for 7 days in order to

**Table 3.** Normalized matrix factor and recovery of abemaciclib, M2, M20 and M18 at low and high concentration levels in six different batches of control human K<sub>2</sub>EDTA plasma

	Nominal concentration (ng/mL)	Normalized matrix factor		Recovery (%)
		Mean	RSD (%)	
Abemaciclib	3	1.01	8.0	105.8
	450	0.98	5.1	90.3
M2	1.5	1.05	6.7	92.2
	225	0.86	8.3	108.2
M20	1.5	1.07	5.8	92.1
	225	0.81	12.5	93.2
M18	0.6	0.96	11.7	92.7
	90	0.75	12.4	94.3

detect whether any of the analytes was also *ex vivo* formed as degradation compound from one of the analytes. Results indicated that abemaciclib and its active metabolites were stable in these matrices, since the mean measured concentration for all samples remained within  $\pm 15\%$ . No further formation of metabolites was detected during this test. Consequently, stability tests were performed with QC samples containing simultaneously all analytes at QC high- and low-concentrations. Stability results at all experimental conditions are presented in Table 4, which prove that abemaciclib, M2, M20 and M18 are stable in human and mouse plasma at room temperature for at least 4 days and at  $-20\text{ }^{\circ}\text{C}$  for at least 3 months. Also, these analytes are stable in both matrices after 3 F/T cycles from  $-20\text{ }^{\circ}\text{C}$  to room temperature,. Moreover, all compounds were found to be stable in the final extract from both matrices.

### Applicability of the method

The applicability of this method was demonstrated by measuring abemaciclib and its active metabolites in mouse and human plasma samples. M2, M20 and M18 are clinically important as they can inhibit CDK4 and CDK6 at a similar potency as abemaciclib (Figure 1) [15]. Based on their abundance in human plasma ( $\geq 13\%$  each one) it is likely that they contribute to the clinical efficacy and safety of abemaciclib [4,5]. Figure 5 illustrates representative chromatograms of plasma samples from a patient and mouse treated with abemaciclib, where in all cases, the parent drug and its active metabolites were identified and quantified, fitting the calibration range. Important inter-species differences between human and mouse samples were observed. While in humans single peaks were detected at the mass transitions of M20 and M18, in mice, more peaks were detected at those mass transitions (Figure 5, panels C1, C2, D1 and D2). These extra peaks in mouse samples correspond to isomers of these metabolites (see "HR-MS measurements for the identification of M20 isomers in mouse samples" section).

**Table 4.** Stability of abemaciclib, M2, M20 and M18 in mouse and human plasma

Analyte	Matrix	Stability conditions	Nominal concentration (ng/mL)	Mean concentration (ng/mL)	Accuracy (% Bias)	Precision (% RSD)	
Abemaciclib	Human plasma	RT, 4 d	3	3.12	4.1	3.2	
			450	433	-3.8	1.7	
		3 F/T (-20 °C/RT)	3	3.28	9.4	8.6	
			450	433	-3.8	5.4	
		-20 °C, 3 m	3	3.28	9.3	0.9	
			450	454	0.9	0.2	
		Final extract	4-8 °C, 4 d	3	2.97	-1.0	3.8
				450	463	3.0	2.1
	Mouse plasma	RT, 4 d	3	3.07	3.8	2.2	
			450	513	14.0	1.8	
			3 F/T (-20 °C/RT)	3	2.95	-1.1	5.6
				450	444	-1.3	2.5
		-20 °C, 3 m	3	2.91	-2.9	4.6	
			450	417	-7.3	6.0	
		Final extract	4-8 °C, 4 d	3	3.05	1.8	5.3
				450	467	3.9	5.6
M2	Human plasma	RT, 4 d	1.5	1.44	-3.8	4.1	
			225	218	-3.1	2.3	
		3 F/T (-20 °C/RT)	1.5	1.64	9.3	6.0	
			225	231	3.0	2.5	
		-20 °C, 3 m	1.5	1.63	8.7	8.8	
			225	229	1.8	3.4	
		Final extract	4-8 °C, 4 d	1.5	1.42	-5.1	2.7
				225	204	-9.3	0.8
	Mouse plasma	RT, 4 d	1.5	1.41	-6.0	0.7	
			225	213	-5.3	11.0	
		3 F/T (-20 °C/RT)	1.5	1.27	-14.9	13.9	
			225	209	-7.0	3.4	
		-20 °C, 3 m	1.5	1.42	-5.3	6.7	
			225	202	-10.4	8.7	
	Final extract	4-8 °C, 4 d	1.5	1.35	-10.0	10.0	
			225	210	-6.8	7.2	

Table 4. Continued

Analyte	Matrix	Stability conditions	Nominal concentration (ng/mL)	Mean concentration (ng/mL)	Accuracy (% Bias)	Precision (% RSD)
M20	Human plasma	RT, 4 d	1.5	1.64	9.6	6.0
			225	254	12.9	5.3
		3 F/T (-20 °C/RT)	1.5	1.76	17.3	5.0
			225	259	15.0	4.3
		-20 °C, 3 m	1.5	1.74	16.2	1.2
			225	257	14.4	4.6
	Final extract	4-8 °C, 4 d	1.5	1.71	14.0	2.5
			225	230	1.5	5.9
	Mouse plasma	RT, 4 d	1.5	1.53	1.8	3.2
			225	245	8.9	1.2
		3 F/T (-20 °C/RT)	1.5	1.55	3.6	11.9
			225	228	1.5	7.6
		-20 °C, 3 m	1.5	1.54	2.4	3.3
			225	229	1.6	3.4
	Final extract	4-8 °C, 4 d	1.5	1.52	1.6	2.7
			225	227	1.0	10.4
M18	Human plasma	RT, 4 d	0.6	0.544	-9.4	1.2
			90	91.0	1.1	6.7
		3 F/T (-20 °C/RT)	0.6	0.630	5.1	13.6
			90	98.2	9.1	2.7
		-20 °C, 3 m	0.6	0.619	3.2	3.6
			90	98.5	9.4	1.4
	Final extract	4-8 °C, 4 d	0.6	0.591	-1.6	3.1
			90	93.4	3.8	1.0
	Mouse plasma	RT, 4 d	0.6	0.530	-11.7	7.2
			90	84.6	-6.1	2.8
		3 F/T (-20 °C/RT)	0.6	0.522	-12.9	6.3
			90	90.4	0.4	1.2
		-20 °C, 3 m	0.6	0.603	0.4	9.0
			90	84.8	-5.8	6.6
	Final extract	4-8 °C, 4 d	0.6	0.539	-10.2	4.8
			90	85.5	-5.0	8.5

RT=Room Temperature, F/T=Freeze-Thaw cycles, d=days, m=months.

In addition, this method was utilized to support pharmacokinetic studies in mice, where the plasma concentration-time curves and areas under the plasma concentration-time curves ( $AUC_{0-4h}$ ) of abemaciclib, M2, M20 and M18 are depicted in Figures 6A and 6B, respectively. All measured samples were within the calibration range for abemaciclib and M2, however for M20, samples that were collected at 0.125 and 0.25 were below the limit of detection (LOD) and the LLOQ, respectively. For M18, samples at these two time points were below the LOD. This is related to the abundance of the metabolites in plasma, as well as the time that is needed for the formation of the metabolites. While M2 and M20 are directly formed from abemaciclib (Figure 1), M18 is formed from these two metabolites, thus involving two metabolic reactions. This pharmacokinetic study showed that the M20 plasma abundance in mice is lower than what is reported for humans [4,5,14]. Furthermore, whereas in humans the abundance of M20 is more comparable to M2, in mice it is significantly lower. This is probably compensated with the formation of the M20 isomers, where the authentic M20 appeared not to be the most abundant in plasma (Figure 5, panel C2). Thus, this method was found to be versatile for the quantitative analysis of abemaciclib, M2, M20 and M18 in both human and mouse plasma samples.

#### **HR-MS measurements for the identification of M20 isomers in mouse samples**

As previously mentioned, several peaks were detected at the M20 and M18 mass transitions in mouse plasma samples. These peaks were also detected in other mouse matrices, like liver, where their signal was higher compared to plasma. For this reason, a liver sample was used for the HR-MS measurements. For these experiments, a column with a lower particle size was used (1.3  $\mu\text{m}$ ) to increase the resolution among the peaks detected at the M18 and M20 mass transitions (Figure 7). Since the response of the M18 detected peaks was too low, these measurements were only performed at M20 mass transition. Extracted ion chromatograms of the parent and product ions are depicted in Figure 8 (panels A1 and A2). Also, the parent and product ion MS spectra of the three detected peaks are presented in Figure 8, together with the accurate  $m/z$  measured in each peak. These values were compared with the theoretical accurate monoisotopic mass of the M20 parent ion, which resulted in a mass difference (ppm) of -6.95 for peak 1, -6.76 for peak 2, and -6.19 for peak 3 (M20). Similarly, this was calculated for the M20 product ion, where a difference of -5.23, 4.74 and -6.70 ppm was estimated for peaks 1, 2 and 3 (M20), respectively. In all comparisons the calculated difference was within 7 ppm, confirming that the three detected peaks are isomers. Since these compounds were separated with a  $C_{18}$  column, we speculate that these compounds are structural isomers, i.e. possibly the hydroxylation occurred in a position different from M20. Although HR-MS measurements for M18 peaks were not performed, it is likely that peaks detected in this mass transition are also structural isomers formed from the various hydroxylated compounds detected at M20 mass transition.

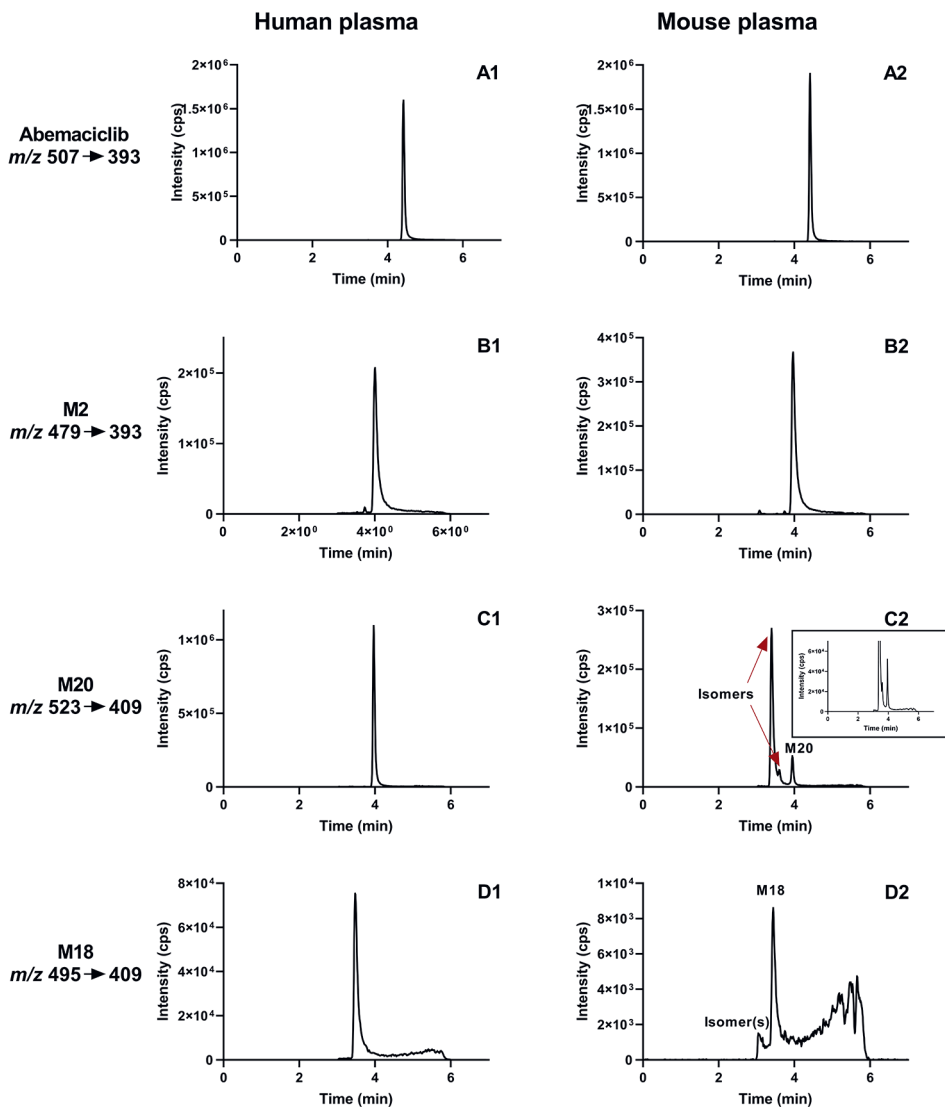


**Figure 5.** Representative chromatograms of abemaciclib (A-series), M2 (B-series), M20 (C-series) and M18 (D-series) obtained from a patient sample that was treated with 50 mg of abemaciclib per day (human plasma), and a mouse dosed with 10 mg/kg abemaciclib (mouse plasma). The patient sample was taken under steady state conditions and the measured concentrations were 54.6 ng/mL for abemaciclib (panel A1), 18.9 ng/mL for M2 (panel B1), 28.3 ng/mL for M20 (panel C1) and 3.15 ng/mL for M18 (panel D1). Mouse plasma sample was collected 1 h after a single oral administration of abemaciclib and 5-fold diluted to obtain the required volume for the sample pre-treatment (50  $\mu$ L); measured concentrations were 308 ng/mL for abemaciclib (panel A2), 160 ng/mL for M2 (panel B2), 7.79 ng/mL for M20 (panel C2) and 2.02 ng/mL for M18 (panel D2).

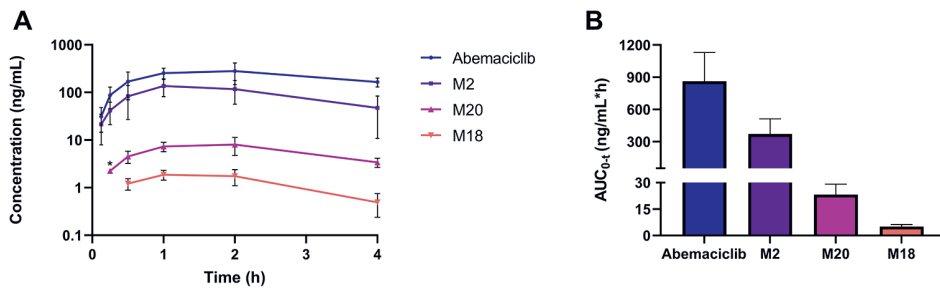


**Figure 6.** Semi-log plasma concentration-time curve (A) and area under the plasma concentration-time curve (B) of abemaciclib, M2, M20 and M18 over 4 h in female FVB mice ( $n = 6$ ) dosed with 10 mg/kg of abemaciclib. Data are presented as mean  $\pm$  SD. \*values below the LLOQ; M20 and M18 were not detected at 0.125 h and at 0.125-1.25 h, respectively.

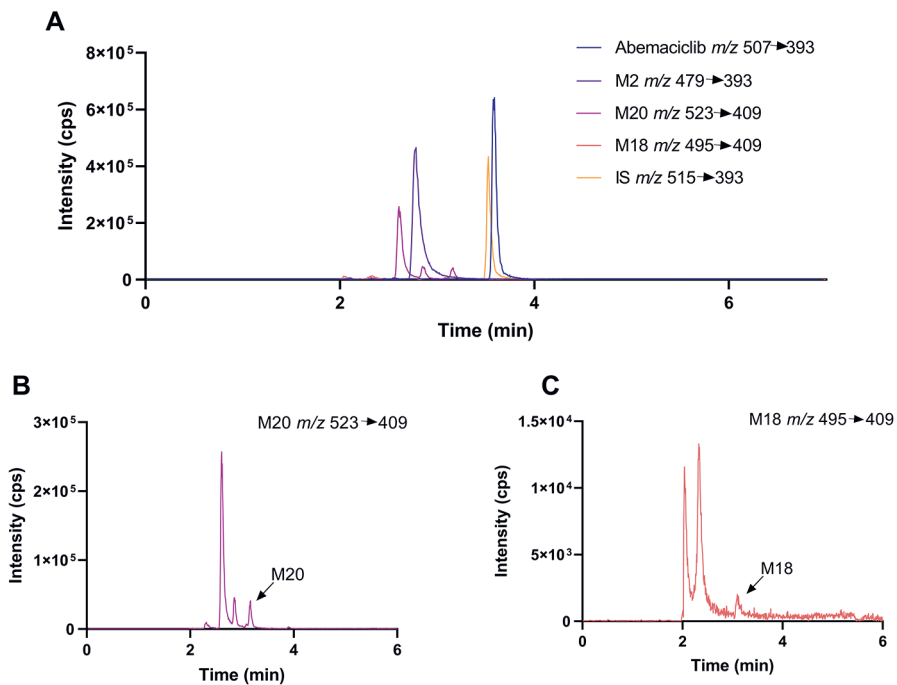


**Figure 7.** Representative chromatograms of a mouse plasma sample obtained with the Column EVO C18 (1.3  $\mu\text{m}$ ) including all analytes (A). Chromatograms at the M20 mass transition (B) and M18 mass transition (C), where separation between the isomers is increased compared to the Kinetex column (Figure 5, panels C2 and D2).



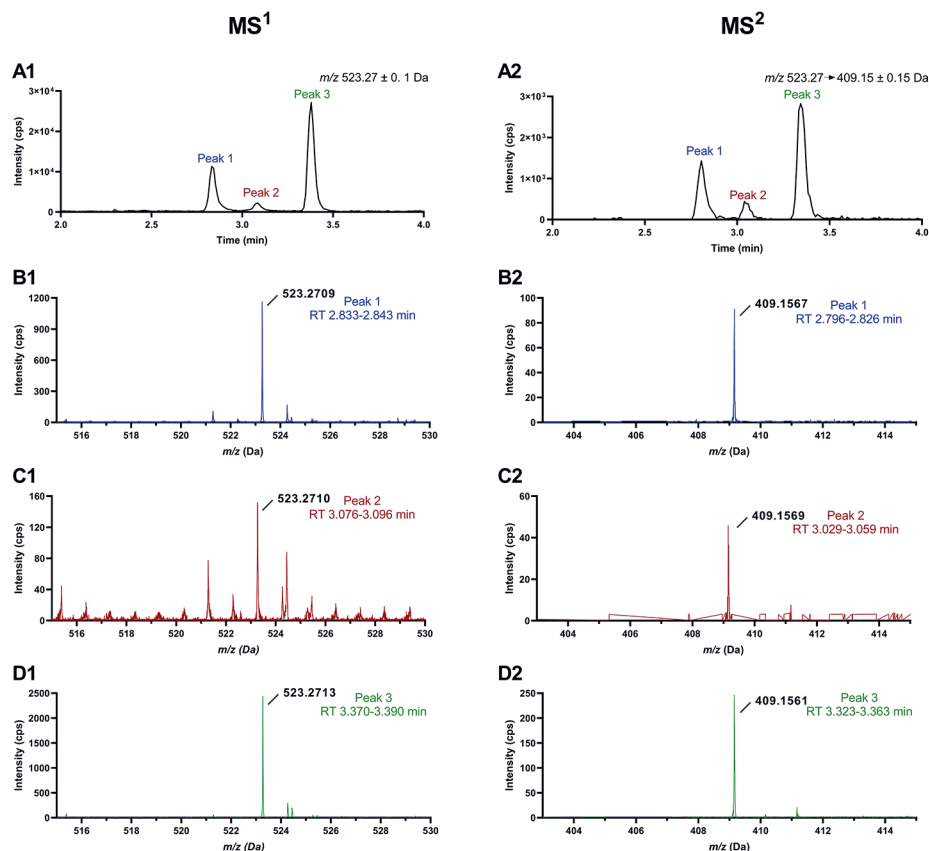


**Figure 8.** Chromatograms acquired at the parent ( $MS^1$ , A1) and product ( $MS^2$ , A2) ions.  $MS^1$  and  $MS^2$  spectra of peak 1 (B1, B2), peak 2 (C1, C2) and peak 3 (D1, D2) with the accurate  $m/z$  values of the detected parent and product ion.

## Conclusions

An UHPLC-MS/MS bioanalytical method for the simultaneous quantification of abemaciclib and its active metabolites (M2, M20 and M18) in human and mouse plasma was developed and validated. Although inter-species differences between humans and mice were encountered, a versatile method for both matrices is provided. This method was demonstrated to be linear, accurate, precise, selective and sensitive for all analytes. However, it was limited by the lack of stable isotopically labeled metabolites to use as internal standards, which resulted in slightly higher variability in the metabolites quantification. Because of this, wider criteria for accuracy and precision were accepted ( $\pm 20\%$  and  $\leq 20\%$ , respectively, for all concentration levels). Nevertheless, it is expected that when these compounds become available, the variability in the metabolites

quantification will decrease. The use of human plasma as a surrogate matrix for an accurate analysis of mouse samples was also verified. Carry-over was detected for all analytes, but several measures were implemented to assure the integrity of the data. Abemaciclib, M2, M20 and M18 were stable in human and mouse plasma under several tested conditions. In addition, the applicability of the method in a preclinical pharmacokinetic study in mice was demonstrated, where all analytes were identified and quantified. Finally, isomers of M20 were detected in mouse samples, which was confirmed by HR-MS measurements.

## References

- [1] L.M. Gelbert, S. Cai, X. Lin, C. Sanchez-Martinez, M. Del Prado, M.J. Lallena, R. Torres, R.T. Ajamie, G.N. Wishart, R.S. Flack, B.L. Neubauer, J. Young, E.M. Chan, P. Iversen, D. Cronier, E. Kreklau, A. De Dios, Preclinical characterization of the CDK4/6 inhibitor LY2835219: In-vivo cell cycle-dependent/independent anti-tumor activities alone/in combination with gemcitabine, *Invest. New Drugs*. 32 (2014) 825–837. <https://doi.org/10.1007/s10637-014-0120-7>.
- [2] B. O'Leary, R.S. Finn, N.C. Turner, Treating cancer with selective CDK4/6 inhibitors, *Nat. Rev. Clin. Oncol*. 13 (2016) 417–430. <https://doi.org/10.1038/nrclinonc.2016.26>.
- [3] Q.Y. Chong, Z.H. Kok, N.L.C. Bui, X. Xiang, A.L.A. Wong, W.P. Yong, G. Sethi, P.E. Lobie, L. Wang, B.C. Goh, A unique CDK4/6 inhibitor: Current and future therapeutic strategies of abemaciclib, *Pharmacol. Res*. 156 (2020) 104686. <https://doi.org/10.1016/j.phrs.2020.104686>.
- [4] US Food and Drug Administration (FDA), INDICATIONS AND USAGE VERZENIO™ ( abemaciclib ), 2017. [https://www.accessdata.fda.gov/drugsatfda\\_docs/label/2020/208716s004lbl.pdf](https://www.accessdata.fda.gov/drugsatfda_docs/label/2020/208716s004lbl.pdf).
- [5] Committee for Medicinal Products for Human Use (CHMP), Public Assessment Report Abemaciclib, (2018). [https://www.ema.europa.eu/en/documents/assessment-report/verzenios-epar-public-assessment-report\\_en.pdf](https://www.ema.europa.eu/en/documents/assessment-report/verzenios-epar-public-assessment-report_en.pdf).
- [6] US Food and Drug Administration (FDA), Safety Testing of Drug Metabolites, (2020). <https://www.fda.gov/media/72279/download>.
- [7] A. Martínez-Chávez, H. Rosing, M. Hillebrand, M. Tibben, A.H. Schinkel, J.H. Beijnen, Development and validation of a bioanalytical method for the quantification of the CDK4/6 inhibitors abemaciclib, palbociclib and ribociclib in human and mouse matrices using liquid chromatography-tandem mass spectrometry, *Anal. Bioanal. Chem*. 411 (2019) 5531–5345. <https://doi.org/10.1007/s00216-019-01932-w>.
- [8] P. Dhakne, A.K. Sahu, M.K. Sharma, P. Sengupta, Simultaneous quantification of abemaciclib and letrozole in rat plasma: method development, validation and pharmacokinetic application, *Biomed. Chromatogr*. 34 (2020). <https://doi.org/10.1002/bmc.4825>.
- [9] A. Maeda, K. Irie, N. Hashimoto, S. Fukushima, H. Ando, A. Okada, H. Ebi, M. Kajita, H. Iwata, M. Sawaki, Serum concentration of the CKD4/6 inhibitor abemaciclib, but not of creatinine, strongly predicts hematological adverse events in patients with breast cancer: a preliminary report, *Invest. New Drugs*. 39 (2021) 272–277. <https://doi.org/10.1007/s10637-020-00994-3>.
- [10] A.A. Kadi, H.W. Darwish, H.A. Abuelizz, T.A. Alsubi, M.W. Attwa, Identification of reactive intermediate formation and bioactivation pathways in Abemaciclib metabolism by LC-MS/MS: In vitro metabolic investigation, *R. Soc. Open Sci*. 6 (2019). <https://doi.org/10.1098/rsos.181714>.
- [11] D. Thakkar, A.S. Kate, Update on metabolism of abemaciclib: In silico, in vitro, and in vivo metabolite identification and characterization using high resolution mass spectrometry, *Drug Test. Anal*. 12 (2020) 331–342. <https://doi.org/10.1002/dta.2725>.
- [12] US Food and Drug Administration, Guidance for Industry Bioanalytical Method Validation, (2018) 1–22. <https://www.fda.gov/files/drugs/published/Bioanalytical-Method-Validation-Guidance-for-Industry.pdf>.
- [13] European Medicines Agency, Guideline on bioanalytical method validation, 44 (2012) 1–23. [https://www.ema.europa.eu/documents/scientific-guideline/guideline-bioanalytical-method-validation\\_en.pdf](https://www.ema.europa.eu/documents/scientific-guideline/guideline-bioanalytical-method-validation_en.pdf).
- [14] M.M. Posada, B.L. Morse, P.K. Turner, P. Kulanthaivel, S.D. Hall, G.L. Dickinson, Predicting Clinical Effects of CYP3A4 Modulators on Abemaciclib and Active Metabolites Exposure Using Physiologically Based Pharmacokinetic Modeling, *J. Clin. Pharmacol*. 60 (2020) 915–930. <https://doi.org/10.1002/jcph.1584>.



# 3

## Development and validation of an LC-MS/MS method for the quantitative analysis of milciclib in human and mouse plasma, mouse tissue homogenates and tissue culture medium

Journal of Pharmaceutical and Biomedical Analysis 2020, 190: 113516

Alejandra Martínez-Chávez  
Matthijs M. Tibben  
Jelle Broeders  
Hilde Rosing  
Alfred H. Schinkel  
Jos H. Beijnen

## Abstract

Milciclib is a promising cyclin-dependent kinase inhibitor currently in phase II clinical trials to treat several types of cancer. The first bioanalytical method for the quantitative analysis of milciclib in several biomatrices using liquid chromatography-tandem mass spectrometry is described here. This method was fully validated in human plasma according to FDA and EMA guidelines, and partially validated in mouse plasma, homogenates of mouse brain, kidney, liver, small intestine, spleen, and tissue culture medium. Palbociclib, an analog compound, was used as internal standard. A simple and fast sample pre-treatment by protein precipitation with acetonitrile was used, leading to efficient extraction of the analyte with recoveries between 95-100%. Chromatographic separation was achieved with a C<sub>18</sub> analytical column and a gradient elution using 10 mM ammonium bicarbonate in water and 10 mM ammonium bicarbonate in water-methanol (1:9, v/v). This assay was selective, accurate, precise and linear in the concentration range of 1-1000 ng/mL. Moreover, samples above the upper limit of quantification can be integrally diluted up to 10-fold prior to analysis. The use of human plasma as a surrogate matrix to quantify milciclib in tissue culture medium and mouse matrices resulted in acceptable accuracy and precision, however tissue culture medium samples required a dilution with human plasma prior the pre-treatment. All performance parameters of the method complied with the acceptance criteria recommended by the guidelines, except for the carry-over, which was slightly above (22.9% of the lower limit of quantification) the recommended percentage (20%). Therefore, additional measures were taken to assure data integrity. Stability of milciclib in all matrices was evaluated, and in some matrices the analyte was unstable under the tested conditions. It is therefore recommended to keep these samples as briefly as possible at room temperature during the pre-treatment, and to store them at -70 °C to avoid analyte degradation. This method was successfully applied to support preclinical pharmacokinetic studies of milciclib.

## Introduction

Cyclin-dependent kinases (CDKs) are key complexes in the regulation of the cell cycle, that are activated when a cyclin (*cyc*) binds to them [1]. CDKs have different roles: they can control the entry of the cell cycle (CDK4/*cycD* and CDK6/*cycD*), the DNA replication (CDK2/*cycE* and *cycA*) and the initiation of mitosis (CDK1/*cycA* and *cycB*) [2]. CDKs, cyclins and the endogenous CDK inhibitors are frequently dysregulated in cancer cells, favoring tumorigenesis [1,3]. This has led to the development of small-molecule CDK inhibitors. So far, three selective CDK4/6 inhibitors, palbociclib, ribociclib and abemaciclib, have been approved by the FDA and EMA to treat cancer, and several other CDK inhibitors, including miliclib, are being investigated in preclinical or clinical studies.

Miliclib is a potent inhibitor mainly for CDK2 ( $IC_{50}$  CDK2/*cycA* 45 nM) and the tropomyosin receptor kinase A (TRKA,  $IC_{50}$  53 nM), an enzyme that is activated in several types of cancer, which leads to the inhibition of apoptosis, inducing cell proliferation [4,5]. Miliclib also inhibits CDK1, CDK4, CDK5, and CDK7 with lower potency ( $IC_{50} \geq 150$  nM) [4]. In addition to the cell cycle arrest via CDK2, it has recently been reported that miliclib reduces angiogenesis and inhibits glucose consumption in tumors by targeting CDK5 and CDK7, respectively [6,7]. Miliclib was developed for oral administration, and is currently being investigated in phase II clinical trials. Preclinical studies have shown the efficacy of miliclib against brain cancers in medulloblastoma and glioma models [8,9]. Miliclib also inhibited tumor growth in a transgenic mouse model for non-small cell lung cancer [10]. In xenografts models, miliclib has shown efficacy against melanoma, ovarian, colon, pancreatic, prostate and non-small cell lung cancer with a tumor growth inhibition from 64 to 91% [11]. In clinical studies, miliclib has been effective against thymic carcinoma and thymoma [12,13]. As a consequence, the European Medicines Agency (EMA) and the U.S. Food and Drug Administration (FDA) granted the "orphan drug" designation to miliclib. In combination with gemcitabine, miliclib was well tolerated and showed clinical benefit in approximately 36% of the patients [14]. Furthermore, miliclib is currently being investigated in phase II clinical studies to treat hepatocellular carcinoma [6,15].

Despite (validated) bioanalytical methods using LC-MS/MS having been used to support some of the studies mentioned above, none of these have been described with respect to either the method settings or their performance [4,11,12,14]. In two of them, only the calibration range is mentioned [11,12]. In drug development, validated bioanalytical methods are pivotal to obtain reliable results and to make critical decisions supporting safety and efficacy of active compounds and/or pharmaceutical formulations [16,17]. The aim of this study is to provide a bioanalytical LC-MS/MS method that could support further pre-clinical and/or clinical research of miliclib. We developed an LC-MS/MS method and fully validated it in human plasma. It was also partially validated in tissue

culture medium and in mouse matrices, including plasma and tissue homogenates of brain, kidney, liver, small intestine and spleen. A preclinical application of this method to pharmacokinetic and tissue distribution studies of milciclib in mice is also presented.

## Material and methods

### Chemicals and reagents

Reference standards of milciclib free base (99.5% pure) and palbociclib free base (100% pure) were obtained from Selleck Chemicals LLC (Houston, TX, USA) and AlsaChim (Illkirch-Graffenstaden, France), respectively. Methanol, water, and formic acid, all ULC-MS grade, and acetonitrile (Supra gradient grade) were supplied by Biosolve Ltd (Valkenswaard, The Netherlands). Ammonium bicarbonate (LC-MS grade) and dimethylsulfoxide (DMSO, Seccosolv) were purchased from Merck (Darmstadt, Germany).

### Blank matrices

K<sub>2</sub>EDTA control human plasma was obtained from BioIVT (Westbury, NY, USA). For the tissue culture medium, the Dulbecco's Modified Eagle Medium glutamax (DMEM, Thermo Fisher Scientific, Waltham, MA, USA) was supplemented with 10% (v/v) Fetal Bovine Serum F7524 (Sigma-Aldrich, Darmstadt, Germany). Heparin plasma and organs from individual male and female mice were obtained from the animal laboratory of The Netherlands Cancer Institute (Amsterdam, The Netherlands, approval number from The Dutch Central Animal Testing Committee AVD3010020173825).

Blank tissue homogenates were prepared with 2% (w/v) bovine serum albumin (BSA, Roche Diagnostics GmbH, Mannheim, Germany) in water. A volume of 3 mL of this solution was added to the liver and small intestine, 2 mL to kidneys and 1 mL to brain and spleen prior the homogenization using the Fast Prep-24™ 5G (MP Biomedicals Inc., Santa Ana, CA, USA). The organ weight to 2% BSA volume ratio (w/v) of the homogenates were approximately 0.4:1 for brain and liver, 0.25:1 for small intestine, 0.2:1 for kidneys, and 0.1:1 for spleen.

### Stock and working solutions

Two independent stock solutions of milciclib with separate weighing were prepared at 1 mg/mL in DMSO. One stock solution was used for the preparation of eight working solutions of calibration standards in the concentration range from 20 to 20,000 ng/mL. The second stock solution was used to prepare working solutions of quality control (QC) samples at concentrations of 20, 60, 1000 and 15,000 ng/mL, and working solutions for tissue culture medium QC samples at 40, 120, 2000 and 30,000 ng/mL. All working solutions were prepared in water-acetonitrile (1:1, v/v).



For the internal standard (IS), a stock solution of palbociclib was prepared in 1% formic acid at 1 mg/mL. The IS-working solution was prepared by diluting this stock solution with water-acetonitrile (1:1, v/v) to obtain a concentration of 100 ng/mL. Stock and working solutions were stored at -20 °C.

### **Calibration standards and quality control samples**

Eight calibration standards at 1, 2.5, 10, 25, 100, 250, 800 and 1000 ng/mL were prepared by diluting the corresponding miliciclib working solutions 20-fold with control human plasma. The same dilution factor was used to prepare the QC samples, obtaining final concentrations of 1 (lower limit of quantification, LLOQ), 3 (LQC), 50 (MQC) and 750 ng/mL (HQC) in human and mouse plasma, and mouse tissue homogenates. QCs in tissue culture medium were prepared at 2 (LLOQ), 6 (LQC), 100 (MQC), and 1500 ng/mL (HQC).

### **Sample pre-treatment**

For plasma samples, both from human and mouse, a volume of 50 µL was processed by adding 20 µL of the IS-working solution and 150 µL of acetonitrile. Then, samples were vortex mixed and centrifuged at 23,100g for 5 min. A volume of 150 µL of the supernatant was transferred to a glass vial with insert, and 1 µL was injected into the LC-MS/MS for analysis. When mouse plasma samples had a volume lower than the required (50 µL), 10 µL of mouse plasma was diluted with 40 µL of control human plasma to obtain the validated volume for the sample pre-treatment.

An aliquot of 100 µL of tissue homogenates was used for the pretreatment and the IS-working solution and acetonitrile were added proportionally based on the plasma samples. Tissue culture medium samples were diluted with control human plasma (1:1, v/v) prior to the pretreatment. Thereafter, the same procedure as described to treat the tissue homogenates was used.

### **Analytical instrumentation and conditions**

An ultra-high performance liquid chromatograph (UHPLC) Nexera X2 (Shimadzu, Kyoto, Japan) was used, which consisted of two binary pumps (LC-30AD model), an autosampler (SIL-30AC<sub>MP</sub>) and a column oven (CTO-20AC). Chromatographic separation was performed using a Gemini C<sub>18</sub> column (50 x 2.0 mm ID, 5 µm, Phenomenex, Torrance, CA) protected by a Gemini C18 (4 x 2 mm) guard column, both maintained at 40 °C. For the elution of the analytes, a gradient was applied using 10 mM ammonium bicarbonate in water (mobile phase A) and 10 mM ammonium bicarbonate in water-methanol (1:9 v/v, mobile phase B) at a flow rate of 0.4 mL/min. Initially, from 0-0.5 min the percentage of B was 50%, from 0.5-1.0 min B increased to 100% and this percentage was kept until 2.5 min, at 2.6 min B decreased at 50% and was maintained until 3.1 min, at 3.6 min B increased again to 100% and was maintained until 4.6 min. At 4.7 min B decreased again to 50%, and the column was conditioned for 1.3 min resulting in a total run time

of 6 min. The increase of 100% B from 3.6 to 4.6 min was included to decrease the memory effect. The temperature of the autosampler was maintained at 20 °C for the tissue culture medium samples, and at 4 °C for the rest of the samples.

The analyte and the internal standard were detected using a Triple Quad 6500+ mass spectrometer (Sciex, Foster City, CA, USA) with a turbo ion spray operated in positive ion mode. A divert valve was used to direct the flow from 1 to 3 min to the mass spectrometer and the remainder was directed to the waste. Selective responses were acquired via multiple reaction monitoring (MRM) using the settings described in Table 1. The Analyst software version 1.6.3 (Sciex) was used for data acquisition and processing.

**Table 1.** MS settings

Parameter	Setting	
Gas 1 (NEB)	50 au	
Gas 2 (Turbo)	50 au	
Curtain gas (CUR)	30 au	
Collision gas (CAD)	9 au	
Ion spray voltage (ISV):	5500 V	
Temperature (TEM)	600°C	
Interface Heater	On	
Dwell time	200 msec	
Entrance potential	10 V	
Compound-dependent settings	Milciclib	Palbociclib
Mass transition ( $m/z$ )	461.1 → 430.2	448.1 → 380.1
Declustering potential (DP)	181 V	166 V
Collision energy (CE)	33 V	39 V
Collision cell exit potential (CXP)	26 V	24 V

### Method validation

This method was fully validated for human plasma according to the FDA and the EMA guidelines for bioanalytical method validation [16,17]. Additionally, the method was partially validated for mouse plasma, mouse tissue homogenates (brain, kidney, liver, small intestine and spleen) and tissue culture medium, including selectivity, intra-run accuracy and precision, dilution integrity and stability, using calibration standards in human plasma.

#### *Calibration model*

Eight non-zero calibration standards (described in section 2.4), a blank and a zero calibration standard (blank spiked with IS) were prepared in duplicate, processed according to section 2.5 and analyzed in each validation run. The relationship between

the analyte concentration and the ratio of the peak areas (miliclib/IS) was described by a linear model with a  $1/x^2$  weighting factor, where  $x$  is the analyte concentration. The difference between the back calculated and nominal concentrations should be within  $\pm 15\%$ , and  $\pm 20\%$  for the LLOQ, in at least 75% of the calibration standards.

#### *Accuracy and precision*

Intra-assay accuracy and precision were assessed by analyzing five replicates of the QC samples at each concentration level (LLOQ, LQC, MQC, and HQC) in all the matrices, including human plasma, mouse plasma, mouse tissue homogenates, and tissue culture medium. Inter-assay accuracy and precision was determined in human plasma by analyzing five replicates of the above described QC samples in three separate analytical runs. The bias (%) between the nominal and the mean measured concentration was calculated to evaluate the accuracy. The intra- and inter-assay precision was determined by calculating the variability using the intra-assay coefficient of variation (%CV) and analysis of variance (ANOVA), respectively. Statistics analyses were performed using validated Microsoft Excel calculation sheets. The bias should be within  $\pm 15\%$  and the CV should be  $\leq 15\%$  for all tested concentration levels, except for the LLOQ, where  $\pm 20\%$  and  $\leq 20\%$  are accepted.

#### *Selectivity*

Blanks and LLOQ samples were prepared in six batches of human plasma, mouse plasma, and mouse tissue homogenates to evaluate the selectivity. For tissue culture medium, the selectivity was tested in one batch. The chromatograms of miliclib and palbociclib (IS) obtained in the blanks were compared with the chromatograms of miliclib in the LLOQ samples to determine potential interferences. The response of the interfering peaks in the blank sample should not exceed 20% of the response for miliclib and 5% of the response for the IS, in an LLOQ sample. Furthermore, at least 4 out of 6 miliclib LLOQ samples should be within  $\pm 20\%$  of the nominal concentration.

#### *Lower limit of quantification*

The LLOQ was set at the lowest calibration level, in which the signal-to-noise ratio should be at least 5. This was determined by comparing the signal of miliclib at this level to the noise obtained in a blank sample, in at least three validation runs.

#### *Carry-over*

Carry-over was investigated by injecting two blanks after the upper limit of quantification (ULOQ) sample in at least three analytical runs. The response at the retention time of miliclib in the first blank was compared with the response of miliclib in an LLOQ sample. Carry-over should not exceed 20% of the response at the LLOQ.

#### *Matrix factor and recovery*

The matrix effect was determined in six batches of control human plasma at LQC and HQC concentrations. For each batch and concentration level, matrix-present samples

(MPS) were prepared. For this, each batch of blank plasma was processed until final extract and spiked with the corresponding QC working solution. The absolute matrix factor (MF) was determined by calculating the ratio of the peak area obtained in the MPS and in the matrix-absent sample (MAS), which was prepared by diluting the working solution with acetonitrile-water (3:1, v/v) to reach the same concentration as the MPS. Additionally, the IS-normalized MF was calculated by dividing the MF of the analyte by the MF of the IS.

The recovery was assessed by comparing the response of processed LQC and HQC samples with the MPS at the correspondent concentration levels. The CV of the IS-normalized MF should be  $\leq 15\%$ .

#### *Dilution integrity*

Dilution integrity was investigated in quintuplicate in human plasma, mouse tissue homogenates and tissue culture medium. For human and mouse matrices, a 10-fold dilution with control human plasma was tested at a miliclib concentration of 5000 ng/mL. For tissue culture medium, a 2-fold dilution with human plasma was tested at a concentration of 1,500 ng/mL. The bias and CV of these samples should be  $\pm 15\%$  and  $\leq 15\%$ , respectively.

#### *Stability*

The stability of miliclib was investigated in all matrices. For human plasma it was evaluated at two concentration levels (LQC and HQC), while for the remaining matrices only at MQC concentration. For every matrix the following stability conditions were assessed: short-term at room temperature (RT), long-term at  $-20\text{ }^{\circ}\text{C}$  (for all matrices) and at  $-70\text{ }^{\circ}\text{C}$  (for mouse tissue homogenates), and freeze-thaw (F/T) cycles from  $-20\text{ }^{\circ}\text{C}$  and/or  $-70\text{ }^{\circ}\text{C}$  to RT. The stability of the final extracts in every matrix at  $2\text{--}8\text{ }^{\circ}\text{C}$  was also determined. Solutions were considered stable if the measured concentration was between 85-115%. Finally, the stability of the stock and working solutions at  $-20\text{ }^{\circ}\text{C}$  was evaluated, and they were considered stable if their response was within  $\pm 5\%$  compared to freshly prepared solutions.

#### **Applicability of the method**

This method was successfully used to support *in vitro* transport studies, as well as *in vivo* pharmacokinetic studies in mice with different genotypes (unpublished data). Mouse studies were conducted according to institutional guidelines complying with the Dutch and European legislation (approval number from The Dutch Central Animal Testing Committee: AVD301002016595). After at least of two hours fasting, 10 mg/kg of miliclib was orally administered to 9-16 weeks old aged female FVB mice ( $n = 6$ ). Blood was collected from the tail tip (approximately 50  $\mu\text{L}$ ) at 0.5, 1, 2, 4, and 8 h. At 24 h, mice were anesthetized and blood was collected via cardiac puncture. All blood samples were centrifuged (9000g,  $4\text{ }^{\circ}\text{C}$  for 6 min) and plasma was obtained using sodium heparin as anticoagulant. Mice were sacrificed by cervical dislocation and

organs were collected and weighed, including brain, kidney, liver, small intestine, and spleen. Tissue homogenates were prepared according to section 2.2. Plasma and tissue homogenates were stored at -20 and -70 °C, respectively until analysis.

## Results and discussion

### Method development

Miliciclib is an analog structure of other CDK inhibitors. It contains a piperazine ring and 2-aminopyrimidine which are also present in palbociclib, ribociclib and abemaciclib, although the substituents are different among them. Since it was not possible to obtain stable isotopically labeled miliciclib, we tested these analog structures to choose a proper internal standard (results not shown). Palbociclib was the compound that showed the most similar chromatographic characteristics compared to miliciclib, and was therefore chosen as internal standard.

Miliciclib and palbociclib MS settings were obtained after performing a compound optimization in the mass spectrometer. Figure 1 shows the MS spectrum for miliciclib (A) and palbociclib (B). Despite the product ion of miliciclib at  $m/z$  402 being the most abundant, the product ion at  $m/z$  430 was selected in the mass transition for this bioanalytical method, because the baseline obtained with the  $m/z$  461→430 mass transition was more stable and the lower signal prevented detector saturation. For palbociclib the most abundant fragment with  $m/z$  380 was selected as product ion.

We have previously described a bioanalytical method for the quantification of the CDK4/6 inhibitors abemaciclib, palbociclib and ribociclib [18]. Since miliciclib is a basic compound with comparable chemical structure to these compounds, the chromatographic conditions selected were similar to this method. Due to the presence of memory-effect, after the elution of the analyte and the internal standard, an extra washing step was included in the gradient. With this cleaning step, the memory effect was reduced, decreasing the carry-over by approximately 60%. Although carry-over was still detected, the quantitative results were not substantially affected.

A very simple and fast protein precipitation was selected for the sample pre-treatment, considering the large number of samples that are generated during pharmacokinetic studies. Acetonitrile in a ratio 3:1 (v/v) to the sample volume was used as precipitation solvent based on the good recovery obtained with analogue compounds [18]. The supernatant was directly injected into the LC-MS/MS. Compared to the plasma aliquot volume used for the pre-treatment, a higher sample aliquot volume (100  $\mu$ L) was used for tissue homogenates to obtain a more representative sample.

During method development, two particular issues were observed for the quantification of miliciclib in tissue culture medium. Firstly, significant negative deviations were obtained in spiked tissue culture medium samples when quantified using human plasma

calibration standards. This is most likely due to the matrix effect of the analyte, which was different from plasma. To solve this matter and considering that the expected concentration in real samples would be relatively high, all samples were diluted with human plasma (1:1, v/v) prior the pre-treatment. Secondly, when the final extract was maintained at low temperatures (i.e. 4 °C), solubility in the final extract decreased, leading to precipitation of the analyte. The accuracy was negatively affected, however this process was reversible. This issue was solved by maintaining the temperature of the autosampler at 20 °C when samples in tissue culture medium were analyzed.

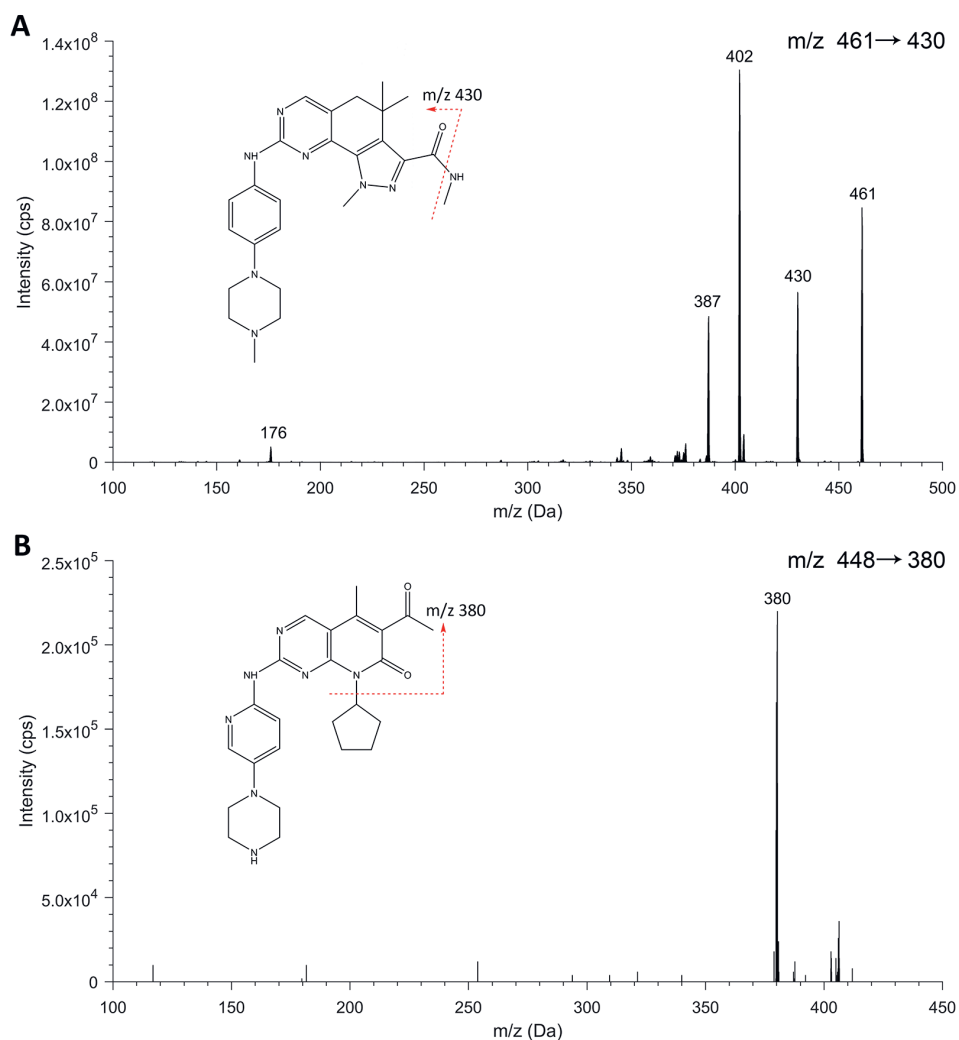


**Figure 1.** Mass spectra with the proposed MS fragmentation pattern of miliclib (A) and the IS palbociclib (B). The red dotted line in the chemical structures indicates the proposed MS fragment selected for quantification.

## Method validation

### Calibration curve

This bioanalytical assay for the quantification of miliclib was linear in the concentration range from 1 to 1000 ng/mL, by using a linear regression with a weighting factor of  $1/x^2$ . Figure 2 shows representative chromatograms of calibration standards at the LLOQ and ULOQ. Linearity was evaluated in twelve analytical runs where calibration curves were injected in duplicate ( $n = 24$ ). Overall, the mean coefficient of correlation was

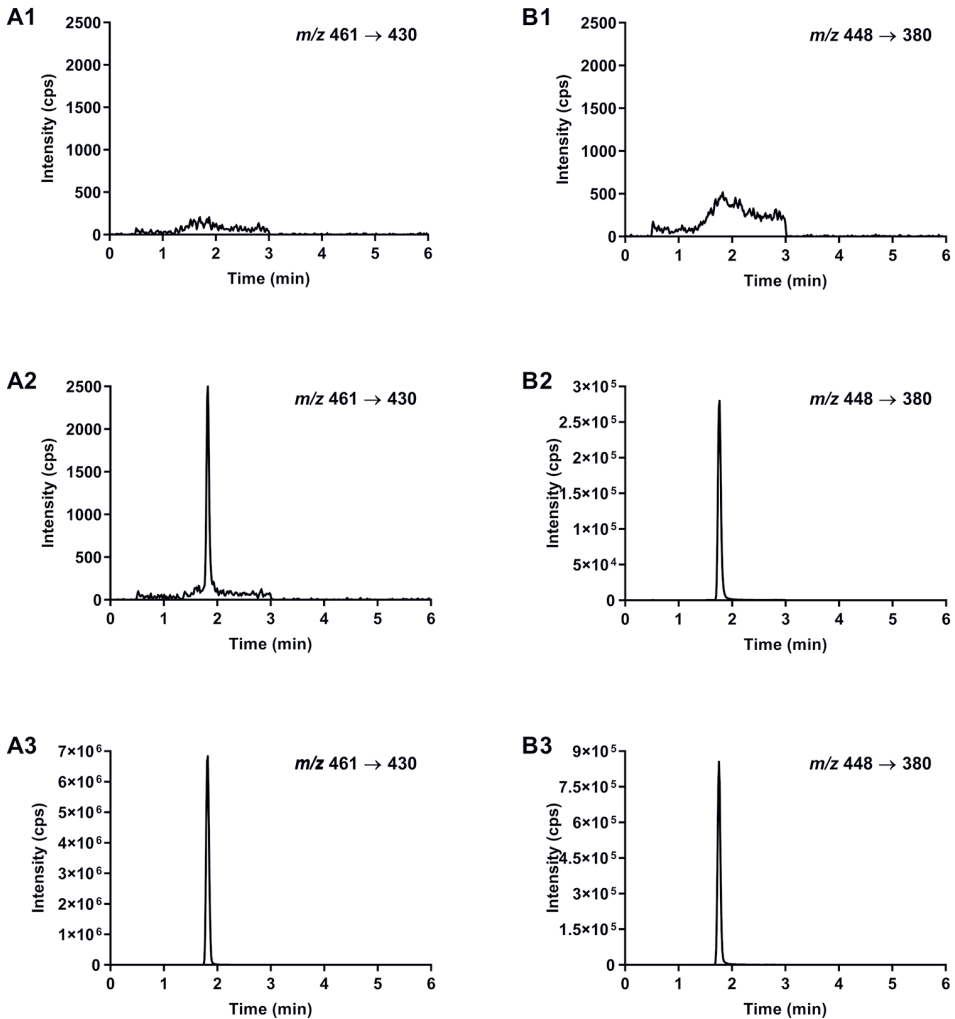


**Figure 2.** Representative chromatograms at the mass transition of miliclib (A-series) and palbociclib (B-series) of a blank human plasma (A1 and B1), blank human plasma spiked at the LLOQ (containing 1 ng/mL of miliclib, A2 and B2) and at the ULOQ (containing 1000 ng/mL of miliclib, A3 and B3).

0.998, and the mean of all back-calculated concentrations was within  $\pm 3.8\%$  of the nominal concentrations ( $CV \leq 10.2\%$ ). Calibration curves in all individual runs complied the acceptance criteria established by the bioanalysis guidelines.

#### *Accuracy and precision*

The results obtained to assess the accuracy and precision of the method are summarized in Table 2. For all matrices, the intra-assay bias and CV were within  $\pm 15\%$  and  $\leq 15\%$ , respectively, in all concentration levels including the LLOQ, complying with the FDA and EMA acceptance criteria for accuracy and precision. Additionally, the inter-assay accuracy and precision was assessed in human plasma, and the obtained data (Table 2) met the acceptance criteria previously indicated. These results also support the use of human plasma as a surrogate matrix for the quantification of milliclib in the non-human matrices used in this study.

#### *Selectivity*

This method was found to be selective for the analysis of milliclib in presence of endogenous compounds. The tested batch of tissue culture medium and the six batches of human plasma and mouse matrices were free from endogenous interferences. Representative chromatograms from blank matrices and samples of milliclib spiked at the LLOQ are depicted in Figure 3 A-series and B-series, respectively, except for human plasma where chromatograms are presented in the A1 and A2 panels from Figure 2. Additionally, the calculated concentrations of the LLOQ samples from all batches were within  $\pm 20\%$  of the nominal concentration for all matrices, except for spleen homogenate where at least 4 out of 6 batches were within this value. Thus, all the matrices complied with the acceptance criteria.

#### *Lower limit of quantification*

Based on the milliclib peak height at the LLOQ and the noise in the blank (Figure 2), the calculated signal-to-noise ratio was at least 16.3. In addition, the bias and the CV for the quantification of milliclib at the LLOQ (1 ng/mL, Table 2) were within acceptance criteria:  $\pm 20\%$  and  $\leq 20\%$ , respectively. These results show that this concentration level has an adequate sensitivity, accuracy and precision for the LLOQ.

#### *Carry-over*

Despite the cleaning step in the gradient, this method showed carry-over for the analyte. For the internal standard, the mean calculated carry-over was 0.1%. Nevertheless, the response in the blank sample produced by the previous ULOQ sample injected was on average 22.9% of the response of the LLOQ. Since this value exceeds the recommendations from the FDA and EMA guidelines, some measures were taken when milliclib samples were analyzed. Samples were injected in ascending order of expected concentrations, and blanks were injected when a high difference



**Table 2.** Accuracy and precision of miliclib in different matrices

Matrix	Nominal concentration (ng/mL)	Intra-assay (n = 5)		Inter-assay (n = 15) <sup>a</sup>	
		Bias (%)	CV (%)	Bias (%)	CV (%)
Human plasma	1	±10.2	≤3.0	-0.7	9.6
	3	±7.0	≤2.9	-3.1	3.6
	50	±4.7	≤2.8	-1.3	3.5
	750	±5.9	≤2.2	-3.1	2.6
Mouse plasma	1	5.8	2.2		
	3	-0.4	2.0		
	50	-1.2	1.9		
	750	-0.1	3.1		
Brain homogenate	1	12.6	2.1		
	3	2.8	1.6		
	50	12.3	2.0		
	750	5.2	2.4		
Kidney homogenate	1	-3.4	2.5		
	3	-7.5	2.4		
	50	-7.7	2.9		
	750	-6.5	1.5		
Liver homogenate	1	13.2	3.8		
	3	3.6	1.8		
	50	1.0	3.0		
	750	-14.4	13.5		
Small intestine homogenate	1	14.4	3.4		
	3	7.5	4.3		
	50	10.2	2.4		
	750	2.8	5.0		
Spleen homogenate	1	-0.3	3.5		
	3	-9.0	2.9		
	50	-10.5	2.4		
	750	-11.5	2.1		
Tissue culture medium	2	-12.4	5.4		
	6	-5.7	2.2		
	100	-3.5	1.7		
	1500	-9.7	1.4		

<sup>a</sup>For inter-assay accuracy and precision five replicates of each concentration level in three different analytical runs were evaluated (n=15)

between a high- and low-concentration sample was expected. In addition, the carry-over factor (CF) was calculated when preclinical samples were analyzed according to the following formula:

$$CF = \frac{\left( \frac{\text{Response}_X \times \text{Mean response}_{\text{blank}}}{\text{Mean response}_{\text{ULOQ}}} \right)}{\text{Response}_{X+1}} \times 100\%$$

where X represents any sample and X+1 represents the consecutive injected sample. Based on the calculated CF value, a strategy was taken as follows: If CF was  $\leq 5\%$  it was concluded that the result of sample X+1 was not significantly affected by sample X, therefore no action was taken. However, if  $CF > 5\%$ , the response of sample X+1 was influenced by sample X, as a consequence, it was necessary to re-inject again sample X+1 at the end of the analytical batch. In this way, data integrity was insured.

#### *Matrix factor and recovery*

The mean matrix factor of miliclib and the internal standard was, respectively, 0.99 and 0.96 at the LQC, and 0.92 and 0.95 at the HQC concentration. The normalized matrix factors were 1.02 and 0.98 for the LQC and HQC concentration levels ( $CV \leq 4.1\%$ ), respectively. The recovery of miliclib was 104.7% and 103.0% at the low and high concentration levels, respectively.

#### *Dilution integrity*

Table 3 shows the accuracy and precision of samples above the ULOQ after dilution with human plasma. For all matrices, the bias between the measured concentration and the nominal concentration prior the dilution was within  $\pm 13.3\%$ , and the CV was  $\leq 5.5\%$ , complying with the acceptance criteria of the followed guidelines.

#### *Stability*

The stability of miliclib at relevant conditions in each matrix is summarized in Table 4. Short-term stability was tested at room temperature, where the analyte was stable in mouse and human plasma for 24 h. Miliclib was stable in tissue homogenates (excluding brain) for at least 4 h, and for 2 h in brain homogenate and tissue culture medium. In contrast, miliclib was unstable in tissue culture medium at room temperature even for 2 h, while immediate processing of spiked samples in this matrix showed a bias of -6.9% with respect to the nominal concentration. Therefore, it is recommended to perform the sample pre-treatment in a short period of time for tissue homogenates, especially brain, and tissue culture medium samples, in order to avoid that results are affected by any instability problem. To determine the appropriate storage conditions, long-term stability of miliclib was evaluated at -20 °C in all matrices. Moreover, since the stability in tissue homogenates is often compromised by the presence of enzymes, in these matrices the stability was also determined at -70 °C. At

**Table 3.** Dilution integrity of miliclib samples

Matrix	Nominal concentration (ng/mL)	Dilution factor	(n = 5)	
			Bias (%)	CV (%)
Human plasma	5000	10	-4.5	0.5
Brain homogenate	5000	10	-4.2	4.7
Kidney homogenate	5000	10	-4.8	4.3
Liver homogenate	5000	10	-13.3	4.0
Small intestine homogenate	5000	10	-3.0	5.5
Spleen homogenate	5000	10	-2.3	2.1
Tissue culture medium	1500	2	-3.3	3.6

-20 °C, the analyte was stable for at least 104 days in plasma samples. After 56 days miliclib was also stable in tissue homogenates stored at -20 °C, except for kidney homogenates. In contrast, at -70 °C the analyte was stable in all tissue homogenates. Tissue culture medium samples were stable after 50 days stored at -20 °C. The freeze-thaw process from -20 °C to room temperature after 3 cycles did not affect the stability of miliclib in mouse and human matrices. In addition, this compound was stable in tissue homogenates after 3 cycles of freeze/thaw from -70 °C to room temperature. For tissue culture medium, stability of miliclib was evaluated in one freeze-thaw cycle, in which the analyte resulted stable. Finally, miliclib was stable at 4-8 °C for (at least) 5 days in the final extracts of human and mouse plasma, brain and liver homogenates, 9 days in kidney, small intestine, and spleen homogenates, and 15 days in tissue culture medium.

The stock and working solutions of miliclib were stable at -20 °C for at least 141 and 76 days, respectively. After these stability tests, it is recommended to store miliclib tissue samples at -70 °C, while plasma and tissue culture medium samples, stock and working solutions can be stored at -20 °C.

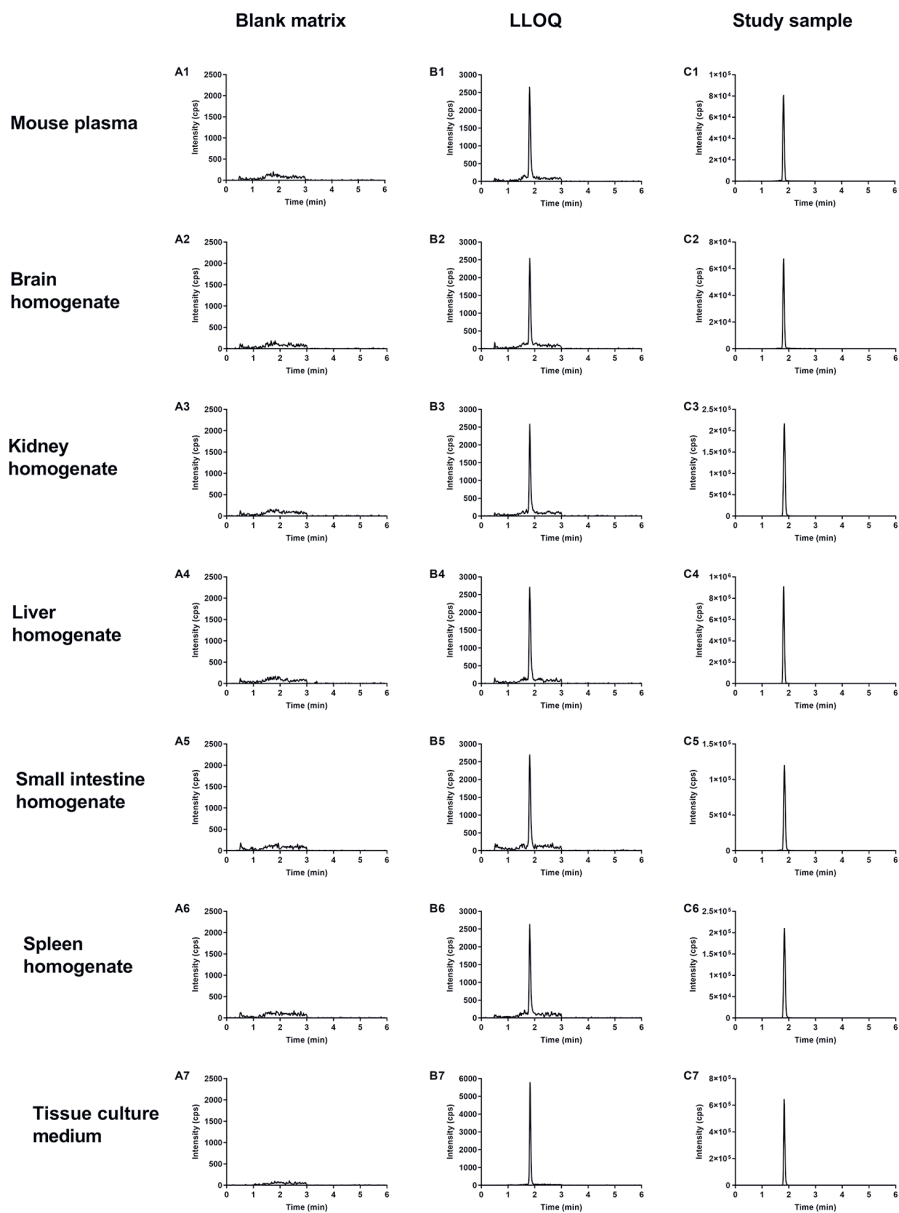


**Figure 3.** Chromatograms at the mass transition of milliciclib ( $m/z$  461  $\rightarrow$  430) of a blank matrix (A-series), a blank matrix spiked at the LLOQ (containing 1 ng/mL of milliciclib, B-series), and representative samples from the preclinical studies (C-series). The matrix is indicated at the beginning of each row. Representative chromatograms of mouse samples (C1-6), which were collected 24 h after oral administration of milliciclib 10 mg/kg. The representative chromatogram of a tissue culture medium sample C7 was collected during an *in vitro* transport experiment of milliciclib using the parental MDCK-II cell line; sample was collected 2 h after the addition of 5  $\mu$ M milliciclib in one of the compartments. Measured concentrations in study samples (ng/mL): mouse plasma (C1), 9.95; brain homogenate (C2), 6.71; kidney homogenate (C3) 48.9; liver homogenate (C4), 70.3; small intestine homogenate (C5), 28.5; spleen homogenate (C6), 50.9; tissue culture medium (C7), 162.

**Table 4.** Stability of miliclib in each tested matrix (n = 3)

Matrix	Type of stability	Stability conditions	Concentration level (ng/mL)	Accuracy (% Bias)	Precision (% CV)
Human plasma	short-term	RT, 24 h	3	2.3	1.2
			750	0.8	0.6
	freeze/thaw cycles	-20 °C/RT, 3 cycles	3	-3.3	2.5
			750	-4.2	2.3
	long-term	-20 °C, 104 d	3	-5.5	2.9
			750	0.3	1.2
	final extract	4-8 °C, 5 d	3	-3.3	17.5
			750	1.7	0.9
Mouse plasma	short-term	RT, 24 h	50	-5.5	0.6
	freeze/thaw cycles	-20 °C/RT, 3 cycles	50	-7.1	1.4
	long-term	-20 °C, 104 d	50	-4.3	2.7
	final extract	4-8 °C, 5 d	50	-8.9	4.5
Brain homogenate	short-term	RT, 2 h	50	8.4	1.8
		RT, 4 h	50	-20.0	2.1
	freeze/thaw cycles	-20 °C/RT, 3 cycles	50	-1.3	0.3
		-70 °C/RT, 3 cycles	50	-0.2	3.0
	long-term	-20 °C, 56 d	50	-3.2	0.4
		-70 °C, 56 d	50	-0.5	2.4
	final extract	4-8 °C, 5 d	50	8.5	0.7
	Kidney homogenate	short-term	RT, 4 h	50	1.2
freeze/thaw cycles		-20 °C/RT, 3 cycles	50	-2.7	1.4
		-70 °C/RT, 3 cycles	50	1.3	3.0
long-term		-20 °C, 56 d	50	-30.5	7.1
		-70 °C, 56 d	50	3.2	0.5
final extract	4-8 °C, 9 d	50	3.5	4.6	
Liver homogenate	short-term	RT, 4 h	50	4.2	6.1
	freeze/thaw cycles	-20 °C/RT, 3 cycles	50	2.4	1.1
		-70 °C/RT, 3 cycles	50	0.7	1.8
	long-term	-20 °C, 56 d	50	-5.9	0.9
		-70 °C, 56 d	50	-6.2	3.5
final extract	4-8 °C, 5 d	50	7.3	4.1	
Small intestine homogenate	short-term	RT, 4 h	50	6.9	1.1
	freeze/thaw cycles	-20 °C/RT, 3 cycles	50	0.3	2.2
		-70 °C/RT, 3 cycles	50	1.9	3.5
	long-term	-20 °C, 56 d	50	11.5	2.0
		-70 °C, 56 d	50	11.9	2.0
final extract	4-8 °C, 9 d	50	-0.6	6.0	

**Table 4.** Continued

Matrix	Type of stability	Stability conditions	Concentration level (ng/mL)	Accuracy (% Bias)	Precision (% CV)
Spleen homogenate	short-term	RT, 4 h	50	-4.7	6.1
	freeze/thaw cycles	-20 °C/RT, 3 cycles	50	0.2	7.0
		-70 °C/RT, 3 cycles	50	1.1	2.3
	long-term	-20 °C, 56 d	50	-1.1	1.2
		-70 °C, 56 d	50	0.3	2.9
final extract	4-8 °C, 9 d	50	3.6	5.2	
Tissue culture medium	short-term	RT, T0	100	-6.9	3.6
		RT, 2 h	100	-44.9	6.3
	freeze/thaw cycles	-20 °C/RT, 1 cycle	100	-9.5	0.7
	long-term	-20 °C, 52 d	100	-14.9	1.8
	final extract	4-8 °C, 15 d	100	12.3	5.4

RT = room temperature, d = days, T0 = immediately processed sample

### Preclinical application of the method

This bioanalytical assay was used to support preclinical *in vitro* and *in vivo* studies of milciclib. Figure 3 C-series depicts representative chromatograms of samples generated in these preclinical studies. The *in vivo* studies aimed to assess the pharmacokinetics of milciclib in mice. As an example, the results obtained for the wild-type mouse strain are presented (Figure 4). The semi-log plasma concentration-time curve of milciclib is presented in Figure 4A, where the time to reach the maximum concentration ( $T_{max}$ ) ranged from 1-8 h and the mean maximum concentration ( $C_{max}$ ) was  $624 \pm 68$  ng/mL. The mean area under the plasma concentration-time curve ( $AUC_{0-24h}$ ) of milciclib was  $7094 \pm 122$  h·ng/mL, due to the lack of points in the terminal phase, the half-life could only be determined in 4 mice, with a mean of  $2.75 \pm 0.13$  h. Milciclib concentration in tissues was calculated in ng/g (Figure 4B), considering the measured concentration in the homogenates, the volume of BSA added to prepare the homogenate and the tissues weight. To determine the tissue distribution of this compound, the tissue-to-plasma concentrations ratios were calculated and presented in Figure 4C, where at 24 h milciclib was poorly distributed in brain, compared to the other tissues. Milciclib was also less distributed in kidneys with respect to liver, small intestine and spleen. All these measured samples were within the calibration range and show that this bioanalytical assay is applicable in preclinical studies of milciclib.

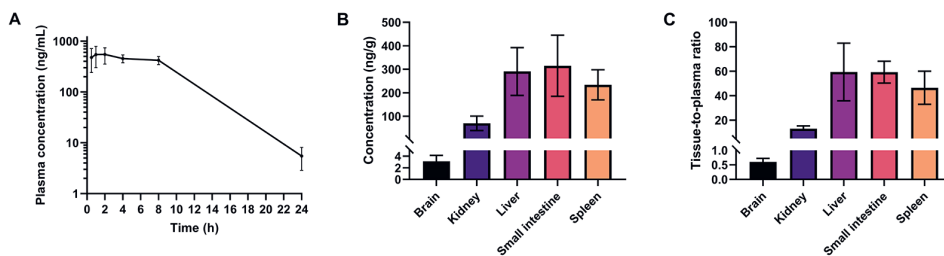


**Figure 4.** Semilog plasma concentration-time curve (A), concentration in tissues (B) and tissue-to-plasma ratio (C) of milliclib over 24 h after oral administration of 10 mg/kg to female FVB mice ( $n = 6$ ). Data are presented as mean  $\pm$  SD.

## Conclusions

The first LC-MS/MS bioanalytical assay for the analysis of milliclib in several matrices was developed and validated following the FDA and EMA guidelines. This method was linear in the calibration range from 1 to 1000 ng/mL, and shown to be selective, accurate and precise for the quantification of milliclib in human plasma, mouse plasma, mouse tissue homogenates, and tissue culture medium. Ten-fold dilution of samples with concentrations above the ULOQ is appropriate for the measurement. Samples in tissue culture medium require special treatment, since a dilution 1:1 (v/v) in human plasma is needed to have an acceptable accuracy and precision. Furthermore, as final extracts of tissue culture medium samples should not be kept at cold temperatures, it is recommended to maintain the autosampler at 20 °C. The use of human plasma as a surrogate matrix to quantify milliclib in tissue culture medium and mouse matrices resulted in acceptable accuracy. To assure stability of milliclib in all tissue homogenates, samples must be stored at -70 °C and processed within 4 h, except brain samples which must be processed within 2 h. Samples in tissue culture medium must be processed immediately to avoid any degradation at room temperature. Plasma samples can be stored at -20 °C. This method has been successfully used to support preclinical studies of milliclib.

## Acknowledgements

The authors acknowledge Lotte van Anandel for the revision of the data generated in this study.

## References

- [1] J. Bai, Y. Li, G. Zhang, Cell cycle regulation and anticancer drug discovery, *Cancer Biol. Med.* 14 (2017) 348–362. <https://doi.org/10.20892/j.issn.2095-3941.2017.0033>.
- [2] Malínková, J. Vylíčil, V. Kryštof, Cyclin-dependent kinase inhibitors for cancer therapy: a patent review (2009 – 2014), *Expert Opin. Ther. Pat.* 25 (2015) 953–970. <https://doi.org/10.1517/13543776.2015.1045414>.
- [3] C. Sánchez-Martínez, M.J. Lallena, S.G. Sanfeliciano, A. de Dios, Cyclin dependent kinase (CDK) inhibitors as anticancer drugs: Recent advances (2015–2019), *Bioorganic Med. Chem. Lett.* 29 (2019). <https://doi.org/10.1016/j.bmcl.2019.126637>.
- [4] M.G. Brasca, N. Amboldi, D. Ballinari, A. Cameron, E. Casale, G. Cervi, M. Colombo, F. Colotta, V. Croci, R. D'Alessio, F. Fiorentini, A. Isacchi, C. Mercurio, W. Moretti, A. Panzeri, W. Pastori, P. Pevarello, F. Quartieri, F. Roletto, G. Traquandi, P. Vianello, A. Vulpetti, M. Ciomei, Identification of N,1,4,4-tetramethyl-8-[[4-(4-methylpiperazin-1-yl)phenyl] amino]-4,5-dihydro-1H-pyrazolo[4,3-h]quinazoline-3-carboxamide (PHA-848125), a potent, orally available cyclin dependent kinase inhibitor, *J. Med. Chem.* (2009). <https://doi.org/10.1021/jm9006559>.
- [5] I.E. Demir, E. Tieftrunk, S. Schorn, H. Friess, G.O. Ceyhan, Nerve growth factor & TrkA as novel therapeutic targets in cancer, *Biochim. Biophys. Acta - Rev. Cancer.* 1866 (2016) 37–50. <https://doi.org/10.1016/j.bbcan.2016.05.003>.
- [6] A. Jindal, A. Thadi, K. Shailubhai, Hepatocellular Carcinoma: Etiology and Current and Future Drugs, *J. Clin. Exp. Hepatol.* 9 (2019) 221–232. <https://doi.org/10.1016/j.jceh.2019.01.004>.
- [7] C. Ghezzi, A. Wong, B.Y. Chen, B. Ribalet, R. Damoiseaux, P.M. Clark, A high-throughput screen identifies that CDK7 activates glucose consumption in lung cancer cells, *Nat. Commun.* 10 (2019) 1–15. <https://doi.org/10.1038/s41467-019-13334-8>.
- [8] C. Albanese, R. Alzani, N. Amboldi, A. Degrassi, C. Festuccia, F. Fiorentini, G.L. Gravina, C. Mercurio, W. Pastori, M.G. Brasca, E. Pesenti, A. Galvani, M. Ciomei, Anti-tumour efficacy on glioma models of PHA-848125, a multi-kinase inhibitor able to cross the blood-brain barrier, *Br. J. Pharmacol.* 169 (2013) 156–166. <https://doi.org/10.1111/bph.12112>.
- [9] S. Bolin, A. Borgenvik, C.U. Persson, A. Sundström, J. Qi, J.E. Bradner, W.A. Weiss, Y.J. Cho, H. Weishaupt, F.J. Swartling, Combined BET bromodomain and CDK2 inhibition in MYC-driven medulloblastoma, *Oncogene.* 37 (2018) 2850–2862. <https://doi.org/10.1038/s41388-018-0135-1>.
- [10] A. Degrassi, M. Russo, C. Nanni, V. Patton, R. Alzani, A.M. Giusti, S. Fanti, M. Ciomei, E. Pesenti, G. Texido, Efficacy of PHA-848125, a cyclin-dependent kinase inhibitor, on the K-RasG12DLA2 lung adenocarcinoma transgenic mouse model: Evaluation by multimodality imaging, *Mol. Cancer Ther.* 9 (2010) 673–681. <https://doi.org/10.1158/1535-7163.MCT-09-0726>.
- [11] C. Albanese, R. Alzani, N. Amboldi, N. Avanzi, D. Ballinari, M.G. Brasca, C. Festuccia, F. Fiorentini, G. Locatelli, W. Pastori, V. Patton, F. Roletto, F. Colotta, A. Galvani, A. Isacchi, J. Moll, E. Pesenti, C. Mercurio, M. Ciomei, Dual targeting of CDK and tropomyosin receptor kinase families by the oral inhibitor PHA-848125, an agent with broad-spectrum antitumor efficacy, *Mol. Cancer Ther.* 9 (2010) 2243–2254. <https://doi.org/10.1158/1535-7163.MCT-10-0190>.
- [12] G.J. Weiss, M. Hidalgo, M.J. Borad, D. Laheru, R. Tibes, R.K. Ramanathan, L. Blaydorn, G. Jameson, A. Jimeno, J.D. Isaacs, A. Scaburri, M.A. Pacciarini, F. Fiorentini, M. Ciomei, D.D. Von Hoff, Phase I study of the safety, tolerability and pharmacokinetics of PHA-848125AC, a dual tropomyosin receptor kinase A and cyclin-dependent kinase inhibitor, in patients with advanced solid malignancies, *Invest. New Drugs.* (2012). <https://doi.org/10.1007/s10637-011-9774-6>.
- [13] B. Besse, M.C. Garassino, A. Rajan, S. Novello, J. Mazieres, G.J. Weiss, D.M. Kocs, J.M. Barnett, C. Davite, P. Crivori, G. Giaccone, Efficacy of miliciclib (PHA-848125AC), a pan-cyclin d-dependent kinase inhibitor, in



two phase II studies with thymic carcinoma (TC) and B3 thymoma (B3T) patients., *J. Clin. Oncol.* 36 (2018) 8519–8519. [https://doi.org/10.1200/jco.2018.36.15\\_suppl.8519](https://doi.org/10.1200/jco.2018.36.15_suppl.8519).

- [14] S. Aspeslagh, K. Shailubhai, R. Bahleda, A. Gazzah, A. Varga, A. Hollebecque, C. Massard, A. Spreafico, M. Reni, J.C. Soria, Phase I dose-escalation study of milciclib in combination with gemcitabine in patients with refractory solid tumors, *Cancer Chemother. Pharmacol.* 79 (2017) 1257–1265. <https://doi.org/10.1007/s00280-017-3303-z>.
- [15] U.S. National Library of Medicine, *ClinicalTrials.gov*, Natl. Institutes Heal. (2020).
- [16] European Medicines Agency, Guideline on bioanalytical method validation, 44 (2012) 1–23. [https://www.ema.europa.eu/documents/scientific-guideline/guideline-bioanalytical-method-validation\\_en.pdf](https://www.ema.europa.eu/documents/scientific-guideline/guideline-bioanalytical-method-validation_en.pdf).
- [17] US Food and Drug Administration, Guidance for Industry Bioanalytical Method Validation, (2018) 1–22. <https://www.fda.gov/files/drugs/published/Bioanalytical-Method-Validation-Guidance-for-Industry.pdf>.
- [18] A. Martínez-Chávez, H. Rosing, M. Hillebrand, M. Tibben, A.H. Schinkel, J.H. Beijnen, Development and validation of a bioanalytical method for the quantification of the CDK4/6 inhibitors abemaciclib, palbociclib and ribociclib in human and mouse matrices using liquid chromatography-tandem mass spectrometry, *Anal. Bioanal. Chem.* 411 (2019) 5531–5345. <https://doi.org/10.1007/s00216-019-01932-w>.



# 4

## Bioanalytical method for the simultaneous quantification of irinotecan and its active metabolite SN-38 in mouse plasma and tissue homogenates using HPLC-fluorescence

Journal of Chromatography B 2020, 1149: 122177

Alejandra Martínez-Chávez  
Hilde Rosing  
Changpei Gan  
Yaogeng Wang  
Alfred H. Schinkel  
Jos H. Beijnen

## Abstract

A simple and rapid bioanalytical method was developed for the simultaneous quantification of irinotecan and SN-38 in mouse plasma and tissue homogenates using High-Performance Liquid Chromatography with Fluorescence detection (HPLC-FL). Camptothecin was used as internal standard and protein precipitation with acetonitrile-methanol (1:1, v/v) followed by acidification with 0.5 M hydrochloric acid was used for sample pre-treatment. The analytes and the internal standard were detected using an excitation and emission wavelength of 368 and 515 nm, respectively. The linearity, selectivity, accuracy and precision, carry-over, limit of detection and lower limit of quantification of the method are described. The method was linear from 7.5 to 1500 ng/mL for irinotecan and from 5 to 1000 ng/mL for SN-38. For all matrices, the accuracy bias and precision variation were within  $\pm 15\%$  and  $\leq 15\%$ , respectively. This method was successfully applied to study the pharmacokinetics of irinotecan and SN-38 using *in vivo* mouse models.

## Introduction

Irinotecan (CPT-11) is an antineoplastic agent indicated to treat metastatic colorectal, pancreatic, ovarian, small and non-small cell lung cancer. [1,2]. Irinotecan is the prodrug of SN-38, which binds to topoisomerase I, producing double-strand breaks in DNA and, therefore, causing cell death. Irinotecan is metabolized into SN-38 mainly by Carboxylesterase (CES) enzymes: CES1, which is strongly expressed in lung and liver, and CES2, mostly expressed in small intestine and kidneys [1,3,4]. Since the CES activity is related to irinotecan efficacy, it is important to clarify the role of each isoenzyme in the irinotecan metabolism.

In addition to predicting the efficacy, safety and toxicity, the quantitative analysis of irinotecan and SN-38 in plasma and tissue homogenates is essential to support either clinical or preclinical studies that provide more insights about this metabolic conversion. Some bioanalytical methods using LC-MS/MS or UHPLC-MS/MS have been described to quantify irinotecan and SN-38 in mouse plasma and tissue homogenates [5–7]. However, their major disadvantage is the necessity of a mass spectrometer, which is more expensive and delicate compared to other detectors. Additionally, the use of a stable isotope of the analyte is needed as an internal standard to correct for the variation in the detector. Despite the popularity of MS/MS detection in bioanalysis, fluorescence (FL) also offers a robust, highly selective, and sensitive detection, as well as fewer problems with instrument instability. In the past years, several bioanalytical assays using a fluorescence detection have been described for irinotecan and/or SN-38 in plasma of different species, but not in tissue homogenates [8–10].

The objective of this work is focused on the development and validation of a simple bioanalytical method using HPLC-FL to quantify simultaneously irinotecan and SN-38 in mouse plasma and tissue homogenates, including liver, kidney, lung, spleen, small intestine, and colon. This method was specifically set up to support preclinical pharmacokinetic experiments focused on the study of the metabolism of irinotecan by the CES enzymes and was applied to measure samples from mouse strains with different expression of these enzymes.

## Materials and methods

### Chemicals and reagents

Irinotecan HCl, SN-38 and camptothecin were obtained from Sigma Aldrich (Darmstadt, Germany). Dimethylsulfoxide (DMSO, SeccoSolv), hydrochloric acid, ammonium acetate and acetic acid glacial (all EMSURE® grade) were from Merck (Darmstadt, Germany). Water (LC-MS grade), acetonitrile (MeCN) and methanol (both HPLC supragradient) were provided by Biosolve Ltd (Valkenswaard, The Netherlands).

Control human K<sub>2</sub>EDTA plasma originated from BioIVT (Hicksville, NY, USA). Mouse plasma and tissues (liver, kidneys, small intestine, colon, spleen, and lungs) were collected from the animal laboratory of the Netherlands Cancer Institute (Amsterdam, The Netherlands). Tissues were homogenized in the Fast Prep-24™ 5G (MP Biomedicals Inc, Santa Ana, California, USA) using 4% bovine serum albumin (BSA) in water. 3 mL of this solution was added to liver and small intestine, 2 mL to kidneys and lungs, and 1 mL to colon and spleen.

### **Stock and working solutions**

An independent stock solution from each analyte at 1 mg/mL in DMSO was used for the preparation of working solutions of calibration standards in the concentration range from 150 to 30,000 ng/mL and 100 to 20,000 ng/mL for irinotecan and SN-38, respectively. A second stock solution from each analyte (1 mg/mL in DMSO) was used for the working solutions of quality control samples, which were prepared at 450, 3000 and 20,000 ng/mL for irinotecan, and at 300, 2000 and 15,000 ng/mL for SN-38. All working solutions were prepared in water-MeCN (1:1, v/v).

### **Calibration standards and quality control samples**

Six non-zero calibration standards were prepared in the range from 7.5 to 1500 ng/mL for irinotecan and from 5 to 1000 ng/mL for SN-38, by diluting working solutions 20-fold with control human plasma. A blank (control matrix spiked with IS) and a double blank (control matrix) were also prepared.

Quality control samples were prepared at three concentration levels: low (QC L), medium (QC M) and high (QC H), by diluting 20-fold the correspondent working solutions in control human plasma, resulting in concentrations of 22.5, 150 and 1000 ng/mL for irinotecan, and 15, 100 and 750 ng/mL for SN-38.

### **Internal standard**

Camptothecin (CPT), a molecule with an analogue structure, was used as an internal standard (IS) and dissolved in DMSO to prepare a stock solution of 50 µg/mL. It was further diluted up to 100 ng/mL with MeCN-MeOH (1:1 v/v) for the working solution.

### **Sample pretreatment**

For plasma samples an aliquot of 50 µL was used for the pretreatment, then 100 µL of the working solution of the internal standard was added followed by 100 µL of MeCN-MeOH (1:1 v/v), except for the double blanks to which 200 µL of MeCN-MeOH (1:1 v/v) was added. For tissue homogenate samples (prepared as described in "Chemical and reagents" section) an aliquot of 100 µL was used for the pretreatment and the reagents were added in the same ratio as explained above. After vortex mixing and centrifugation of the samples (23,100 g and 4 °C for 10 minutes), 100 µL of supernatant was acidified with 10 µL of 0.5 M HCl. Subsequently, samples were vortex

mixed again and transferred to a vial. 10  $\mu\text{L}$  of the final extract was injected into the HPLC-FL system for analysis.

### HPLC-FL system

An Agilent 1100 chromatograph (Palo Alto, CA, USA) was used, which consisted of a binary pump, a degasser, an autosampler and a column oven (Models G1312A, G1379A, G1367A, G1316A, respectively). To achieve the chromatographic separation, a Zorbax SB C18 column (150 x 2.1 mm ID, 5 $\mu\text{m}$ ) protected by a C18 (4 x 2 mm) guard column (Phenomenex, Torrance, CA, USA) was used. Analytes were eluted using 20 mM ammonium acetate in water pH 3.5 (eluent A) and acetonitrile (eluent B) at a flow rate of 0.3 mL/min. A modified gradient program from Guo *et al.* was used for the elution of the analytes: initially eluent B was kept at 25% for 2.7 min, in 2.3 min B increased to 29%, in 2 min B increased to 66%, in 1 min B increased to 90%, and it was kept for 0.5 min. At 8.5 min, B decreased from 90% to the initial conditions (25%) in 0.5 min, and it was maintained for 3 min to condition the analytical column [11]. The temperatures of the autosampler and oven were set at 6 and 35 °C, respectively. The Jasco FP-920 E fluorescence detector (Easton, Maryland, USA) with a 16  $\mu\text{L}$  flow cell was used to monitor the analytes and the internal standard with the following settings: the emission band width was set at 40 nm, for the filter response settings a CR (analog) filter was selected with a slow (SLW) response, and a gain of 100 was selected. The excitation and emission wavelengths were, respectively, 368 and 515 nm to detect irinotecan, SN-38 and CPT.

### Method validation

A partial validation of the method was performed, where the linearity, limit of detection (LOD), lower limit of quantification (LLOQ), selectivity, carry-over, accuracy and precision were evaluated.

Linearity was determined using the 6 non-zero calibration standards prepared as described in 2.4, which were prepared and analyzed in duplicate in at least three analytical runs. The concentration-response correlation for both analytes was described using a linear regression with a 1/x weighting factor ( $x$  = analyte concentration).

To determine the selectivity, at least one batch from each blank matrix was evaluated for interferences at the analytes and IS retention times. LOD and LLOQ were determined based on the signal-to-noise ratio.

Carry-over was tested in at least three analytical runs, where two double blank samples were injected after the upper limit of quantification (ULOQ). The response obtained at the retention time of each analyte in the double blanks was compared to the LLOQ response of each analyte.

Intra- and inter-assay accuracy and precision were evaluated in control human plasma at three concentration levels (QC L, QC M and QC H). For mouse matrices, accuracy and precision was tested in one day at one concentration level 300 and 200 ng/mL for irinotecan and SN-38, respectively. These spiked samples were quantified using calibration standards in human plasma. The bias between the nominal and measured concentrations within- and between-run was determined to evaluate the accuracy. ANOVA was used to determine the within- and between-run precision of the method at each concentration level according to the following formulas:

$$\text{Within-run precision} = \frac{\sqrt{MS_W}}{M} \times 100 \%$$

$$\text{Between-run precision} = \frac{\sqrt{\frac{MS_B - MS_W}{n}}}{M} \times 100 \%$$

where,  $MS_W$  is the within-run mean square,  $MS_B$  is the between-run mean square,  $M$  is the mean of all measured concentrations, and  $n$  is the number of determinations per group [12].

### **Applicability of the method**

This method was developed to support preclinical investigation of the irinotecan conversion into SN-38 by CES enzymes in mouse models (unpublished data). Animal housing and mouse studies were conducted according to institutional guidelines complying with Dutch and European Union legislation. All experiments were approved by the institutional board for the care and use of laboratory animals. Irinotecan HCl trihydrate was intravenously or orally administered at a dose of 20 mg/kg. After intravenous administration of irinotecan, blood was collected from the tip of the tail at several time points (0.125, 0.25, 0.5, 1 and 2 h) in heparin-coated tubes. Prior the last time point at 4 h, mice were anaesthetized with isoflurane, and blood was collected by cardiac puncture. In a separate experiment, irinotecan was orally administered to mice; prior to organ collection, mice were sacrificed by cervical dislocation and the tissues (liver, kidneys, small intestine, colon, spleen and lungs) were collected and weighed. Tissues were homogenized as described in 2.1. Blood samples were centrifuged (9000g, 4 °C, for 6 min) to obtain plasma. To complete the volume needed for the sample pretreatment, 10 µL of mouse plasma was diluted with 40 µL of control human plasma, when necessary.



## Results and discussion

### HPLC-FL method development

Irinotecan and SN-38 are determined in this bioanalytical method after acidifying the final extract with 0.5 M HCl to favor the conversion to the lactone ring. Irinotecan and SN-38 molecules have a lactone ring which can be reversibly hydrolyzed into a carboxylate form (Figure 1). This hydrolysis depends mainly on pH: at pH < 5 the lactone form is favored, while at pH > 9 the carboxylate form is formed [2,13,14]. Only the lactone form can bind the topoisomerase I, however, it has been previously described that the quantification of the lactone and carboxylate forms (total irinotecan and SN-38), is as clinically relevant as the quantification of the lactone form, since the pharmacokinetics of both forms is correlated [2,15,16].

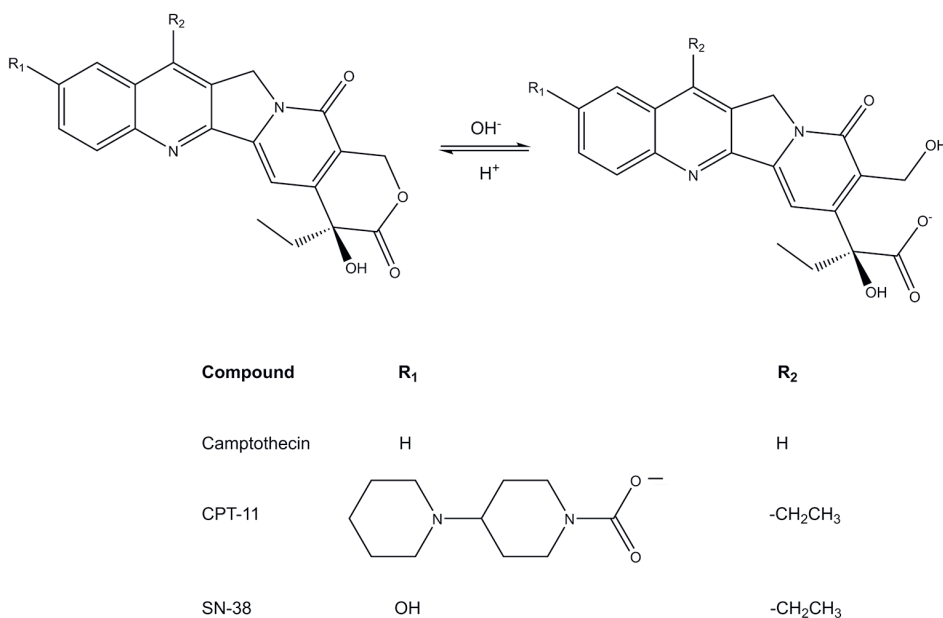


**Figure 1.** Chemical structures (lactone and carboxylate forms) of irinotecan (CPT-11), SN-38 and camptothecin.

### Method validation

The typical chromatograms obtained after spiking the analytes and internal standard in human plasma at the lower and upper limit of quantification are shown in Figure 2 (A and B, respectively). The resolution between the peaks was always > 2.5 between irinotecan and SN-38 and > 1.5 between SN-38 and camptothecin.

The selectivity of the method was evaluated in all the previously described matrices. In Figure 2 C-J the chromatograms obtained with blank matrices are shown, where no interferences were observed at the retention times of the analytes. The method was selective for all the matrices tested, since no peaks were detected at the retention times of the analytes.

The LOD and the LLOQ for irinotecan were 1.3 and 7.5 ng/mL, respectively, and for SN-38 1.7 and 5 ng/mL, respectively. Both parameters were estimated based on the signal-to-noise ratio (S/N) for each analyte. The LOD was calculated considering a S/N  $\geq 3$  and the LLOQ was selected considering a S/N of at least  $\geq 5$ ; for both analytes the bias of the back-calculated concentration was within  $\pm 20\%$  of the nominal concentrations.

The calibration range for irinotecan and SN-38 was selected as wide as possible due to the high variability in the study samples. It was limited by the capacity of the fluorescence detector, which is based on the S/N ratio for the LLOQ and the signal saturation for the irinotecan ULOQ. The calibration curves for both analytes were linear using a weighting factor of  $1/x$  in the range of 7.5-1500 ng/mL for irinotecan and 5-1000 ng/mL for SN-38. The correlation coefficient of the calibration model was 0.9988 for irinotecan and 0.9993 for SN-38.

No peak was detected in the double blank samples injected after the ULOQ, neither for irinotecan nor for SN-38, therefore there was not carry-over for the established concentration ranges.

**Table 1.** Intra- and inter-assay precision and accuracy for irinotecan and SN-38 in human plasma

Analyte	Nominal concentration (ng/mL)	Intra-assay (n = 3)		Inter-assay (n = 25 in 10 analytical batches)	
		Accuracy (% Bias)	Precision (% CV)	Accuracy (% Bias)	Precision (% CV)
Irinotecan	22.5	-3.2	3.3	-8.3	4.5
	150	4.6	2.8	-7.7	6.3
	1000	2.0	2.8	-0.8	2.2
SN-38	15	-4.0	5.0	-4.8	1.8
	100	0.9	1.4	-5.7	3.8
	750	2.8	1.5	-0.4	2.6

The intra- and inter-assay accuracy and precision of this method is shown in Table 2, where the bias and the coefficient of variation were within  $\pm 15\%$  and  $\leq 15\%$ , respectively for both analytes. The accuracy and precision obtained for the mouse matrices are summarized in Table 3, where all the results met the criteria previously mentioned. Prior experiments indicate that approximately 85.8% of irinotecan and 102% of SN-38 are recovered after processing human plasma samples with the described sample pre-treatment at concentrations within the calibration range.

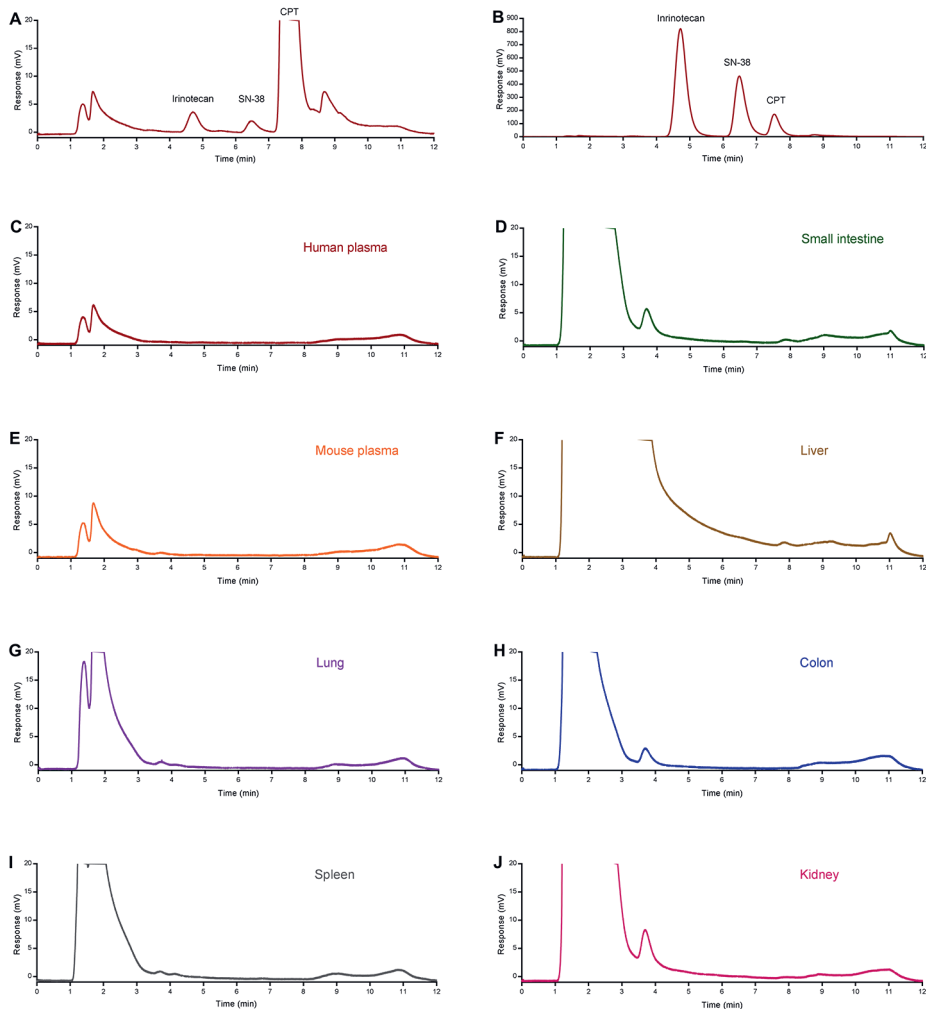


**Figure 2.** Representative chromatograms of human plasma spiked with irinotecan, SN-38 and the internal standard at the LLOQ (A) and ULOQ (B). Chromatograms obtained after processing blank samples from different matrices (C-J).

**Table 2.** Accuracy and precision in mouse matrices (n = 3, one analytical batch)

Matrix	Irinotecan (nominal concentration 300 ng/mL)		SN-38 (nominal concentration 200 ng/mL)	
	Accuracy (% Bias)	Precision (% CV)	Accuracy (% Bias)	Precision (% CV)
Mouse plasma	13.5	1.5	3.7	0.7
Liver homogenate	-1.5	2.5	3.6	0.7
Kidney homogenate	0.2	0.3	4.1	0.9
Spleen homogenate	8.6	0.9	6.8	2.3
Small intestine homogenate	7.5	3.1	2.6	1.4
Colon homogenate	10.5	5.0	5.2	5.8
Lung homogenate	10.6	1.4	4.3	0.6

### Application of the method

This bioanalytical method developed was used to support *in vivo* studies of the conversion of irinotecan into SN-38 by CES enzymes. Figure 3 shows the measured concentrations in each matrix. Plasma samples were diluted 1:5 (v/v) to complete the sample volume required for the pre-treatment. The calibration ranges included for mouse plasma are corrected for this dilution factor (Figure 3A, B). Figures 3C and D show the measured concentrations in each tissue homogenate for irinotecan and SN-38, respectively. Most of the measured samples fit in the calibration range for both compounds. Irinotecan was abundant in liver and small intestine homogenate samples, in some of them the concentration of irinotecan was above the ULOQ, where it was necessary to dilute the samples to properly quantify it. Lung homogenates showed low concentrations for irinotecan, where 30% of the samples were below the LLOQ and above the LOD, and 25% were below the LOD. For SN-38, none of the samples exceeded the ULOQ. For most matrices the concentration of SN-38 was within the calibration range, except for lung and spleen homogenates, where SN-38 had a very low distribution and this was reflected in the negligible measured concentrations (Figure 3D). For the other matrices there was a high difference in SN-38 concentration among the measured samples (Figure 3D), showing that this method is useful for either normal or negligible conversion of irinotecan into SN-38.

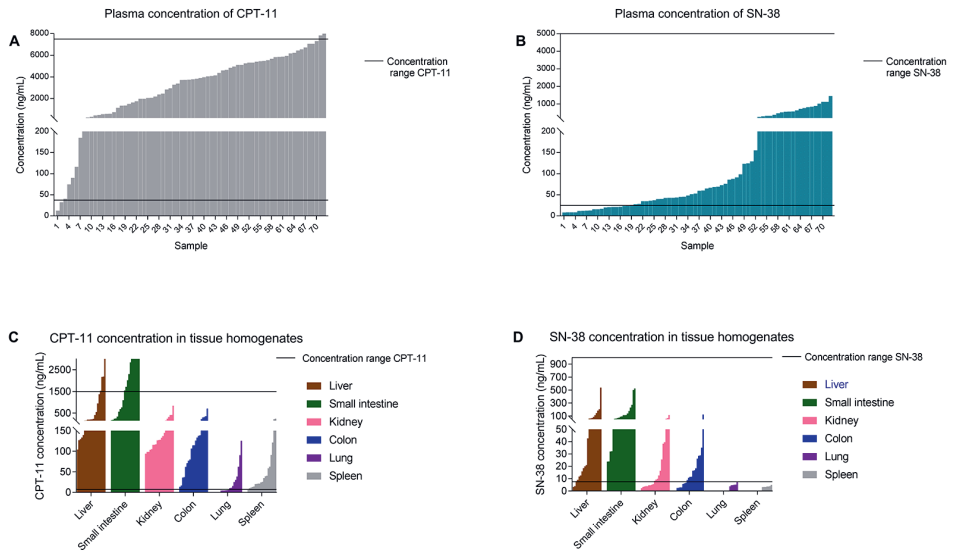


**Figure 3.** Measured concentrations of irinotecan (CPT-11) and SN-38 (ng/mL) in mouse plasma samples (A-B), and tissue homogenates (C-D). The concentration range of the bioanalytical method is indicated in the graphs with a black line; for plasma samples the dilution factor (5x) is considered in the indicated range.

## Conclusions

A bioanalytical assay for irinotecan and SN-38 in plasma and tissue homogenates using HPLC-FL is described. We showed that this method is linear, accurate, precise, selective and sensitive to simultaneously measure the total irinotecan and SN-38 in mouse plasma and tissue homogenate samples using human plasma as a surrogate matrix. This method was successfully applied to study the conversion of irinotecan into SN-38 *in vivo*.

## References

- [1] F.M. de Man, A.K.L. Goey, R.H.N. van Schaik, R.H.J. Mathijssen, S. Bins, Individualization of Irinotecan Treatment: A Review of Pharmacokinetics, Pharmacodynamics, and Pharmacogenetics, *Clin. Pharmacokinet.* (2018). <https://doi.org/10.1007/s40262-018-0644-7>.
- [2] R. Mullangi, P. Ahlawat, N.R. Srinivas, Irinotecan and its active metabolite, SN-38: Review of bioanalytical methods and recent update from clinical pharmacology perspectives, *Biomed. Chromatogr.* 24 (2010) 104–123. <https://doi.org/10.1002/bmc.1345>.
- [3] T. Satoh, M. Hosokawa, Carboxylesterases: Structure, function and polymorphism, *Biomol. Ther.* 17 (2009) 335–347. <https://doi.org/10.4062/biomolther.2009.17.4.335>.
- [4] R. Humerickhouse, K. Lohrbach, L. Li, W.F. Bosron, M.E. Dolan, Characterization of CPT-11 hydrolysis by human liver carboxylesterase isoforms hCE-1 and hCE-2, *Cancer Res.* 60 (2000) 1189–1192.
- [5] S. Bardin, W. Guo, J.L. Johnson, S. Khan, A. Ahmad, J.X. Duggan, J. Ayoub, I. Ahmad, Liquid chromatographic-tandem mass spectrometric assay for the simultaneous quantification of Camptosar® and its metabolite SN-38 in mouse plasma and tissues, *J. Chromatogr. A.* 1073 (2005) 249–255. <https://doi.org/10.1016/j.chroma.2004.08.060>.
- [6] S. Basu, M. Zeng, T. Yin, S. Gao, M. Hu, Development and validation of an UPLC-MS/MS method for the quantification of irinotecan, SN-38 and SN-38 glucuronide in plasma, urine, feces, liver and kidney: Application to a pharmacokinetic study of irinotecan in rats, *J. Chromatogr. B Anal. Technol. Biomed. Life Sci.* 1015–1016 (2016) 34–41. <https://doi.org/10.1016/j.jchromb.2016.02.012>.
- [7] S. Khan, A. Ahmad, W. Guo, Y.F. Wang, A. Abu-Qare, I. Ahmad, A simple and sensitive LC/MS/MS assay for 7-ethyl-10-hydroxycamptothecin (SN-38) in mouse plasma and tissues: Application to pharmacokinetic study of liposome entrapped SN-38 (LE-SN38), *J. Pharm. Biomed. Anal.* 37 (2005) 135–142. <https://doi.org/10.1016/j.jpba.2004.09.053>.
- [8] N. Taneja, V. Gota, M. Gurjar, K.K. Singh, Development and validation of high-performance liquid chromatographic method for quantification of irinotecan and its active metabolite SN-38 in colon tumor bearing NOD/SCID mice plasma samples: Application to pharmacokinetic study, *Acta Chromatogr.* 31 (2019) 166–172. <https://doi.org/10.1556/1326.2018.00370>.
- [9] F. D'Esposito, B.N. Tattam, I. Ramzan, M. Murray, A liquid chromatography/electrospray ionization mass spectrometry (LC-MS/MS) assay for the determination of irinotecan (CPT-11) and its two major metabolites in human liver microsomal incubations and human plasma samples, *J. Chromatogr. B Anal. Technol. Biomed. Life Sci.* 875 (2008) 522–530. <https://doi.org/10.1016/j.jchromb.2008.10.011>.
- [10] X. Yang, Z. Hu, Y.C. Sui, B.C. Goh, W. Duan, E. Chan, S. Zhou, Simultaneous determination of the lactone and carboxylate forms of irinotecan (CPT-11) and its active metabolite SN-38 by high-performance liquid chromatography: Application to plasma pharmacokinetic studies in the rat, *J. Chromatogr. B Anal. Technol. Biomed. Life Sci.* 821 (2005) 221–228. <https://doi.org/10.1016/j.jchromb.2005.05.010>.
- [11] W. Guo, A. Ahmad, S. Khan, F. Dahhani, Y.F. Wang, I. Ahmad, Determination by liquid chromatography with fluorescence detection of total 7-ethyl-10-hydroxy-camptothecin ( SN-38 ) in beagle dog plasma after intravenous administration of liposome-based SN-38 ( LE - SN38 ), *J. Chromatogr. B Anal. Technol. Biomed. Life Sci.* 791 (2003) 85–92. [https://doi.org/10.1016/S1570-0232\(03\)00210-1](https://doi.org/10.1016/S1570-0232(03)00210-1).
- [12] H. Rosing, M.J.X. Hillebrand, J.M. Jimeno, A. Gómez, P. Floriano, G. Faircloth, L. Cameron, R.E.C. Henrar, J.B. Vermorken, A. Bult, J.H. Beijnen, Analysis of ecteinascidin 743, a new potent marine-derived anticancer drug, in human plasma by high-performance liquid chromatography in combination with solid-phase extraction, *J. Chromatogr. B Biomed. Appl.* 710 (1998) 183–189. [https://doi.org/10.1016/S0378-4347\(98\)00143-1](https://doi.org/10.1016/S0378-4347(98)00143-1).
- [13] J. Fassberg, V.J. Stella, A Kinetic and Mechanistic Study of the Hydrolysis of Camptothecin and Some Analogues, *J. Pharm. Sci.* 81 (1992) 676–684.

- [14] G. Boyd, J.F. Smyth, D.I. Jodrell, J. Cummings, High-Performance Liquid Chromatographic Technique for the Simultaneous Determination of Lactone and Hydroxy Acid Forms of Camptothecin and SN-38 in Tissue Culture Media and Cancer Cells, *Anal. Biochem.* 297 (2001) 15–24. <https://doi.org/10.1006/abio.2001.5317>.
- [15] L.P. Rivory, E. Chatelut, P. Canal, A. Mathieu-Boué, J. Robert, Kinetics of the in Vivo Interconversion of the Carboxylate and Lactone Forms of Irinotecan (CPT-11) and of Its Metabolite SN-38 in Patients, *Cancer Res.* 54 (1994) 6330–6333. [https://doi.org/10.1016/0959-8049\(95\)96205-R](https://doi.org/10.1016/0959-8049(95)96205-R).
- [16] L.P. Rivory, J. Robert, Reversed-phase high-performance liquid chromatographic method for the simultaneous quantitation of the carboxylate and lactone forms of the camptothecin derivative irinotecan, CPT-11, and its metabolite SN-38 in plasma, *J. Chromatogr. B Biomed. Sci. Appl.* 661 (1994) 133–141. [https://doi.org/10.1016/0378-4347\(94\)00340-8](https://doi.org/10.1016/0378-4347(94)00340-8).





## **PART II**

The impact of drug transporters and drug-metabolizing enzymes on the pharmacokinetics of the cyclin-dependent kinase inhibitors



# 5

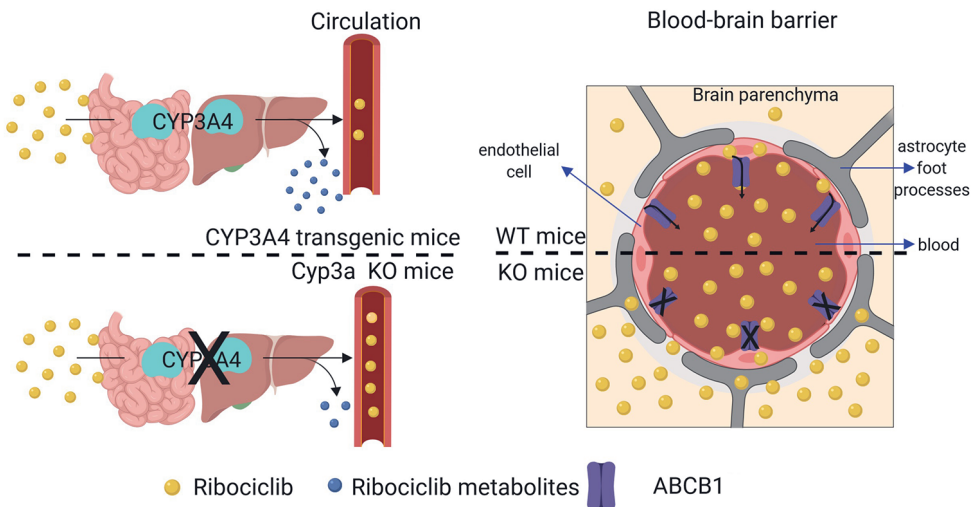
## P-glycoprotein limits ribociclib brain exposure and CYP3A4 restricts its oral bioavailability

Molecular Pharmaceutics 2019, 16: 3842-3852

Alejandra Martínez-Chávez  
Stéphanie van Hoppe  
Hilde Rosing  
Maria C. Lebre  
Matthijs M. Tibben  
Jos H. Beijnen  
Alfred H. Schinkel

## Abstract

Ribociclib is a CDK4/6 inhibitor recently approved for the treatment of some types of breast cancer in combination with an aromatase inhibitor. It is currently investigated in the clinic to treat other malignancies, including brain tumors. Using *in vitro* and genetically modified mouse models, we investigated the effect of the multidrug efflux transporters ABCB1 and ABCG2, and the drug-metabolizing CYP3A enzymes on ribociclib pharmacokinetics and tissue distribution. *In vitro*, ribociclib was avidly transported by human ABCB1, but not by human ABCG2 and only modestly by mouse *Abcg2*. Upon oral administration at 20 mg/kg, the plasma  $AUC_{0-24h}$  of ribociclib was increased by 2.3-fold, and its terminal elimination was delayed in *Abcb1a/1b<sup>-/-</sup>;Abcg2<sup>-/-</sup>* compared to wild-type mice. The brain-to-plasma ratios of ribociclib were increased by at least 23-fold relative to wild-type mice in *Abcb1a/1b<sup>-/-</sup>;Abcg2<sup>-/-</sup>* and *Abc1a/1b<sup>-/-</sup>* mice, but not noticeably in *Abcg2<sup>-/-</sup>* mice. Oral coadministration of elacridar, an ABCB1 and ABCG2 inhibitor, increased the brain penetration of ribociclib in wild-type mice to the same level as seen in *Abcb1a/1b<sup>-/-</sup>;Abcg2<sup>-/-</sup>* mice. Plasma exposure of ribociclib further decreased by 3.8-fold when transgenic human CYP3A4 was overexpressed in *Cyp3a*-deficient mice. Ribociclib penetration into the brain is thus drastically limited by ABCB1 in the blood-brain barrier, but coadministration of elacridar can fully reverse this process. Moreover, human CYP3A4 can extensively metabolize ribociclib and strongly restrict its oral bioavailability. The insights obtained from this study may be useful to further optimize the clinical application of ribociclib, especially for the treatment of (metastatic) brain tumors.



## Introduction

In recent years, a new class of compounds was successfully introduced in the clinic for breast cancer treatment. These are inhibitors of the cyclin-dependent kinases 4 and 6 (CDK4/6), enzymes that regulate cell cycle progression through the G1/S transition [1]. To date, three CDK4/6 inhibitors have been approved by the US Food and Drug Administration (FDA) and the European Medicines Agency (EMA): palbociclib (2015), ribociclib (2017) and abemaciclib (2017-2018). These compounds are registered for the treatment of advanced-stage and/or metastatic hormone receptor-positive (HR<sup>+</sup>) and HER2-negative (HER2<sup>-</sup>) breast cancer after menopause in combination with an aromatase inhibitor. Recently, the FDA expanded the indication for ribociclib to treat also pre/perimenopausal women with the above-mentioned subtypes of breast cancer [2].

Ribociclib (Supplementary Figure S1) is an orally bioavailable small molecule that binds to the ATP-binding cleft of CDK4/6, leading to the inhibition of these enzymes (IC<sub>50</sub> 10 and 39 nM, respectively). After a dosage of 600 mg/day in the clinic, ribociclib is rapidly absorbed with a maximum plasma concentration between 1-5 h, and a half-life that ranges from 33 to 42 h. In addition to breast cancer, the efficacy of ribociclib to treat other malignancies including melanoma, non-small cell lung cancer, liposarcoma, glioblastoma, gynecologic cancers, prostate cancer and others is currently investigated in clinical trials [3,4].

Drug disposition and therefore drug efficacy can be affected by the drug efflux transporters P-glycoprotein (P-gp; MDR1; ABCB1) and Breast Cancer Resistance Protein (BCRP; ABCG2), which belong to the ATP-binding cassette (ABC) superfamily [5]. These efflux transporters are expressed in the apical membrane of organs with absorptive and eliminatory functions, like intestine, liver and kidneys, as well as in various blood-tissue barriers, including the blood-brain barrier (BBB). Their function is to accelerate the elimination and limit the tissue penetration of xenobiotics, including drugs [5,6]. In addition, efficacy of transported anticancer agents can also be directly affected since both proteins can be expressed in some cancer cells. Indeed, several mechanisms involved in the upregulation of ABCB1 and/or ABCG2 in some cancer treatments have been described to be associated with multidrug resistance in breast cancer [7-9].

Many anticancer agents are transport substrates of ABCB1 and/or ABCG2. Specifically within the CDK4/6 inhibitors, abemaciclib and palbociclib are substrates for human ABCB1 and mouse *Abcg2*, and for both compounds the penetration of the BBB improves when *Abcb1a/1b* is absent in rodents. For palbociclib, it was shown that its brain penetration is also restricted by mouse *Abcg2* [10,11]. According to the manufacturer, ribociclib is a weak substrate for ABCB1, but Sorf *et al.* showed that ribociclib is markedly transported by human ABCB1 *in vitro* [12,13]. However, the *in vivo* effects of the ABC efflux transporters on ribociclib disposition have not been described hitherto.

In preclinical studies in rats, ribociclib distributed extensively to most tissues except for the brain [1]. Because ABCB1 and ABCG2 are expressed at the BBB, they could potentially limit the brain accumulation of ribociclib. Breast cancer can often metastasize to the brain, therefore it would be preferable to use an anticancer agent that can readily penetrate into the brain. As ribociclib is orally administered, ABCB1 and ABCG2 might also significantly impact on its oral bioavailability.

Similar to drug transporters, drug-metabolizing enzymes and their inter- and intraindividual variabilities can affect the therapeutic efficacy and safety of drugs, since they can lead to deactivation, either directly or by facilitating its excretion from the body, or to bioactivation to form active and/or toxic compounds. In humans, CYP3A isoenzymes comprise the largest portion of cytochrome P450 (CYP450) enzymes in the liver, where CYP3A4 is the most abundant [14,15]. Ribociclib is mainly hepatically metabolized through CYP3A4. Three circulating metabolites of ribociclib have been reported, including M13 (N-hydroxylation), M4 (N-demethylation) and M1 (secondary glucuronide), but their contribution to the clinical activity is negligible [3,12,16]. In a drug-drug interaction study (DDI) it was found that the CYP3A inhibitor ritonavir could substantially increase the plasma exposure of ribociclib [12,16]. Using defined *in vivo* models we wanted to study how ribociclib exposure is affected by CYP3A4. In this study, we aimed to investigate the interaction of ribociclib with the efflux transporters ABCB1 and ABCG2 *in vitro* as well as *in vivo*, in order to assess their effects on oral bioavailability and tissue accumulation of ribociclib. We also studied the effect of co-administration of the ABCB1 and ABCG2 inhibitor elacridar. Finally, we determined to what extent ribociclib oral bioavailability and tissue accumulation is affected by CYP3A.

## Materials and methods

### Drugs

Ribociclib free base was purchased from Alsachim (Illkirch-Graffenstaden, France). Zosuquidar free base was supplied by Sequoia Research Products (Pangbourne, UK). Ko143 was obtained from Tocris Bioscience (Bristol, UK), and elacridar free base from Carbosynth Limited (Berkshire, UK).

### *In vitro* transport assays

#### *Cell culture*

Parental Madin-Darby Canine Kidney (MDCK-II) cells and subclones transduced with human hABCB1 [17,18], hABCG2 [19], and mouse mAbcg2 [20] were cultured in DMEM glutamax (Gibco, Thermo Fisher Scientific, Waltham, MA), supplemented with 10% Fetal Bovine Serum F7524 (FBS, Sigma-Aldrich, Darmstadt, Germany) and 1% penicillin-streptomycin 10000 U/mL (Gibco) at 37 °C in 5% CO<sub>2</sub>. Cells were cultured for at least 2 weeks before the start of the transport assays, reaching a passage number of 15 for

the parental, 10 for the hABCB1, 14 for the hABCG2, and 11 for the mAbcg2 cell line when seeded in the Transwell supports.

#### *Transport assays*

Cell lines were seeded in 12-well Transwell® permeable supports (Corning Life Sciences, Tewksbury, MA) using inserts with 12 mm internal diameter polycarbonate membrane (3 µm pore size), at a density of  $2.5 \times 10^5$  cells per well. Cells were cultured for 3 days until a monolayer with tight junctions was formed. The tightness was evaluated by measuring the transepithelial electrical resistance (TEER). On day 3, cells were washed with Dulbecco's phosphate-buffered saline (DPBS, Gibco) prior to a 1 h pre-incubation with DMEM supplemented only with 10% FBS, and containing 5 µM zosuquidar (ABCB1 inhibitor) and/or 5 µM Ko143 (ABCG2 inhibitor), when appropriate. 5 µM of the inhibitors was selected to ensure complete inhibition of even avid substrates of the respective ABC transporters. Thereafter, this medium was replaced with FBS-supplemented DMEM in the acceptor compartment, and with 5 µM ribociclib in FBS-supplemented DMEM in the donor compartment. For the inhibition experiments, the appropriate inhibitor(s) were added to both compartments. The total volume in each compartment was 0.75 mL for the apical and 1.5 mL for the basolateral side. Transport assays were independently performed in either the apical-to-basolateral (AB) or the basolateral-to-apical direction (BA). Transwell plates were incubated at 37 °C in 5% CO<sub>2</sub>. At 1, 2, 4, and 8 h, 50 µL samples were taken from the acceptor compartment. Sample volumes were not replaced, and drug transport calculations were corrected for the change in volume and amount of removed drug. Monolayer integrity was assessed after the transport experiment by re-measuring the TEER. For all cell lines TEERs were above 95 Ohm.cm<sup>2</sup> before the start of the transport experiment, and they were not decreased when re-measured after 8 h at the end of the experiment. Inhibitor additions also did not negatively affect the TEER. Samples were stored at -20 °C until analysis.

#### *Sample measurement and calculations*

Ribociclib was quantified by liquid chromatography-tandem mass spectrometry (LC-MS/MS) using a modification of a previously described bioanalytical method [21]. A different concentration range was used (20 to 2500 ng/mL), and in order to maintain linearity within the new range the collision energy in the MS detector was decreased to 35 V for ribociclib and the injection volume was reduced to 1 µL. Calibration standards and quality control samples were prepared in FBS-supplemented DMEM. <sup>2</sup>H<sub>6</sub>-ribociclib (AlsaChim) was used as an internal standard and added to each sample prior to sample pretreatment. Proteins were precipitated with acetonitrile and after centrifugation (10 min, 23,100 g) the supernatant was injected into the LC-MS/MS system. A partial validation was performed after these changes. Linearity, selectivity, accuracy, precision, lower limit of quantification (LLOQ), carry-over, dilution integrity and stability were evaluated and found to be satisfactory according to international standards [22,23].

The amount of ribociclib transported at each time point was calculated. Active transport due to efflux transporters was expressed by the efflux ratio ( $r$ ), which is determined by the apparent permeability coefficient ( $P_{app}$ ) from basolateral-to-apical transported drug divided by the  $P_{app}$  from apical-to-basolateral translocated drug. 1000 pmol transport at 8 h corresponds to an approximate apparent permeability coefficient ( $P_{app}$ ) of  $6.2 \times 10^{-6}$  cm/s.

### ***In vivo* pharmacokinetics and tissue distribution of ribociclib**

#### *Animals*

Female (FVB) WT, *Abcb1a/1b*<sup>-/-</sup> [24], *Abcg2*<sup>-/-</sup> [20], *Abc1a/1b*<sup>-/-</sup>;*Abcg2*<sup>-/-</sup> [25], *Cyp3a*<sup>-/-</sup> [26], and *Cyp3aXAV* mice were used between 9-16 weeks of age. The homozygous CYP3A4-humanized transgenic mice (*Cyp3aXAV*, with CYP3A4 expression in both liver and intestine) were generated by cross-breeding of transgenic mice with stable human CYP3A4 expression in liver or intestine, respectively, in a *Cyp3a*<sup>-/-</sup> background [27]. Animals were housed in a temperature-controlled environment with a 12 h light and 12 h dark cycle. Food (Transbreed, SDS Diets, Technilab-BMI, Someren, The Netherlands) and acidified water were provided *ad libitum*. Mice were housed and handled according to institutional guidelines complying with Dutch and EU legislation. All experiments were reviewed and approved by the institutional animal care and use committee.

#### *Pharmacokinetic and tissue distribution experiments*

After at least 2 h of fasting, a dose of 20 mg/kg of ribociclib was orally administered, using a formulation containing 2 mg/mL of ribociclib in DMSO:Tween 80:10 mM HCl in water (5:5:90, v/v). Approximately 50  $\mu$ L of blood was collected from the tip of the tail in heparin-coated microvette® tubes (Sarstedt AG & Co., Nümbrecht, Germany) at 0.25, 0.5, 1, 3, and 8 h, or 0.25, 0.5, 1, 2, and 4 h, for the 24 and 8 h experiment, respectively. At either 8 or 24 h after administration, blood was collected by cardiac puncture under deep isoflurane anesthesia. The mice were then sacrificed by cervical dislocation and organs, including brain, liver, kidneys, spleen and small intestine (cleaned from fecal content) were collected and weighed. Plasma was obtained from blood samples after 6 minutes centrifugation at 9000g and 4°C.

Tissue homogenates were prepared using the Fast Prep-24™ 5G homogenizer (MP Biomedicals Inc, Santa Ana, CA). For this, Bovine Serum Albumin (BSA, Fraction V), obtained from Roche Diagnostics GmbH (Mannheim, Germany), was dissolved at a concentration of 4% (w/v) in distilled water (B Braun Medical, Melsungen, Germany). 3 mL of this solution was added to liver and small intestine, 2 mL to kidneys, and 1 mL to brain and spleen prior to the homogenization. All samples were stored at -20°C or -70°C until analysis.

#### *Effect of elacridar on ribociclib pharmacokinetics and brain accumulation*

After at least 2 h of fasting, vehicle or 50 mg/kg of elacridar were orally administered (5 mg/mL of elacridar in DMSO-cremophor EL-water (1:2:7, v/v)) to WT and



*Abcb1a/1b;Abcg2*<sup>-/-</sup> mice. Subsequently, after 15 minutes, 20 mg/kg of ribociclib was orally administered to each mouse. Blood samples were collected from the tip of the tail at 0.25, 0.5, 1 and 2 h. At the terminal time point (4 h), blood was collected by cardiac puncture under isoflurane anesthesia; brain and liver were collected and their homogenates were prepared as described above.

#### *Ribociclib quantification, pharmacokinetic calculation and statistics*

Ribociclib concentrations in plasma and tissue homogenates were determined using the previously described LC-MS/MS bioanalytical method [21].

All pharmacokinetic parameters were calculated with a non-compartmental model using the add-in PKSolver program in Microsoft Excel [28]. In addition to ribociclib concentration in tissues, tissue-to-plasma ratios and tissue accumulation of ribociclib were calculated by dividing by plasma concentration at the terminal time-point, and by the area under the plasma concentration-time curve ( $AUC_{0-t}$ ), respectively. Statistical analysis was done using the software GraphPad Prism 7 (GraphPad software, San Diego, CA). All data were log-transformed before statistical analysis. Student's t and one-way ANOVA statistical tests were applied when two and multiple groups were compared, respectively. The Bonferroni post-hoc test was used for multiple comparisons. Differences were considered statistically significant when  $P < 0.05$ .

## Results

### ***In vitro* transport of ribociclib**

To determine whether and to what extent ribociclib is a transport substrate of ABCB1 and ABCG2, an *in vitro* transwell assay was performed using the polarized parental Madin-Darby Canine Kidney (MDCK-II) cell line and subclones overexpressing hABCB1, hABCG2 and mAbcg2. In the parental MDCK-II cell line, ribociclib (added at 5  $\mu$ M) was modestly transported to the apical side (efflux ratio  $r = 2.1$ , Figure 1A). This transport was completely inhibited by the ABCB1 inhibitor zosuquidar ( $r = 1.1$ , Figure 1B). This suggests that the ribociclib transport was due to the low-level endogenous canine ABCB1 known to be expressed in the parental MDCK-II cell line [29]. In the MDCK-II-hABCB1 cells, ribociclib was strongly transported to the apical side ( $r = 13.5$ , Figure 1C) and this transport was completely inhibited by zosuquidar ( $r = 1.2$ , Figure 1D). In transport experiments performed with MDCK-II-hABCG2 and MDCK-II-mAbcg2 cells, zosuquidar was added to inhibit the background activity of the endogenous canine ABCB1. In the hABCG2-transduced cell line, ribociclib was not noticeably actively transported to the apical side, since translocation rates in both directions were similar. Furthermore, the efflux ratios without and with the ABCG2 inhibitor Ko143 were comparable (1.1 and 1.0, respectively, Figures 1E and 1F). However, ribociclib was modestly transported in the apical direction in the MDCK-II-mAbcg2 cell line ( $r = 1.9$ )

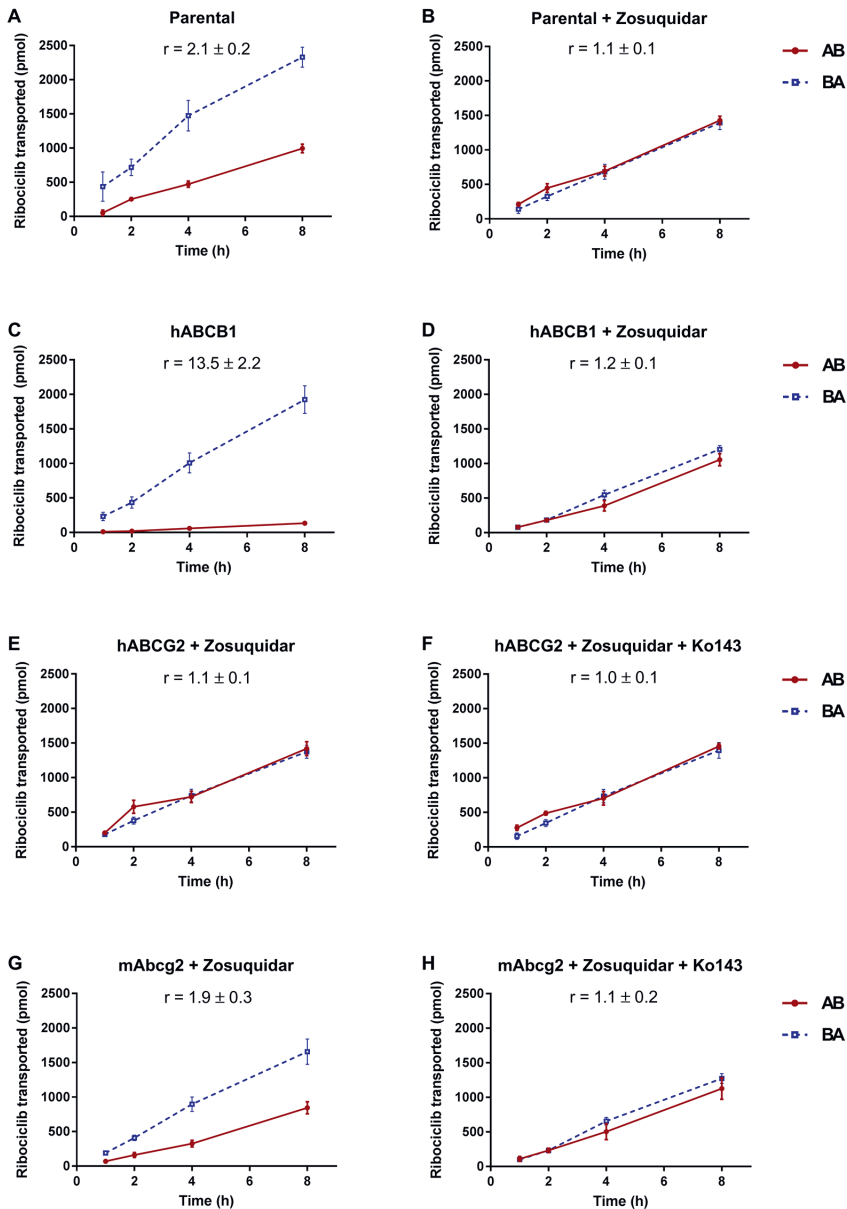


**Figure 1.** *In vitro* transport of ribociclib evaluated in MDCK-II cells either non-transduced (A, B) or transduced with human ABCB1 (C, D), human ABCG2 (E, F) or murine Abcg2 (G, H) cDNA. At  $t = 0$ , ribociclib ( $5 \mu\text{M}$ ) was added in the donor compartment, either apical to assess apical-to-basolateral translocation, or basolateral to assess basolateral-to-apical transport. At 1, 2, 4 and 8 h, the concentration in the acceptor compartment was measured and plotted in the graphs as total transported amount ( $n = 3$ ). D-H: zosuquidar was added to inhibit human and/or endogenous canine ABCB1. F and H: Ko143 was added for the inhibition of human and murine ABCG2.  $r =$  efflux ratio. Translocation from the apical to the basolateral compartment (AB). Translocation from the basolateral to apical compartment (BA). Data are presented as mean  $\pm$  SD. 1000 pmol transport at 8 h corresponds to an approximate apparent permeability coefficient ( $P_{\text{app}}$ ) of  $6.2 \times 10^{-6} \text{ cm}^2/\text{s}$ .

and Ko143 inhibited this transport completely ( $r = 1.1$ ) (Figures 1G and 1H). Ribociclib thus appears to be a very good transport substrate of hABCB1, whereas it is not noticeably transported by hABCG2 and only modestly by mAbcg2 *in vitro*.

### Effect of ABCB1 and ABCG2 on ribociclib pharmacokinetics and tissue distribution in mice

Based on the *in vitro* transport results, we evaluated a possible effect of both transporters on ribociclib plasma pharmacokinetics (oral bioavailability) and tissue distribution. A 24 h pilot experiment was performed in WT and *Abcb1a/1b*<sup>-/-</sup>;*Abcg2*<sup>-/-</sup> mice. Since ribociclib is prescribed to treat breast cancer, which mostly occurs in women, female mice were used. Ribociclib was orally administered at 20 mg/kg, resulting in similar plasma concentrations as seen in patients after a single oral dose of 600 mg [30,31]. As shown in Figure 2, in the absence of *Abcb1a/1b* and *Abcg2*, the area under the plasma-concentration-time curve (AUC) significantly increased by 2.3-fold compared to WT mice ( $P < 0.001$ , Table 1). Furthermore, ribociclib showed a slower elimination in *Abcb1a/1b*<sup>-/-</sup>;*Abcg2*<sup>-/-</sup> mice compared to WT mice, especially beyond 3 and 8 h after oral administration, which is reflected in the increase in the plasma concentration at 24 h (Supplementary Figure S2). However, the maximum plasma concentration ( $C_{\max}$ ) of ribociclib and the time to reach it ( $T_{\max}$ ) were not significantly different between the two mouse strains (Table 1,  $P > 0.05$ ).

Ribociclib was also quantified in brain, liver, kidney, spleen and small intestine tissue 24 h after oral administration. Interestingly, the brain concentration of ribociclib was vastly increased in the *Abcb1a/1b*<sup>-/-</sup>;*Abcg2*<sup>-/-</sup> mice. This increase was not only dependent on the higher plasma concentration in this strain, since the brain-to-plasma ratio ( $K_{p,\text{brain}}$ ) was also dramatically increased by around 30-fold ( $P < 0.001$ , Figure 3A-C, Table 1). In other organs like liver, ribociclib concentrations were also significantly increased in *Abcb1a/1b*<sup>-/-</sup>;*Abcg2*<sup>-/-</sup> compared to WT mice. However, this increase was primarily associated with the higher ribociclib plasma concentration at the terminal time point, since there was no difference between both strains after correction for the plasma concentration (Figure 3D-F, Supplementary Figure S3). For kidneys and spleen the organ-to-plasma ratios in *Abcb1a/1b*<sup>-/-</sup>;*Abcg2*<sup>-/-</sup> mice were moderately lower than in WT mice, whereas the tissue accumulations were moderately higher, suggesting that the difference may have been primarily caused by the substantial difference in plasma concentration between the strains at 24 h (Supplementary Figure S3). In general, ribociclib was highly distributed in organs compared to plasma, since all tested organ-to-plasma ratios showed a mean higher than 25 in WT mice except for the brain, where the ratio was just below 1 (Table 1, Figure 3, Supplementary Figure S3).

To further investigate the single and combined effects of these transporters on plasma pharmacokinetics and tissue distribution of ribociclib, we performed a second experiment with oral ribociclib at 20 mg/kg which was terminated at 8 h, when ribociclib plasma concentrations were still relatively high. In addition to WT and *Abcb1a/1b*<sup>-/-</sup>

; *Abcg2*<sup>-/-</sup> mice, also single *Abcb1a/1b*<sup>-/-</sup> and *Abcg2*<sup>-/-</sup> mouse strains were included. As shown in Figure 4A and Table 2, the ribociclib plasma AUC<sub>0-8h</sub> was not significantly different among the mouse strains ( $P > 0.05$ ). Most other pharmacokinetic parameters were not significantly different either. However, the elimination from 1 h on was slower when *Abcb1a/1b* was absent in both the *Abcb1a/1b*<sup>-/-</sup> and especially the *Abcb1a/1b*;*Abcg2*<sup>-/-</sup> mice (Supplementary Figure S4A), which is consistent with what we observed in the pilot experiment, albeit a bit less pronounced. Thus, *Abcb1a/1b* may be an important factor for the intermediate and late elimination phases of ribociclib.

The ABC efflux transporters further had a profound effect at 8 h on the brain accumulation of ribociclib, but not in the other organs (Figure 5, Supplementary Figure S5). The brain-to-plasma ratio was increased by 26-fold ( $P < 0.001$ , Table 2, Figure 5A-C) in the absence of *Abcb1a/1b* and *Abcg2*. Similarly, in the single *Abcb1a/1b*<sup>-/-</sup> mice, the brain-to-plasma ratio was increased by 30-fold ( $P < 0.001$ , Table 2). In contrast, single *Abcg2*<sup>-/-</sup> mice did not demonstrate any effect on brain accumulation, since the brain-to-plasma ratio was comparable to that in WT mice ( $P > 0.05$ , Table 2, Figure 5A-C). These results suggest that the brain accumulation of ribociclib is extensively limited by *Abcb1a/1b* in the BBB, whereas *Abcg2* does not have a significant effect. This is further supported by the lack of significant differences between *Abcb1a/1b*<sup>-/-</sup> and *Abcb1a/1b*<sup>-/-</sup>;*Abcg2*<sup>-/-</sup> mice (Figure 5B, C).

### Effect of CYP3A on ribociclib pharmacokinetics and tissue distribution in mice

To investigate the interaction between ribociclib and murine *Cyp3a*, a 24 h oral ribociclib (20 mg/kg) pilot experiment was performed, where the pharmacokinetics between WT and the *Cyp3a*<sup>-/-</sup> mice were compared. As shown in Figure 2 and Table 1, when *Cyp3a*

**Table 1.** Pharmacokinetic parameters over 24 h after oral administration of 20 mg/kg ribociclib to female WT, *Abcb1a/1b*<sup>-/-</sup>;*Abcg2*<sup>-/-</sup> and *Cyp3a*<sup>-/-</sup> mice.

Parameter	Genotype		
	WT	<i>Abcb1a/1b</i> <sup>-/-</sup> ; <i>Abcg2</i> <sup>-/-</sup>	<i>Cyp3a</i> <sup>-/-</sup>
AUC <sub>0-24h</sub> (h*ng/mL)	6885 ± 1215	15775 ± 2515***	11967 ± 2427**
Fold change AUC <sub>0-24h</sub>	1.0	2.3	1.7
T <sub>max</sub> (h)	0.5-1.0	0.5-8.0	0.5
C <sub>max</sub> (ng/mL)	1036 ± 352	1308 ± 226	1739 ± 127**
C <sub>brain</sub> (ng/g)	3.3 ± 0.5	1690 ± 668***	5.4 ± 1.6**
K <sub>p,brain</sub>	0.70 ± 0.19	24.8 ± 7.9***	0.67 ± 0.15
Fold increase K <sub>p,brain</sub>	1.0	35.5	1.0
P <sub>brain</sub> (*10 <sup>-3</sup> h <sup>-1</sup> )	0.5 ± 0.2	108.2 ± 32.3***	0.5 ± 0.3

Data are presented as mean ± SD, except for T<sub>max</sub> (n = 5-6). AUC<sub>0-24h</sub>, area under the plasma concentration-time curve; C<sub>max</sub>, maximum concentration in plasma; T<sub>max</sub>, time point (h) of maximum plasma concentration; C<sub>brain</sub>, brain concentration; K<sub>p,brain</sub>, brain-to-plasma ratio; P<sub>brain</sub>, brain accumulation, calculated by determining the ribociclib brain concentration at 24 h relative to the AUC<sub>0-24h</sub>. Data were log-transformed for statistical analysis. \*\*,  $P < 0.01$ ; \*\*\*,  $P < 0.001$  compared to WT mice. *Cyp3a* data were treated separately for statistical analysis.

was knocked out, the plasma AUC and  $C_{max}$  of ribociclib significantly increased by 1.7-fold ( $P < 0.01$ ) but the  $T_{max}$  was similar. These results suggest that mCyp3a-mediated metabolism significantly limits ribociclib plasma exposure. The tissue distribution of ribociclib between both strains was also compared, but no relevant differences between the two groups were evident considering the higher plasma exposure in *Cyp3a*<sup>-/-</sup> mice (Figure 3 and Supplementary Figure S3).

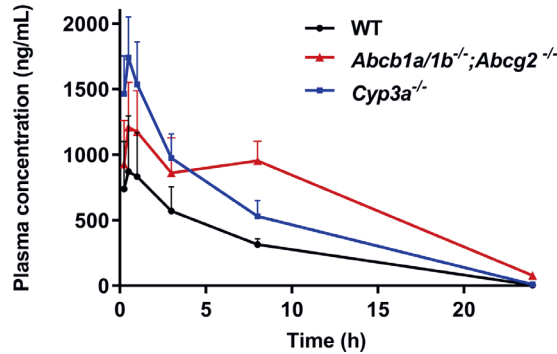


**Figure 2.** Plasma concentration-time curves of ribociclib over 24 h in female WT, *Abcb1a/1b*<sup>-/-</sup>;*Abcg2*<sup>-/-</sup>, and *Cyp3a*<sup>-/-</sup> mice after oral administration of 20 mg/kg. Data are presented as mean  $\pm$  SD ( $n = 6$ ).

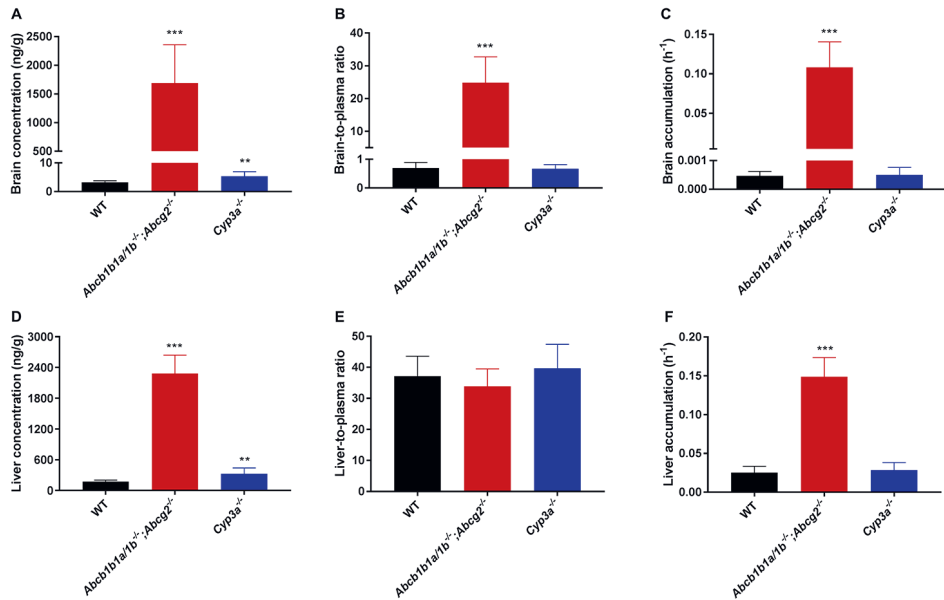


**Figure 3.** Brain and liver concentration (A, D), tissue-to-plasma ratio (B, E), and tissue accumulation (C, F) of ribociclib in WT, *Abcb1a/1b*<sup>-/-</sup>;*Abcg2*<sup>-/-</sup>, and *Cyp3a*<sup>-/-</sup> mice 24 h after oral administration of 20 mg/kg of ribociclib. Data are presented as mean  $\pm$  SD ( $n = 6$ ). \*\*,  $P < 0.01$ ; \*\*\*,  $P < 0.001$  compared to WT mice.

**Table 2.** Pharmacokinetic parameters over 8 h after oral administration of 20 mg/kg ribociclib to female WT, *Abcb1a1/1b<sup>-/-</sup>*, *Abcg2<sup>-/-</sup>*, *Abcb1a1/1b<sup>-/-</sup>;Abcg2<sup>-/-</sup>*, *Cyp3a<sup>-/-</sup>*, *Cyp3a<sup>-/-</sup>;Cyp3aXAV* mice.

Parameter	Genotype				
	WT	<i>Abcb1a1/1b<sup>-/-</sup></i>	<i>Abcb1a1/1b<sup>-/-</sup>;Abcg2<sup>-/-</sup></i>	<i>Cyp3a<sup>-/-</sup></i>	<i>Cyp3aXAV</i>
AUC <sub>0-8h</sub> (h*ng/mL)	5901 ± 1760	7616 ± 1014	6576 ± 719	7021 ± 2586	1834 ± 490###
Fold change AUC <sub>0-8h</sub>	1.0	1.3	1.1	1.2	0.31
T <sub>max</sub> (h)	0.25-2	0.5-2	0.5-2	0.5-1	0.25-0.5
C <sub>max</sub> (ng/mL)	1774 ± 833	1565 ± 441	1288 ± 182	1963 ± 791	546 ± 260###
C <sub>brain</sub> (ng/g)	80.4 ± 28.2	76.1 ± 19.6	4066 ± 888***	77.4 ± 17.0	27.1 ± 8.4###
K <sub>p,brain</sub>	0.25 ± 0.09	0.40 ± 0.15	7.83 ± 2.55***	0.23 ± 0.07	0.35 ± 0.15
Fold increase K <sub>p,brain</sub>	1.0	1.6	26.4	0.9	1.4
P <sub>brain</sub> (*10 <sup>-3</sup> h <sup>-1</sup> )	14.1 ± 3.6	12.3 ± 3.6	535 ± 95***	635 ± 70***	15.3 ± 5.2

Data are presented as mean ± SD, except for T<sub>max</sub> (n = 6-8), AUC<sub>0-8h</sub>, area under the plasma concentration-time curve; C<sub>max</sub>, maximum concentration in plasma; T<sub>max</sub>, time point (h) of maximum plasma concentration; C<sub>brain</sub>, brain concentration; K<sub>p,brain</sub>, brain-to-plasma ratio; P<sub>brain</sub>, brain accumulation, calculated by determining the ribociclib brain concentration at 8 h relative to the AUC<sub>0-24h</sub>. Data were log-transformed for statistical analysis. \*\*\*, P < 0.001 compared to WT mice. ###, P < 0.001 compared to *Cyp3a<sup>-/-</sup>* mice. CYP3A groups were treated separately for the statistical analysis.

To study the possible *in vivo* impact of human CYP3A4, a transgenic mouse strain with expression of human CYP3A4 in liver and small intestine in a *Cyp3a<sup>-/-</sup>* background (*Cyp3aXAV* mice) was included in a subsequent 8-h experiment. Ribociclib pharmacokinetics and tissue distribution were compared among the three mouse genotypes over 8 h after oral administration of ribociclib at 20 mg/kg. Plasma exposure of ribociclib decreased markedly in the *Cyp3aXAV* mice compared to *Cyp3a<sup>-/-</sup>* mice, with a 3.8-fold reduced plasma AUC<sub>0-8h</sub> ( $P < 0.001$ , Figure 4B, Table 2). In addition, the ribociclib C<sub>max</sub> significantly decreased by around 70% in the CYP3aXAV mice ( $P < 0.001$ , Table 2). Also, in this experiment the plasma AUC was somewhat higher in *Cyp3a<sup>-/-</sup>* than in WT mice, but the difference was not significant. There was again no meaningful difference in organ exposure among the three strains considering the differences in plasma exposure (Figure 5, Supplementary Figure S5). These results support that ribociclib is extensively metabolized *in vivo* via human CYP3A4, resulting in reduced systemic exposure, but without a strong effect on tissue distribution of the drug.

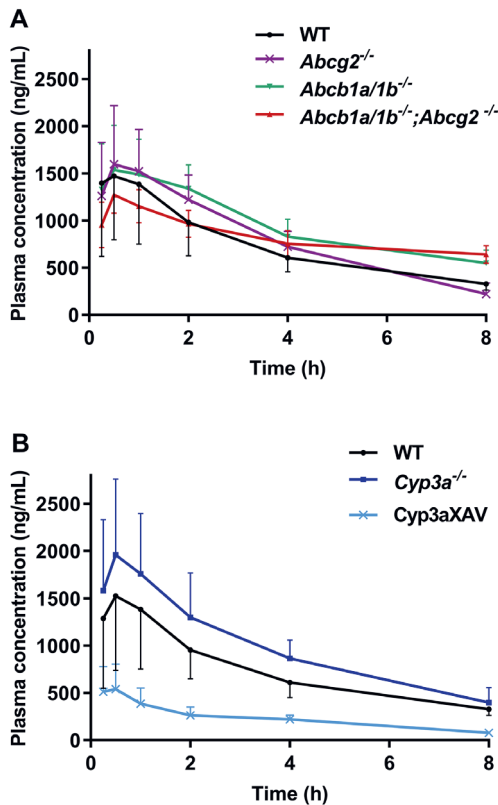


**Figure 4.** Plasma concentration-time curves of ribociclib over 8 h in female WT, *Abcg2<sup>-/-</sup>*, *Abcb1a/1b<sup>-/-</sup>*, *Abcb1a/1b<sup>-/-</sup>;Abcg2<sup>-/-</sup>* (A), and female WT, *Cyp3a<sup>-/-</sup>*, *Cyp3aXAV* (B) mice after oral administration of 20 mg/kg ribociclib. Data are presented as mean  $\pm$  SD ( $n = 6-8$ ).

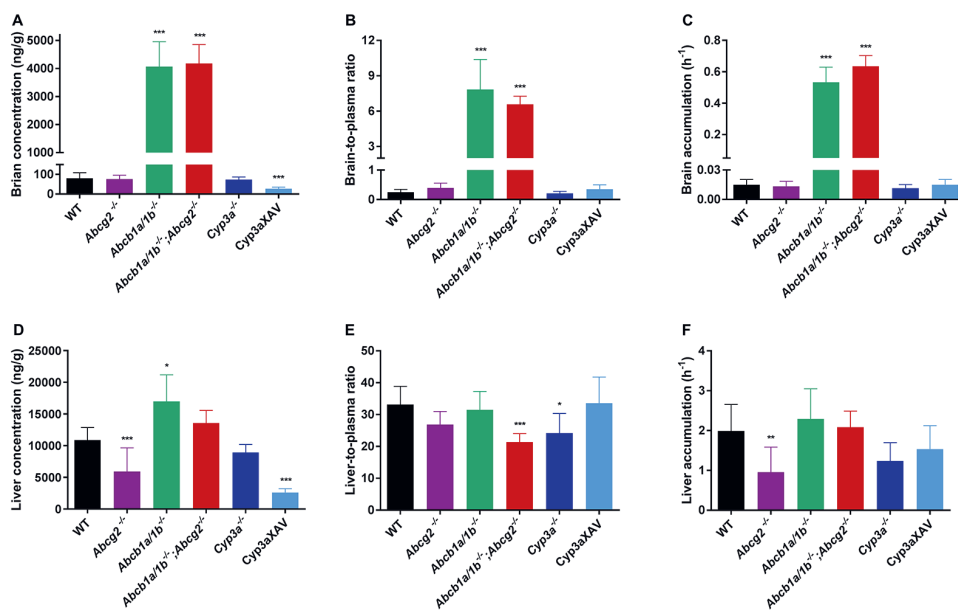


**Figure 5.** Brain and liver concentration (A, D), tissue-to-plasma ratio (B, E), and tissue accumulation (C, F) of ribociclib in WT, *Abcb1a/1b*<sup>-/-</sup>, *Abcg2*<sup>-/-</sup>, *Abcb1a/1b*<sup>-/-</sup>;*Abcg2*<sup>-/-</sup>, *Cyp3a*<sup>-/-</sup>, and *Cyp3aXAV* mice 8 h after oral administration of 20 mg/kg of ribociclib. Data are presented as mean  $\pm$  SD (n = 6-8). \*,  $P < 0.05$ ; \*\*,  $P < 0.01$ ; \*\*\*,  $P < 0.001$  compared to WT mice.

### Effect of elacridar on ribociclib oral bioavailability and brain accumulation

Since the brain accumulation of ribociclib was strongly affected by *Abcb1a/1b*, we investigated whether coadministration of elacridar, a dual inhibitor for ABCB1 and ABCG2, could enhance the ribociclib brain accumulation. Elacridar (50 mg/kg) or vehicle were orally administered 15 minutes prior to the administration of ribociclib (20 mg/kg) to WT and *Abcb1a/1b*;*Abcg2*<sup>-/-</sup> mice. In order to optimally assess the effects of elacridar, the experiment was terminated at 4h, which is around the reported median  $T_{\max}$  of elacridar in mice receiving a similar oral elacridar dose [32], and while ribociclib plasma concentrations were still high. The plasma  $AUC_{0-4h}$  and the  $C_{\max}$  were respectively 2.3-fold and 2.6-fold higher in WT mice treated with elacridar compared to WT mice treated with vehicle ( $P < 0.001$ , Table 3, Supplementary Figure S6). High inter-individual variation was observed in the WT mice treated with elacridar compared to other groups, especially during the first two hours. This may perhaps be explained by inter-individual variation in the elacridar exposure of the *Abcb1a/1b* and *Abcg2* transporters.

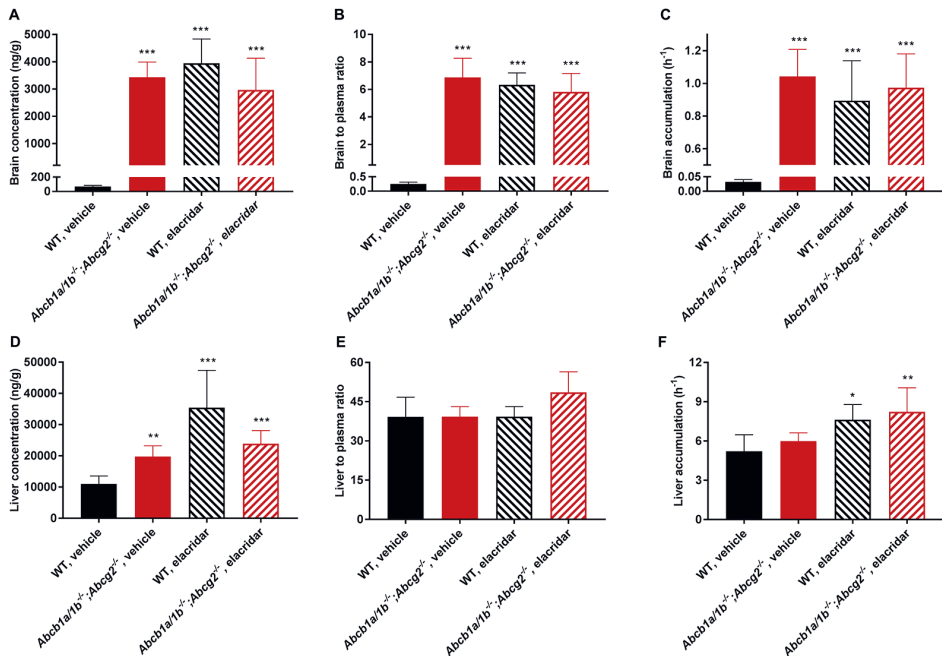
Strong evidence of full *Abcb1a/1b* inhibition by elacridar at the BBB was found (Figure 6A-C, Table 3). In the vehicle-treated groups, the brain-to-plasma ratio at 4 h was 28-fold higher in *Abcb1a/1b*;*Abcg2*<sup>-/-</sup> compared to WT mice ( $P < 0.001$ , Table 3), similar to the results found at 8 and 24 h. In elacridar-treated WT mice, the brain-to-plasma ratio



**Table 3.** Effect of elacridar on pharmacokinetic parameters over 4 h after oral administration of 20 mg/kg ribociclib to female WT and *Abcb1a/1b*<sup>-/-</sup>;*Abcg2*<sup>-/-</sup> mice.

Parameter	Genotype			
	Vehicle		Elacridar	
	WT	<i>Abcb1a/1b</i> <sup>-/-</sup> ; <i>Abcg2</i> <sup>-/-</sup>	WT	<i>Abcb1a/1b</i> <sup>-/-</sup> ; <i>Abcg2</i> <sup>-/-</sup>
AUC <sub>0-4h</sub> (h*ng/mL)	2134 ± 273	3305 ± 436	4804 ± 1695***	2976 ± 636
Fold change AUC <sub>0-4h</sub>	1.0	1.5	2.3	1.4
T <sub>max</sub> (h)	0.25-1	0.5-2	0.25-0.5	0.25-2
C <sub>max</sub> (ng/mL)	809 ± 119	1129 ± 114	2132 ± 1191**	1134 ± 350
C <sub>brain</sub> (ng/g)	69.1 ± 15.7	3430 ± 557***	3945 ± 890***	2965 ± 1163***
K <sub>p,brain</sub>	0.25 ± 0.07	6.88 ± 1.40***	6.34 ± 0.86***	5.80 ± 1.30***
Fold increase K <sub>p,brain</sub>	1.0	27.5	24.9	23.2
P <sub>brain</sub> (*10 <sup>-3</sup> h <sup>-1</sup> )	32.7 ± 7.8	1043 ± 165***	894 ± 244***	934 ± 207***

Data are presented as mean ± SD, except for T<sub>max</sub> (n = 6). AUC<sub>0-4h</sub>, area under the plasma concentration-time curve; C<sub>max</sub>, maximum concentration in plasma; T<sub>max</sub>, time point (h) of maximum plasma concentration; C<sub>brain</sub>, brain concentration; K<sub>p,brain</sub>, brain-to-plasma ratio; P<sub>brain</sub>, brain accumulation, calculated by determining the ribociclib brain concentration at 4 h relative to the AUC<sub>0-4h</sub>. Data were log-transformed for statistical analysis. \*\*, P < 0.01; \*\*\*, P < 0.001 compared to vehicle-treated WT mice.

**Figure 6.** Brain and liver concentration (A, D), brain-to-plasma ratio (B, E), and brain accumulation (C, F) of ribociclib in WT and *Abcb1a/1b*<sup>-/-</sup>;*Abcg2*<sup>-/-</sup> mice 4 h after oral administration of 20 mg/kg of ribociclib with oral vehicle or elacridar coadministration (50 mg/kg). Data are presented as mean ± SD (n = 5-6). \*, P < 0.05; \*\*, P < 0.01; \*\*\*, P < 0.001 compared to vehicle-treated WT mice.

dramatically increased by 25-fold compared to the vehicle-treated group ( $P < 0.001$ , Table 3, Figure 6B). This value was essentially the same as that in vehicle- or elacridar-treated *Abcb1a/1b;Abcg2*<sup>-/-</sup> mice ( $P > 0.05$ , Table 3, Figure 6B). This indicates that elacridar could completely inhibit *Abcb1a/1b* in the BBB. Moreover, since the brain-to-plasma ratios were not significantly different between the *Abcb1a/1b;Abcg2*<sup>-/-</sup> vehicle and elacridar groups, it appears that the elacridar effect was specifically due to the inhibition of m*Abcb1a/1b*, and not due to interaction with other systems. In the liver elacridar coadministration with ribociclib did not cause significant changes in the tissue-to-plasma ratios in either WT or *Abcb1a/1b;Abcg2*<sup>-/-</sup> mice ( $P > 0.05$ , Figure 6E).

## Discussion

In this study we show that ribociclib is a good transport substrate of hABCB1, but not noticeably of hABCG2 and a poor substrate of m*Abcg2* *in vitro*. *In vivo* only m*Abcb1a/1b* had a significant impact on ribociclib pharmacokinetics and tissue distribution in mice. The oral bioavailability of ribociclib was significantly affected by the absence of *Abcb1a/1b* and *Abcg2*, increasing the  $AUC_{0-24h}$  by 2.3-fold. Ribociclib brain accumulation was drastically increased (at least 23-fold) when *Abcb1a/1b* was knocked out, demonstrating that this transporter plays an important role in the BBB in limiting the brain penetration of ribociclib. In contrast, ribociclib distribution to liver, kidneys, spleen and small intestine was not markedly affected by *Abcb1a/1b* and *Abcg2*. We further showed that elacridar coadministration can completely inhibit *Abcb1a/1b* activity at the BBB, dramatically enhancing the brain accumulation of ribociclib. Oral bioavailability of ribociclib was further extensively affected by transgenic human CYP3A4, decreasing the  $AUC_{0-8h}$  by 3.8-fold, in line with extensive ribociclib metabolism by human CYP3A4. As the present study was nearing completion, Sorf *et al.* showed that ribociclib is a transport substrate of hABCB1 but not of hABCG2 [13]. These results are consistent with our data, but they contrast with the FDA and EMA documentation stating that ribociclib is a weak substrate of ABCB1, which is therefore unlikely to affect ribociclib exposure [12,16]. We also evaluated the transport in mouse *Abcg2* overexpressing cells where the efflux transport was 1.9. According to the International Transporter Consortium, since the efflux ratio is  $< 2$ , ribociclib is considered a poor or non-*Abcg2* substrate [5]. For ribociclib, this consideration was reflected in our *in vivo* results, where only *Abcb1a/1b* had an impact on ribociclib plasma pharmacokinetics and tissue distribution, whereas mouse *Abcg2* did not have any noticeable effect. It is thus very unlikely that hABCG2 will have a noticeable impact on human ribociclib pharmacokinetics and tissue distribution.

Our results suggest that *Abcb1a/1b* primarily has an impact on the elimination of ribociclib, which was slower when this transporter was absent (Figures S1 and S3), significantly increasing the ribociclib  $AUC_{0-24h}$  by 2.3-fold ( $P < 0.001$ , Table 1, Figure 2).

This effect was clear beyond 4 and 8 hours, but at earlier time points this effect was not evident. This may partly explain why only the plasma  $AUC_{0-24h}$  was significantly affected and not the  $AUC_{0-8h}$  and  $AUC_{0-4h}$ . Ribociclib is mostly excreted via feces, where unchanged ribociclib amounts have been reported from 10.2% (in beagle dogs) to 17.3% (in humans) of the dose, and to a lesser extent in urine (12.1% in humans) [12,16]. Based on our data, we speculate that Abcb1a/1b could mediate hepatobiliary excretion and/or direct intestinal excretion of ribociclib, or reduce its intestinal re-uptake when the intestinal luminal concentration is relatively low. Each of these processes, or a combination thereof, could explain the delayed elimination of ribociclib that we observed in the absence of Abcb1a/1b.

The most striking finding was that Abcb1a/1b was responsible for limiting the ribociclib brain accumulation. So far, the penetration of ribociclib into the central nervous system (CNS) has not been fully characterized and there is controversial information about the ability of ribociclib to penetrate into the brain [33,34]. Although, according to the FDA and EMA information, ribociclib showed a low or absent brain penetration in rats [12,16], Patel *et al.* reported that ribociclib penetrates into the CNS in mouse models especially in brain tumors [35]. It is worth noting that the BBB or blood-tumor barrier (BTB) is often partly disturbed in brain metastases of breast cancer mouse models, resulting in variably increased drug levels and passive permeability in the metastases [36,37]. However, variation in permeability is high, and the BTB is rarely completely disrupted. Consequently, only ~10% of brain metastases is expected to be leaky enough to allow efficacious drug concentrations of conventional chemotherapeutics into the lesions. Additional measures to further enhance permeability of the BBB and BTB might therefore improve therapy responses. In the present study we found that in the WT situation, the brain-to-plasma ratio was 0.25 at 4 and 8 h after oral administration of 20 mg/kg of ribociclib (Tables 2 and 3). Therefore, ribociclib is able to significantly cross the BBB even in WT mice, but its penetration to the brain is still dramatically limited by Abcb1a/1b.

The high efflux ratio in ABCB1-overexpressing cells *in vitro* correlates well with the *in vivo* role of Abcb1a/1b in the BBB. This implies that also in the human situation ABCB1 activity may limit ribociclib penetration into the brain. There is a lot of interest in ribociclib brain penetration since clinical investigation in pediatric patients with neuroblastoma or malignant rhabdoid tumors showed that ribociclib displayed preliminary signs of brain tumor stabilization [38,39]. Currently, several phase I/II clinical trials are ongoing to investigate the efficacy of ribociclib in brain tumors either alone or in combination with everolimus [33]. In addition, drugs that cross the BBB are needed since metastatic brain tumors are the most common type of brain tumors, occurring in approximately 20 to 40% of cancer patients [10,40]. Interestingly, the incidence of such metastases is rising due to several factors, including the improved therapeutic efficacy of many modern targeted drugs against tumors occurring outside of the CNS [10,40,41]. Among metastatic brain tumors, breast cancer presents the

second highest frequency in brain metastasis, just after lung cancer [10,40,41]. Here, we also showed that the coadministration of 50 mg/kg of elacridar with ribociclib completely inhibits Abcb1a/1b in the BBB, increasing the brain penetration to the same extent as when Abcb1a/1b was ablated. Therefore, the efficacy of ribociclib to treat (metastatic) brain tumors in the clinic could potentially be enhanced by inhibiting hABCB1, since we have shown that ribociclib is also highly transported by hABCB1. Furthermore, since cancer cells themselves also often express ABCB1, they can be intrinsically resistant to ribociclib therapy, and ABCB1 inhibitors (like elacridar) could be coadministered to improve the efficacy of ribociclib against such tumors.

Overlap in substrate specificities has been observed between CYP enzymes and the ABC transporters, which has led to the idea that they may work synergistically to promote drug elimination [42]. Our CYP3A studies show that ribociclib is eliminated by both mouse *Cyp3a* and human CYP3A4. Oral bioavailability of ribociclib is affected by these metabolic enzymes but to different extents; while in the *Cyp3a*<sup>-/-</sup> mice the plasma AUC was barely affected, in the CYP3A4 transgenic mice the AUC was strongly decreased. The modest difference in AUCs between *Cyp3a*<sup>-/-</sup> and WT mice suggests that the contribution of mouse *Cyp3a* to the ribociclib metabolism is minor, and hence, ribociclib metabolism in mice could be accomplished also by other enzymes. Ribociclib was primarily metabolized by CYP3A4/5 (approximately 78%) and Flavin-containing monooxygenase 3 (FMO3, approximately 20%) *in vitro*, whereas *in vivo* studies in rats showed that the metabolism was dominated by direct phase II sulfation [12,16]. Probably also in *Cyp3a*<sup>-/-</sup> mice, some of these non-CYP3A enzymes could take over ribociclib metabolism. In contrast, the human CYP3A4 markedly limited the oral bioavailability of ribociclib, decreasing the AUC<sub>0-8h</sub> by 3.8-fold. This suggests that hepatic and intestinal CYP3A4 contributes to a high extent to the first-pass metabolism of ribociclib. The overall effect of transgenic CYP3A4 in our mouse models (3.8-fold decrease in AUC) was similar to the ritonavir effect found in humans (3.2-fold increase in AUC) when ritonavir was coadministered with ribociclib. Our results thus further support that, in the human situation, ribociclib is extensively metabolized via CYP3A4 and its oral bioavailability is strongly restricted by this enzyme. CYP3A4 has a wide substrate specificity and it can be strongly inhibited and/or induced by many different drugs and food components. Furthermore, genetic polymorphisms can also markedly affect its activity. All these factors might potentially contribute to high levels of variation in CYP3A4 activity, which may impact on oral bioavailability; thus, plasma concentrations of ribociclib should be carefully monitored in patients to ensure optimal therapeutic exposure [14,15].

## Conclusions

This study shows that ribociclib is avidly transported by ABCB1. This transporter dramatically restricts the brain penetration of ribociclib *in vivo*, whereas it does not considerably affect the relative ribociclib distribution in other tissues. Our results

further suggest that ABCB1 can play a significant role in ribociclib elimination. In contrast, ABCG2 does not have any noticeable effect on ribociclib plasma pharmacokinetics and tissue distribution. Moreover, coadministration of elacridar can completely inhibit the activity of ABCB1 at the BBB, dramatically improving the brain penetration of ribociclib. Our experiments also support that the oral bioavailability of ribociclib is markedly limited by human CYP3A4 activity, but this does not affect the relative tissue distribution. The risk of high variation in oral exposure due to variable CYP3A4 activity must thus be considered while using ribociclib in patients. The insights gained from this study may be useful to further improve the efficacy of ribociclib in the clinic, especially for the treatment of (metastatic) brain tumors.

---

#### *Acknowledgements*

The authors thank Margarida Martins for assistance in executing the *in vivo* mouse experiments and Ioannis Zavrakidis for advice on statistical calculations and analysis.

## References

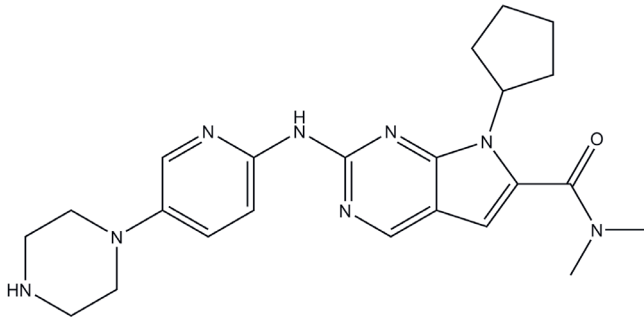
- [1] D. Kwapisz, Cyclin-dependent kinase 4/6 inhibitors in breast cancer: palbociclib, ribociclib, and abemaciclib, *Breast Cancer Res. Treat.* 166 (2017) 41–54. <https://doi.org/10.1007/s10549-017-4385-3>.
- [2] D. Romero, Expanding ribociclib use, *Nat. Rev. Clin. Oncol.* 15 (2018) 470–471.
- [3] D. Tripathy, A. Bardia, W.R. Sellers, Ribociclib (LEE011): Mechanism of Action and Clinical Impact of This Selective Cyclin-Dependent Kinase 4/6 Inhibitor in Various Solid Tumors, *Clin. Cancer Res.* 23 (2017) 3251–3262. <https://doi.org/10.1158/1078-0432.CCR-16-3157>.
- [4] G. Curigliano, C. Criscitiello, A. Esposito, M. Intra, S. Minucci, Pharmacokinetic drug evaluation of ribociclib for the treatment of metastatic, hormone-positive breast cancer, *Expert Opin. Drug Metab. Toxicol.* 13 (2017) 575–581. <https://doi.org/10.1080/17425255.2017.1318848>.
- [5] K.M. Giacomini, S.-M. Huang, D.J. Tweedie, L.Z. Benet, K.L.R. Brouwer, X. Chu, A. Dahlin, R. Evers, V. Fischer, K.M. Hillgren, K.A. Hoffmaster, T. Ishikawa, D. Keppler, R.B. Kim, C.A. Lee, M. Niemi, J.W. Polli, Y. Sugiyama, P.W. Swaan, J.A. Ware, S.H. Wright, S. Wah Yee, M.J. Zamek-Gliszczynski, L. Zhang, Membrane transporters in drug development, *Nat. Rev. Drug Discov.* 9 (2010) 215–236. <https://doi.org/10.1038/nrd3028>.
- [6] A.H. Schinkel, J.W. Jonker, Mammalian drug efflux transporters of the ATP binding cassette (ABC) family: An overview, *Adv. Drug Deliv. Rev.* 64 (2012) 138–153. <https://doi.org/10.1016/j.addr.2012.09.027>.
- [7] B. Mittal, S. Tulsyan, R. Mittal, The effect of ABCB1 polymorphisms on the outcome of breast cancer treatment, *Pharmgenomics. Pers. Med.* 9 (2016) 47. <https://doi.org/10.2147/PGPM.S86672>.
- [8] K. Natarajan, Y. Xie, M.R. Baer, D.D. Ross, Role of breast cancer resistance protein (BCRP/ABCG2) in cancer drug resistance, *Biochem. Pharmacol.* 83 (2012) 1084–1103. <https://doi.org/10.1016/j.bcp.2012.01.002>.
- [9] T. Kuo, Roles of multidrug resistance genes in breast cancer chemoresistance, in: D. Yu, M.-C. Hung (Eds.), *Breast Cancer Chemosensitivity*, Springer Science, New York, USA, 2007: pp. 23–28.
- [10] T.J. Raub, G.N. Wishart, P. Kulanthaivel, B.A. Staton, R.T. Ajamie, G.A. Sawada, L.M. Gelbert, H.E. Shannon, C. Sanchez-Martinez, A. De Dios, Brain exposure of two selective dual CDK4 and CDK6 inhibitors and the antitumor activity of CDK4 and CDK6 inhibition in combination with temozolomide in an intracranial glioblastoma xenograft, *Drug Metab. Dispos.* 43 (2015) 1360–1371. <https://doi.org/10.1124/dmd.114.062745>.
- [11] M. de Gooijer, P. Zhang, N. Thota, I. Mayayo-peralta, L. Buil, J.H. Beijnen, O. Van Tellingen, P-glycoprotein and breast cancer resistance protein restrict the brain penetration of the CDK4/6 inhibitor palbociclib, *Invest. New Drugs.* 33 (2015) 1012–1019. <https://doi.org/10.1007/s10637-015-0266-y>.
- [12] FDA (Center of drug evaluation and research), Multidiscipline review of ribociclib, 2017.
- [13] A. Sorf, J. Hofman, R. Kučera, F. Staud, M. Ceckova, Ribociclib shows potential for pharmacokinetic drug-drug interactions being a substrate of ABCB1 and potent inhibitor of ABCB1, ABCG2 and CYP450 isoforms in vitro, *Biochem. Pharmacol.* 154 (2018) 10–17. <https://doi.org/10.1016/j.bcp.2018.04.013>.
- [14] L. Elens, T. Van Gelder, D.A. Hesselink, V. Haufroid, R.H.N. Van Schaik, CYP3A4\*22: Promising newly identified CYP3A4 variant allele for personalizing pharmacotherapy, *Pharmacogenomics.* 14 (2013) 47–62. <https://doi.org/10.2217/pgs.12.187>.
- [15] B. Rochat, Role of Cytochrome P450 Activity in the Fate of Anticancer Agents and in Drug Resistance, *Clin. Pharmacokinet.* 44 (2005) 349–366. <https://doi.org/10.2165/00003088-200544040-00002>.
- [16] European Medicines Agency, Assessment report of ribociclib, 2017.
- [17] E. Bakos, R. Evers, G. Szakacs, G.E. Tusnady, E. Welker, K. Szabo, M. de Haas, L. van Deemter, P. Borst, a Varadi, B. Sarkadi, Functional multidrug resistance protein (MRP1) lacking the N-terminal transmembrane domain, *J. Biol. Chem.* 273 (1998) 32167–32175. <https://doi.org/10.1074/jbc.273.48.32167>.

- [18] R. Evers, M. Kool, L. van Deemter, H. Janssen, J. Calafat, L.C. Oomen, C.C. Paulusma, R.P. Oude Elferink, F. Baas, A.H. Schinkel, P. Borst, Drug export activity of the human canalicular multispecific organic anion transporter in polarized kidney MDCK cells expressing cMOAT (MRP2) cDNA, *J. Clin. Invest.* 101 (1998) 1310–1319. <https://doi.org/10.1172/JCI928>.
- [19] B. Poller, E. Wagenaar, S.C. Tang, A.H. Schinkel, Double-transduced MDCKII cells to study human P-glycoprotein (ABCB1) and breast cancer resistance protein (ABCG2) interplay in drug transport across the blood-brain barrier, *Mol. Pharm.* 8 (2011) 571–582. <https://doi.org/10.1021/mp1003898>.
- [20] J.W. Jonker, Role of Breast Cancer Resistance Protein in the Bioavailability and Fetal Penetration of Topotecan, *J. Natl. Cancer Inst.* 92 (2000) 1651–1656. <https://doi.org/10.1093/jnci/92.20.1651>.
- [21] A. Martínez-Chávez, H. Rosing, M. Hillebrand, M. Tibben, A.H. Schinkel, J.H. Beijnen, Development and validation of a bioanalytical method for the quantification of the CDK4/6 inhibitors abemaciclib, palbociclib and ribociclib in human and mouse matrices using liquid chromatography-tandem mass spectrometry, *Anal. Bioanal. Chem.* 411 (2019) 5531–5345. <https://doi.org/10.1007/s00216-019-01932-w>.
- [22] FDA, Guidance for Industry Bioanalytical Method Validation, (2018) 1–22.
- [23] European Medicines Agency, Guideline on bioanalytical method validation, 44 (2012) 1–23. [https://www.ema.europa.eu/documents/scientific-guideline/guideline-bioanalytical-method-validation\\_en.pdf](https://www.ema.europa.eu/documents/scientific-guideline/guideline-bioanalytical-method-validation_en.pdf).
- [24] A.H. Schinkel, U. Mayer, E. Wagenaar, C.A.A.M. Mol, L. Van Deemter, J.J.M. Smit, M.A. Van Der Valk, A.C. Voordouw, H. Spits, O. Van Tellingen, M. Zijlman, W. Fibbe, P. Borst, Normal viability and altered pharmacokinetics in mice lacking mdr1-type (drug-transporting) P-glycoproteins, *Proc. Natl. Acad. Sci.* 94 (1997) 4028–4033. <https://doi.org/10.1073/pnas.94.8.4028>.
- [25] J.W. Jonker, J. Freeman, E. Bolscher, S. Musters, A.J. Alvi, I. Titley, A.H. Schinkel, T.C. Dale, Contribution of the ABC Transporters Bcrp1 and Mdr1a/1b to the Side Population Phenotype in Mammary Gland and Bone Marrow of Mice, *Stem Cells.* 23 (2005) 1059–1065. <https://doi.org/10.1634/stemcells.2005-0150>.
- [26] R.A.B. Van Waterschoot, J.S. Lagas, E. Wagenaar, C.M.M. Van Der Kruijssen, A.E. Van Herwaarden, J.Y. Song, R.W. Rooswinkel, O. Van Tellingen, H. Rosing, J.H. Beijnen, A.H. Schinkel, Absence of both cytochrome P450 3A and P-glycoprotein dramatically increases docetaxel oral bioavailability and risk of intestinal toxicity, *Cancer Res.* 69 (2009) 8996–9002. <https://doi.org/10.1158/0008-5472.CAN-09-2915>.
- [27] A.E. Van Herwaarden, E. Wagenaar, C.M.M. Van Der Kruijssen, R.A.B. Van Waterschoot, J.W. Smit, J. Song, M.A. Van Der Valk, O. Van Tellingen, J.W.A. Van Der Hoorn, H. Rosing, J.H. Beijnen, A.H. Schinkel, Knockout of cytochrome P450 3A yields new mouse models for understanding xenobiotic metabolism, *J. Clin. Invest.* 117 (2007) 3583–3592. <https://doi.org/10.1172/JCI33435>.
- [28] Y. Zhang, M. Huo, J. Zhou, S. Xie, PKSolver: An add-in program for pharmacokinetic and pharmacodynamic data analysis in Microsoft Excel, *Comput. Methods Programs Biomed.* 99 (2010) 306–314. <https://doi.org/10.1016/j.cmpb.2010.01.007>.
- [29] D. Gartzke, J. Delzer, L. Laplanche, Y. Uchida, Y. Hoshi, M. Tachikawa, T. Terasaki, J. Sydor, G. Fricker, Genomic knockout of endogenous canine P-glycoprotein in wild-type, human P-glycoprotein and human BCRP transfected MDCKII cell lines by zinc finger nucleases, *Pharm. Res.* 32 (2015) 2060–2071. <https://doi.org/10.1007/s11095-014-1599-5>.
- [30] T.S. Samant, S. Dhuria, Y. Lu, M. Laisney, S. Yang, A. Grandeur, M. Mueller-zsigmondy, K. Umehara, F. Huth, M. Miller, C. Germa, M. Elmeliegy, Ribociclib Bioavailability Is Not Affected by Gastric pH Changes or Food Intake : In Silico and Clinical Evaluations, *Clin. Pharmacol. Ther.* 104 (2018) 374–383. <https://doi.org/10.1002/cpt.940>.
- [31] T. Doi, B. Hewes, T. Kakizume, T. Tajima, N. Ishikawa, Y. Yamada, Phase I study of single-agent ribociclib in Japanese patients with advanced solid tumors, *Cancer Sci.* 109 (2018) 193–198. <https://doi.org/10.1111/cas.13428>.
- [32] K.W. Ward, L.M. Azzarano, Preclinical pharmacokinetic properties of the P-glycoprotein inhibitor GF120918A in the mouse, rat, dog, and monkey, *J. Pharmacol. Exp. Ther.* 310 (2004) 703–709. <https://doi.org/10.1124/jpet.104.068288>.

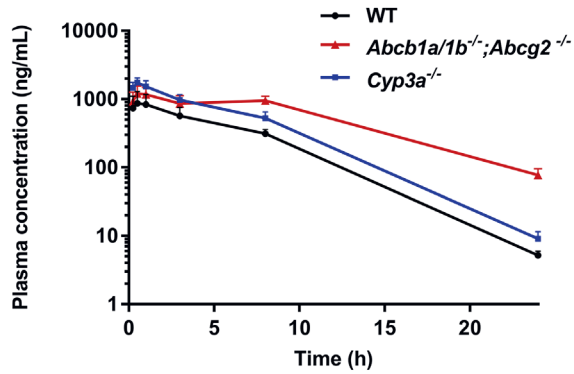
- [33] B.A. Duso, D. Trapani, G. Viale, C. Criscitiello, P. D'Amico, C. Belli, L. Mazzeola, M. Locatelli, I. Minchella, G. Curigliano, Clinical efficacy of ribociclib as a first-line therapy for HR-positive, advanced breast cancer, *Expert Opin. Pharmacother.* 19 (2018) 299–305. <https://doi.org/10.1080/14656566.2018.1429407>.
- [34] D. Kwapisz, Cyclin-dependent kinase 4/6 inhibitors in hormone receptor-positive early breast cancer: preliminary results and ongoing studies, *Breast Cancer.* 25 (2018) 506–516. <https://doi.org/10.1007/s12282-018-0864-6>.
- [35] Y. Patel, A. Davis, A. Kala, J. Roberts, M. Jacus, S. Baker, M. Roussel, C. Stewart, PDTB-12. CNS Penetration of the CDK4/6 inhibitor ribociclib (LEE011) in non-tumor bearing mice and mice bearing orthotopic pediatric brain tumors, *Neuro. Oncol.* 18 (2016) 2–3.
- [36] P.R. Lockman, R.K. Mittapalli, K.S. Taskar, V. Rudraraju, B. Gril, K.A. Bohn, C.E. Adkins, A. Roberts, H.R. Thorsheim, J.A. Gaasch, S. Huang, D. Palmieri, P.S. Steeg, Q.R. Smith, Heterogeneous blood-tumor barrier permeability determines drug efficacy in experimental brain metastases of breast cancer, *Clin. Cancer Res.* 16 (2010) 5664–5678. <https://doi.org/10.1158/1078-0432.CCR-10-1564>.
- [37] C.E. Adkins, A.S. Mohammad, T.B. Terrell-Hall, E.L. Dolan, N. Shah, E. Sechrest, J. Griffith, P.R. Lockman, Characterization of passive permeability at the blood-tumor barrier in five preclinical models of brain metastases of breast cancer, *Clin. Exp. Metastasis.* 33 (2016) 373–383. <https://doi.org/10.1007/s10585-016-9784-z>.
- [38] B. Geoerger, F. Bourdeaut, S.G. DuBois, M. Fischer, T. Cash, J.R. Dobson, A. Marabelle, G.W. Robinson, J.I. Geller, F. Bourdeaut, M. Motta, S. Parasuraman, S. Modak, S.G. Bhansali, S.N. Chi, A. Matano, A.D.J. Pearson, B. Geoerger, N.G. Gottardo, A Phase I Study of the CDK4/6 Inhibitor Ribociclib (LEE011) in Pediatric Patients with Malignant Rhabdoid Tumors, Neuroblastoma, and Other Solid Tumors, *Clin. Cancer Res.* 23 (2017) 2433–2441. <https://doi.org/10.1158/1078-0432.ccr-16-2898>.
- [39] Novartis, Pediatric Oncology Subcommittee of the Oncologic Drugs Advisory Committee Briefing Document LEE011, (2013) 1–19. <https://www.pharmamedtechbi.com/~media/Supporting Documents/The Pink Sheet DAILY/2013/November/114 novartis preview.pdf>.
- [40] R.A. Patchell, The management of brain metastases, *Cancer Treat. Rev.* 29 (2003) 533–540. [https://doi.org/10.1016/S0305-7372\(03\)00105-1](https://doi.org/10.1016/S0305-7372(03)00105-1).
- [41] P.S. Steeg, K.A. Camphausen, Q.R. Smith, Brain metastases as preventive and therapeutic targets, *Nat. Rev. Cancer.* 11 (2011) 352–363. <https://doi.org/10.1038/nrc3053>.
- [42] G. Szakács, A. Váradi, C. Özvegy-Laczkó, B. Sarkadi, The role of ABC transporters in drug absorption, distribution, metabolism, excretion and toxicity (ADME-Tox), *Drug Discov. Today.* 13 (2008) 379–393. <https://doi.org/10.1016/j.drudis.2007.12.010>.

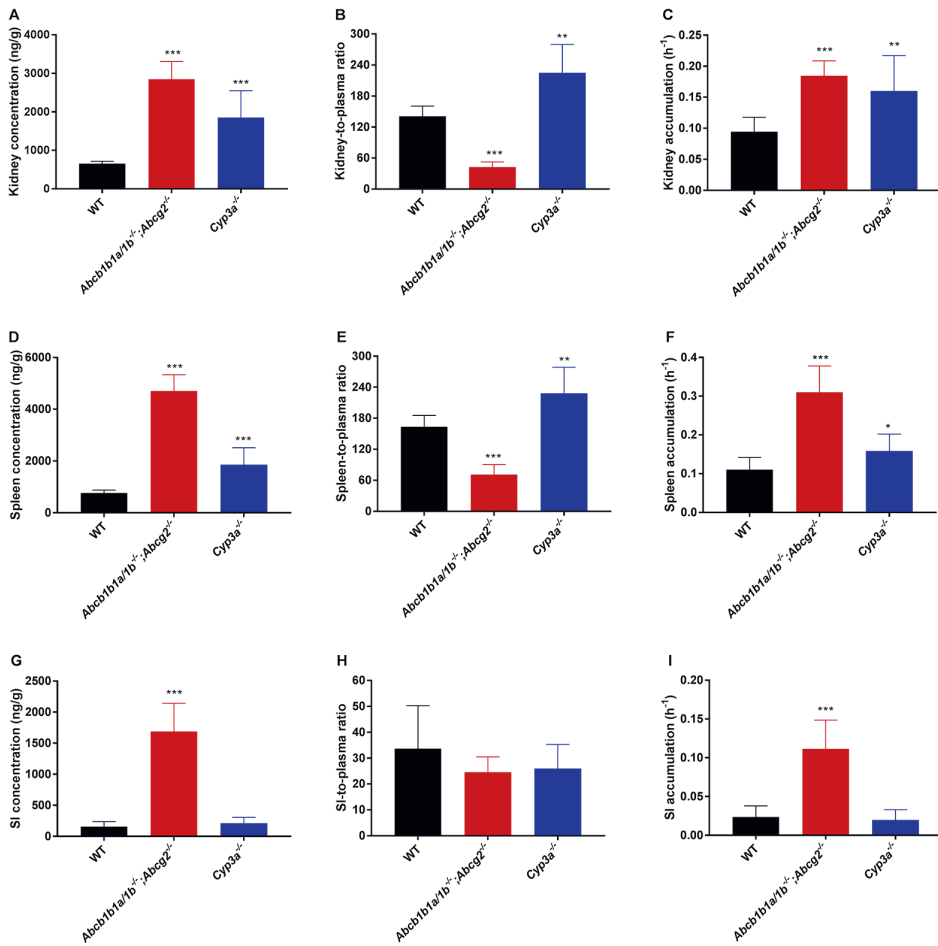


## Supplementary material

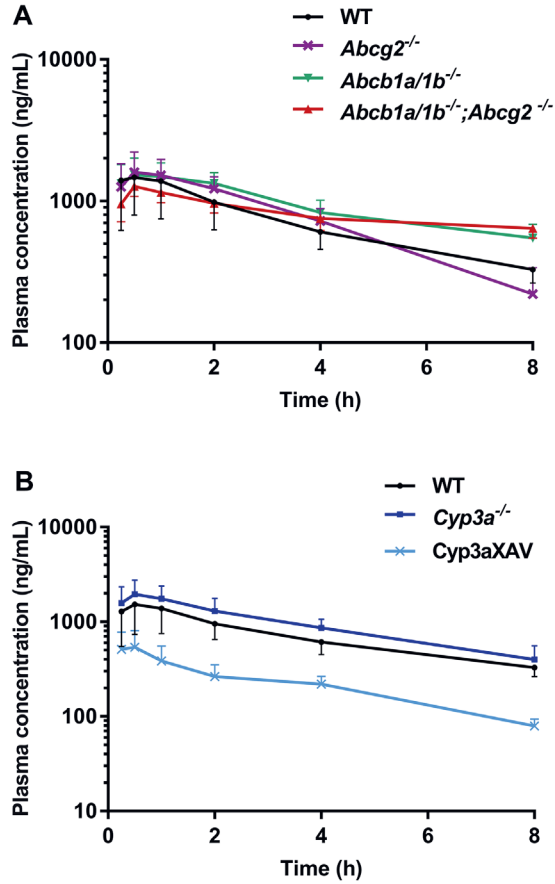


Supplementary Figure S1. Chemical structure of ribociclib.

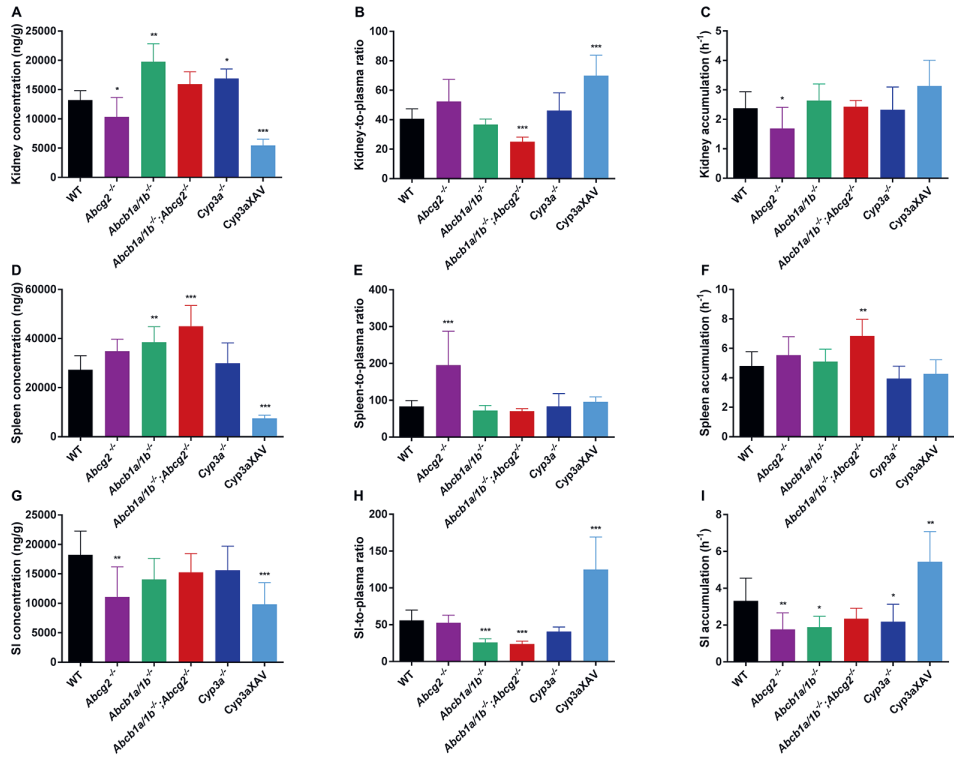
Supplementary Figure S2. Semi-log plot of plasma concentration-time curves of ribociclib over 24 h in female WT, *Abcb1a/1b*<sup>-/-</sup>;*Abcg2*<sup>-/-</sup>, and *Cyp3a*<sup>-/-</sup> mice after oral administration of 20 mg/kg. Data are presented as mean  $\pm$  SD (n = 6).



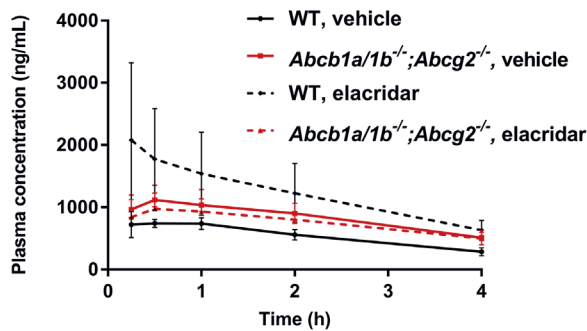
**Supplementary Figure S3.** Kidney, spleen and small intestinal tissue concentration (A, D, G), tissue-to-plasma ratio (B, E, H), and tissue accumulation (C, F, I) of ribociclib in female WT, *Abcb1a/1b*<sup>-/-</sup>; *Abcg2*<sup>-/-</sup>, and *Cyp3a*<sup>-/-</sup> mice 24 h after oral administration of 20 mg/kg of ribociclib. Data are presented as mean ± SD (n = 6). \*, P < 0.05; \*\*, P < 0.01; \*\*\*, P < 0.001 compared to WT mice.



**Supplementary Figure S4.** Semi-log plot of plasma concentration-time curves of ribociclib over 8 h in female WT, *Abcg2*<sup>-/-</sup>, *Abcb1a/1b*<sup>-/-</sup>, *Abcb1a/1b*<sup>-/-</sup>;*Abcg2*<sup>-/-</sup> (A), and WT, *Cyp3a*<sup>-/-</sup>, *Cyp3aXAV* (B) mice after oral administration of 20 mg/kg ribociclib. Data are presented as mean ± SD (n = 6-8).



**Supplementary Figure S5.** Kidney, spleen and small intestinal (SI) tissue concentration (A, D, G), tissue-to-plasma ratio (B, E, H), and tissue accumulation (C, F, I) of ribociclib in female WT, *Abcb1a/1b*<sup>-/-</sup>;*Abcg2*<sup>-/-</sup>, and *Cyp3a*<sup>-/-</sup> mice 8 h after oral administration of 20 mg/kg of ribociclib. Data are presented as mean ± SD (n = 6). \*, P < 0.05; \*\*, P < 0.01; \*\*\*, P < 0.001 compared to WT mice.



**Supplementary Figure S6.** Plasma concentration-time curves of ribociclib over 4 h in female WT and *Abcb1a/1b*<sup>-/-</sup>;*Abcg2*<sup>-/-</sup> mice after oral administration of 20 mg/kg ribociclib with oral vehicle or elacridar coadministration (50 mg/kg). Data are presented as mean ± SD (n = 5-6).





# 6

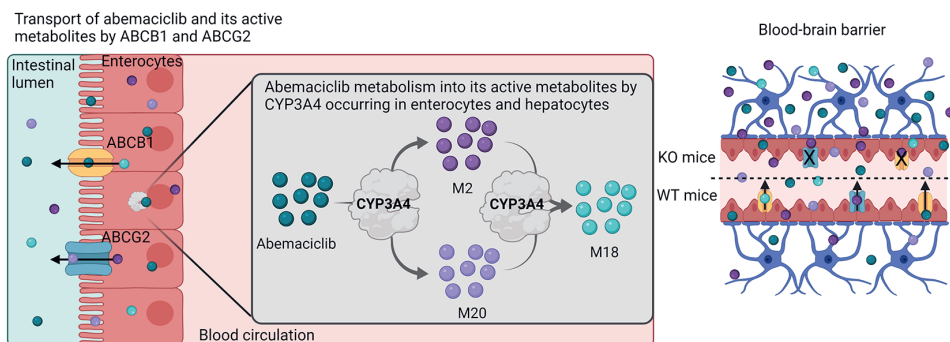
ABCB1 and ABCG2 limit brain penetration and,  
together with CYP3A4, total plasma exposure of  
abemaciclib and its active metabolites

*Submitted*

Alejandra Martínez-Chávez  
Nancy H. C. Loos  
Maria C. Lebre  
Matthijs M. Tibben  
Hilde Rosing  
Jos H. Beijnen  
Alfred H. Schinkel

## Abstract

Abemaciclib is the third cyclin-dependent kinase (CDK) 4/6 inhibitor approved for the treatment of breast cancer and currently under investigation for other malignancies, including brain cancer. Primarily CYP3A4 metabolizes abemaciclib, forming three active metabolites (M2, M20 and M18) that are likely relevant for abemaciclib efficacy and toxicity. We investigated the impact of ABCB1 (P-gp), ABCG2 (BCRP) and CYP3A on the pharmacokinetics and tissue distribution of abemaciclib and its metabolites using genetically modified mice. *In vitro*, abemaciclib was efficiently transported by hABCB1 and mAbcg2, and slightly by hABCG2, but the active metabolites were transported even better. Upon oral administration of 10 mg/kg abemaciclib, absence of *Abcg2* and especially *Abcb1a/1b* significantly increased the plasma  $AUC_{0-24h}$  and  $C_{max}$  of M2 and M18. Furthermore, the relative brain penetration of abemaciclib, M2 and M20 was dramatically increased by 25-, 4- and 60-fold, respectively, in *Abcb1a/1b;Abcg2*<sup>-/-</sup> mice, and to a lesser extent in single *Abcb1a/1b*<sup>-/-</sup> or *Abcg2*<sup>-/-</sup> mice. The recovery of all active compounds in the small intestine content was profoundly reduced in *Abcb1a/1b;Abcg2*<sup>-/-</sup> mice, with smaller effects in single *Abcb1a/1b*<sup>-/-</sup> and *Abcg2*<sup>-/-</sup> mice. Our results indicate that *Abcb1a/1b* and *Abcg2* cooperatively and profoundly limit the brain penetration of abemaciclib and its active metabolites, and likely also participate in their hepatobiliary or direct intestinal elimination. Moreover, transgenic human CYP3A4 drastically reduced the abemaciclib plasma  $AUC_{0-24h}$  and  $C_{max}$  by 7.5- and 5.6-fold, respectively, relative to *Cyp3a*<sup>-/-</sup> mice. These insights may help to optimize the clinical development of abemaciclib, especially for the treatment of brain malignancies.





## Introduction

Breast cancer is the most prevalent diagnosed malignancy worldwide and the leading global cause of cancer mortality in women, with an incidence increase expected for the coming years [1,2]. An important improvement in the treatment of patients with advanced or metastatic breast cancer was the recent development and approval of cyclin-dependent kinase 4 and 6 (CDK4/6) inhibitors. CDK4 and 6 form a complex with cyclin D that phosphorylates the retinoblastoma protein, resulting in release of the E2F transcription factor and progression of the cell cycle. Thus, inhibition of CDK4 and 6 leads to cell cycle arrest. Apart from breast cancer, dysregulation of the cell cycle due to aberrations in the CDK4/6 pathway has been encountered in other cancer types, which might expand the use of these inhibitors [3]. Abemaciclib was the third CDK4/6 inhibitor approved by the European Medicines Agency (EMA) and the U.S. Food and Drug Administration (FDA) for the treatment of hormone receptor-positive and human epidermal growth factor receptor (HER) 2-negative breast cancer in combination therapy, and it is the only agent in this class that can be used as monotherapy [4].

In the clinic, abemaciclib is orally administered showing a slow absorption, with a median time to maximum plasma concentration ( $t_{max}$ ) of 4 h and high inter-individual variation in its pharmacokinetics. At steady state, for the doses of 150 mg (combined treatment) and 200 mg (monotherapy), the area under the plasma concentration-time curve of abemaciclib ( $AUC_{0-\infty}$ ) is 2390 and 3000 ng/mL·h (equivalent to 4718 and 5922 nM), and the maximum plasma concentration ( $C_{max}$ ) is 169 and 197 ng/mL (equivalent to 334 and 389 nM), respectively [5]. Abemaciclib is primarily metabolized by CYP3A4, forming three active metabolites: *N*-desethylabemaciclib (M2), hydroxyabemaciclib (M20), and hydroxy-*N*-desethylabemaciclib (M18), combining the modifications of M2 and M20 (Figure 1). These metabolites have even higher affinity for CDK4 and CDK6 than abemaciclib, with half-maximal inhibitory concentrations ( $IC_{50}$ ) of 1.2 and 1.3 nM for M2, 1.5 and 1.9 nM for M20, and 1.2 and 2.7 nM for M18, *versus* 2.0 and 9.6 nM for abemaciclib, based on a cell-free kinase assay. In addition, these metabolites are abundant in human plasma, with the AUCs of abemaciclib, M2, M20, and M18 accounting for 34%, 13%, 26%, and 5% of the total radioactivity, respectively. The protein binding of these metabolites was also comparable to that of abemaciclib (96.3%). Moreover, the excretion of abemaciclib occurred mainly through feces, mostly as metabolites [6,7]. Altogether, it is likely that the therapeutic effect of abemaciclib is due at least in part also to these active metabolites.

Currently, several clinical studies involving abemaciclib are investigating its efficacy for the treatment of other cancer types including brain cancers, such as gliomas and brain metastases arising from solid tumors with CDK4/6 mutations [8]. However, brain cancer treatment remains challenging in part due to the low penetration of most anticancer drugs into the brain, caused mainly by the blood-brain barrier (BBB). This barrier,

formed by endothelial cells with intercellular tight junctions, expresses various transporters that control the entry of compounds into the brain [9,10]. Although many drugs have promising physicochemical characteristics to cross the BBB by passive diffusion, their brain penetration is still restricted by the ATP-binding cassette (ABC) efflux transporters expressed at the BBB [10,11].

The apical ABC transporters are transmembrane proteins expressed in the apical membrane of cells, that utilize ATP hydrolysis to extrude endogenous and exogenous compounds. P-glycoprotein (ABCB1, P-gp, MDR1) and the breast cancer resistance protein (ABCG2, BCRP) are important transporters for drugs because they have a wide substrate specificity and can control the disposition of substrate compounds. Apart from limiting the brain penetration, these ABC transporters can control the net absorption and elimination of drugs, which can impact drug pharmacokinetics [12–14]. They are expressed in the intestinal epithelial cells, where substrates are translocated into the intestinal lumen, and in the proximal tubule of nephrons and in the bile canalicular membrane of hepatocytes, where substrates are transported from blood into the urine and bile, respectively [12,14]. Furthermore, the efficacy of anticancer drugs can be compromised by the overexpression of ABCB1 and ABCG2 in tumor cells, conferring multidrug resistance since many of these drugs are readily transported substrates [15,16].

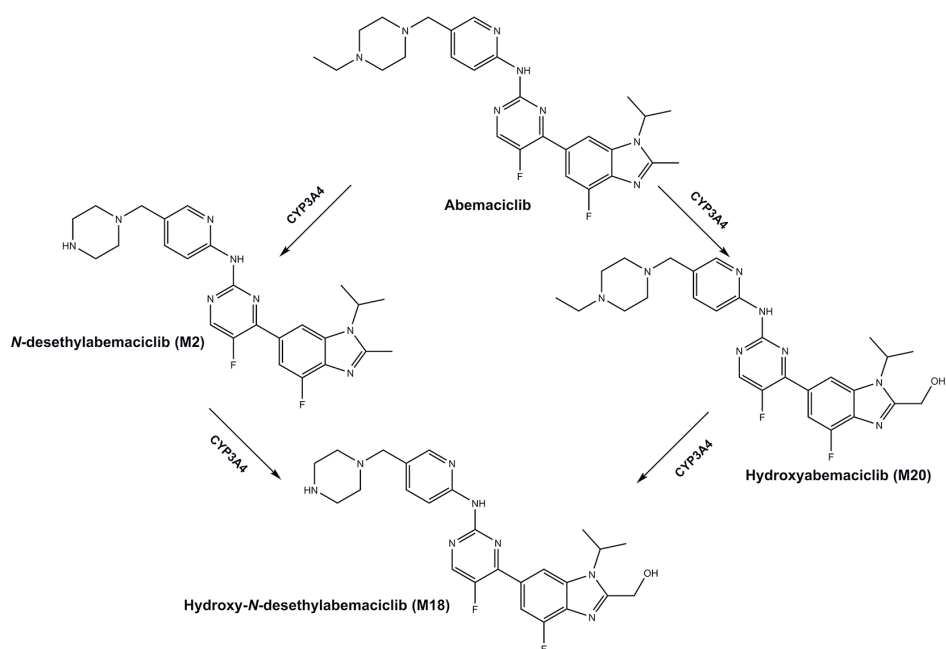


**Figure 1.** Abemaciclib metabolism by CYP3A4 with the primary formation of N-desethylabemaciclib (M2) and hydroxyabemaciclib (M20). Subsequently, hydroxy-N-desethylabemaciclib (M18) is formed, combining the modifications in M2 and M20.

A previous study reported that abemaciclib is a good substrate of human (h) ABCB1 and mouse (m) *Abcg2* *in vitro*, and that the brain penetration of abemaciclib increased around 3-fold in *Abcb1*-deficient mice or in rats previously dosed with an ABCB1 inhibitor [17]. The *in vitro* and *in vivo* influence of ABCB1 on the transport and disposition of M2, M20 and M18 has not been reported so far, nor the influence of ABCG2 on the disposition of any of the abemaciclib active compounds. Since abemaciclib active metabolites probably contribute to the clinical efficacy and safety profile of this drug, it is important to further characterize the disposition of these compounds and to determine the role of ABC transporters in their pharmacokinetics. Thus, the objective of this study was to determine whether abemaciclib and its active metabolites (M2, M20 and M18) are transported by ABCB1 and ABCG2 *in vitro*. Furthermore, using genetically modified mouse models, we investigated the single and combined effects of these ABC transporters on the tissue distribution and oral plasma exposure of abemaciclib and its metabolites. Finally, we explored the *in vivo* role of CYP3A4 in the pharmacokinetics of all abemaciclib active compounds.

## Materials and methods

### Drugs and chemicals

Abemaciclib was purchased from Alsachim (Illkirch-Graffenstaden, France), N-desethylabemaciclib from Clearsynth (Mumbai, India), and hydroxyabemaciclib (M20) and hydroxy-N-desethylabemaciclib hydrochloride (M18) from MedChemExpress LLC (Monmouth Junction, NJ). Zosuquidar and Ko143 were obtained from Sequoia Research Products (Pangbourne, UK) and Tocris Bioscience (Bristol, UK), respectively. Dimethylsulfoxide (DMSO) was supplied by Sigma Aldrich and potassium dihydrogen phosphate from Merck (Darmstadt, Germany). Isoflurane was purchased from Pharmachemie (Haarlem, The Netherlands) and heparin 5000 IU/mL from Leo Pharma (Breda, The Netherlands). Bovine serum albumin (BSA) fraction V was obtained from Roche Diagnostics GmbH (Mannheim, Germany).

For cell culture, Dulbecco's Modified Essential Medium (DMEM) glutamax, penicillin-streptomycin 10,000 U/L, and Dulbecco's Phosphate-Buffered saline (DPBS) were supplied by Life Technologies and Fetal Bovine Serum (FBS) was purchased from Serana (Pessin, Germany).

### *In vitro* transport studies

#### *Cell culture*

Human (h)ABCB1-, hABCG2- or mouse (m)*Abcg2*-overexpressing Madin-Darby Canine Kidney (MDCK-II) cell lines were previously generated in our institute [18–21]. These subclones together with the parental MDCK-II line were cultured at 37 °C and 5% CO<sub>2</sub>

in supplemented DMEM, in which FBS and penicillin-streptomycin were added at 10% and 1% (v/v), respectively. All cell lines were cultured for a minimum of 2 weeks before the transport experiment.

#### *Working solutions*

Independent stock solutions of abemaciclib, M2, M20, M18, zosuquidar and Ko143 were prepared in DMSO. From these, on the day of experiment, three working solutions containing abemaciclib and its metabolites were freshly prepared by diluting the stock solutions in FBS-supplemented DMEM at concentrations of 0.5  $\mu\text{M}$  for abemaciclib and 1  $\mu\text{M}$  each for M2, M20 and M18. One of these working solutions was also spiked with zosuquidar and another with zosuquidar and Ko143 at 3  $\mu\text{M}$  for both inhibitors.

#### *Transport experiment*

Cells were seeded in 12-well Transwell permeable supports (Corning Life Sciences, Tewksbury, MA) with a polycarbonate membrane (3  $\mu\text{m}$  pore size, 1.2 cm diameter) at a density of  $2.5 \times 10^5$  cells/well. On days 1 and 2 after seeding, supplemented DMEM was refreshed, while monolayers with tight junctions were formed in each well. The integrity of these monolayers was assessed by measuring the transepithelial electrical resistance (TEER) prior to the experiment, where all the values were within the reference for each cell line ( $\geq 70 \Omega \text{ cm}^2$  for the parental and hABCG2-overexpressing,  $\geq 200 \Omega \text{ cm}^2$  for the hABCB1-overexpressing, and  $\geq 140 \Omega \text{ cm}^2$  for the mAbcg2-overexpressing cell lines). On day 3, the transport experiment was performed. Cell monolayers were first washed with DPBS, and thereafter pre-incubated for 1 h with only FBS-supplemented DMEM, 3  $\mu\text{M}$  zosuquidar or 3  $\mu\text{M}$  Ko143 and zosuquidar. Zosuquidar was used to inhibit the endogenous and the human ABCB1, and Ko143 was used to inhibit the murine and human ABCG2. After pre-incubation, the medium was removed and working solutions containing abemaciclib and its metabolites, either alone or in combination with the appropriate inhibitor(s), were added in the donor compartment, and FBS-supplemented DMEM, either with or without inhibitors, was added in the acceptor compartment. Transport experiments were conducted in triplicate and independently in both directions: from apical-to-basolateral (A-B) and from basolateral-to-apical (B-A). Transwell plates were maintained at 37°C and 5%  $\text{CO}_2$  during the experiment, and 50  $\mu\text{L}$  was sampled from the acceptor compartment at 1, 2, and 4 h. The TEER was re-measured after the last time point, and in all cases it did not decrease, demonstrating the integrity of the monolayer throughout the experiment. All samples were stored at -20 °C until analysis.

#### *Bioanalysis of samples*

Abemaciclib, M2, M20 and M18 were quantified in samples collected during the transport assay, using a liquid chromatography-tandem mass spectrometry (LC-MS/MS) bioanalytical method that we developed [22]. Calibrators and quality control samples were prepared in FBS-supplemented DMEM, and the linearity, accuracy and precision were maintained throughout the calibration range.

### Calculations

For abemaciclib, M2, M20 and M18 each, the total amount transported was calculated correcting for the sampled volume and the removed compound in the acceptor compartment at the previous time points. Active transport was evaluated by the relative transport ratio, which was calculated for each compound by dividing the transported amount over 4 h in the B-A direction by the transported amount over 4 h in the A-B direction.

## Plasma pharmacokinetic and tissue distribution studies

### Animals

Female mice (FVB strain background) from various genotypes, including wild-type, *Abcb1a/1b*<sup>-/-</sup>, *Abcg2*<sup>-/-</sup>, *Abcb1a/1b*<sup>-/-</sup>;*Abcg2*<sup>-/-</sup>, *Cyp3a*<sup>-/-</sup>, and *Cyp3aXAV* (humanized mouse model with expression of CYP3A4 in liver and small intestine in *Cyp3a*-deficient mice) were used between 9 and 16 weeks of age [21,23,24]. Animals received a standard diet (Transbreed, SDS Diets, Technilab-BMI, Someren, The Netherlands) and acidified water *ad libitum*. They were housed with controlled temperature and in a 12 h light/dark cycle. Mouse housing and handling was conducted according to institutional guidelines complying with Dutch and EU Legislation. Studies were reviewed and approved by the internal animal care and use committee (project approval number from The Dutch Central Animal Testing Committee: AVD301002016595).

### Pharmacokinetic experiments

Mice were fasted for at least 2 h before oral administration of 10 mg/kg abemaciclib, formulated in a dosing solution containing 1 mg of abemaciclib per mL of 25 mM phosphate buffer (KH<sub>2</sub>PO<sub>4</sub>) pH 3 / DMSO (95:5, v/v). Blood was withdrawn by tail cut in heparin-coated microvettes (Sarstedt, Nümbrecht, Germany) at 0.5, 1, 2, 4, and 8 h or at 0.125, 0.25, 0.5, 1 and 2 h for the experiments terminated at 24 and 4 h, respectively. At the terminal time point (24 or 4 h) blood was collected by cardiac puncture under isoflurane anesthesia, and heparin was used as anticoagulant. Mice were then directly sacrificed by cervical dislocation and brain, liver, small intestine, small intestine content, kidneys, lungs and spleen were collected and weighed.

Plasma was separated from blood cells by centrifugation at 9000g and 4 °C for 6 min. Tissues were homogenized with 4% (w/v) BSA in water using the Fast Prep-24 5G grinder (MP Biomedicals Inc., Santa Ana, CA). One mL of 4% BSA was added to brain and spleen, 2 mL to lungs, kidneys and small intestine content, and 3 mL to liver and small intestine tissue.

Plasma samples and tissue homogenates were stored at -20 and -70 °C, respectively, until bioanalytical measurement.

### *Bioanalysis of mouse samples*

Abemaciclib, M2, M20 and M18 were quantified or semi-quantified in plasma and tissue homogenate samples using an LC-MS/MS bioanalytical method that was previously developed [22]. Abemaciclib and M2 were quantified using appropriate reference standards in the calibration range from 0.2-400 ng/mL. M18 and M20 were semi-quantified based on the calibration curve of abemaciclib, since the relevant reference standards were not available when the *in vivo* experiments were performed.

### *Pharmacokinetic calculations and statistics*

For each compound, plasma pharmacokinetic parameters, including the area under the plasma concentration-time curve ( $AUC_{0-t}$ ), maximum concentration ( $C_{max}$ ) and time to reach the maximum concentration ( $t_{max}$ ) were calculated using the add-in PK Solver program for Microsoft Excel [25]. The tissue-to-plasma ratio and the tissue accumulation were calculated by dividing the tissue concentration by the plasma concentration and the plasma  $AUC_{0-t}$ , respectively. Statistical analysis was performed using the GraphPad Prism 9.1.0 software (GraphPad, San Diego, CA). For two- and multiple-group comparisons, student's t and one-way ANOVA tests were used, respectively. When  $P < 0.05$ , differences were considered statistically significant. The Bonferroni *post-hoc* analysis was used for multiple comparisons.

## Results

### **Abemaciclib and its active metabolites are transported by ABCB1 and ABCG2 *in vitro***

Transport efficacy of abemaciclib, M2, M20, and M18 by ABCB1 and ABCG2 was investigated *in vitro* in a simultaneous transport assay of abemaciclib (0.5  $\mu$ M) and the metabolites (each 1  $\mu$ M; total compound concentration: 3.5  $\mu$ M) across polarized MDCK-II monolayers formed with parental, hABCB1-, hABCG2- or mAbcg2-overexpressing cells. In the parental cell line, abemaciclib was similarly translocated in both directions, apical-to-basolateral (BA) and basolateral-to-apical (BA), yielding a relative transport ratio ( $r$ ) of 1.1 (Figure 2A). In the presence of zosuquidar, which was added to inhibit the endogenous canine ABCB1 [26], this was slightly but not significantly reduced ( $r = 0.8$ , Figure 2B). In the hABCB1-transduced cell line, abemaciclib was clearly apically transported ( $r = 4.4$ , Figure 2C), and this transport was completely inhibited by zosuquidar ( $r = 1.0$ , Figure 2D), indicating that abemaciclib is a good substrate of ABCB1. For hABCG2- and mAbcg2-transduced cells, zosuquidar was added to inhibit any potential background transport by the endogenous canine ABCB1. Low apically directed transport of abemaciclib was detected in the hABCG2-overexpressing cell line ( $r = 1.4$ , Figure 2E), and extensive transport for the mAbcg2-transduced cell line ( $r = 10.0$ , Figure 2G). In both cases, the ABCG2 inhibitor Ko143 abrogated the active transport, yielding  $r = 0.8$  and 1.0, respectively (Figures 2F and 2H).

All three abemaciclib active metabolites were even better substrates of ABCB1 and ABCG2 than the parent drug, with both higher transport ratios and absolute amounts of drug transported, even after correction for the 2-fold higher starting concentrations of the metabolites. Firstly, M2 was actively transported by the endogenous canine and human ABCB1, with relative transport ratios of 3.6 and 29.4, respectively (Figure 3A and C). M2 was also transported extensively by hABCG2 ( $r = 14.4$ , Figure 3E) and mAbcg2 ( $r = 46.3$ , Figure 3G). Active transport of M2 was completely inhibited by zosuquidar and/or Ko143 ( $r = 0.7 - 0.9$ , Figure 3B, D, F and H). Secondly, in the parental cell line, M20 was slightly transported to the apical side ( $r = 1.3$ , Figure 4A), whereas in the MDCK-II-hABCB1 cell line, it was efficiently transported ( $r = 9.9$ , Figure 4C). M20 was also an excellent substrate of both hABCG2 ( $r = 5.0$ , Figure 4E) and mAbcg2 ( $r = 36.4$ , Figure 4G). Active transport of M20 in these cell lines was completely suppressed by adding the ABCB1 and/or ABCG2 inhibitors ( $r = 0.7 - 1.0$ , Figure 4B, D, F and H). Finally, M18 transepithelial transport by ABCB1 and ABCG2 is depicted in Figure 5, demonstrating efficient transport even in the parental MDCK-II cell line ( $r = 9.5$ , Figure 5A). Moreover, M18 was avidly transported in the apical direction in cells overexpressing hABCB1 ( $r = 38.5$ ), hABCG2 ( $r = 31.2$ ) and mAbcg2 ( $r = 35.6$ ) (Figures 5C, E, G). All transport was markedly inhibited with zosuquidar and/or Ko143 ( $r = 0.8 - 1.2$ , Figures 5B, D, F, and H). In summary, abemaciclib, M2, M20 and M18 are good to excellent transport substrates of both ABCB1 and ABCG2.

### Plasma exposure of total abemaciclib active compounds is limited by ABCB1 and ABCG2

The potential effect of ABCB1 and ABCG2 on the pharmacokinetics of abemaciclib, M2, M20 and M18 was investigated in an *in vivo* pilot study using wild-type and *Abcb1a/1b;Abcg2*<sup>-/-</sup> mice, where 10 mg/kg of abemaciclib was orally administered. In wild-type mice, abemaciclib was the most abundant compound in plasma, followed by M2, while M20 and M18 were relatively low. Figure 6A-D shows the plasma concentration time curves of these compounds and the active compounds combined (Figure 6E). For abemaciclib, the  $AUC_{0-24h}$  and  $C_{max}$  in *Abcb1a/1b;Abcg2*<sup>-/-</sup> mice were not significantly different from those in wild-type mice (Figure 6A, Table 1,  $P > 0.05$ ). In contrast, M2 plasma  $AUC_{0-24h}$  and  $C_{max}$  were 5.3- and 3.0-fold increased, respectively, in *Abcb1a/1b;Abcg2*<sup>-/-</sup> compared to wild-type mice (Figure 6B, Table 2,  $P < 0.001$ ). Consequently, the plasma  $AUC_{0-24h}$  of M2 in *Abcb1a/1b;Abcg2*<sup>-/-</sup> mice was even higher than that of abemaciclib. The  $AUC_{0-24h}$  and  $C_{max}$  of M20 were not significantly different between the two mouse strains (Figure 6C, Table 3,  $P > 0.05$ ). Finally, M18 plasma exposure was significantly increased in the absence of *Abcb1a/1b* and *Abcg2* (Figure 6D, Table 4). Due to the very low concentrations of M18 detected in wild-type mice, an increase of (at least) 3.5-fold in the  $AUC_{0-24h}$  in *Abcb1a/1b;Abcg2*<sup>-/-</sup> mice could only be estimated.

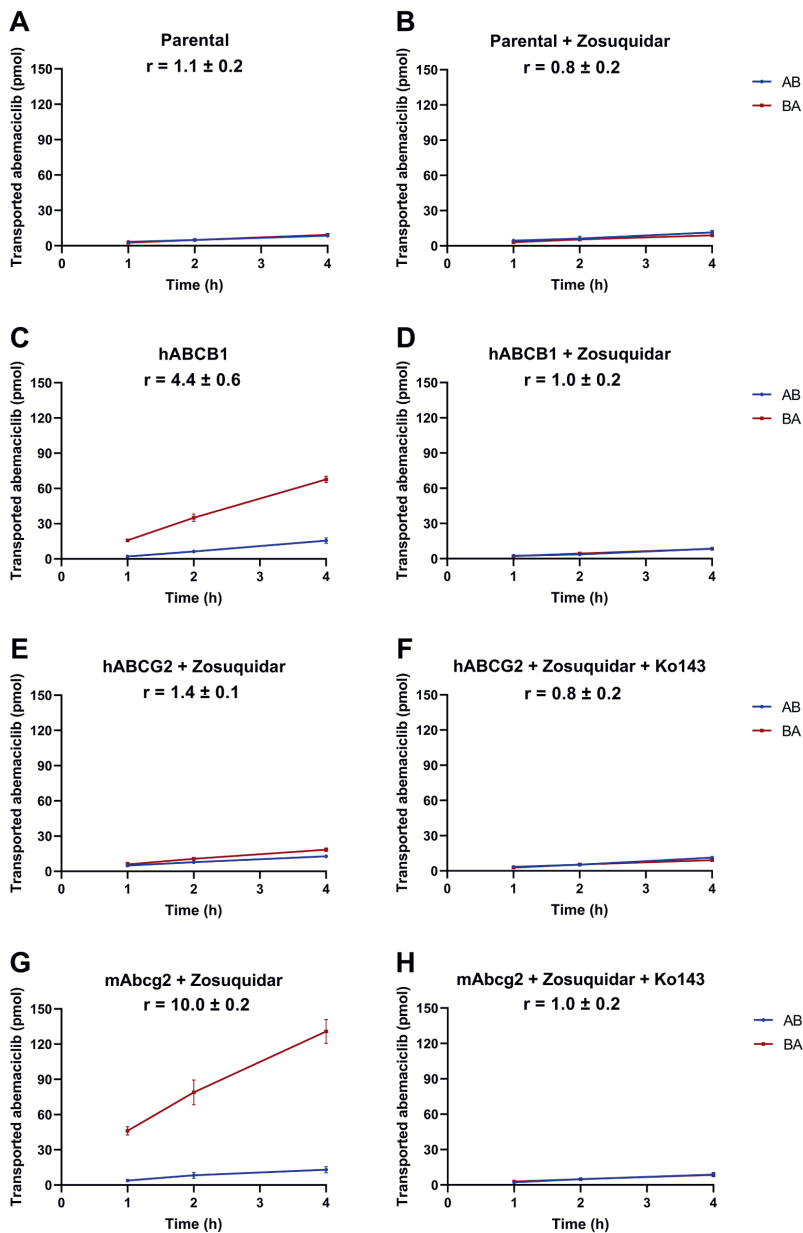


**Figure 2.** *In vitro* bidirectional transport of abemaciclib (0.5  $\mu\text{M}$ ) across MCDK-II cell monolayers formed with parental (A, B) or human ABCB1 (C, D), human ABCG2 (E, F), or murine Abcg2 (G, H) overexpressing cell lines. At  $t = 0$  abemaciclib (as well as M2, M20, and M18 at 1  $\mu\text{M}$  each) was added in the donor compartment, and at 1, 2, and 4 h the total transported amount of abemaciclib in the acceptor compartment was determined. Apical-to-basolateral (AB) transport is presented with the red line and basolateral-to-apical (BA) transport with the blue line. Zosuquidar (3  $\mu\text{M}$ ) was added to inhibit the human and/or the endogenous ABCB1, while Ko143 (3  $\mu\text{M}$ ) was added to inhibit the human or murine ABCG2. Data are presented as mean  $\pm$  SD ( $n = 3$ ),  $r$  = relative transport ratio  $\pm$  SD.



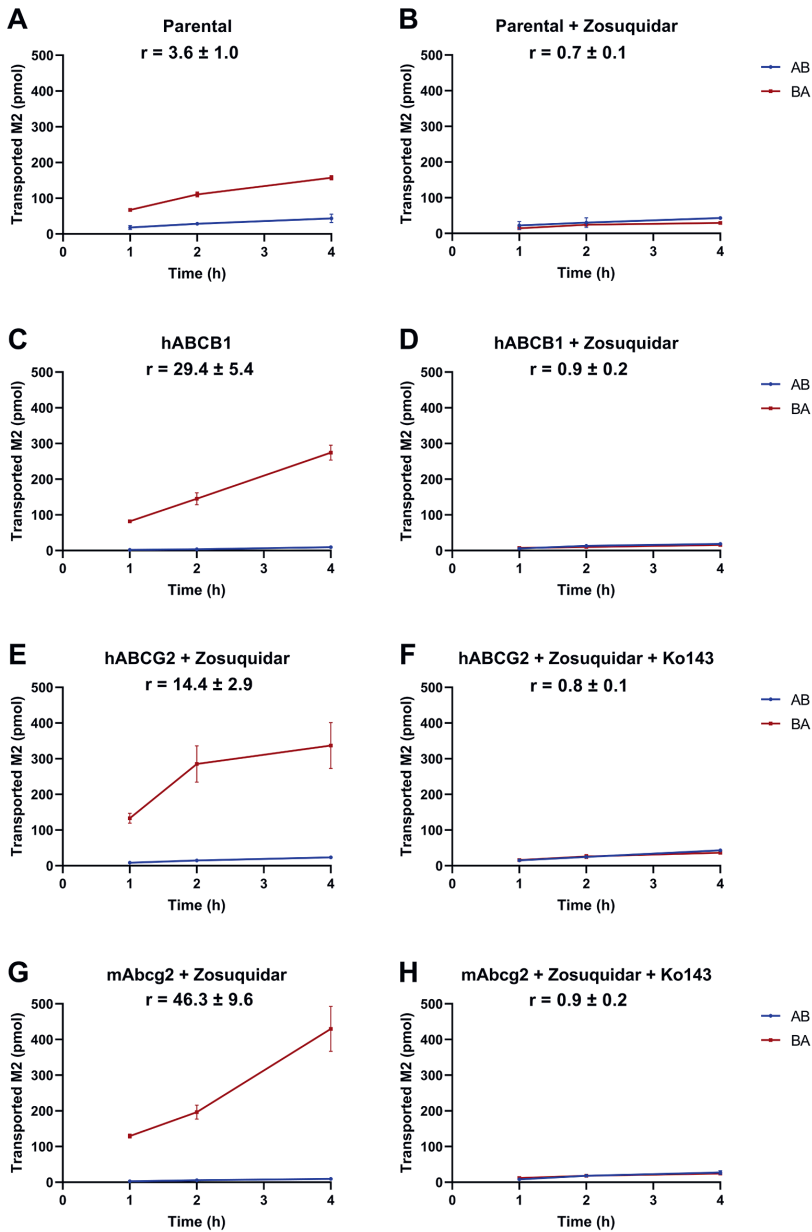


**Figure 3.** *In vitro* bidirectional transport of N-desethylabemaciclib (M2, 1  $\mu$ M) across MCDK-II cell monolayers formed with parental (A, B) or human ABCB1 (C, D), human ABCG2 (E, F), or mouse Abcg2 (G, H) overexpressing cell lines. At  $t = 0$  M2 (as well as abemaciclib at 0.5  $\mu$ M and M20 and M18 at 1  $\mu$ M each) was added in the donor compartment, and at 1, 2, and 4 h the total transported amount of M2 in the acceptor compartment was determined. Apical-to-basolateral (AB) transport is presented with the red line and basolateral-to-apical (BA) transport with the blue line. Zosuquidar (3  $\mu$ M) was added to inhibit the human and/or the endogenous ABCB1, while Ko143 (3  $\mu$ M) was added to inhibit the human or mouse ABCG2. Data are presented as mean  $\pm$  SD ( $n = 3$ ),  $r$  = relative transport ratio  $\pm$  SD.

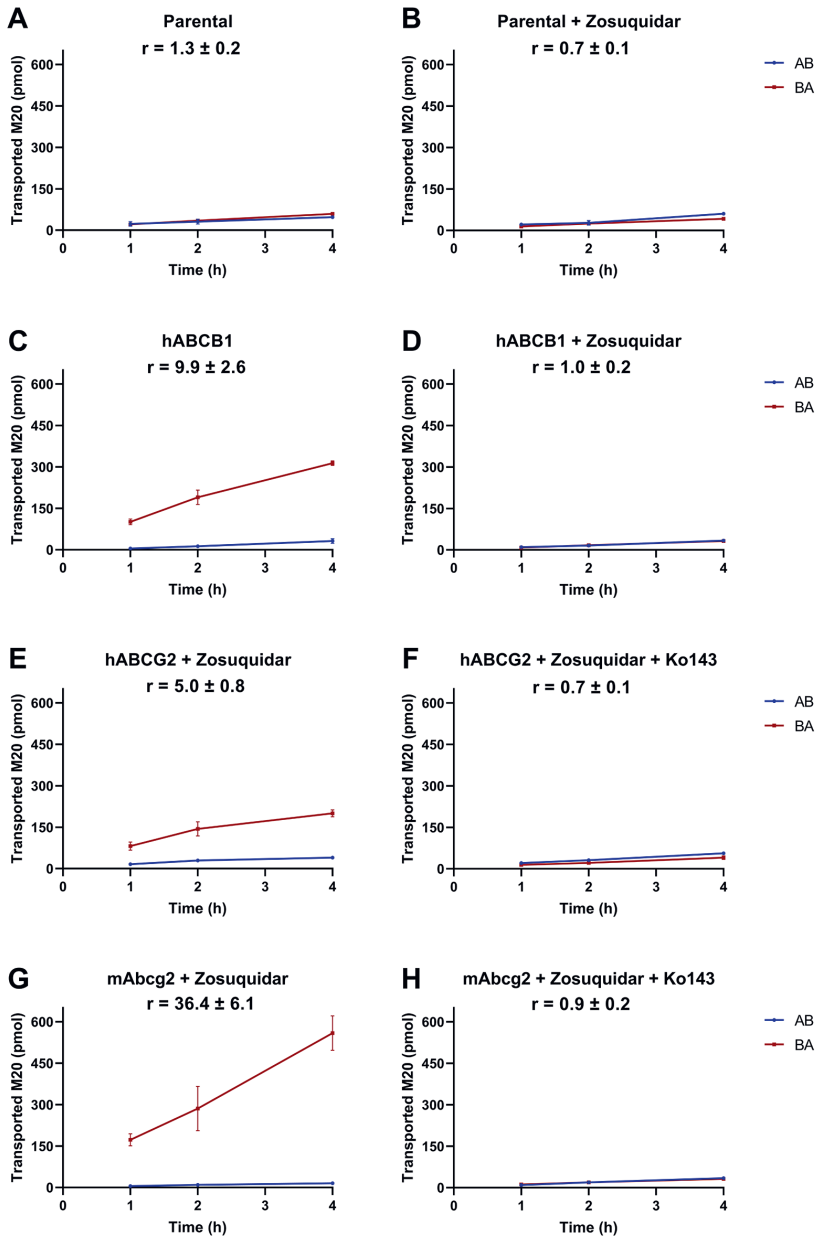


**Figure 4.** *In vitro* bidirectional transport of hydroxyabemaciclib (M20, 1  $\mu$ M) across MCDK-II cell monolayers formed with parental (A, B) or human ABCB1 (C, D), human ABCG2 (E, F), or mouse Abcg2 (G, H) overexpressing cell lines. At  $t = 0$  M20 (as well as abemaciclib at 0.5  $\mu$ M and M2 and M18 at 1  $\mu$ M each) was added in the donor compartment, and at 1, 2, and 4 h the total transported amount of M20 in the acceptor compartment was determined. Apical-to-basolateral (AB) transport is presented with the red line and basolateral-to-apical (BA) transport with the blue line. Zosuquidar (3  $\mu$ M) was added to inhibit the human and/or the endogenous ABCB1, while Ko143 (3  $\mu$ M) was added to inhibit the human or mouse ABCG2. Data are presented as mean  $\pm$  SD ( $n = 3$ ),  $r$  = relative transport ratio  $\pm$  SD.

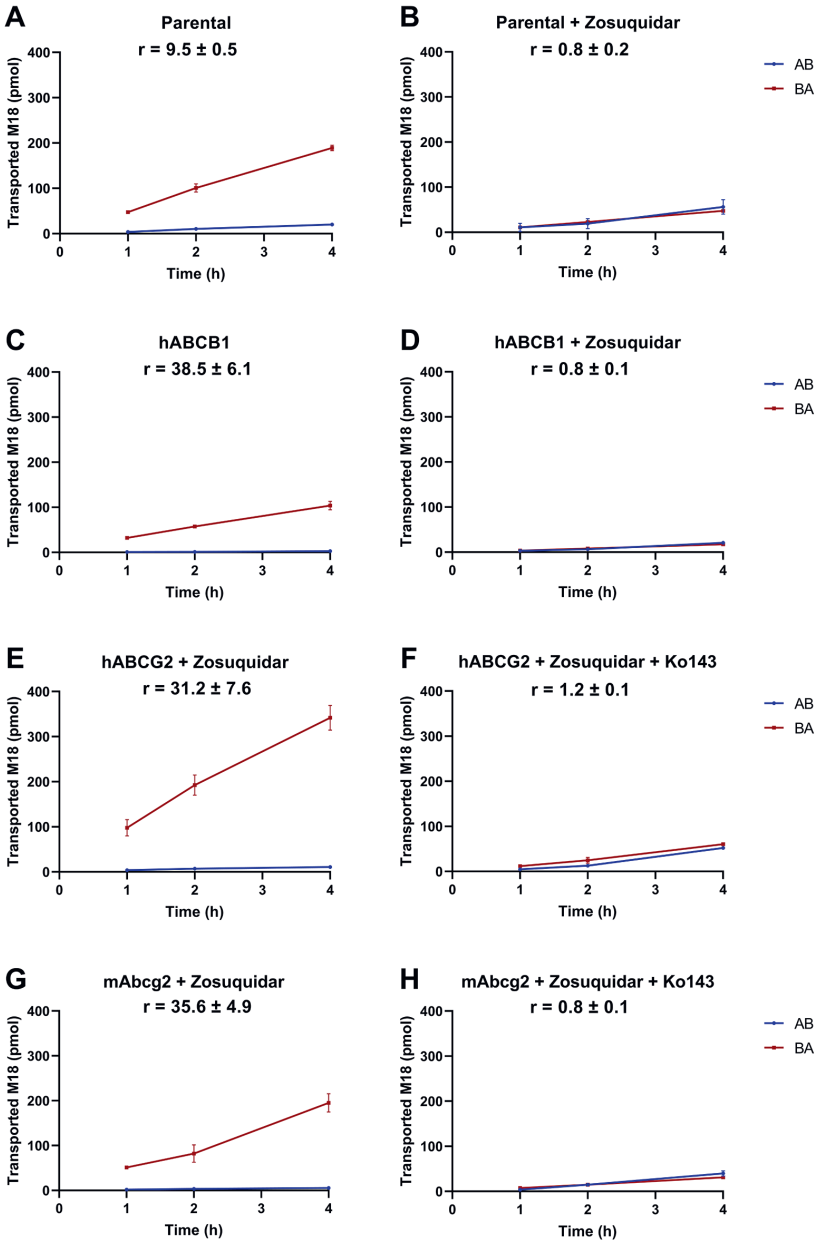


**Figure 5.** *In vitro* bidirectional transport of hydroxy-N-desethylabemaciclib (M18, 1  $\mu$ M) across MCDK-II cell monolayers formed with parental (A, B) or human ABCB1 (C, D), human ABCG2 (E, F), or mouse Abcg2 (G, H) overexpressing cell lines. At t = 0 M18 (as well as abemaciclib at 0.5  $\mu$ M and M2 and M20 at 1  $\mu$ M each) was added in the donor compartment, and at 1, 2, and 4 h the total transported amount of M18 in the acceptor compartment was determined. Apical-to-basolateral (AB) transport is presented with the red line and basolateral-to-apical (BA) transport with the blue line. Zosuquidar (3  $\mu$ M) was added to inhibit the human and/or the endogenous ABCB1, while Ko143 (3  $\mu$ M) was added to inhibit the human or mouse ABCG2. Data are presented as mean  $\pm$  SD (n = 3), r = relative transport ratio  $\pm$  SD.

6

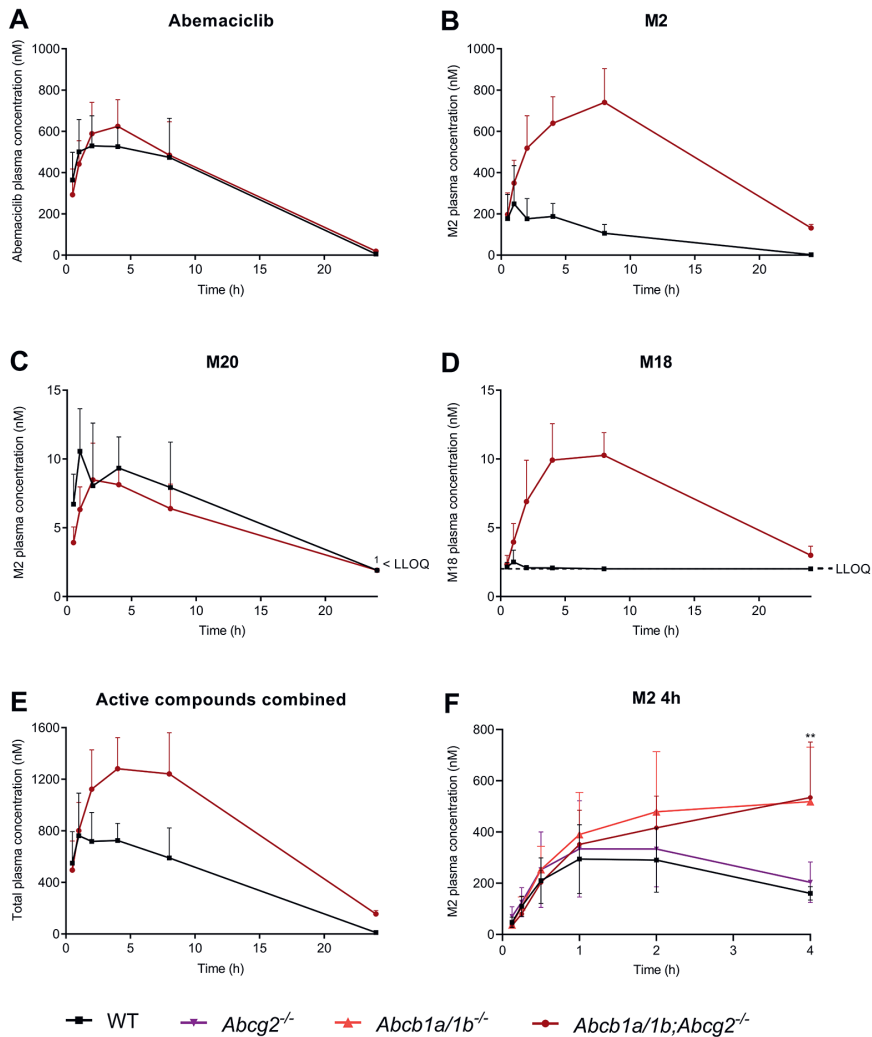


**Figure 6.** Plasma concentration-time curves of abemaciclib (A), M2 (B), M20 (C), M18 (D) and all active compounds combined (E) after oral administration of 10 mg/kg abemaciclib over 24 h in female wild-type (WT) and *Abcb1a/1b;Abcg2*<sup>-/-</sup> mice. Panel F depicts the plasma concentration-time curve of M2 from a separate experiment over 4 h, with female wild-type (WT), *Abcg2*<sup>-/-</sup>, *Abcb1a/1b*<sup>-/-</sup> and *Abcb1a/1b;Abcg2*<sup>-/-</sup> mice. Data are presented as mean  $\pm$  SD (n = 6 - 7). 'LLOQ represents the lower limit of quantification of the bioanalytical method.

**Table 1.** Pharmacokinetic parameters of abemaciclib 4 or 24 h after oral administration of 10 mg/kg abemaciclib to female wild-type, *Abcg2<sup>-/-</sup>*, *Abcb1a/1b<sup>-/-</sup>* and *Abcb1a/1b<sup>-/-</sup>Abcg2<sup>-/-</sup>* mice <sup>a</sup>

Parameter	Genotype					
	4 h					
	Wild-type	<i>Abcb1a/1b<sup>-/-</sup></i>	<i>Abcb1a/1b<sup>-/-</sup>Abcg2<sup>-/-</sup></i>	Wild-type		
AUC <sub>0-t</sub> (nm·h)	1937 ± 486	2281 ± 607	1629 ± 599	1182 ± 421	7808 ± 1857	8231 ± 1749
Fold change AUC <sub>0-t</sub>	-	1.2	0.8	0.6	-	1.1
t <sub>max</sub> (h)	2 (1-2)	2 (2-4)	2 (2-4)	2 (1-4)	3 (1-8)	4 (2-8)
C <sub>max</sub> (nM)	657 ± 206	739 ± 175	508 ± 205	386 ± 140	636 ± 58	723 ± 85
C <sub>brain</sub> (pmol/g)	173 ± 29	241 ± 48*	1822 ± 664***	3181 ± 997***	3.05 ± 1.38	304 ± 99***
K <sub>p,brain</sub>	0.45 ± 0.04	0.49 ± 0.11	4.38 ± 0.59***	12.6 ± 7.9***	0.667 ± 0.207	16.7 ± 1.9***
Fold increase K <sub>p,brain</sub>	-	1.1	9.7	28	-	25
SIC (% of dose)	2.66 ± 0.81	2.39 ± 0.68	2.00 ± 1.04	0.673 ± 0.261***	ND	ND
K <sub>p,SIC</sub> × 10 <sup>-3</sup>	7.0 ± 2.4	4.7 ± 1.5	4.9 ± 0.9	1.8 ± 0.9***	ND	ND
Fold change K <sub>p,SIC</sub>	-	0.67	0.7	0.26	ND	ND
P <sub>SIC</sub> (h <sup>-1</sup> × 10 <sup>3</sup> )	1.51 ± 0.77	1.12 ± 0.42	1.19 ± 0.24	0.643 ± 0.358*	ND	ND
Fold change P <sub>SIC</sub>	-	0.74	0.79	0.43	ND	ND

<sup>a</sup>Data are presented as mean ± SD (n=6 - 7), except for t<sub>max</sub> where the median (range) is presented. AUC<sub>0-t</sub>, area under the plasma concentration-time curve from 0 to the last time point (t = 4 or 24 h); C<sub>max</sub>, maximum plasma concentration; t<sub>max</sub>, time point (h) of maximum plasma concentration; C<sub>brain</sub>, brain concentration; K<sub>p,brain</sub>, brain-to-plasma ratio; P<sub>brain</sub>, brain accumulation; SIC, small intestine content; K<sub>p,SIC</sub>, small intestine content (% of dose)-to-plasma ratio; P<sub>SIC</sub>, small intestine content (% of dose) accumulation. ND = not determined. \*, *P* < 0.05; \*\*, *P* < 0.01; \*\*\*, *P* < 0.001 compared to wild-type mice.

**Table 2.** Pharmacokinetic parameters of M2 4 or 24 h after oral administration of 10 mg/kg abemaciclib to female wild-type, *Abcg2*<sup>-/-</sup>, *Abcb1a/1b*<sup>-/-</sup> and *Abcb1a/1b;Abcg2*<sup>-/-</sup> mice<sup>a</sup>

Parameter	Genotype					
	4 h			24 h		
	Wild-type	<i>Abcg2</i> <sup>-/-</sup>	<i>Abcb1a/1b</i> <sup>-/-</sup>	<i>Abcb1a/1b;Abcg2</i> <sup>-/-</sup>	Wild-type	<i>Abcb1a/1b;Abcg2</i> <sup>-/-</sup>
AUC <sub>0-t</sub> (nm·h)	933 ± 341	1082 ± 485	1236 ± 290	1375 ± 453	2184 ± 430	11519 ± 1576***
Fold change AUC <sub>0-t</sub>	-	1.2	1.3	1.5	-	5.3
t <sub>max</sub> (h)	1 (1-2)	2 (1-2)	2 (1-4)	4 (1-4)	3 (1-4)	4 (2-8)
C <sub>max</sub> (nM)	307 ± 121	364 ± 172	423 ± 122	479 ± 184	266 ± 172	789 ± 125***
C <sub>brain</sub> (pmol/g)	16.2 ± 3.5	37.0 ± 21.6***	89.1 ± 33.7***	391 ± 73***	6.60 ± 1.65	1689 ± 127***
K <sub>p,brain</sub>	0.102 ± 0.023	0.198 ± 0.118	0.178 ± 0.053	0.911 ± 0.345***	3.12 ± 1.39	12.9 ± 1.6***
Fold increase K <sub>p,brain</sub>	-	1.9	1.7	8.9	-	4.1
SIC (% of dose)	5.25 ± 1.30	4.03 ± 1.06	4.51 ± 0.69	0.797 ± 0.226***	ND	ND
K <sub>p,SIC</sub> × 10 <sup>-3</sup>	33.4 ± 9.3	21.4 ± 5.3**	9.5 ± 2.9***	1.9 ± 0.8***	ND	ND
Fold change K <sub>p,SIC</sub>	-	0.64	0.28	0.06	ND	ND
P <sub>SIC</sub> (h <sup>-1</sup> × 10 <sup>-3</sup> )	6.16 ± 2.59	4.15 ± 1.38	3.80 ± 0.95	0.624 ± 0.241***	ND	ND
Fold change P <sub>SIC</sub>	-	0.67	0.62	0.10	ND	ND

<sup>a</sup>Data are presented as mean ± SD (n=6 - 7), except for t<sub>max</sub>, where the median (range) is presented. AUC<sub>0-t</sub>, area under the plasma concentration-time curve from 0 to the last time point (t = 4 or 24 h); C<sub>max</sub>, maximum plasma concentration; t<sub>max</sub>, time point (h) of maximum plasma concentration; C<sub>brain</sub>, brain concentration; K<sub>p,brain</sub>, brain-to-plasma ratio; P<sub>SIC</sub>, brain accumulation; SIC, small intestine content; K<sub>p,SIC</sub>, small intestine content (% of dose)-to-plasma ratio; P<sub>SIC</sub>, small intestine content (% of dose) accumulation. ND = not determined. \*\*, P < 0.01; \*\*\*, P < 0.001 compared to wild-type mice.

**Table 3.** Pharmacokinetic parameters of M20 4 or 24 h after oral administration of 10 mg/kg abemaciclib to female wild-type, *Abcg2*<sup>-/-</sup>, *Abcb1a/1b*<sup>-/-</sup> and *Abcb1a/1b;Abcg2*<sup>-/-</sup> mice <sup>a</sup>

Parameter	Genotype					
	4 h			24 h		
	Wild-type	<i>Abcg2</i> <sup>-/-</sup>	<i>Abcb1a/1b;Abcg2</i> <sup>-/-</sup>	Wild-type	<i>Abcb1a/1b;Abcg2</i> <sup>-/-</sup>	<i>Abcb1a/1b;Abcg2</i> <sup>-/-</sup>
AUC <sub>0-t</sub> (nm·h)	43.9 ± 13.7	42.1 ± 9.8	32.4 ± 12.5	149 ± 31	123 ± 17	123 ± 17
Fold change AUC <sub>0-t</sub>	-	1.0	0.7	-	0.6	0.8
t <sub>max</sub> (h)	2	2	2	2 (1-2)	2 (1-2)	3 (2-8)
C <sub>max</sub> (nM)	16.8 ± 6.6	15.1 ± 3.7	11.1 ± 4.8	11.7 ± 2.52	9.5 ± 2.0	9.5 ± 2.0
C <sub>brain</sub> (pmol/g)	0.867 ± 0.082	1.91 ± 0.46***	7.34 ± 1.90***	0.817 ± 0.817 <sup>b</sup>	29.2 ± 6.1***	29.2 ± 6.1***
K <sub>p,brain</sub>	0.146 ± 0.040	0.322 ± 0.110**	1.23 ± 0.54***	8.75 ± 4.37***	ND <sup>c</sup>	ND <sup>c</sup>
Fold increase K <sub>p,brain</sub>	-	2.2	8.4	60	ND <sup>c</sup>	ND <sup>c</sup>
SIC (% of dose)	0.128 ± 0.027	0.92 ± 0.019*	0.051 ± 0.018***	0.009 ± 0.002***	ND	ND
K <sub>p,SIC</sub> × 10 <sup>-3</sup>	21.3 ± 6.4	16.1 ± 7.1	8.6 ± 3.9**	1.8 ± 1.0***	ND	ND
Fold change K <sub>p,SIC</sub>	-	0.76	0.40	0.08	ND	ND
P <sub>SIC</sub> (h <sup>-1</sup> × 10 <sup>3</sup> )	3.17 ± 1.28	2.32 ± 0.81	1.72 ± 0.71*	0.371 ± 0.174***	ND	ND
Fold change P <sub>SIC</sub>	-	0.73	0.54	0.12	ND	ND

<sup>a</sup> Data are presented as mean ± SD (n=6 - 7), except for t<sub>max</sub> where the median (range) is presented. AUC<sub>0-t</sub> area under the plasma concentration-time curve from 0 to the last time point (t = 4 or 24 h); C<sub>max</sub>, maximum plasma concentration; t<sub>max</sub>, time point (h) of maximum plasma concentration; C<sub>brain</sub>, brain concentration; K<sub>p,brain</sub>, brain-to-plasma ratio; P<sub>SIC</sub>, brain accumulation; SIC, small intestine content; K<sub>p,SIC</sub>, small intestine content (% of dose)-to-plasma ratio; P<sub>SIC</sub>, small intestine content (% of dose) accumulation. ND = not determined. \*, P < 0.05; \*\*, P < 0.01; \*\*\*, P < 0.001 compared to wild-type mice.

<sup>b</sup> Brain concentrations were detected but below the lower limit of quantification (LLOQ), therefore the LLOQ ± LLOQ was used for the calculations and the statistical analysis.

<sup>c</sup> Not determined as M20 was undetectable in plasma at 24 h.

**Table 4.** Pharmacokinetic parameters of M18 4 or 24 h after oral administration of 10 mg/kg abemaciclib to female wild-type, *Abcg2*<sup>-/-</sup>, *Abcb1a/1b*<sup>-/-</sup> and *Abcb1a/1b;Abcg2*<sup>-/-</sup> mice<sup>a</sup>

Parameter	Genotype					
	4 h		24 h			
	Wild-type	<i>Abcg2</i> <sup>-/-</sup>	<i>Abcb1a/1b</i> <sup>-/-</sup>	<i>Abcb1a/1b;Abcg2</i> <sup>-/-</sup>	Wild-type	<i>Abcb1a/1b;Abcg2</i> <sup>-/-</sup>
AUC <sub>0-t</sub> (nM·h)	10.7 ± 10.4	12.6 ± 5.5	15.8 ± 6.8	31.4 ± 9.0***	48.7 ± 48.7 <sup>c</sup>	171 ± 15
Fold change AUC <sub>0-t</sub>	-	1.2	1.5	2.9	-	3.5
t <sub>max</sub> (h)	1.5 (1-2)	2 (1-2)	2 (1-4)	4 (2-4)	0.5 (0.5-1)	8 (4-8)
C <sub>max</sub> (nM)	3.85 ± 0.91	4.79 ± 2.33	5.74 ± 2.59	11.6 ± 3.1***	2.51	11.4 ± 2.3
C <sub>brain</sub> (pmol/g)	> 0.867 <sup>b</sup>	0.586 ± 0.552	1.44 ± 1.06	1.84 ± 0.37	> 0.867 <sup>b</sup>	8.78 ± 1.56
K <sub>p,brain</sub>	ND	0.311 ± 0.349	0.324 ± 0.228	0.182 ± 0.047	ND	3.07 ± 1.00
Fold increase K <sub>p,brain</sub>	ND	ND	ND	ND	ND	ND
SIC (% of dose)	ND	0.049 ± 0.049	0.084 ± 0.053	0.062 ± 0.016	ND	0.006 ± 0.001
K <sub>p,SIC</sub> × 10 <sup>-3</sup>	ND	ND	ND	ND	ND	ND
Fold change K <sub>p,SIC</sub>	0.226 ± 0.070	0.128 ± 0.038**	0.308 ± 0.062*	0.035 ± 0.010***	ND	ND
P <sub>SIC</sub> (h <sup>-1</sup> × 10 <sup>3</sup> )	147 ± 69	66 ± 25**	79.2 ± 24.6*	3.3 ± 0.8***	ND	ND
Fold change P <sub>SIC</sub>	-	0.45	0.54	0.02	ND	ND

<sup>a</sup> Data are presented as mean ± SD (n = 6-7), except for t<sub>max</sub>, where the median (range) is presented. AUC<sub>0-t</sub>, area under the plasma concentration-time curve from 0 to the last time point (t = 4 or 24 h); C<sub>max</sub>, maximum plasma concentration; t<sub>max</sub>, time point (h) of maximum plasma concentration; C<sub>brain</sub>, brain concentration; K<sub>p,brain</sub>, brain-to-plasma ratio; P<sub>SIC</sub>, brain accumulation; SIC, small intestine content; K<sub>p,SIC</sub>, small intestine content (% of dose)-to-plasma ratio; P<sub>SIC</sub>, small intestine content (% of dose) accumulation. ND = not determined. \*, P < 0.05; \*\*, P < 0.01; \*\*\*, P < 0.001 compared to wild-type mice.

<sup>b</sup> M18 was not detected in wild-type mice. This value represents the estimated LLOQ.

<sup>c</sup> Due to low M18 concentration levels LLOQ ± LLOQ was used for the pharmacokinetic calculations.



In the semi-log plasma concentration-time curves of abemaciclib and M2 (Supplemental Figure 1A and B), the terminal slopes indicated a slower elimination of these compounds in *Abcb1a/1b;Abcg2*<sup>-/-</sup> than in wild-type mice. While for abemaciclib this was observed only after 8 h, for M2 this occurred after 2 h, resulting in increases in elimination half-lives of 1.5- and 2.9-fold for abemaciclib ( $P < 0.01$ ) and M2 ( $P < 0.001$ ), respectively.

To study the separate pharmacokinetic roles of *Abcg2* and *Abcb1a/1b*, a follow-up experiment included single *Abcg2* and *Abcb1a/1b* knockout strains, and was terminated 4 h after oral abemaciclib administration to allow analysis at relatively high drug and metabolite concentrations. Like in the 24 h experiment, no statistically significant differences in plasma  $AUC_{0-4h}$  and  $C_{max}$  were found between the four strains for abemaciclib and M20 (Supplemental Figures 2A and C, Tables 1 and 3,  $P > 0.05$ ). The plasma  $AUC_{0-4h}$  of M2 was also not significantly different among the strains. However, as in the 24 h experiment, at 4 h the M2 plasma concentration in *Abcb1a/1b;Abcg2*<sup>-/-</sup> and *Abcb1a/1b*<sup>-/-</sup> mice was significantly higher than the wild-type concentration (Figure 6F,  $P < 0.01$ ). For M18, a significantly increased exposure ( $AUC_{0-4h}$  and  $C_{max}$ ) was again observed in *Abcb1a/1b;Abcg2*<sup>-/-</sup> mice (Supplemental Figure 2D, Table 4,  $P < 0.001$ ) compared to the wild-type situation, but not in the single *Abcg2*<sup>-/-</sup> and *Abcb1a/1b*<sup>-/-</sup> mice. In summary, the total plasma exposure of abemaciclib active compounds is restricted by *Abcb1a/1b* and/or *Abcg2* as depicted in Figure 6E, mainly due to effects on M2. Furthermore, as shown in Supplemental Figure 1E, these efflux transporters contribute to the terminal elimination of the total abemaciclib active compounds from plasma.

### **ABCB1 and ABCG2 restrict the brain penetration of abemaciclib and its active metabolites**

The impact of ABCB1 and ABCG2 on the tissue distribution of abemaciclib active compounds was first investigated in the 24-h pilot experiment, where abemaciclib, M2, M20 and M18 were measured in brain and other tissues from wild-type and *Abcb1a/1b;Abcg2*<sup>-/-</sup> mice. Overall, exposure of all abemaciclib active compounds was dramatically increased in *Abcg2*- and *Abcb1a/1b*-deficient mice compared to the wild-type situation (Tables 1-4, Supplemental Figures 3A, 3C and 4A,  $P < 0.001$ ). A dramatic increase in the brain-to-plasma ratio of abemaciclib (25-fold) and M2 (4-fold) was detected in *Abcb1a/1b;Abcg2*<sup>-/-</sup> mice, compared to wild-type mice (Tables 1 and 2, Supplemental Figures 3B and D,  $P < 0.001$ ). This indicates that the higher brain exposure was due to the lack of ABC transporters at the blood-brain barrier and not only the higher plasma exposure. Brain-to-plasma ratios of M20 and M18 could not be determined at 24 h due to the low plasma levels of these metabolites. Although M18 was poorly detected in brain and plasma, in general, an increase in brain exposure was observed in *Abcb1a/1b;Abcg2*<sup>-/-</sup> mice compared to wild-type, in which M18 was not even detectable in brain (Table 4).

Tissue concentrations were also measured in the above-described 4-h oral abemaciclib pharmacokinetic experiment including wild-type, *Abcg2*<sup>-/-</sup>, *Abcb1a/1b*<sup>-/-</sup>, and *Abcb1a/1b;Abcg2*<sup>-/-</sup> mice, to investigate the individual and combined functions of Abcg2 and Abcb1a/1b at the BBB. The brain concentration of each of the abemaciclib active compounds was again drastically increased in *Abcb1a/1b;Abcg2*<sup>-/-</sup> mice, and to a lesser extent when only one of the ABC transporters was ablated (Figure 7A, C, E, G, and Supplemental Figure 4B). For abemaciclib, the brain-to-plasma ratio was increased by 28-fold in *Abcb1a/1b;Abcg2*<sup>-/-</sup> mice, and by 9.7-fold in *Abcb1a/1b*<sup>-/-</sup> mice compared to the wild-type situation (Figure 7B, Table 1,  $P < 0.001$ ). No significant increase was detected in *Abcg2*-deficient mice. For M2, the brain-to-plasma ratios were not significantly increased in *Abcg2*<sup>-/-</sup> and *Abcb1a/1b*<sup>-/-</sup> mice (1.9 and 1.7-fold, respectively;  $P > 0.05$ ), but in *Abcb1a/1b;Abcg2*<sup>-/-</sup> mice, the M2 brain-to-plasma ratio was 8.9-fold higher ( $P < 0.001$ ) compared to wild-type (Table 2, Figure 7D). The brain-to-plasma ratios of M20 were 2.2-, 8.4-, and 60-fold higher in *Abcg2*<sup>-/-</sup>, *Abcb1a/1b*<sup>-/-</sup> and *Abcb1a/1b;Abcg2*<sup>-/-</sup> mice, respectively (Table 3, Figure 7F,  $P < 0.01$  or  $P < 0.001$ ). Finally, although M18 levels in wild-type brain were still undetectable, an increase in brain concentration was detected in the knockout strains, although reliable comparisons between the strains were limited due to the low concentrations of this compound (Table 4, Figure 7H).

Interestingly, the M2 brain-to-plasma ratio in *Abcb1a/1b;Abcg2*<sup>-/-</sup> mice was around 10-fold higher at 24 h compared to that at 4 h, which is primarily a consequence of the increase in absolute M2 brain concentration between 4 and 24 h (compare Figure 7C and Supplemental Figure 3C). In contrast, abemaciclib brain concentration was strongly decreasing between 4 and 24 h, mostly following the plasma concentration (Figure 7A and Supplemental Figure 3A). Thus, while abemaciclib is cleared quite efficiently from the knockout brain, M2 seems to accumulate. Collectively, these results indicate that both Abcb1 and Abcg2 are cooperatively limiting the brain penetration of abemaciclib, M2, M20 and M18.

### **ABCB1 and ABCG2 participate in the elimination of abemaciclib active compounds**

To evaluate the possible impact of Abcb1a/1b and Abcg2 on the further tissue distribution of abemaciclib, M2, M20 and M18, several organs were collected in the 24 and 4 h pharmacokinetic experiments. Interestingly, in the small intestinal content collected in the 4 h experiment, the percentage of abemaciclib, M2, M20 and M18 recovered with respect to the original abemaciclib dose was markedly decreased in *Abcb1a/1b;Abcg2*<sup>-/-</sup> mice compared to the wild-type situation. In single *Abcg2* or *Abcb1a/1b* deficient mice, abemaciclib active compounds were also decreased, but to a lesser extent (Figure 8 A, C, E and G). These effects were more pronounced for the metabolites than for abemaciclib, since the ratio between the percentage of dose present in the small intestine content and the plasma concentration was more extensively reduced for the metabolites than for abemaciclib (Tables 1-4, Figure 8).

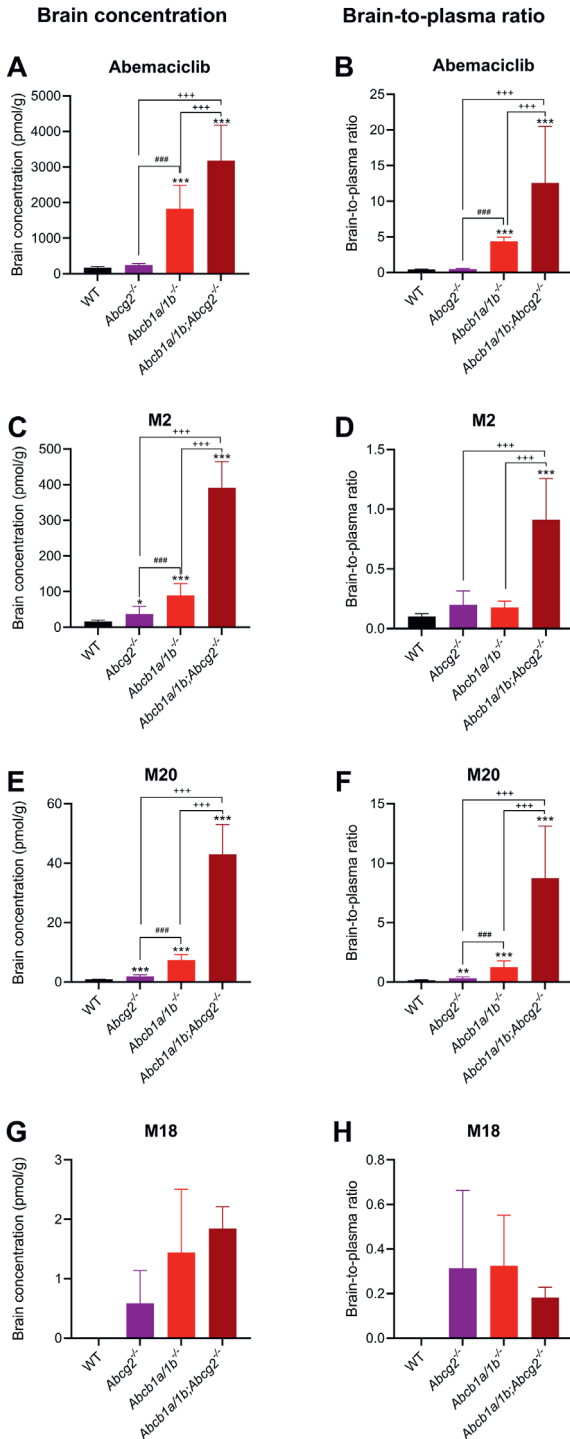


**Figure 7.** Brain concentration (A, C, E, and G) and brain-to-plasma ratio (B, D, F and H) of abemaciclib, M2, M20 and M18 in female wild-type (WT), *Abcg2*<sup>-/-</sup>, *Abcb1a/1b*<sup>-/-</sup> and *Abcb1a/1b*<sup>-/-</sup>;*Abcg2*<sup>-/-</sup> mice 4 h after oral administration of 10 mg/kg abemaciclib. Data are presented as mean ± SD (n = 6 - 7). \* *P* < 0.05; \*\* *P* < 0.01; \*\*\* *P* < 0.001 compared to WT mice; ### *P* < 0.001 compared to *Abcb1a/1b*;*Abcg2*<sup>-/-</sup> mice; ### *P* < 0.001 compared to *Abcg2*<sup>-/-</sup> mice. M18 was not detected in wild-type mice.

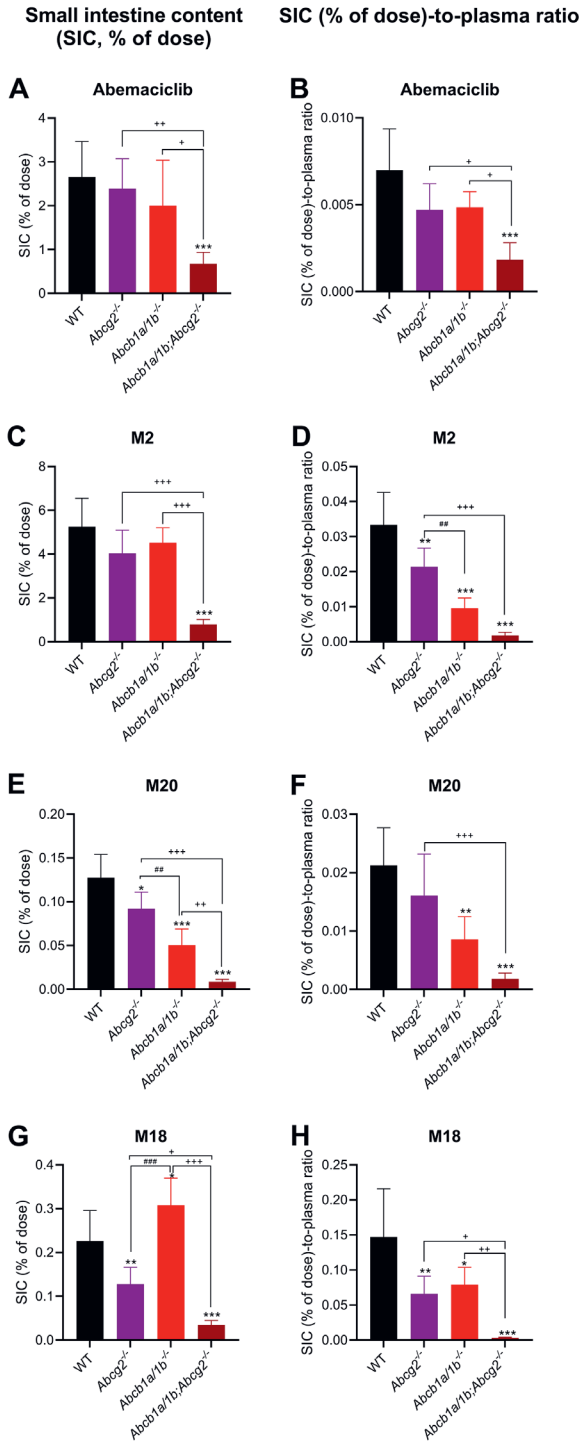


**Figure 8.** Small intestine content percentage of dose (A, C, E and G) and small intestine content (% of dose)-to-plasma ratio (B, D, F and H) of abemaciclib, M2, M20 and M18 in female wild-type (WT), *Abcg2*<sup>-/-</sup>, *Abcb1a/1b*<sup>-/-</sup> and *Abcb1a/1b;Abcg2*<sup>-/-</sup> mice 4 h after oral administration of 10 mg/kg abemaciclib. Data are presented as mean  $\pm$  SD (n = 6 - 7). \*  $P < 0.05$ ; \*\*  $P < 0.01$ ; \*\*\*  $P < 0.001$  compared to WT mice; +  $P < 0.05$ , ++  $P < 0.01$ , +++  $P < 0.001$  compared to *Abcb1a/1b;Abcg2*<sup>-/-</sup> mice; #  $P < 0.01$ ; ###  $P < 0.001$  compared to *Abcg2*<sup>-/-</sup> mice.

The small intestine tissue concentrations appeared to mainly reflect the intestinal content concentrations, as markedly reduced small intestine tissue-to-plasma ratios were also detected for all compounds in *Abcb1a/1b;Abcg2*<sup>-/-</sup> mice at 4 h (Supplemental Figure 8). The intestinal content results could be explained by the hepatobiliary excretion of abemaciclib and its active metabolites or by the effective pumping (back) of these compounds from the intestinal epithelium into the intestinal lumen, or a combination of both processes. Both processes can be mediated by *Abcb1* and *Abcg2*, and would be profoundly reduced when both transporters are ablated.

The distribution of active compounds to liver and other measured tissues was not significantly or relevantly affected at 4 and 24 h by either one or both ABC transporters, resulting in similar liver-to-plasma ratios between all strains (Supplemental Figures 5-7 and 9-11).

#### **Oral bioavailability of abemaciclib and its active metabolites is limited by CYP3A4**

The effects of *Cyp3a* and CYP3A4 on the plasma exposure and tissue distribution of abemaciclib and its active metabolites were assessed in a 24-h pharmacokinetic study, where female wild-type, *Cyp3a*<sup>-/-</sup> and transgenic *Cyp3aXAV* mice (humanized model that expresses the human CYP3A4 in liver and small intestine in a *Cyp3a*<sup>-/-</sup> background) were included. We found that the plasma exposure of abemaciclib was markedly increased ( $AUC_{0-24h}$  and  $C_{max}$  by 3.1- and 2.6-fold, respectively) in *Cyp3a*-deficient compared to wild-type mice (Figure 9A, Table 5,  $P < 0.001$ ). In contrast, relative to *Cyp3a*<sup>-/-</sup> mice, in *Cyp3AXAV* mice the  $AUC_{0-24h}$  and  $C_{max}$  were profoundly reduced by 7.5- and 5.6-fold, respectively. When compared to the wild-type situation, these parameters were also significantly reduced.

The active metabolites M2, M20 and M18 were still formed to some extent in the absence of *Cyp3a*, presumably by other drug-metabolizing enzymes (Figure 9). For M2 and M20 the impact of mouse *Cyp3a* and human CYP3A4 was also investigated, but not for M18, which was mostly unquantifiable or undetectable in the three mouse strains. Plotting of the plasma metabolite-to-abemaciclib ratios over time (Supplemental Figure 12) showed that relative M2 formation was strongly decreased in *Cyp3a*<sup>-/-</sup> mice, and then markedly recovered in *Cyp3aXAV* mice (panel A), suggesting that both mouse *Cyp3a* and human CYP3A4 are major factors in M2 formation. In contrast, relative M20 formation was hardly altered in the *Cyp3a*<sup>-/-</sup> mice (panel B), but strongly increased in the *Cyp3aXAV* mice. This suggests that mouse *Cyp3a* has at best a minor role in M20 formation (compared to other non-*Cyp3a* enzymes), whereas human CYP3A4 plays a prominent role. This would also be consistent with the much more prominent formation of M20 relative to M2 in human plasma than in mouse plasma [27].

With respect to the absolute plasma exposure of these metabolites, M2 was not significantly different among the three mouse strains (although initial formation was

delayed in *Cyp3a*<sup>-/-</sup> mice), whereas the AUC<sub>0-24h</sub> and C<sub>max</sub> of M20 were considerably increased in *Cyp3a*-deficient mice (Figure 9C, Table 5, *P* < 0.001). Moreover, M20 AUC<sub>0-24h</sub> and C<sub>max</sub> were again decreased by 2- and 1.6-fold, respectively, upon the expression of human CYP3A4. However, the M20-to-abemaciclib ratios in plasma suggest that these differences were primarily a consequence of the high abemaciclib plasma exposure in *Cyp3a*-deficient mice (Figure 9A and Supplemental Figure 12B). Overall, considering the total plasma exposure of abemaciclib active compounds in the studied mouse models, it is clear that CYP3A4 is the most important factor limiting the plasma exposure of abemaciclib active compounds (Figure 9E).

Concerning the role of CYP3A in tissue disposition, in some cases an increase or decrease of abemaciclib and/or M2 concentrations was detected, but this was generally a consequence of the altered plasma exposure in the corresponding strain. Therefore no relevant effects of CYP3A on relative tissue distribution were observed (Supplemental Figures 3, 5 and 6).

**Table 5** Pharmacokinetic parameters of abemaciclib, M2 and M20 24 h after oral administration of 10 mg/kg abemaciclib to female wild-type, *Cyp3a*<sup>-/-</sup> and *Cyp3aXAV* mice <sup>a</sup>

	Parameter	Genotype		
		Wild-type	<i>Cyp3a</i> <sup>-/-</sup>	<i>Cyp3XAV</i>
Abemaciclib	AUC <sub>0-24h</sub> (nM·h)	7808 ± 1837	24236 ± 2700***	3200 ± 791****
	Fold change AUC <sub>0-24h</sub>	-	3.1	0.4
	t <sub>max</sub> (h)	3 (1-8)	6 (2-8)	1 (0.5-8)
	C <sub>max</sub> (nM)	636 ± 58	1661 ± 160***	294 ± 46****
	Fold change C <sub>max</sub>	-	2.6	0.46
M2	AUC <sub>0-24h</sub> (nM·h)	2184 ± 430	1497 ± 137	2079 ± 618
	Fold change AUC <sub>0-24h</sub>	-	0.7	1.0
	t <sub>max</sub> (h)	3 (1-4)	6 (2-8)	1 (0.5-4)
	C <sub>max</sub> (nM)	266 ± 172	113 ± 18	226 ± 54
	Fold change C <sub>max</sub>	-	0.4	0.8
M20	AUC <sub>0-24h</sub> (nM·h)	149 ± 31	365 ± 41***	182 ± 33###
	Fold change AUC <sub>0-24h</sub>	-	2.4	1.2
	t <sub>max</sub> (h)	2 (1-8)	8 (4-8)	1 (1-8)
	C <sub>max</sub> (nM)	11.7 ± 2.2	24.6 ± 2.5***	15.4 ± 3.2###
	Fold change C <sub>max</sub>	-	2.1	1.3

<sup>a</sup> Data are presented as mean ± SD (n=6), except for t<sub>max</sub> where the median (range) is presented. AUC<sub>0-24h</sub> area under the plasma concentration-time curve from 0 to 24 h; C<sub>max</sub> maximum plasma concentration; t<sub>max</sub> time point (h) of maximum plasma concentration. \*\*, *P* < 0.01; \*\*\*, *P* < 0.001 compared to wild-type mice. ###, *P* < 0.001.

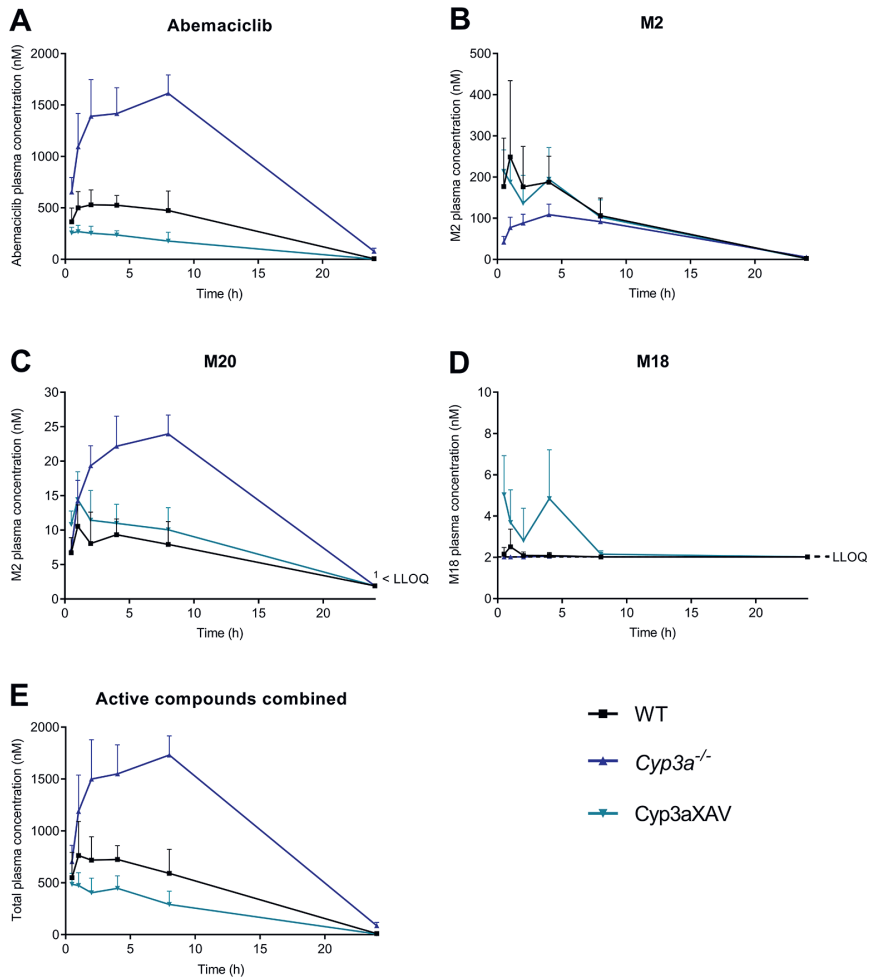


**Figure 9.** Plasma concentration-time curves of abemaciclib (A), M2 (B), M20 (C), M18 (D) and all active compounds combined (E) after oral administration of 10 mg/kg abemaciclib over 24 h in female wild-type (WT), *Cyp3a*<sup>-/-</sup> and *Cyp3aXAV* mice. Data are presented as mean  $\pm$  SD (n = 6). †LLOQ represents the lower limit of quantification of the bioanalytical method.

## Discussion

Our *in vitro* results confirm that abemaciclib is efficiently transported by hABCB1 and mAbcg2, and modestly by hABCG2. Additionally, abemaciclib metabolites M2, M20 and M18 are excellent substrates of hABCB1, hABCG2 and mAbcg2; and, despite the low expression of the endogenous canine ABCB1 [26], M2 and M18 are markedly transported by the canine ABCB1. *In vivo*, the total plasma exposure of all active compounds over 24 h after abemaciclib oral administration was increased in *Abcb1a/1b*

and Abcg2-deficient mice. This is mostly due to the significant increase of the M2 AUC<sub>0-24h</sub> (by 5.3-fold) in this mouse strain, where Abcb1a/1b appears to play a dominant role in limiting the plasma exposure of M2 compared to Abcg2. Furthermore, the lack of both Abcb1a/1b and Abcg2 drastically reduced the amount of all active compounds present in the small intestine content. Moreover, in the absence of both Abcb1 and Abcg2, the brain penetration of each of the abemaciclib active compounds dramatically increased, and to a lesser extent when only one efflux transporter was ablated. This indicates the relevant role of each of the transporters in limiting the penetration of abemaciclib active compounds across the BBB. Finally, human CYP3A4 extensively contributed to the metabolic clearance of abemaciclib, by reducing its plasma exposure 7.5-fold compared to Cyp3a-deficient mice. Human CYP3A4 also appeared to form more actively both M2 and M20, compared to the mouse Cyp3a, which also showed a very limited capacity to produce M20.

To the best of our knowledge, this is the first study demonstrating the extensive active transport of the abemaciclib active metabolites by ABCB1 and ABCG2 *in vitro*. Consistent with our data, Raub *et al.*, reported that abemaciclib was transported by hABCB1 and mAbcg2, with efflux transport ratios (4.1 and 11 for hABCB1 and mAbcg2, respectively) similar to the relative transport ratios we obtained (4.4 and 10, respectively) [17]. Moreover, in accordance with our results, FDA and EMA reports state that abemaciclib and M2 are substrates of ABCB1 and ABCG2 [6,7]. In general, M2, M20 and M18 were better substrates for ABCB1 and ABCG2 than abemaciclib. Interestingly, both structural metabolic modifications of abemaciclib to form M2 and M20 (i.e. the *N*-desethylation and the hydroxylation on the methyl group of the benzimidazole ring) led to a profound increase in the apically-directed transport by ABCB1 and ABCG2. Between them, the *N*-desethylation had the highest impact, resulting in higher relative transport ratios for M2 than for M20 in all cell lines. The combination of both structural modifications increased the apically-directed transport by hABCB1 and hABCG2 even further, as observed for M18, except in mAbcg2-overexpressing cells, which had a similar relative transport ratio compared to M2.

In our *in vitro* study, we simultaneously assessed the transepithelial transport of abemaciclib and its active metabolites. This is in some ways more representative of an *in vivo* situation, where these molecules are simultaneously exposed to the efflux transporters. Relatively low concentrations of each compound were used in this experiment, reaching a total concentration of 3.5  $\mu\text{M}$ , in order to minimize the risk of transporter saturation or cell toxicity during the experiment. The latter was reflected in the cell monolayer integrity being maintained throughout the experiment. It has been suggested that abemaciclib can inhibit ABCB1 and ABCG2 [6,7,28], therefore an abemaciclib concentration of 0.5  $\mu\text{M}$  was used to decrease the risk of potential inhibitory interactions from abemaciclib. Usually we use 5 or 2  $\mu\text{M}$  of single substrates



to be tested in these transport assays. No relevant inhibition by abemaciclib (if any) was detected in this study, as abemaciclib and its active metabolites were all efficiently transported by ABCB1 and ABCG2. These results therefore suggest that it is feasible to simultaneously test 4 different (albeit structurally related) transport substrates in this type of assay.

The *in vivo* single and combined effects of ABCB1 and ABCG2 on the plasma pharmacokinetics and tissue distribution of abemaciclib and its active metabolites have to our knowledge not been described before. In the clinic, abemaciclib has shown high variability in its plasma exposure. After oral administration of 10 mg/kg abemaciclib, the  $C_{\max}$  obtained in the wild-type mice was similar to the geometric mean  $C_{\max}$  reported in humans at steady state with a 200 mg dose [29]. The abemaciclib and M2 plasma exposure in mice was above the concentrations needed for a pharmacodynamic effect in all the mouse models, (based on their potency and protein binding), while for M20 and M18 it was below the therapeutic levels. This was expected for M18, being in line with the human situation; however, for M20 higher plasma concentrations were expected. Similarly, in other pre-clinical species, like rat and dog, low M20 plasma exposure has been reported [6]. We speculate that the much lower relative M20 plasma concentrations in mice are due to species differences in CYP3A-mediated metabolism, with human CYP3A4 being relatively proficient in forming M20. In mice it might also be due (in part) to the formation of several additional M20 isomers (i.e. compounds with the hydroxyl group in different position of the molecule), as we detected these compounds in the mouse samples [22].

Our study showed that the plasma exposure of abemaciclib and M20 was not significantly affected by Abcb1a/1b and/or Abcg2. However, the  $AUC_{0-24h}$  and  $C_{\max}$  of M2 and M18 were markedly increased in the absence of both Abcb1a/1b and Abcg2, probably due to a reduced elimination of these metabolites. In line with our results, M2 was the most abundant compound eliminated by feces in several species (rats, dogs and humans) [7]. Thus the combination of its abundance and diminished elimination impacted on its plasma exposure in the ABC transporter-deficient mice. Consistent with our *in vitro* data, also *in vivo* M2 and M18 appear to be (even) better substrates of both ABCB1 and ABCG2 than abemaciclib and M20. Based on our results, ABCB1 and ABCG2 are unlikely to influence the plasma exposure of abemaciclib and M20 in humans; however, the plasma exposure of M2 and M18 could increase by complete inhibition of both transporters. Probably the M18 increase might not be of interest, as its abundance is relatively low also in humans. However, the possible increase of M2 could potentially be clinically relevant, as M2 is abundant in human plasma. For this reason, it might be useful to monitor plasma concentrations of all abemaciclib active compounds, especially M2, in patients concomitantly treated with abemaciclib and ABCB1 and/or ABCG2 inhibitors.

We hypothesize that the increased plasma exposure of M2 and M18 may be a consequence of the reduced hepatobiliary or direct intestinal elimination, or a combination of both processes occurring in *Abcb1a/1b;Abcg2*<sup>-/-</sup> mice. Indeed, lower amounts of M2 and M18 were measured in the small intestine content of these mice, compared to the wild-type situation. Significantly reduced amounts of M2 and M18 were also found in the small intestine content of single *Abcg2*<sup>-/-</sup> and *Abcb1a/1b*<sup>-/-</sup> mice. The amount of abemaciclib and M20 was significantly reduced in the combination *Abcb1a/1b;Abcg2*<sup>-/-</sup> mice. While the abemaciclib amount in the small intestine content was impacted only by the lack of both transporters, the M20 present in the intestinal lumen was also affected by the lack of *Abcb1a/1b*. It is worth noting that in wild-type mice, the percentage of dose recovered for M2 after 4 h (5.3%) was even higher than for abemaciclib itself (2.7%), and this remained true after correction for relative plasma concentrations (Figure 6 panels A-D) or exposure (not shown). This suggests that M2 is more efficiently extruded into the intestinal content than abemaciclib itself. This would be consistent with M2 being a more efficiently transported substrate for the ABC transporters than abemaciclib, as was indeed found in Figures 1 and 2. Liver penetration was not significantly altered by *Abcb1a/1b* and/or *Abcg2* deficiency. Although one would expect that the reduced hepatobiliary excretion of these compounds might impact on their liver accumulation, possibly the reduced concentrations in the intrahepatic bile might be compensated by the higher concentrations in the hepatocytes. This, combined with the rapid liver equilibration with blood may result in an overall unchanged liver penetration. In contrast, the small intestine tissue appeared to primarily reflect what happened in the small intestine lumen, with a reduced accumulation of the abemaciclib active compounds.

Although abemaciclib, M2 and M20 can somewhat cross the BBB, our study demonstrates that their combined brain exposure is profoundly restricted by both ABCB1 and ABCG2. Overall, the total brain exposure of active compounds was 19-fold higher at 4 h, and 179-fold higher at 24 h after oral administration of abemaciclib in *Abcb1a/1b;Abcg2*<sup>-/-</sup> compared to WT mice (Supplemental Figure 6). Also the total brain concentration decreased only modestly (1.8-fold) between 4 and 24 h in the knockout strain, whereas in the wild-type strain it decreased 17-fold. The parent drug and M20 were more affected by the transporters at 4 h, where their brain-to-plasma ratio was drastically increased by 28- and 60-fold, respectively, in mice lacking both efflux transporters (Figure 5). In line with our findings, Raub *et al.* previously reported that in *Abcb1a/1b*-deficient mice the brain penetration of abemaciclib increased from 3- to 7-fold compared to wild-type mice at 5 or 60 min after intravenous administration [17]. In our study M2 penetration was also significantly affected, since its brain-to-plasma ratio increased 8.9-fold at 4 h when the transporters were ablated. Due to the low brain concentrations of M18 in wild-type mice, the effect of ABC transporters on the M18 brain penetration could not be quantified.

Whereas the brain penetration of abemaciclib and M20 was clearly more affected by Abcb1a/1b than Abcg2, no significant differences in brain-to-plasma ratios between Abcb1a/1b and Abcg2 knockout strains were detected for M2 and M18 (Figure 5). Consistent with our *in vitro* experiment and the small intestine content data, this suggests an increased transport efficacy of Abcg2 for M2 and M18, compared to abemaciclib and M20. When plasma exposure of all active compounds was (close to) the maximum levels (i.e. 4 h after oral administration), abemaciclib appears to be the most relevant compound for the brain pharmacodynamic effect in a normal situation, exhibiting the highest absolute brain concentration and brain-to-plasma ratio among all the active compounds. Together with abemaciclib, M20 may potentially also be important for the brain pharmacodynamic effect in humans at an early time point, since M20 abundance in human plasma is much higher compared to mice. On the other hand, at later time points M2 seems to be more relevant, since it accumulated in brain over the time, especially in the absence of Abcb1a/1b and Abcg2, reaching considerably higher brain concentrations and brain-to-plasma ratio at 24 h after oral administration of abemaciclib (Supplemental Figure 5, Table 2). Similarly, in *Abcb1a/1b;Abcg2*<sup>-/-</sup> mice M2 was found to also accumulate in kidney and lung with increased tissue concentrations at 24 h compared to 4h (Supplemental Figures 8, 11 and 13), and to be retained in liver and small intestine, showing tissue-to-plasma ratios higher at 24 h than at 4h (Supplemental Figures 7, 9 and 10).

The potential use of abemaciclib in the treatment of brain malignancies seems promising due to two relevant factors. First, the inhibition of CDK4 and CDK6 could be efficacious in the treatment of some brain malignancies, including glioblastoma, as molecular alterations in the CDK4/6-retinoblastoma pathway have been identified in these cancers. Similarly, brain metastases from cancers with these molecular aberrations can occur, with breast cancer the second most frequent malignancy that metastasizes to the brain [30,31]. Second, consistent with previous reports [17,32], our study showed a decent brain penetration of abemaciclib (and its metabolites) in the wild-type situation. A phase I clinical study in breast cancer patients with brain metastases suggested that the total concentration of abemaciclib and its active metabolites in brain tissue at steady state led to an efficacious CDK4/6 inhibition. Nevertheless, most of the patients presented disease progression, causing treatment discontinuation. Although the causes of this were not clear, suboptimal brain exposure in some patients cannot be discounted. Our results suggest that the co-administration of an efficacious ABCB1 and ABCG2 inhibitor with abemaciclib could dramatically enhance the brain exposure of all abemaciclib active compounds, assuring pharmacologically relevant concentrations in brain. As tumor cells themselves can also overexpress ABCB1 and ABCG2, the inhibition of these transporters could further be beneficial to improve the tumor exposure of abemaciclib active compounds. Often brain lesions can produce a leaky BBB, which could lead one to question the impact of the BBB ABC transporters. However, it has been demonstrated that ABCB1 and

ABCG2 are still expressed in the vasculature of these brain tumors, limiting the brain exposure of drugs regardless of the extent of leakiness [33].

This study further showed the substrate specificity of mouse Cyp3a and human CYP3A4 for metabolizing abemaciclib *in vivo*. Human CYP3A4 decreased the abemaciclib  $AUC_{0-24h}$  by 7.5-fold when overexpressed in the hepatocytes and enterocytes of mice. This pronounced effect of CYP3A4 is in line with the prescription recommendations of avoiding concomitant administration of abemaciclib with (strong) CYP3A4 modulators [27,29]. As an excellent substrate of CYP3A4, abemaciclib exposure is highly susceptible to variations in CYP3A4 activity, caused for instance by drugs or food components that induce or inhibit this drug-metabolizing enzyme or by genetic polymorphisms [34,35]. Thus, the reported high inter-individual variability of abemaciclib plasma exposure could be due (in part) to high variation in CYP3A4 activity. However, as the primary CYP3A4-generated metabolites (M2, M20, M18) are also pharmacodynamically active, the effective total therapeutic exposure may be less affected by altered CYP3A4 activity than would be suggested by only looking at the abemaciclib plasma concentrations. The data in Figure 7E suggest that complete inhibition of CYP3A4 activity would still result in a pronounced increase in effective exposure to all active abemaciclib compounds.

Comparing all the CDK4/6 inhibitors used in the clinic, abemaciclib brain exposure was affected by both ABCB1 and ABCG2, similarly to palbociclib, whereas ribociclib brain exposure was only limited by ABCB1 [17,36,37]. Moreover, the plasma exposure of all these CDK4/6 inhibitors is restricted by the extensive metabolism by human CYP3A4. Using the same mouse models, we previously reported that the  $AUC_{0-24h}$  of ribociclib was 3.8-fold reduced upon the expression of the human CYP3A4, while for abemaciclib this led to a 7.5-fold decrease in its  $AUC_{0-24h}$ . Although studies of palbociclib in these mouse models were not performed, based on the clinical DDI studies it was concluded that also palbociclib is extensively metabolized by CYP3A4.

## Conclusions

Collectively, this study confirmed that abemaciclib is a substrate of ABCB1 and ABCG2 and demonstrated that its active metabolites are excellent substrates of both efflux transporters. While the plasma pharmacokinetics of abemaciclib and M20 were not affected by Abcb1a/1b and Abcg2, the M2  $AUC_{0-24h}$  and  $C_{max}$  were markedly increased in the absence of both transporters, with Abcb1a/1b apparently dominant. This marked increase could be due to a reduced excretion of this compound when these transporters are ablated. Moreover, Abcb1a/1b and Abcg2 showed cooperative restriction of the brain exposure and penetration of abemaciclib and its active metabolites. Additionally, Abcb1a/1b and Abcg2 participated in the (hepatobiliary or direct intestinal) elimination

of all abemaciclib active compounds. Finally, the extensive metabolism of abemaciclib by CYP3A4 is confirmed, with CYP3A4 the protein that most affects the plasma exposure of overall active compounds. Both human CYP3A4 and mouse Cyp3a can metabolize abemaciclib, however inter-species differences between these enzymes were encountered, where human CYP3A4 appeared to be more active in forming M2 and especially M20. These insights might be relevant for the clinical use of abemaciclib, especially in glioblastoma or brain metastasis treatments, since the brain exposure of all active compounds could potentially be enhanced by the co-administration of abemaciclib with an efficacious ABCB1 and ABCG2 inhibitor such as elacridar.

---

*Acknowledgements*

The authors thank Wenlong Li for assistance in executing the *in vivo* mouse experiments.

## References

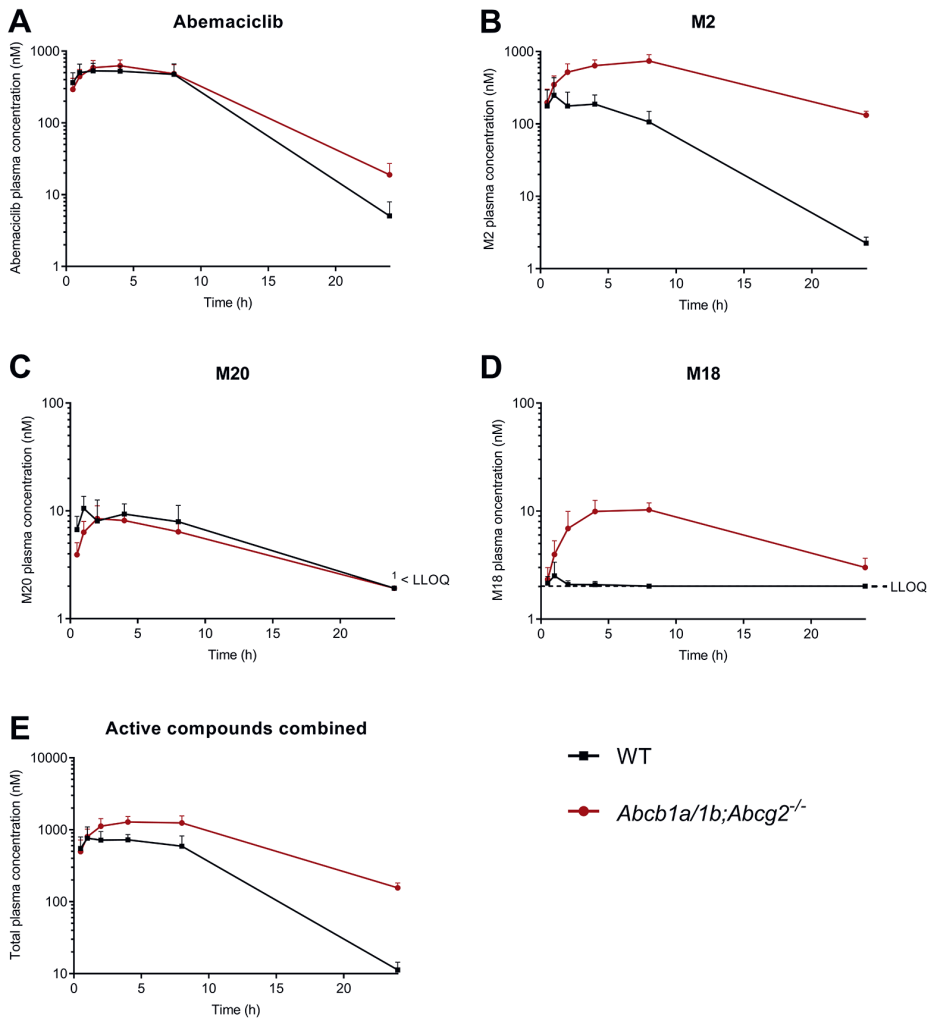
- [1] N. Harbeck, F. Penault-Llorca, J. Cortes, M. Gnant, N. Houssami, P. Poortmans, K. Ruddy, J. Tsang, F. Cardoso, *Breast cancer*, 2019. <https://doi.org/10.1038/s41572-019-0111-2>.
- [2] H. Sung, J. Ferlay, R.L. Siegel, M. Laversanne, I. Soerjomataram, A. Jemal, F. Bray, *Global cancer statistics 2020: GLOBOCAN estimates of incidence and mortality worldwide for 36 cancers in 185 countries*, *CA. Cancer J. Clin.* 0 (2021) 1–41. <https://doi.org/10.3322/caac.21660>.
- [3] B. O'Leary, R.S. Finn, N.C. Turner, *Treating cancer with selective CDK4/6 inhibitors*, *Nat. Rev. Clin. Oncol.* 13 (2016) 417–430. <https://doi.org/10.1038/nrclinonc.2016.26>.
- [4] L.M. Gelbert, S. Cai, X. Lin, C. Sanchez-Martinez, M. Del Prado, M.J. Lallena, R. Torres, R.T. Ajamie, G.N. Wishart, R.S. Flack, B.L. Neubauer, J. Young, E.M. Chan, P. Iversen, D. Cronier, E. Kreklau, A. De Dios, *Preclinical characterization of the CDK4/6 inhibitor LY2835219: In-vivo cell cycle-dependent/independent anti-tumor activities alone/in combination with gemcitabine*, *Invest. New Drugs.* 32 (2014) 825–837. <https://doi.org/10.1007/s10637-014-0120-7>.
- [5] A. Patnaik, L.S. Rosen, S.M. Tolaney, A.W. Tolcher, J.W. Goldman, L. Gandhi, K.P. Papadopoulos, M. Beeram, D.W. Rasco, J.F. Hilton, A. Nasir, R.P. Beckmann, A.E. Schade, A.D. Fulford, T.S. Nguyen, R. Martinez, P. Kulanthaivel, L.Q. Li, M. Frenzel, D.M. Cronier, E.M. Chan, K.T. Flaherty, P.Y. Wen, G.I. Shapiro, *Efficacy and safety of Abemaciclib, an inhibitor of CDK4 and CDK6, for patients with breast cancer, non-small cell lung cancer, and other solid tumors*, *Cancer Discov.* 6 (2016) 740–753. <https://doi.org/10.1158/2159-8290.CD-16-0095>.
- [6] FDA Center for drug evaluation and Rsearch, *Multi-discipline Review of Abemaciclib*, 2017.
- [7] Committee for Medicinal Products for Human Use (CHMP), *Public Assessment Report Abemaciclib*, (2018). [https://www.ema.europa.eu/en/documents/assessment-report/verzenios-epar-public-assessment-report\\_en.pdf](https://www.ema.europa.eu/en/documents/assessment-report/verzenios-epar-public-assessment-report_en.pdf).
- [8] Q.Y. Chong, Z.H. Kok, N.L.C. Bui, X. Xiang, A.L.A. Wong, W.P. Yong, G. Sethi, P.E. Lobie, L. Wang, B.C. Goh, *A unique CDK4/6 inhibitor: Current and future therapeutic strategies of abemaciclib*, *Pharmacol. Res.* 156 (2020) 104686. <https://doi.org/10.1016/j.phrs.2020.104686>.
- [9] X. Bao, J. Wu, Y. Xie, S. Kim, S. Michelhaugh, J. Jiang, S. Mittal, N. Sanai, J. Li, *Protein Expression and Functional Relevance of Efflux and Uptake Drug Transporters at the Blood-Brain Barrier of Human Brain and Glioblastoma*, *Clin. Pharmacol. Ther.* 107 (2020) 1116–1127. <https://doi.org/10.1002/cpt.1710>.
- [10] J.T. Henderson, M. Piquette-Miller, *Blood-brain barrier: an impediment to neuropharmaceuticals*, *Clin. Pharmacol. Ther.* 97 (2015) 308–313. <https://doi.org/10.1002/cpt.77>.
- [11] W.M. Pardridge, *Drug transport across the blood-brain barrier*, *J. Cereb. Blood Flow Metab.* 32 (2012) 1959–1972. <https://doi.org/10.1038/jcbfm.2012.126>.
- [12] A.H. Schinkel, J.W. Jonker, *Mammalian drug efflux transporters of the ATP binding cassette (ABC) family: An overview*, *Adv. Drug Deliv. Rev.* 64 (2012) 138–153. <https://doi.org/10.1016/j.addr.2012.09.027>.
- [13] G. Szakács, A. Váradi, C. Özvegy-Laczka, B. Sarkadi, *The role of ABC transporters in drug absorption, distribution, metabolism, excretion and toxicity (ADME-Tox)*, *Drug Discov. Today.* 13 (2008) 379–393. <https://doi.org/10.1016/j.drudis.2007.12.010>.
- [14] K.M. Giacomini, S. Huang, Tweedie DJ, L.Z. Benet, *Membrane transporters in drug development. The International Transporter Consortium.*, *Nat. Re Drug Discov.* (2010). <https://doi.org/10.1038/nrd3028>. Membrane.
- [15] J.H. Lin, M. Yamazaki, *Clinical Relevance of P-Glycoprotein in Drug Therapy*, *Drug Metab. Rev.* 35 (2003) 417–454. <https://doi.org/10.1081/DMR-120026871>.

- [16] K. Natarajan, Y. Xie, M.R. Baer, D.D. Ross, Role of breast cancer resistance protein (BCRP/ABCG2) in cancer drug resistance, *Biochem. Pharmacol.* 83 (2012) 1084–1103. <https://doi.org/10.1016/j.bcp.2012.01.002>.
- [17] T.J. Raub, G.N. Wishart, P. Kulanthaivel, B.A. Staton, R.T. Ajamie, G.A. Sawada, L.M. Gelbert, H.E. Shannon, C. Sanchez-Martinez, A. De Dios, Brain exposure of two selective dual CDK4 and CDK6 inhibitors and the antitumor activity of CDK4 and CDK6 inhibition in combination with temozolomide in an intracranial glioblastoma xenograft, *Drug Metab. Dispos.* 43 (2015) 1360–1371. <https://doi.org/10.1124/dmd.114.062745>.
- [18] E. Bakos, R. Evers, G. Szakacs, G.E. Tusnady, E. Welker, K. Szabo, M. de Haas, L. van Deemter, P. Borst, a Varadi, B. Sarkadi, Functional multidrug resistance protein (MRP1) lacking the N-terminal transmembrane domain, *J. Biol. Chem.* 273 (1998) 32167–32175. <https://doi.org/10.1074/jbc.273.48.32167>.
- [19] R. Evers, M. Kool, L. van Deemter, H. Janssen, J. Calafat, L.C. Oomen, C.C. Paulusma, R.P. Oude Elferink, F. Baas, A.H. Schinkel, P. Borst, Drug export activity of the human canalicular multispecific organic anion transporter in polarized kidney MDCK cells expressing cMOAT (MRP2) cDNA., *J. Clin. Invest.* 101 (1998) 1310–1319. <https://doi.org/10.1172/JCI928>.
- [20] B. Poller, E. Wagenaar, S.C. Tang, A.H. Schinkel, Double-transduced MDCKII cells to study human P-glycoprotein (ABCB1) and breast cancer resistance protein (ABCG2) interplay in drug transport across the blood-brain barrier, *Mol. Pharm.* 8 (2011) 571–582. <https://doi.org/10.1021/mp1003898>.
- [21] J.W. Jonker, Role of Breast Cancer Resistance Protein in the Bioavailability and Fetal Penetration of Topotecan, *J. Natl. Cancer Inst.* 92 (2000) 1651–1656. <https://doi.org/10.1093/jnci/92.20.1651>.
- [22] A. Martínez-Chávez, M.M. Tibben, K.A.M. de Jong, H. Rosing, A.H. Schinkel, J.H. Beijnen, Simultaneous quantification of abemaciclib and its active metabolites in human and mouse plasma by UHPLC-MS / MS, *J. Pharm. Biomed. Anal.* (2021) [in press].
- [23] A.H. Schinkel, U. Mayer, E. Wagenaar, C.A.A.M. Mol, L. Van Deemter, J.J.M. Smit, M.A. Van Der Valk, A.C. Voordouw, H. Spits, O. Van Tellingen, M. Zijlman, W. Fibbe, P. Borst, Normal viability and altered pharmacokinetics in mice lacking mdr1-type (drug-transporting) P-glycoproteins, *Proc. Natl. Acad. Sci.* 94 (1997) 4028–4033. <https://doi.org/10.1073/pnas.94.8.4028>.
- [24] R.A.B. Van Waterschoot, J.S. Lagas, E. Wagenaar, C.M.M. Van Der Kruijssen, A.E. Van Herwaarden, J.Y. Song, R.W. Rooswinkel, O. Van Tellingen, H. Rosing, J.H. Beijnen, A.H. Schinkel, Absence of both cytochrome P450 3A and P-glycoprotein dramatically increases docetaxel oral bioavailability and risk of intestinal toxicity, *Cancer Res.* 69 (2009) 8996–9002. <https://doi.org/10.1158/0008-5472.CAN-09-2915>.
- [25] Y. Zhang, M. Huo, J. Zhou, S. Xie, PKSolver: An add-in program for pharmacokinetic and pharmacodynamic data analysis in Microsoft Excel, *Comput. Methods Programs Biomed.* 99 (2010) 306–314. <https://doi.org/10.1016/j.cmpb.2010.01.007>.
- [26] D. Gartzke, J. Delzer, L. Laplanche, Y. Uchida, Y. Hoshi, M. Tachikawa, T. Terasaki, J. Sydor, G. Fricker, Genomic knockout of endogenous canine P-glycoprotein in wild-type, human P-glycoprotein and human BCRP transfected MDCKII cell lines by zinc finger nucleases, *Pharm. Res.* 32 (2015) 2060–2071. <https://doi.org/10.1007/s11095-014-1599-5>.
- [27] M.M. Posada, B.L. Morse, P.K. Turner, P. Kulanthaivel, S.D. Hall, G.L. Dickinson, Predicting Clinical Effects of CYP3A4 Modulators on Abemaciclib and Active Metabolites Exposure Using Physiologically Based Pharmacokinetic Modeling, *J. Clin. Pharmacol.* 60 (2020) 915–930. <https://doi.org/10.1002/jcph.1584>.
- [28] T. Wu, Z. Chen, K.K.W. To, X. Fang, F. Wang, B. Cheng, L. Fu, Effect of abemaciclib (LY2835219) on enhancement of chemotherapeutic agents in ABCB1 and ABCG2 overexpressing cells in vitro and in vivo, *Biochem. Pharmacol.* 124 (2017) 29–42. <https://doi.org/10.1016/j.bcp.2016.10.015>.
- [29] S.L. Groenland, A. Martínez-Chávez, M.G.J. van Dongen, J.H. Beijnen, A.H. Schinkel, A.D.R. Huitema, N. Steeghs, Clinical Pharmacokinetics and Pharmacodynamics of the Cyclin-Dependent Kinase 4 and 6 Inhibitors Palbociclib, Ribociclib, and Abemaciclib, *Clin. Pharmacokinet.* (2020). <https://doi.org/10.1007/s40262-020-00930-x>.

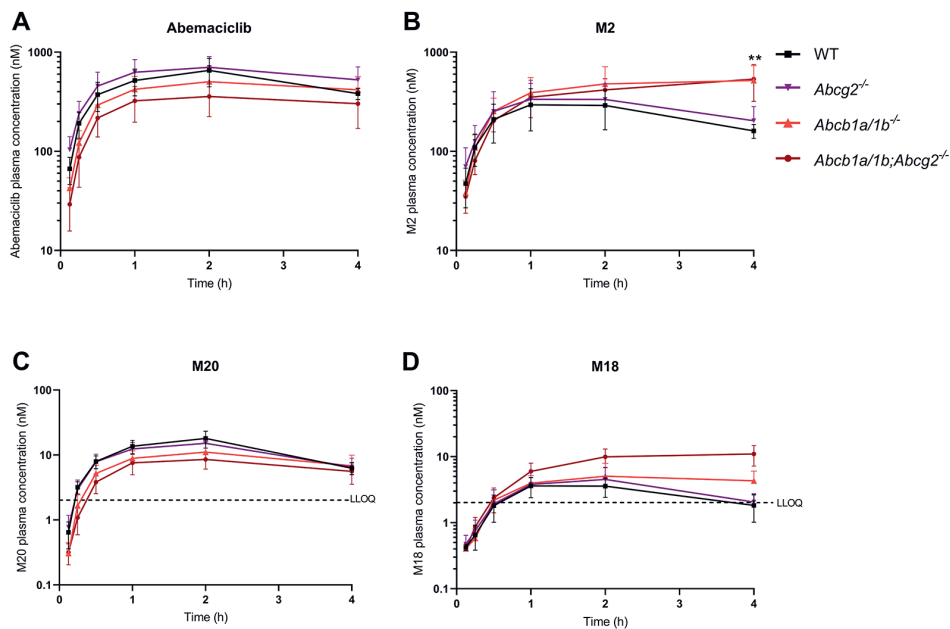
- [30] R.A. Patchell, The management of brain metastases, *Cancer Treat. Rev.* 29 (2003) 533–540. [https://doi.org/10.1016/S0305-7372\(03\)00105-1](https://doi.org/10.1016/S0305-7372(03)00105-1).
- [31] P.S. Steeg, K.A. Camphausen, Q.R. Smith, Brain metastases as preventive and therapeutic targets, *Nat. Rev. Cancer.* 11 (2011) 352–363. <https://doi.org/10.1038/nrc3053>.
- [32] S.M. Tolaney, S. Sahebjam, E. LeRhun, T. Bachelot, P. Kabos, A. Awada, D. Yardley, A. Chan, P. Conte, V. Diéras, N.U. Lin, M. Bear, S.C. Chapman, Z. Yang, Y. Chen, C.K. Anders, A Phase II Study of Abemaciclib in Patients with Brain Metastases Secondary to Hormone Receptor – Positive Breast Cancer, *Clin. Cancer Res.* 26 (2021) 5310–5319. <https://doi.org/10.1158/1078-0432.CCR-20-1764>.
- [33] M.C. de Gooijer, E.M. Kemper, L.C.M. Buil, C.H. Citirikaya, T. Buckle, J.H. Beijnen, O. van Tellingen, ATP-binding cassette transporters restrict drug delivery and efficacy against brain tumors even when blood-brain barrier integrity is lost II ATP-binding cassette transporters restrict drug delivery and efficacy against brain tumors even when blood-brain , *Cell Reports Med.* 2 (2021) 100184. <https://doi.org/10.1016/j.xcrm.2020.100184>.
- [34] B. Rochat, Role of Cytochrome P450 Activity in the Fate of Anticancer Agents and in Drug Resistance, *Clin. Pharmacokinet.* 44 (2005) 349–366. <https://doi.org/10.2165/00003088-200544040-00002>.
- [35] L. Elens, T. Van Gelder, D.A. Hesselink, V. Haufroid, R.H.N. Van Schaik, CYP3A4\*22: Promising newly identified CYP3A4 variant allele for personalizing pharmacotherapy, *Pharmacogenomics.* 14 (2013) 47–62. <https://doi.org/10.2217/pgs.12.187>.
- [36] M. de Gooijer, P. Zhang, N. Thota, I. Mayayo-peralta, L. Buil, J.H. Beijnen, O. Van Tellingen, P-glycoprotein and breast cancer resistance protein restrict the brain penetration of the CDK4/6 inhibitor palbociclib, *Invest. New Drugs.* 33 (2015) 1012–1019. <https://doi.org/10.1007/s10637-015-0266-y>.
- [37] A. Martínez-Chávez, S. van Hoppe, H. Rosing, M. C. Lebre, M. Tibben, J. H. Beijnen, A. H. Schinkel, P-glycoprotein Limits Ribociclib Brain Exposure and CYP3A4 Restricts Its Oral Bioavailability, *Mol. Pharm.* 0 (2019) null-null. <https://doi.org/10.1021/acs.molpharmaceut.9b00475>.



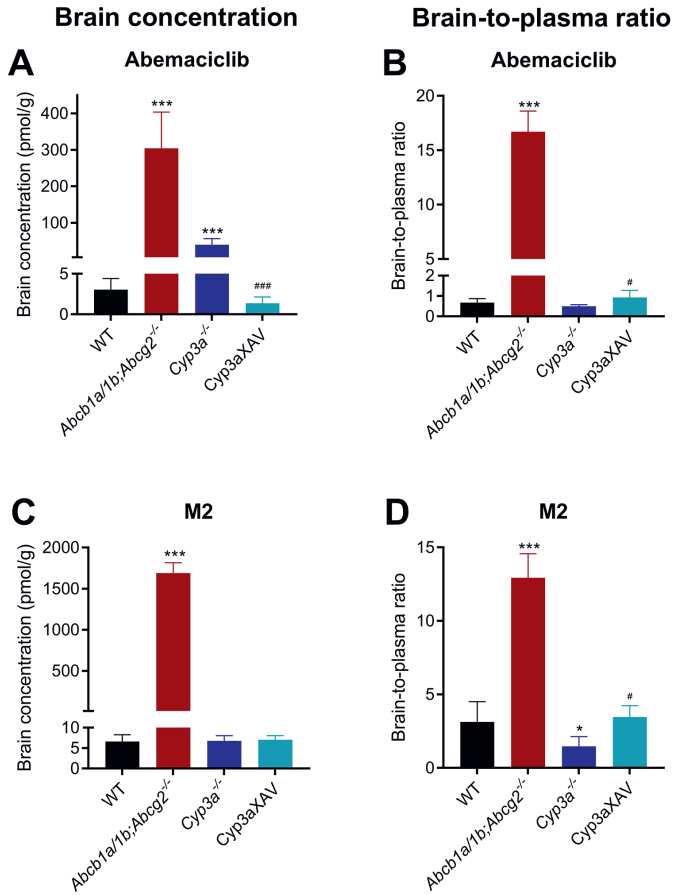
## Supplementary material



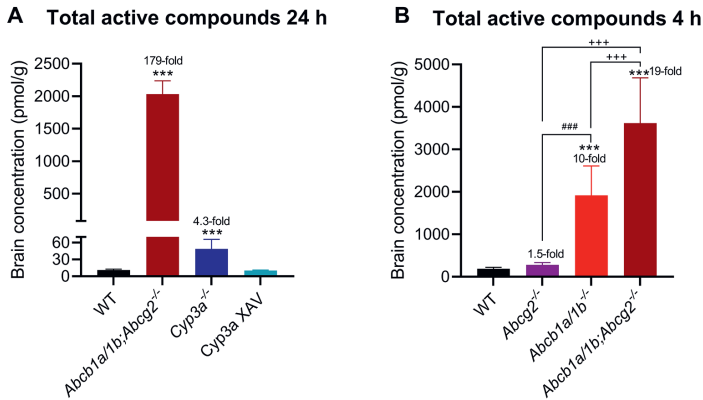
**Supplemental Figure 1.** Semi-log plasma concentration-time curves of abemaciclib (A), M2 (B), M20 (C), M18 (D) and all active compounds combined (E) over 24 h in female wild-type (WT) and *Abcb1a/1b;Abcg2<sup>-/-</sup>* mice after oral administration of 10 mg/kg abemaciclib. Data are presented as mean  $\pm$  SD (n = 6). <sup>1</sup> Values below the lower limit of quantification (LLOQ).



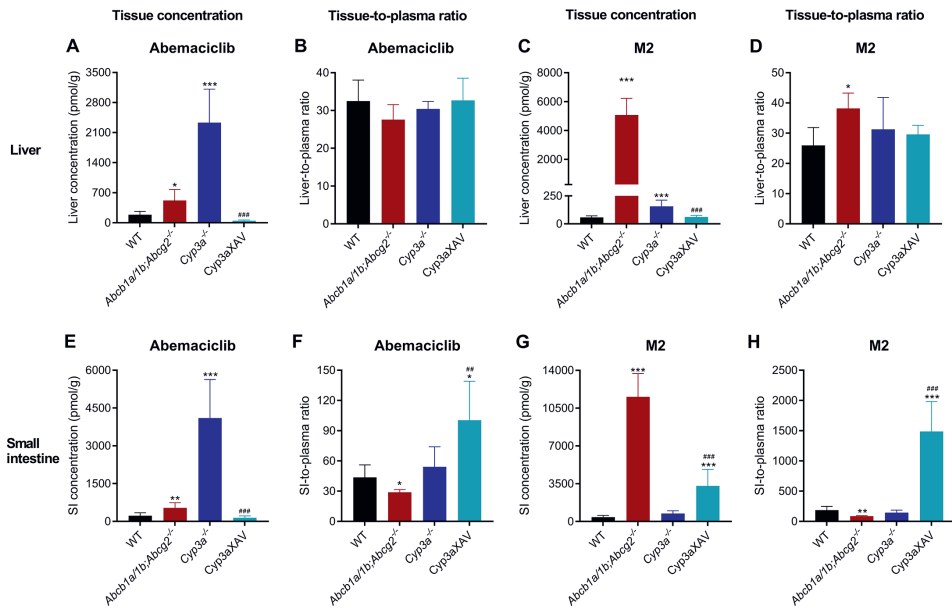
**Supplemental Figure 2.** Semi-log plasma concentration-time curves of abemaciclib (A), M2 (B), M20 (C), and M18 (D) over 4 h in female wild-type (WT), *Abcg2*<sup>-/-</sup>, *Abcb1a/1b*<sup>-/-</sup> and *Abcb1a/1b;Abcg2*<sup>-/-</sup> mice after oral administration of 10 mg/kg abemaciclib. Data are presented as mean  $\pm$  SD (n = 6 - 7). \*\*  $P < 0.01$  compared to WT mice. LLOQ represents the lower limit of quantification of the bioanalytical method.



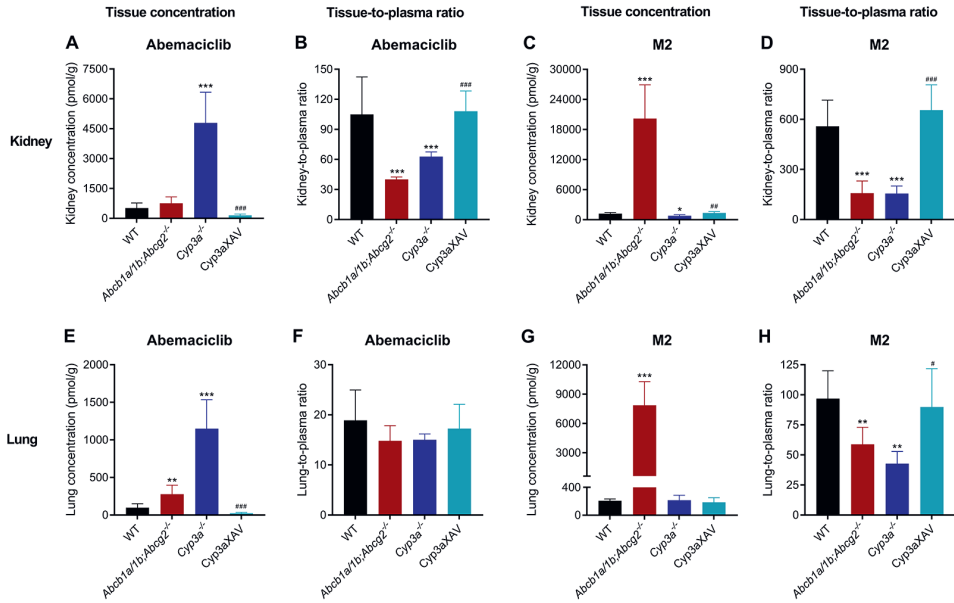
**Supplemental Figure 3.** Brain concentration (A and C) and brain-to-plasma ratio (B and D) of abemaciclib and M2 in female wild-type (WT), *Abcb1a/1b;Abcg2*<sup>-/-</sup>, *Cyp3a*<sup>-/-</sup> and *Cyp3aXAV* mice 24 h after oral administration of 10 mg/kg abemaciclib. Data are presented as mean ± SD (n = 6 - 7). \* *P* < 0.05; \*\* *P* < 0.01; \*\*\* *P* < 0.001 compared to WT mice; # *P* < 0.05; ## *P* < 0.01, ### *P* < 0.001 compared to *Cyp3a*<sup>-/-</sup> mice. M18 was not detected in wild-type, *Cyp3a*<sup>-/-</sup> and *Cyp3aXAV* mice.



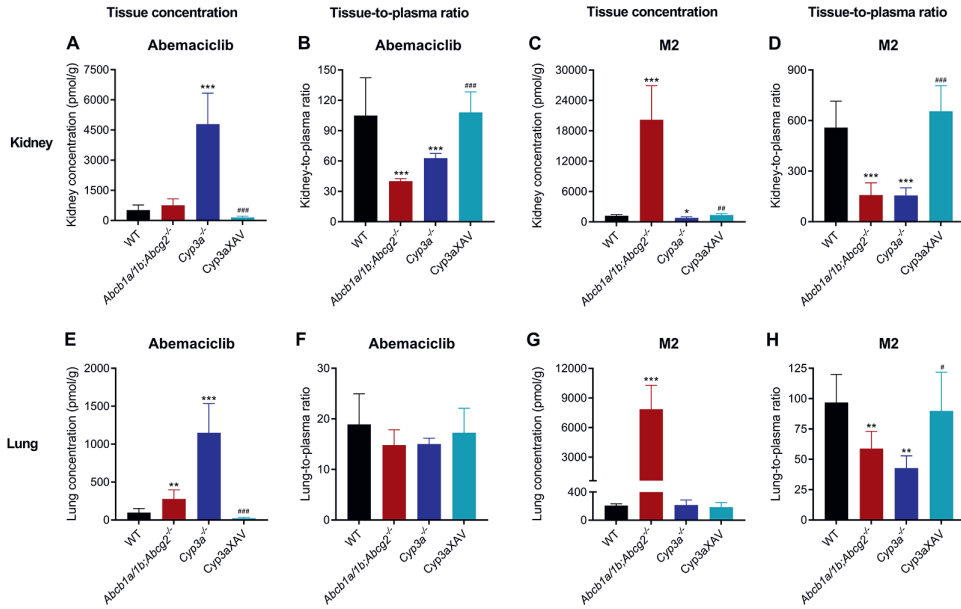
**Supplemental Figure 4.** Total brain concentration of all abemaciclib active compounds combined (including abemaciclib, M2, M20 and M18) in female wild-type (WT), *Abcb1a/1b;Abcg2<sup>-/-</sup>*, *Cyp3a<sup>-/-</sup>* and *Cyp3aXAV* mice 24 h after oral administration of 10mg/kg abemaciclib (A), and in wild-type (WT), *Abcb1a/1b;Abcg2<sup>-/-</sup>*, *Abcb1a/1b<sup>-/-</sup>* and *Abcg2<sup>-/-</sup>* mice 4 h after oral administration of 10 mg/kg abemaciclib (B). Fold difference relative to WT values is indicated. Data are presented as mean  $\pm$  SD (n = 6 - 7); \*\*\*  $P < 0.001$  compared to WT mice; \*\*\*  $P < 0.001$  compared to *Abcb1a/1b;Abcg2<sup>-/-</sup>* mice; ###  $P < 0.001$  compared to *Abcg2<sup>-/-</sup>* mice.



**Supplemental Figure 5.** Liver concentration (A and C), liver-to-plasma ratio (B and D), small intestine concentration (E and G) and small intestine-to-plasma ratio (F and H) of abemaciclib and M2 in female wild-type (WT), *Abcb1a/1b;Abcg2<sup>-/-</sup>*, *Cyp3a<sup>-/-</sup>* and *Cyp3aXAV* mice 24 h after oral administration of 10 mg/kg abemaciclib. Data are presented as mean  $\pm$  SD (n = 5 - 6). \*  $P < 0.05$ ; \*\*  $P < 0.01$ ; \*\*\*  $P < 0.001$  compared to WT mice; ##  $P < 0.01$ ; ###  $P < 0.001$  compared to *Cyp3a<sup>-/-</sup>* mice.



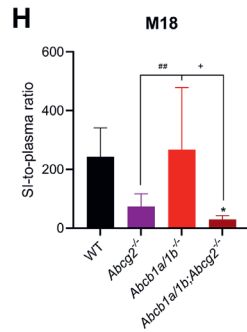
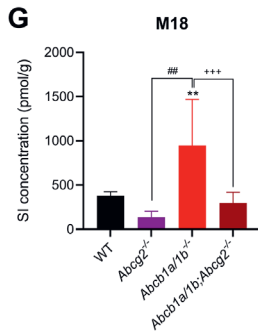
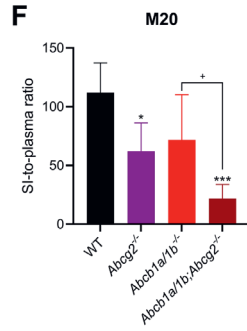
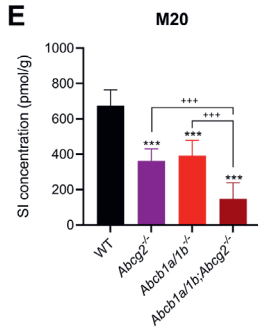
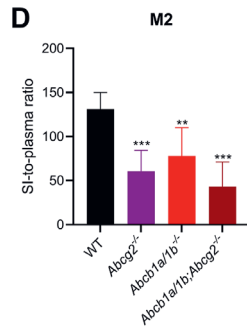
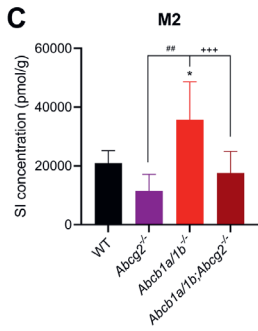
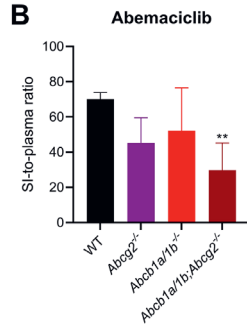
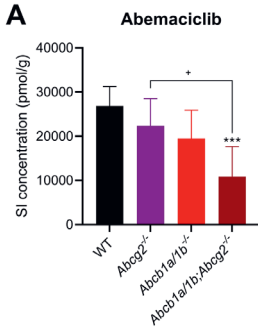
**Supplemental Figure 6.** Kidney concentration (A and C), kidney-to-plasma ratio (B and D), lung concentration (E and G) and lung-to-plasma ratio (F and H) of abemaciclib or M2 in female wild-type (WT), *Abcb1a/1b;Abcg2<sup>-/-</sup>*, *Cyp3a<sup>-/-</sup>* and *Cyp3aXAV* mice 24 h after oral administration of 10 mg/kg abemaciclib. Data are presented as mean  $\pm$  SD (n = 5 - 6). \*  $P < 0.05$ ; \*\*  $P < 0.01$ ; \*\*\*  $P < 0.001$  compared to WT mice; #  $P < 0.05$ ; ##  $P < 0.01$ ; ###  $P < 0.001$  compared to *Cyp3a<sup>-/-</sup>* mice.



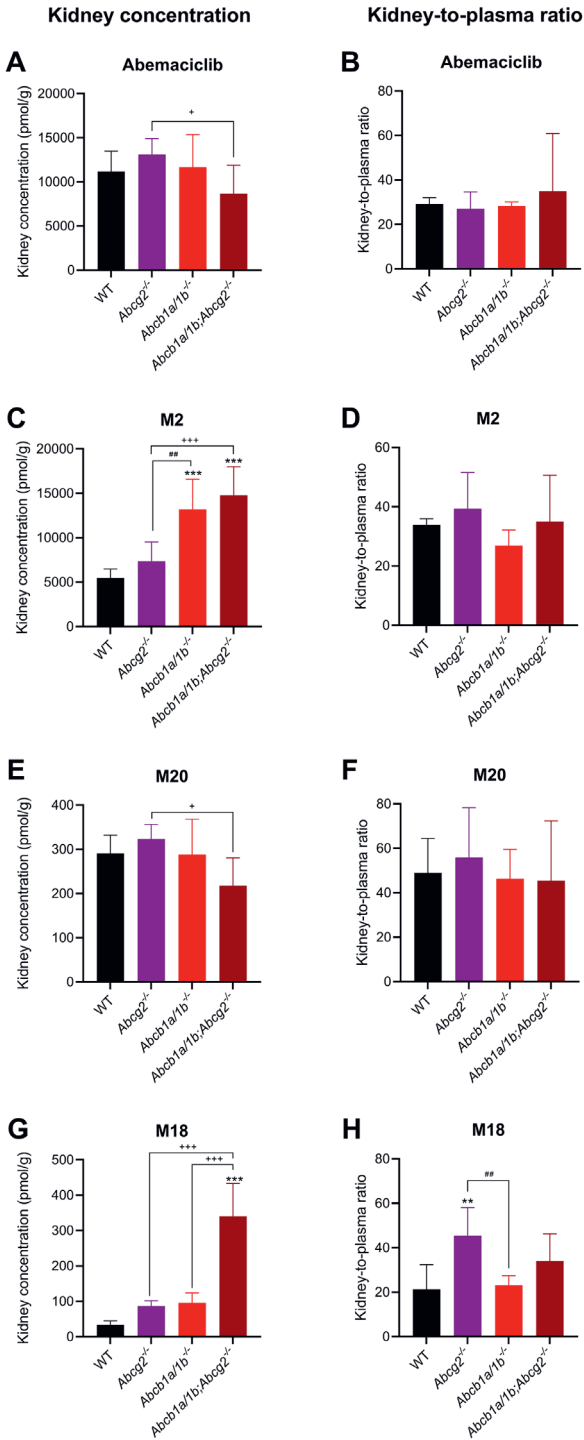
**Supplemental Figure 7.** Liver concentration (A, C, E and G) and liver-to-plasma ratio (B, D, F and H) of abemaciclib, M2, M20 and M18 in female wild-type (WT), *Abcg2<sup>-/-</sup>*, *Abcb1a/1b<sup>-/-</sup>* and *Abcb1a/1b;Abcg2<sup>-/-</sup>* mice 4 h after oral administration of 10 mg/kg abemaciclib. Data are presented as mean  $\pm$  SD (n = 6 - 7). \*  $P < 0.05$ ; \*\*\*  $P < 0.001$  compared to WT mice; +  $P < 0.05$ ; ++  $P < 0.01$ ; +++  $P < 0.001$  compared to *Abcb1a/1b;Abcg2<sup>-/-</sup>* mice; ###  $P < 0.001$  compared to *Abcg2<sup>-/-</sup>* mice.

Small intestine concentration

Small intestine-to-plasma ratio

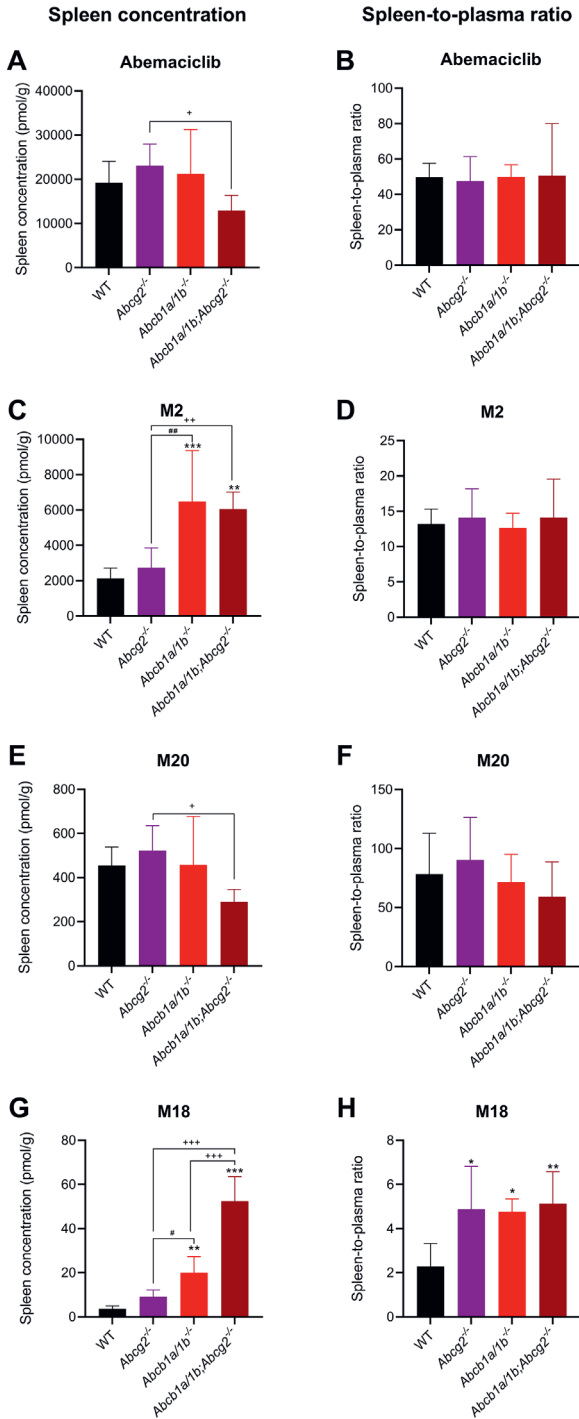


**Supplemental Figure 8.** Small intestine tissue concentration (A, C, E and G) and small intestine tissue-to-plasma ratio (B, D, F and H) of abemaciclib, M2, M20 and M18 in female wild-type (WT), *Abcg2*<sup>-/-</sup>, *Abcb1a/1b*<sup>-/-</sup> and *Abcb1a/1b*<sup>-/-</sup>;*Abcg2*<sup>-/-</sup> mice 4 h after oral administration of 10 mg/kg abemaciclib. Data are presented as mean ± SD (n = 6 - 7). \* *P* < 0.05; \*\* *P* < 0.01; \*\*\* *P* < 0.001 compared to WT mice; + *P* < 0.05; +++ *P* < 0.001 compared to *Abcb1a/1b*<sup>-/-</sup> mice; ## *P* < 0.01 compared to *Abcg2*<sup>-/-</sup> mice.

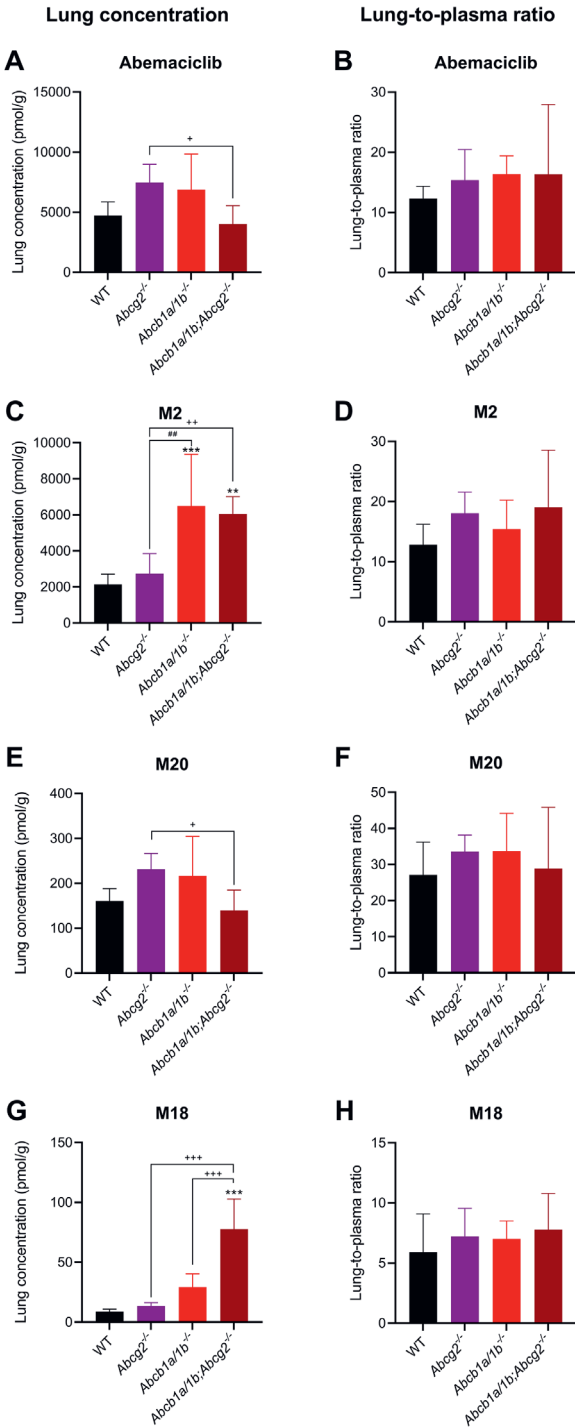


**Supplemental Figure 9.** Kidney concentration (A, C, E and G) and kidney-to-plasma ratio (B, D, F and H) of abemaciclib, M2, M20 and M18 in female wild-type (WT), *Abcg2*<sup>-/-</sup>, *Abcb1a/1b*<sup>-/-</sup> and *Abcb1a/1b;Abcg2*<sup>-/-</sup> mice 4 h after oral administration of 10 mg/kg abemaciclib. Data are presented as mean ± SD (n = 6 - 7). \*\* P < 0.01; \*\*\* P < 0.001 compared to WT mice; + P < 0.05; \*\*\* P < 0.001 compared to *Abcb1a/1b;Abcg2*<sup>-/-</sup> mice; # P < 0.01 compared to *Abcg2*<sup>-/-</sup> mice.

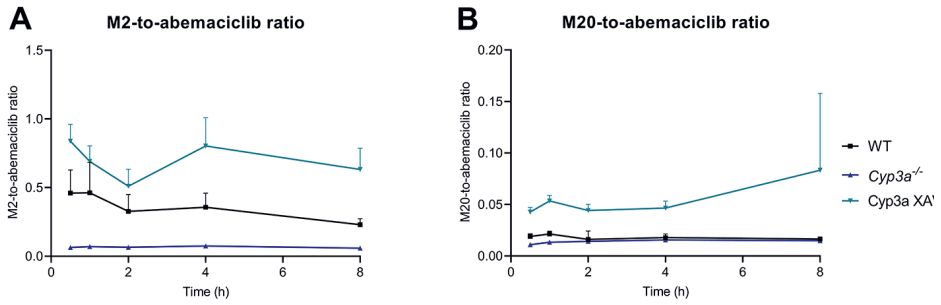




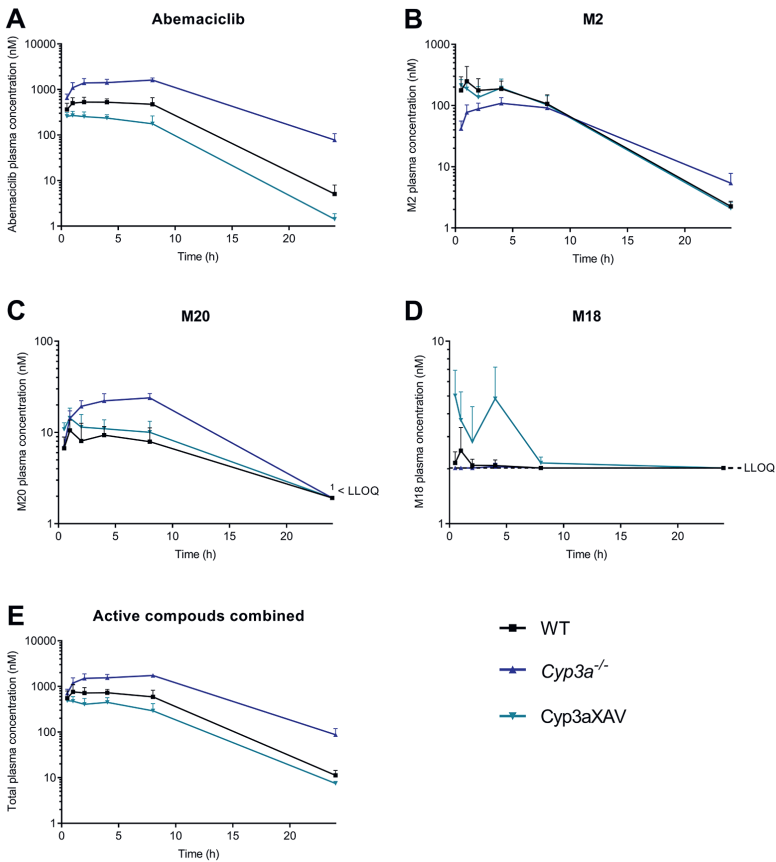
**Supplemental Figure 10.** Spleen concentration (A, C, E and G) and spleen-to-plasma ratio (B, D, F and H) of abemaciclib, M2, M20 and M18 in female wild-type (WT), *Abcg2*<sup>-/-</sup>, *Abcb1a/1b*<sup>-/-</sup> and *Abcb1a/1b;Abcg2*<sup>-/-</sup> mice 4 h after oral administration of 10 mg/kg abemaciclib. Data are presented as mean ± SD (n = 6 - 7). \* *P* < 0.05; \*\* *P* < 0.01; \*\*\* *P* < 0.001 compared to WT mice; # *P* < 0.05; ## *P* < 0.01 compared to *Abcb1a/1b;Abcg2*<sup>-/-</sup> mice.



**Supplemental Figure 11.** Lung concentration (A, C, E and G) and lung-to-plasma ratio (B, D, F and H) of abemaciclib, M2, M20 and M18 in female wild-type (WT), *Abcg2*<sup>-/-</sup>, *Abcb1a/1b*<sup>-/-</sup>, and *Abcb1a/1b;Abcg2*<sup>-/-</sup> mice 4 h after oral administration of 10 mg/kg abemaciclib. Data are presented as mean ± SD (n = 6 - 7). \*\* *P* < 0.01; \*\*\* *P* < 0.001 compared to WT mice; \* *P* < 0.05; \*\* *P* < 0.01; \*\*\* *P* < 0.001 compared to *Abcb1a/1b;Abcg2*<sup>-/-</sup> mice; # *P* < 0.01 compared to *Abcg2*<sup>-/-</sup> mice.



**Supplemental Figure 12.** Metabolite-to-abemaciclib ratio of M2 (A) and M20 (B) in plasma of wild-type, *Cyp3a*<sup>-/-</sup> and *Cyp3a*XAV mice over 8 h after oral administration of 10 mg/kg abemaciclib. Data are presented as mean ± SD (n = 6).



**Supplemental Figure 13.** Semi-log plasma concentration-time curves of abemaciclib (A), M2 (B), M20 (C), M18 (D) and all active compounds combined (E) over 24 h in female wild-type (WT), *Cyp3a*<sup>-/-</sup> and *Cyp3a*XAV mice after oral administration of 10 mg/kg abemaciclib. Data are presented as mean ± SD (n = 6). <sup>1</sup>, Values below the lower limit of quantification (LLOQ).



# 7

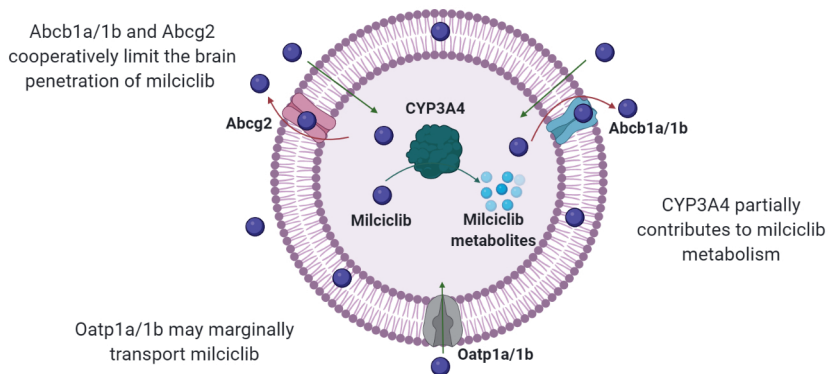
## The role of drug efflux and uptake transporters ABCB1 (P-gp), ABCG2 (BCRP) and OATP1A/1B and of CYP3A4 in the pharmacokinetics of the CDK inhibitor milciclib

European Journal of Pharmaceutical Sciences 2021, 190: 113516

Alejandra Martínez-Chávez  
Jelle Broeders  
Maria C. Lebre  
Matthijs M. Tibben  
Hilde Rosing  
Jos H. Beijnen  
Alfred H. Schinkel

## Abstract

The promising anticancer drug milciclib potently inhibits cyclin-dependent kinase (CDK) 2 and tropomyosin receptor kinase (TRK) A, and is currently in phase II clinical studies. To characterize factors affecting milciclib pharmacokinetics, we investigated whether milciclib is a substrate of the multidrug efflux and uptake transporters ABCB1 (P-gp), ABCG2 (BCRP), and OATP1A/1B, and the drug-metabolizing enzyme CYP3A4, using genetically-modified mouse models and Madin-Darby Canine Kidney (MDCK-II) cells. *In vitro*, milciclib was transported by mAbcg2, and this was inhibited by the ABCG2 inhibitor Ko143. Upon oral administration of milciclib, its plasma exposure in *Abcb1a/1b*<sup>-/-</sup>, *Abcg2*<sup>-/-</sup>, and *Abcb1a/1b;Abcg2*<sup>-/-</sup> mice was similar to that found in wild-type mice. Milciclib showed good brain penetration even in wild-type mice (brain-to-plasma ratio of 1.2), but this was further increased by 5.2-fold when both *Abcb1* and *Abcg2* were ablated, and to a lesser extent in single *Abcb1*- or *Abcg2*-deficient mice. *Oatp1a/1b* deficiency had only a minor impact on the milciclib plasma AUC<sub>0-24h</sub> and C<sub>max</sub>. The milciclib AUC<sub>0-8h</sub> increased 1.9-fold in *Cyp3a*<sup>-/-</sup> mice but decreased only 1.3-fold upon overexpression of human CYP3A4. Thus, ABCB1 and ABCG2 cooperatively limit milciclib brain penetration. The low impact of OATP1 and CYP3A4 could be clinically favorable for milciclib, reducing the risks of unintended drug-drug interactions or interindividual variation in CYP3A4 activity.



## Introduction

Miliclib (PHA-848125, Supplemental Figure 1) is a promising small-molecule anticancer drug that is currently in phase II clinical studies. It potently inhibits the complex formed between cyclin-dependent kinase (CDK) 2 and cyclin A, and the tropomyosin receptor kinase (TRK) A, with a half-maximal inhibitory concentration ( $IC_{50}$ ) of 45 and 53 nM, respectively [1,2]. Alterations in both targets (e.g. CDK2 amplification or TRKA activation) have been identified in various cancers. Their inhibition leads to cell cycle arrest via CDK2 and to reduction in cell proliferation [3,4]. In addition, miliclib can inhibit other CDKs, albeit with lower potency ( $IC_{50} >150$  nM). Interestingly, inhibition of CDK7 by miliclib has been associated with a reduction in glucose consumption in cancer cells, while CDK5 inhibition has been related with antiangiogenic effects of miliclib [5–7].

In preclinical studies, miliclib showed efficacy against various cancers in several human xenograft mouse models, including ovarian, colon, pancreatic, melanoma and non-small cell lung cancer, with a maximal tumor growth inhibition between 70 and 91% after administration of 40 mg/kg miliclib twice a day for 10 consecutive days. In addition, with this schedule miliclib produced tumor stabilization or regression in two glioma xenograft mouse models (U251 and U87MG) with a maximal tumor growth inhibition between 71 and 80% [2,8]. Phase I clinical studies in cancer patients with solid tumors demonstrated a safe use of miliclib, either alone or in combination with gemcitabine. The most common adverse effects included nausea and vomiting (both manageable with conventional anti-emetic treatment), diarrhea, fatigue and neurologic effects, which were reversible after treatment discontinuation and further treated primarily using (re-)hydration [9,10]. Furthermore, miliclib showed efficacy for thymoma and thymic carcinoma treatment, obtaining Orphan Drug designations by the U.S. Food and Drug Administration (FDA) and the European Medicine Agency (EMA) [11–13]. Phase II clinical studies to determine the efficacy of miliclib as monotherapy in hepatocellular carcinoma are ongoing [14].

In patients, miliclib is absorbed with a median time to reach the maximum plasma concentration ( $t_{max}$ ) ranging between 2 and 4 h after oral administration of miliclib maleate capsules. After repeated doses and upon reaching the steady state, miliclib accumulated with a factor of 3, and the elimination half-life was approximately 33 h. At the recommended phase II dose (150 mg/day with a schedule of 7 days on/7 days off in 2 week cycle), on day 7 the mean maximum plasma concentration ( $C_{max}$ ) and the mean area under the plasma concentration-time curve ( $AUC_{0-24}$ ) were 1.5  $\mu$ M (CV = 33%) and 25  $\mu$ M·h (CV = 34%). Miliclib plasma exposure showed a dose-proportional increase up to 200 mg/day [9].

Pharmacokinetics of drugs including miliclib can be influenced by drug transporters, since these can affect the absorption, distribution, metabolism and excretion of drugs,

often with clinically relevant (pharmacodynamic) consequences [15,16]. In this study we focus on two major families of transmembrane drug transporters: the ATP-binding cassette (ABC) transporters and the organic anion-transporting polypeptides (OATPs).

The ABC transporters use the energy from ATP hydrolysis to translocate both endogenous and exogenous compounds to the extracellular compartment. Among them, P-glycoprotein (ABCB1, P-gp, MDR1) and the Breast Cancer Resistance Protein (ABCG2, BCRP) are the most relevant efflux transporters for drugs, because of their wide substrate specificity and influence on drug disposition [15,16]. Expressed in the apical membrane of enterocytes, ABCB1 and ABCG2 can control the net absorption of drugs, as they extrude substrate drugs from the intestinal epithelium into the intestinal lumen. They also facilitate the elimination of substrate drugs in the bile canicular membrane of hepatocytes and the apical membrane of proximal tubules of nephrons, where substrate drugs are pumped out from blood into the bile and urine, respectively. Finally, ABCB1 and ABCG2 are expressed in brain capillary endothelial cells, limiting the penetration of substrates into the brain at the blood-brain barrier [15,17]. In addition, ABCB1 and ABCG2, when overexpressed in tumor cells, can confer resistance to anticancer drugs [18,19].

OATPs are primarily uptake transporters, where OATP1A and OATP1B have been demonstrated to impact the pharmacokinetics of several drugs. They are expressed in the sinusoidal membrane of hepatocytes (OATP1B1 and OATP1B3), the distal tubules of nephrons (OATP1A2), and at the blood-brain barrier (OATP1A2) [20,21]. Whether miliclib is a substrate of the drug transporters ABCB1, ABCG2, OATP1A and OATP1B has not been reported so far.

The pharmacokinetics of drugs is also often strongly affected by drug-metabolizing enzymes. The Cytochrome P450 (CYP) 3A family participates in the metabolism of numerous clinically used drugs, including anticancer agents, facilitating drug elimination. Importantly, these enzymes can be markedly induced or inhibited by dietary compounds or other drugs. This, together with their broad substrate specificity, can lead to several drug-drug interactions. CYP3A4 and CYP3A5 are the most abundant isoforms in liver. In addition, various polymorphisms of CYP3A4 and CYP3A5 have been identified in humans, leading to high inter-individual variation in CYP3A activity [22]. *In vitro* studies indicate that miliclib is partially metabolized by the CYP3A4 isoform, with a contribution of approximately 15%. However, to what extent CYP3A4 influences the oral exposure of miliclib in an *in vivo* context has not been reported so far [1]. In addition, it has been suggested that several metabolic pathways are involved in miliclib metabolism, although further information is not publicly available [23].

For investigational drugs like miliclib, it is important to determine their potential interaction with these drug transporters and CYP enzymes, since this could help to



predict clinical drug-drug interactions [24]. Thus, the objective of this study is to investigate the interaction between miliclib and ABCB1, ABCG2, OATP1A/1B, and CYP3A4. An *in vitro* transport study as well as *in vivo* studies in various mouse models with different genotypes were performed to determine the potential impact of these drug transporters and CYP3A on miliclib pharmacokinetics.

## Materials and methods

### Drugs, chemicals and reagents

Miliclib free base was purchased from Selleck Chemicals (Houston, TX). Zosuquidar was supplied by Sequoia Research Products (Pangbourne, UK), and Ko143 was obtained from Tocris Bioscience (Bristol, UK).

DMSO was obtained from Sigma-Aldrich (Steinheim, Germany) and potassium dihydrogen phosphate from Merck (Darmstadt, Germany). Heparin 5000 IU/mL was supplied by Leo Pharma (Breda, The Netherlands), isoflurane by Pharmachemie (Harlem, The Netherlands), and bovine serum albumin (BSA, fraction V) was purchased from Roche Diagnostics GmbH (Mannheim, Germany).

Cell culture products, including Dulbecco's Modified Essential Medium glutamax (DMEM), Dulbecco's phosphate-buffered saline (DPBS) and penicillin-streptomycin 10,000 U/mL were purchased from Life Technologies (Carlsbad, CA). Fetal Bovine Serum (FBS) was supplied by Sigma-Aldrich (Steinheim, Germany).

### Cell culture

The parental Madin-Darby Canine Kidney (MDCK-II) cells were used, as well as its subclones transduced with human (h)ABCB1, hABCG2 or mouse (m)Abcg2, which were generated previously in our group [25–28]. Cells were cultured at 37°C and 5% CO<sub>2</sub> in supplemented culture medium (DMEM with 10% (v/v) FBS and 1% (v/v) of penicillin-streptomycin). Cells were maintained in culture for at least 2 weeks prior to the transport studies, reaching a passage number between 11 and 15.

### *in vitro* transport studies

Transport experiments were carried out in 12-well Transwell permeable supports (Corning Life Sciences, Tewksbury, MA) with 12 mm internal diameter inserts, containing a polycarbonate membrane (3 µm pore size). Cells were seeded at a density of 2.5 × 10<sup>5</sup> cells/well. Supplemented culture medium was refreshed on day 1 and 2 after seeding, while the cells formed a monolayer with tight junctions. This was assessed by transepithelial electrical resistance (TEER) measurement prior the experiment, where all monolayers showed TEER values within the reference values for each cell line (≥ 70 Ω cm<sup>2</sup> for the parental and hABCG2-transduced, ≥ 200 Ω cm<sup>2</sup> for the hABCB1-

transduced, and  $\geq 140 \Omega \text{ cm}^2$  for the mAbcg2-transduced cell line). On day 3, after washing with DPBS, cells were pre-incubated during 1 h with 10% FBS-supplemented medium, 5  $\mu\text{M}$  zosuquidar (ABCB1 inhibitor) and/or 5  $\mu\text{M}$  Ko143 (ABCG2 inhibitor). Subsequently, the pre-incubation medium was replaced with FBS-supplemented medium containing 4  $\mu\text{M}$  miliclib in the donor compartment and no miliclib in the acceptor compartment. For inhibition experiments, these solutions contained Zosuquidar and/or Ko143 at 5  $\mu\text{M}$ . Transport experiments were performed independently in both directions: apical-to-basolateral (A-B) or basolateral to apical (B-A). Transwell plates were incubated at 37°C in 5%  $\text{CO}_2$  and samples of 50  $\mu\text{L}$  were collected from the acceptor compartment at 1, 2, 4 and 8 h. After the last time point, the integrity of the monolayer throughout the experiment was confirmed by re-measuring the TEER. In all cases TEER values were not decreased at the end of the experiment. All experiments were conducted in triplicate. Samples were stored at -20°C until their analysis according to the LC-MS/MS method described below.

The total miliclib transported at each time point was calculated considering the remaining volume in the acceptor compartment, and corrected for the removed drug from previous samplings. Active transport was determined by the efflux ratio (ER), which was calculated by dividing the apparent permeability coefficient ( $P_{\text{app}}$ ) for basolateral-to-apical transport by the  $P_{\text{app}}$  for apical-to-basolateral transport for miliclib. Papp was calculated according to the following formula:

$$P_{\text{app}} = \frac{dQ}{dt} \times \frac{1}{AC_0}$$

Where  $dQ/dt$  is the transport rate (pmol/s) obtained from the linear regression of miliclib transport amount vs time, A is the insert surface area ( $\text{cm}^2$ ) and  $C_0$  is the initial concentration in the donor compartment (pmol/mL).

### Animals

FVB wild-type (WT) and genetically modified mice were used, including *Abcb1a/1b*<sup>-/-</sup>; *Abcg2*<sup>-/-</sup>, *Abcb1a/1b*<sup>-/-</sup>, *Abcg2*<sup>-/-</sup>, *Oatp1a/1b*<sup>-/-</sup>, *Cyp3a*<sup>-/-</sup> and *Cyp3aXAV* (CYP3A4-humanized transgenic mice with expression in liver and small intestine in a *Cyp3a*<sup>-/-</sup> background), which were previously generated in our institute [29–34]. Based on availability, female mice within 9–16 weeks old were used. They were housed in an environment with controlled temperature and 12 h light/dark cycle, receiving water and a standard diet (Transbreed, SDS Diets, Technilab-BMI, Someren, The Netherlands) *ad libitum*. Animal housing and studies were conducted according to institutional guidelines complying with the Dutch and EU Legislation (approval number from The Dutch Central Animal Testing Committee: AVD301002016595). All experiments were approved by the institutional animal care and use committee.

### ***in vivo* pharmacokinetic studies**

The influence of transporters on miliclib pharmacokinetics was investigated in two experiments, which were terminated at 24 or 4 h, while for the assessment of CYP3A impact the experiments were terminated at 24 or 8 h. In each experiment, six mice were used per strain. A miliclib dosing solution was formulated at 1 mg of drug per mL of vehicle, which consisted of 25 mM phosphate buffer pH 3:DMSO (95:5, v/v). Miliclib was orally administered to the mice at 10 mg/kg, after at least 2 h of fasting. Approximately 50  $\mu$ L of blood was drawn from the tip of the tail at intermediate time points in heparin-coated microvette tubes (Sarstedt, Numbrecht, Germany). For the 4 h experiment the intermediate time points were 0.125, 0.25, 0.5, 1 and 2 h, for the 8 h experiment they were 0.25, 0.5, 1, 2, and 4 h, and for the 24 h experiment the intermediate time points were 0.5, 1, 2, 4, and 8 h. At the terminal point (24, 8 or 4 h) at least 600  $\mu$ L of blood was collected via cardiac puncture under isoflurane anesthesia using heparin as anticoagulant. Thereafter, mice were sacrificed by cervical dislocation, and tissues were collected including brain, liver, small intestine, kidneys, spleen and thymus.

Tissues were weighed and homogenized with 2% BSA in water (w/v) using the grinder FastPrep-24 (MP-Biomedicals, Santa Ana, CA). For this, 0.5 mL was added to thymus, 1 mL to brain and spleen, 2 mL to kidneys, and 3 mL to liver and small intestine. Tissue homogenates were stored at -70°C until analysis.

From blood samples, plasma was obtained after centrifugation (9000g, 4°C, 6 min) and stored at -20°C prior to analysis.

### **Quantification of miliclib using liquid chromatography-tandem mass spectrometry (LC-MS/MS)**

Miliclib was quantified in all samples generated in the transport and pharmacokinetic studies according to the validated bioanalytical method previously described using liquid chromatography-tandem mass spectrometry [35].

### **Pharmacokinetic calculations and statistics**

Pharmacokinetic parameters were calculated using the add-in PK solver in Microsoft Excel [36]. The area under the plasma concentration-time curves until the last time point ( $AUC_{0-t}$ ) was determined by the linear trapezoidal method. The  $C_{max}$  and the  $t_{max}$  were obtained directly from the plasma concentration-time curves. Tissue-to-plasma ratios were calculated by dividing the concentration in tissues by the plasma concentration. Statistical analyses were performed using GraphPad Prism 7 (San Diego, CA). For two and multiple group comparisons, student's t test and ANOVA were used, respectively. Bonferroni post-hoc correction was used to account for multiple comparisons. Differences were considered statistically significant when  $P < 0.05$ .

## Results

### ***In vitro* transport of miliclib by ABCB1 and ABCG2**

In order to study the interaction of miliclib with the ABCB1 and ABCG2 transporters in an *in vitro* context, we evaluated the bidirectional transport of miliclib (at 4  $\mu\text{M}$ ) across polarized monolayers formed by parental and hABCB1-, hABCG2- and mAbcg2-transduced MDCK-II cells (Figure 1). In the parental and the hABCB1 cell lines, the apical-to-basolateral transport of miliclib was slightly higher than the basolateral-to-apical transport, resulting in efflux ratios (ERs) of 1.3 and 1.2, respectively (Figures 1A and 1C). When the ABCB1 inhibitor zosuquidar was added, the efflux ratio was slightly reduced in both cell lines (ER = 0.9, Figures 1B and 1D). These data suggest that miliclib is a weak transport substrate for human ABCB1. Zosuquidar was added in the hABCG2 and mAbcg2 experiments to inhibit any putative activity of the endogenous canine Abcb1 expressed in these cell lines. For hABCG2 no active transport was noticeable, since the efflux ratio was 1.0, both with and without the ABCG2 inhibitor Ko143 (Figure 1E and 1F). However, in the mAbcg2 monolayer miliclib was clearly transported in the apical direction (ER = 2.1, Figure 1G), and this was completely inhibited by Ko143 (ER = 1.0, Figure 1H). This indicates that miliclib is a transport substrate of mAbcg2.

### **Effect of Abcb1 and Abcg2 on miliclib plasma pharmacokinetics**

We further investigated the *in vivo* effects of Abcb1 and Abcg2 on the plasma pharmacokinetics and tissue distribution of miliclib. First, a 24-h pharmacokinetic experiment was performed in wild-type and *Abcb1a/1b*<sup>-/-</sup>;*Abcg2*<sup>-/-</sup> mice. Then, a second experiment with a 4-h terminal time point was performed, where the single *Abcb1a/1b*<sup>-/-</sup> and *Abcg2*<sup>-/-</sup> strains were also included.

Oral administration of 10 mg/kg miliclib in wild-type mice resulted in a similar plasma level ( $C_{\text{max}}$ ) of miliclib as that seen at steady state in humans [9]. The plasma concentration-time curves of miliclib in the 24-h and 4-h experiments are depicted in Figure 2A and 2B, respectively. In both experiments, the area under the plasma concentration-time curves (AUCs) of miliclib were not significantly different among the different mouse strains (Table 1). No significant differences were found either for the maximum plasma concentration ( $C_{\text{max}}$ ) among the wild-type and the Abcb1- and/or Abcg2-deficient mice. High variation in the time point to reach the maximum concentration ( $t_{\text{max}}$ ) was observed in all mouse strains, primarily reflecting an effective plateauing of the plasma concentration between about 1 and 4 h (Figure 2, Table 1). The terminal elimination of miliclib (beyond 8 h) appeared to be slower in *Abcb1a/1b*<sup>-/-</sup>;*Abcg2*<sup>-/-</sup> mice compared to wild-type, as observed in the semi-log plasma concentration-time curve at 24 h (Supplemental Figure 2). This is also reflected in the estimated terminal half-lives ( $t_{1/2}$ ), which were 2.8 and 3.5 h for wild-type and *Abcb1a/1b*<sup>-/-</sup>;*Abcg2*<sup>-/-</sup> mice, respectively ( $P < 0.001$ ).

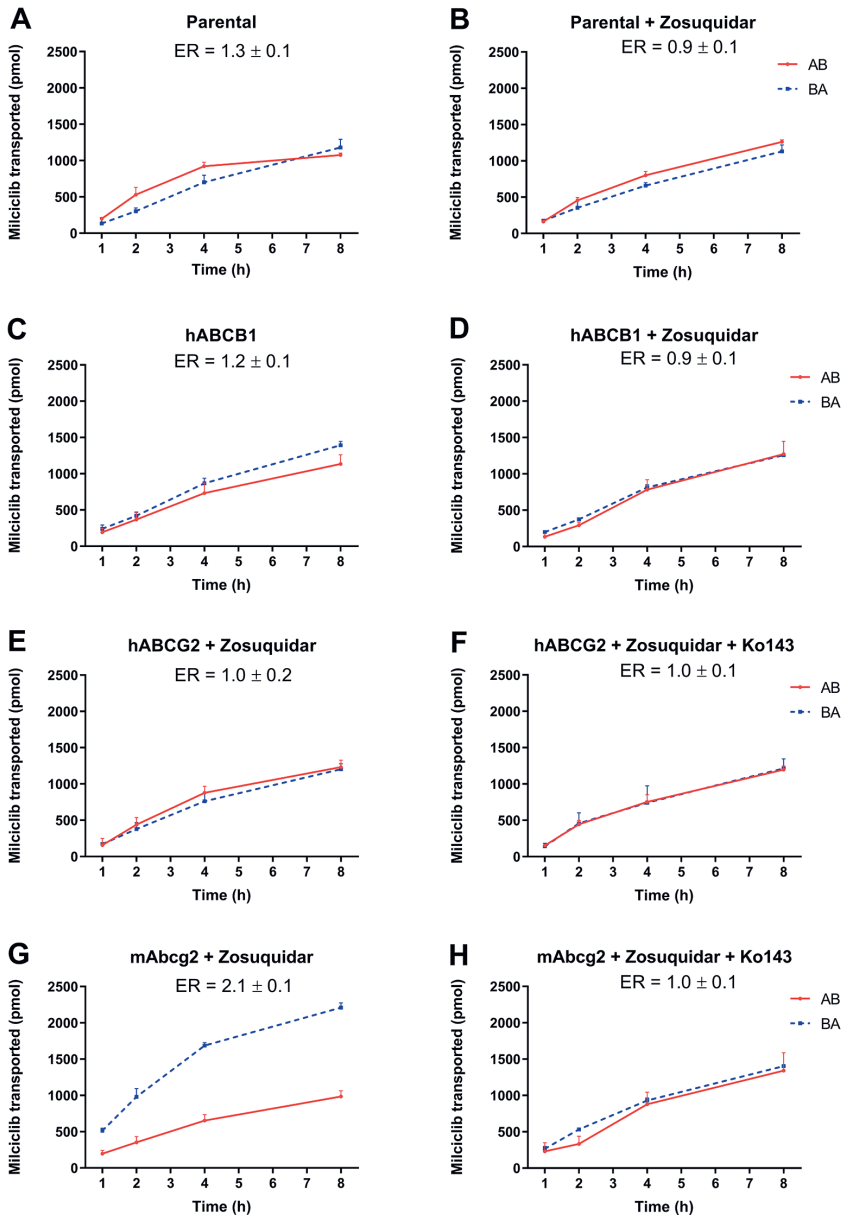


**Figure 1.** *In vitro* bidirectional transport of miliciclib (4  $\mu$ M) using MCDK-II cells parental (A, B) or transduced with human ABCB1 (C, D), human ABCG2 (E, F), or murine Abcg2 (G, H) cDNA. At  $t = 0$  miliciclib was added in the donor compartment. At 1, 2, 4 and 8 h miliciclib was quantified in the acceptor compartment and plotted as total transported amount. Apical-to-basolateral (AB) transport is depicted with the red line and basolateral-to-apical (BA) transport is shown with the dotted blue line. Zosuquidar (5  $\mu$ M) was added to inhibit the human and/or the endogenous ABCB1, while Ko143 (5  $\mu$ M) was added to inhibit the human or murine ABCG2. Data are presented as mean  $\pm$  SD ( $n = 3$ ), ER = efflux transport ratio. Respective  $P_{app}$  values ( $\times 10^{-6}$  cm/s) for BA and AB transport in each panel were: Panel A, 9.2 and 7.1; Panel B, 8.3 and 9.2; Panel C, 10.1 and 8.2; Panel D, 9.3 and 10.1; Panel E, 8.9 and 9.1; Panel F, 8.9 and 8.7; Panel G, 14.3 and 6.8; Panel H, 9.7 and 10.0.

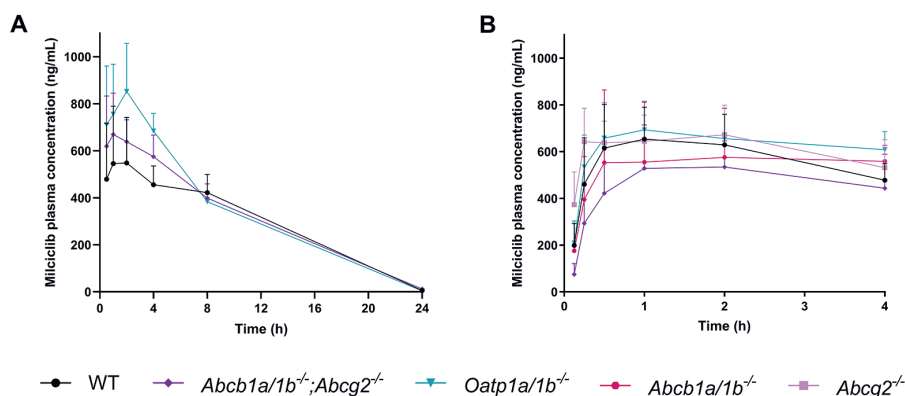


**Figure 2.** Plasma concentration-time curves of miliclib over 24 h (A) and 4 h (B) in wild-type (WT), *Abcb1a/1b*<sup>-/-</sup>; *Abcg2*<sup>-/-</sup>, *Oatp1a/1b*<sup>-/-</sup>, *Abcb1a/1b*<sup>-/-</sup> and *Abcg2*<sup>-/-</sup> female mice after oral administration of 10 mg/kg miliclib. Data are presented as mean  $\pm$  SD (n = 6).

**Table 1.** Plasma pharmacokinetic parameters and brain penetration of miliclib in wild-type, *Abcb1a/1b*<sup>-/-</sup>; *Abcg2*<sup>-/-</sup>, *Abcb1a/1b*<sup>-/-</sup> and *Abcg2*<sup>-/-</sup> female mice over 24 or 4 h after 10 mg/kg miliclib oral administration<sup>a</sup>

Parameter	Genotype					
	24 h		4 h			
	Wild-type	<i>Abcb1a/1b</i> <sup>-/-</sup> ; <i>Abcg2</i> <sup>-/-</sup>	Wild-type	<i>Abcg2</i> <sup>-/-</sup>	<i>Abcb1a/1b</i> <sup>-/-</sup>	<i>Abcb1a/1b</i> <sup>-/-</sup> ; <i>Abcg2</i> <sup>-/-</sup>
AUC <sub>0-t</sub> (h·ng/mL)	7094 $\pm$ 301	7576 $\pm$ 922	2254 $\pm$ 346	2430 $\pm$ 401	2142 $\pm$ 698	1863 $\pm$ 492
Fold change AUC <sub>0-t</sub>	-	1.1	-	1.1	1.0	0.8
t <sub>max</sub> (h)	1-8	0.5-4	0.5-4	0.25-4	0.5-4	1-4
C <sub>max</sub> (ng/mL)	624 $\pm$ 167	737 $\pm$ 128	697 $\pm$ 121	694 $\pm$ 108	678 $\pm$ 222	599 $\pm$ 118
C <sub>brain</sub> (ng/g)	3.12 $\pm$ 1.00	28.16 $\pm$ 8.02***	556 $\pm$ 70	768 $\pm$ 136	1518 $\pm$ 243***	2619 $\pm$ 561***
Brain-to-plasma ratio	0.60 $\pm$ 0.12	2.35 $\pm$ 0.43***	1.19 $\pm$ 0.26	1.47 $\pm$ 0.17	2.71 $\pm$ 0.24***	6.13 $\pm$ 0.93***
Fold increase brain-to-plasma ratio	-	3.9	-	1.2	2.3	5.2

<sup>a</sup> Data are presented as mean  $\pm$  SD (n=6), except for t<sub>max</sub> where the range is presented. AUC<sub>0-t</sub>, area under the plasma concentration-time curve from 0 to the last time point (t = 24 or 4 h); C<sub>max</sub>, maximum plasma concentration; t<sub>max</sub>, time point (h) of maximum plasma concentration; C<sub>brain</sub>, brain concentration. \*\*\*, P < 0.001 compared to wild-type mice

### Effect of *Abcb1* and *Abcg2* on the brain penetration of miliclib

For both experiments (24 and 4 h) tissues where ABCB1 and ABCG2 are highly expressed were collected at the terminal time point, including liver, small intestine, kidney and brain, as well as spleen. Thymus was collected only in the 4 h experiment. This was in order to determine whether the miliclib tissue distribution was affected by these efflux transporters.

At 24 h, the brain concentration was considerably (about 9-fold) increased in *Abcb1a/1b*<sup>-/-</sup>; *Abcg2*<sup>-/-</sup> compared to wild-type mice (Figure 3, Table 1,  $P < 0.001$ ). The brain-to-plasma ratio was calculated to ascertain whether this increase was due to the lack of the efflux transporters in the brain and not only due to the higher plasma concentration in *Abcb1a/1b*<sup>-/-</sup>; *Abcg2*<sup>-/-</sup> mice at 24 h. As shown in Figure 3B and Table 1, the brain-to-plasma ratio was also increased by 3.9-fold ( $P < 0.001$ ) in the absence of Abcb1 and Abcg2. For the other tissues, including liver, despite the (significant) increase in their miliclib concentration in *Abcb1a/1b*<sup>-/-</sup>; *Abcg2*<sup>-/-</sup> mice, the corresponding tissue-to plasma ratios were generally not significantly or meaningfully different from those in the wild-type mice (Figure 3E, F and Supplemental Figure 3).

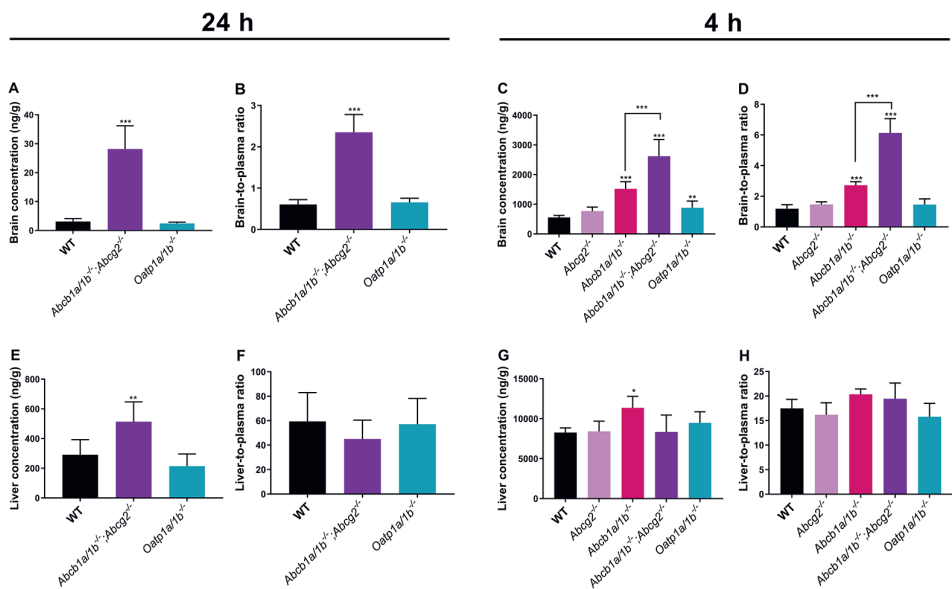


**Figure 3.** Brain (A, C) and liver (E, G) concentrations and tissue-to-plasma ratios (brain: B, D; liver F, H) of miliclib in wild-type (WT), *Abcb1a/1b*<sup>-/-</sup>; *Abcg2*<sup>-/-</sup>, *Oatp1a/1b*<sup>-/-</sup>, *Abcb1a/1b*<sup>-/-</sup> and *Abcg2*<sup>-/-</sup> female mice at 24 or 4 h after oral administration of 10 mg/kg miliclib. Data are presented as mean  $\pm$  SD (n = 6). \*,  $P < 0.05$ ; \*\*,  $P < 0.01$ ; \*\*\*,  $P < 0.001$  compared to wild-type mice.

We further investigated the individual and combined effects of Abcb1 and Abcg2 on limiting the brain penetration of miliclib. This experiment was terminated when the plasma concentration of miliclib was not much below the  $C_{\max}$  (i.e. 4 h after oral administration), in view of its higher relevance for overall tissue exposure. At 4h the brain-to-plasma ratio of miliclib was significantly increased by 2.3-fold in the *Abcb1a/1b*-deficient mice, compared to wild-type ( $P < 0.001$ ). In contrast, although a slight increase in the brain penetration was observed in the mice lacking Abcg2, this was not significantly different from wild-type mice. Interestingly, the brain-to-plasma

ratio in the *Abcb1a/1b*<sup>-/-</sup>;*Abcg2*<sup>-/-</sup> mice was 5.2-fold higher than in the wild-type mice ( $P < 0.001$ ). This value was also significantly higher than that in *Abcb1a/1b*<sup>-/-</sup> mice ( $P < 0.001$ ). Importantly, miliclib intrinsically exhibited good brain penetration even in the wild-type situation, where the mean drug concentration in the brain was 119% of the plasma concentration at 4 h and 60% at 24 h. These results suggest that *Abcb1* and *Abcg2* together limit the brain penetration of miliclib, but that even in their presence a considerable amount of the drug crosses the blood-brain barrier.

For the other tissues we tested, no significant changes were observed among the different mouse genotypes (Figures 3G, H and Supplemental Figure 3).

### Effect of *Oatp1a/1b* on miliclib plasma levels and tissue distribution

The possible effects of *Oatp1a/1b* proteins on miliclib pharmacokinetics were investigated in two different experiments with terminal time points at 24 and 4 h. As shown in Table 2 and Figure 2A, in the 24 h-experiment, the miliclib plasma concentration was slightly higher prior to the 8 h time point in the *Oatp1a/1b*-deficient mice, which resulted in a statistically significant minor increase in the plasma  $AUC_{0-24\text{ h}}$  and  $C_{\text{max}}$  (by 1.1- and 1.8-fold, respectively) compared to the wild-type situation ( $P < 0.05$ ). In the 4 h experiment, minor increases in miliclib plasma exposure were observed for the *Oatp1a/1b*<sup>-/-</sup> mice, but in this case they were not significantly different (Figure 2B, Table 2). In addition, no relevant or significant effects of *Oatp1a/1b* ablation were observed for the tissue distribution of miliclib including liver uptake, which is usually the most sensitive parameter to detect functional effects of *Oatp1a/1b* (Figure 3 and Supplemental Figure 3). In summary, our results suggest that *Oatp1a/1b* proteins have at best a minor effect (if any) on miliclib plasma exposure and tissue distribution.

### Metabolism of miliclib by CYP3A

The effect of possible CYP3A-mediated metabolism on miliclib pharmacokinetics was also investigated using *in vivo* mouse models. First, a pilot experiment over 24 h was performed in wild-type and *Cyp3a*<sup>-/-</sup> mice. Plasma exposure of miliclib was significantly higher in *Cyp3a*-deficient mice, especially before 8 h, where the  $AUC_{0-24\text{ h}}$  and the  $C_{\text{max}}$  increased by 1.2- ( $P < 0.001$ ) and 1.8-fold ( $P < 0.01$ ), respectively (Table 3, Figure 4A, Supplemental Figure 4). Based on these results, a second experiment was performed, in which miliclib pharmacokinetics was also investigated in *Cyp3aXAV* mice (a transgenic strain with expression of the human CYP3A4 in liver and small intestine in a *Cyp3a*<sup>-/-</sup> background), as well as in wild-type and *Cyp3a*<sup>-/-</sup> mice. This study was terminated at 8 h (Figure 4B). Again, in the absence of *Cyp3a*, the  $AUC_{0-8\text{ h}}$  and the  $C_{\text{max}}$  significantly increased by 1.9- and 1.8-fold, respectively (Table 3, Figure 4B, both  $P < 0.001$ ). The expression of human CYP3A4 in mice significantly decreased the plasma exposure of miliclib by 1.3-fold compared to *Cyp3a*-deficient mice ( $P < 0.01$ ), but not back to the level seen in wild-type mice (Figure 4B, Table 3). The data suggest that miliclib plasma levels are modestly restricted by mouse *Cyp3a*-mediated metabolism, and only slightly by human CYP3A4-mediated metabolism.



**Table 2.** Plasma pharmacokinetic parameters and brain penetration of miliclib in wild-type and *Oatp1a/1b*<sup>-/-</sup> female mice over 24 or 4 h after 10 mg/kg miliclib oral administration<sup>a</sup>

Parameter	Genotype			
	24 h		4 h	
	Wild-type	<i>Oatp1a/1b</i> <sup>-/-</sup>	Wild-type	<i>Oatp1a/1b</i> <sup>-/-</sup>
AUC <sub>0-t</sub> (h·ng/mL)	7094 ± 301	8116 ± 631**	2254 ± 346	2485 ± 341
Fold change AUC <sub>0-t</sub>	-	1.1	-	1.1
t <sub>max</sub> (h)	1-8	0.5-4	0.5-4	0.5-4
C <sub>max</sub> (ng/mL)	624 ± 167	1140 ± 225*	697 ± 121	734 ± 133
C <sub>brain</sub> (ng/g)	3.12 ± 1.00	2.44 ± 0.46	556 ± 70	883 ± 226**
Brain-to-plasma ratio	0.60 ± 0.12	0.66 ± 0.10	1.19 ± 0.26	1.46 ± 0.37
Fold increase brain-to-plasma ratio	-	1.1	-	1.2
C <sub>liver</sub> (ng/g)	291 ± 102	214 ± 82	8270 ± 578	9482 ± 1392
Liver-to-plasma ratio	59.4 ± 23.5	57.1 ± 21.1	17.5 ± 1.8	15.8 ± 2.7
Fold increase liver-to-plasma ratio	-	1.0	-	0.9

<sup>a</sup>Data are presented as mean ± SD (n=6), except for t<sub>max</sub> where the range is presented. AUC<sub>0-t</sub>, area under the plasma concentration-time curve from 0 to the last time point (t = 24 or 4 h); C<sub>max</sub>, maximum plasma concentration; t<sub>max</sub>, time point (h) of maximum plasma concentration; C<sub>brain</sub>, brain concentration. \*, P < 0.05; \*\*, P < 0.01 compared to wild-type mice.

In addition, the tissue exposure and penetration of miliclib were investigated in the above-mentioned mouse strains. No significant changes were observed in miliclib concentrations at 24 h, but minor increases in tissue concentrations were observed at 8 h, including brain, spleen, kidney, and thymus, when *Cyp3a* was knocked out. This is most likely a consequence of the higher plasma exposure in this mouse strain, as no relevant changes were observed in the tissue-to-plasma ratios either at 24 h or 8 h (Supplemental Figure 5).

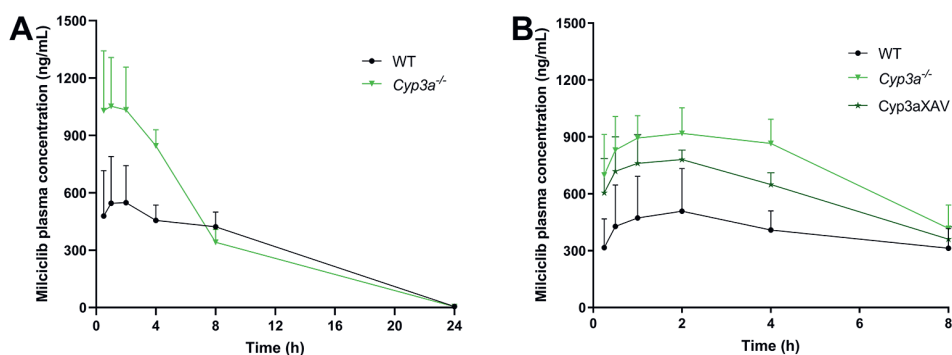
### Toxicity of miliclib in ABC transporter and *Cyp3a* knockout mice

Importantly, during the execution of the *in vivo* experiments, some discomfort was observed in several (but not all) knockout mice at approximately 3 h after oral administration of miliclib. This was revealed by the abnormal behavior of mice, characterized mainly by hunched position, squinted eyes, loss of activity and increased breathing rate. These adverse effects of miliclib were assessed as ranging from mild to moderate [37], with considerable interindividual variation, and eventually disappeared from 6 to 8 h after oral administration in all affected mice. The effects were more pronounced in *Abcb1a/1b*<sup>-/-</sup>; *Abcg2*<sup>-/-</sup> and *Cyp3a*<sup>-/-</sup> mice, although they were observed in all mouse strains, except for the wild-type and *Oatp1*-deficient mice. The side effects showed no simple relationship with miliclib plasma concentrations. For instance, the effects were evident in *Abcb1a/1b*; *Abcg2*<sup>-/-</sup> mice, in which the miliclib plasma concentrations were similar to those in wild-type mice (Figure 2A, B), which showed no adverse effects.

**Table 3.** Plasma pharmacokinetic parameters of miliclib in wild-type, *Cyp3a<sup>-/-</sup>*, and *Cyp3aXAV* female mice over 24 or 8 h after 10 mg/kg miliclib oral administration<sup>a</sup>

Parameter	Genotype				
	24 h		8 h		
	Wild-type	<i>Cyp3a<sup>-/-</sup></i>	Wild-type	<i>Cyp3a<sup>-/-</sup></i>	<i>Cyp3aXAV</i>
AUC <sub>0-t</sub> (h·ng/mL)	7094 ± 301	8842 ± 668***	3206 ± 711	5966 ± 518***	4638 ± 81***#
Fold change AUC <sub>0-t</sub>	-	1.2	-	1.9	1.4
t <sub>max</sub> (h)	1-8	0.5-4	0.5-8	0.5-4	1-2
C <sub>max</sub> (ng/mL)	624 ± 167	1140 ± 225**	558 ± 177	990 ± 109***	813 ± 103*
Fold change C <sub>max</sub>	-	1.8	-	1.8	1.5

<sup>a</sup>Data are presented as mean ± SD (n=6), except for t<sub>max</sub> where the range is presented. AUC<sub>0-t</sub>, area under the plasma concentration-time curve from 0 to the last time point (t = 24 or 8 h); C<sub>max</sub>, maximum plasma concentration; t<sub>max</sub>, time point (h) of maximum plasma concentration. \*, P < 0.05; \*\*, P < 0.01; \*\*\*, P < 0.001 compared to wild-type mice; #, P < 0.01 compared to *Cyp3a<sup>-/-</sup>*.

**Figure 4.** Plasma concentration-time curves of miliclib over 24 h (A) and 8 h (B) in wild-type (WT) and *Cyp3a<sup>-/-</sup>* and *Cyp3aXAV* female mice after oral administration of 10 mg/kg miliclib. Data are presented as mean ± SD (n = 6).

## Discussion

This study shows that *in vitro* miliclib was clearly transported by mAbcg2, and slightly or not noticeably by hABCb1 and hBCG2, respectively. *In vivo*, none of the efflux transporters significantly impacted the plasma exposure of miliclib. However, the relative brain penetration of miliclib was markedly increased (by at least 3.9-fold) when both *Abcb1* and *Abcg2* were ablated, revealing the importance of both transporters in limiting the miliclib penetration at the BBB. Our results further suggest that *Oatp1* could at best have a minor impact on miliclib plasma exposure. In addition, we found that miliclib plasma exposure is slightly limited by human CYP3A4, decreasing the miliclib AUC<sub>0-8h</sub> by 1.3-fold.

To the best of our knowledge, this is the first reported study that investigates the role of efflux and uptake transporters in miliciclib pharmacokinetics. Although both tested efflux transporters did not significantly impact the oral bioavailability of miliciclib, a slower elimination of the drug was observed beyond 8 h when both efflux transporters were knocked out. As a result, a significantly higher plasma concentration at the 24 h time point ( $P < 0.01$ ) was detected. It is likely that Abcb1 and Abcg2 could modestly contribute to the hepatic elimination of miliciclib, since around 70% of miliciclib, including both unchanged drug and metabolites, was excreted via feces in rats [23]. Hypothetically, the absence of both efflux transporters might result in increased intestinal (re)uptake and ultimately uptake of the drug into the blood, and possibly reduced hepatobiliary excretion.

The brain penetration of miliciclib considerably increased in the absence of both Abcb1 and Abcg2. Single Abcb1a/1b-deficient mice also showed an increase in miliciclib brain penetration, albeit to a lesser extent. In contrast, the miliciclib brain penetration of single *Abcg2*<sup>-/-</sup> mice did not significantly increase with respect to wild-type, possibly because Abcb1 takes over most of the function of Abcg2. These results show that Abcb1 and Abcg2 have a cooperative effect in limiting the miliciclib penetration into the brain, with Abcb1a/1b being more dominant than Abcg2. Similar results of the single and combined effects of Abcg2 and Abcb1 have been observed for other targeted anticancer agents, including the CDK4/6 inhibitor palbociclib, which is an analogous compound to miliciclib [38–40]. This apparent cooperative effect between Abcb1 and Abcg2 is most likely simply due to their separate and combined net efflux activity at the BBB, without the need to invoke any direct physical interaction between both transporters [41].

Overall, whereas our *in vitro* data showed that miliciclib is barely transported by the human ABCB1, the *in vivo* studies clearly demonstrated that miliciclib is a substrate of mouse Abcb1, thus limiting its brain penetration. This could perhaps be explained by interspecies differences, but also by the experimental model: while the *in vivo* studies reflect the effects at the BBB, the cell monolayer model is more comparable with the intestinal absorption process, in which also in the *in vivo* situation no significant impact of Abcb1 was observed on miliciclib plasma exposure [42]. This could relate to an effectively much higher miliciclib concentration in the intestinal lumen vs the blood concentration, saturating Abcb1-mediated transport in the enterocytes, but not in the BBB. The murine Abcg2 modestly transported miliciclib under *in vitro* circumstances, while in the *in vivo* situation a significant effect was detected in the BBB: it was shown to cooperate with Abcb1 in limiting the miliciclib brain penetration. Collectively, the combined *in vitro* and *in vivo* results suggest that miliciclib is a moderate transport substrate of ABCB1 and ABCG2, and both transporters limit its brain penetration, but its plasma exposure is not likely to be affected by them.

Compared to most anticancer drugs, miliciclib showed a good inherent brain penetration even in wild-type mice, where the miliciclib concentration was higher in brain than in plasma at 4 h. This is mostly in line with a previous report, with higher miliciclib

concentrations observed in rat brain than in plasma at 2, 6, and 24 h [8]. However, at 24 h our study showed a brain-to-plasma ratio of 0.7, which could be explained by an interspecies difference or by the analytical technique used for milciclib quantification: while our study measured specifically the unchanged drug, the referred study measured total radioactivity, which is unable to discriminate between the parental drug and its metabolites [8]. Compared to the currently approved CDK inhibitors, milciclib was able to penetrate the brain to a high extent, comparable to abemaciclib. In the wild-type situation and at time points close to the  $C_{max}$ , while ribociclib and palbociclib showed poor brain penetration (brain-to-plasma ratios  $\leq 0.25$ ), abemaciclib was reported to have a similar brain-to-plasma ratio to milciclib (1.2) [43,44].

The good brain penetration of milciclib might be beneficial for the treatment of brain cancers and, based on our results, this could potentially be even further enhanced by the coadministration of an ABCB1 and ABCG2 inhibitor (e.g. elacridar). Some studies have already demonstrated the potential use of milciclib to treat brain tumors, either as a single agent or in synergistic coadministration with temozolomide [8,45]. This is further supported by the identification of some mechanistic alterations involving CDK2 (the main target of milciclib) in glioblastoma and medulloblastoma [45,46]. In addition, thymic and hepatocellular carcinoma, types of cancer in which milciclib treatment is being investigated, can metastasize to the brain [47,48]. Although brain metastasis is quite rare with these types of cancer, when it occurs it has a very poor prognosis, so a drug that readily penetrates the brain could be beneficial in these patients. It is further important to consider that cancer cells themselves can overexpress ABCB1 and/or ABCG2, and thus become intrinsically resistant to milciclib treatment. Thus, in addition to enhancing the brain penetration, ABC transporter inhibitors could also be used to improve the antitumor effect of milciclib in such tumors.

Our study demonstrated that milciclib is eliminated by both mouse Cyp3a and human CYP3A4, and therefore the plasma exposure of milciclib is significantly affected by them, albeit to different extents. Milciclib was more efficiently eliminated by mouse Cyp3a compared to human CYP3A4, based on the changes in plasma  $AUC_{0-8h}$ . CYP3A4/Cyp3a effects were especially evident before 8 hours (Figure 4), suggesting that perhaps at later time points, at lower plasma levels, alternative clearance mechanisms with lower effective  $K_m$  might dominate the removal of milciclib. For instance, milciclib could be metabolized by another enzyme with higher affinity but lower  $V_{max}$ , resulting in a saturation of this alternative elimination mechanism when higher milciclib concentrations are present in plasma, and therefore, CYP3A4/Cyp3a will then make a comparatively more substantial contribution to milciclib elimination.

The minor contribution of human CYP3A4 to milciclib elimination is in line with previous reports, where *in vitro* incubations with human CYP3A4 supersomes showed a reduction of only 15% of the milciclib initial amount [1]. It has been suggested that milciclib metabolism involves more than one enzymatic pathway, with the formation of M1

(NMS-867734, N-oxidation of the N-methyl piperazine moiety) being the major route [10,23]. In this study, we estimated that the contribution of CYP3A4 to miliciclib elimination in mice is  $< 25\%$ . Based on this value, miliciclib clearance by CYP3A4 in humans may not be significantly affected by drug-drug interactions [24]. Thus, the small contribution of CYP3A4 to miliciclib clearance can be considered beneficial due to the low risk of miliciclib plasma exposure changes by either CYP3A4-modulating compounds or genetic polymorphisms. Direct scientific evidence to support the low risk of clinically relevant drug-drug interactions of miliciclib as a perpetrator drug is still lacking. However, it has been reported that miliciclib may not be a CYP3A inducer since it did not activate CYP3A gene transcription. Moreover, although it competitively inhibited CYP3A4, this occurred at concentrations higher than the reported  $C_{\max}$  ( $K_i \geq 2.4 \mu\text{M}$ ) [23]. Considering all this information, it is likely that miliciclib is not substantially affected by drug-drug interactions via ABCB1, ABCG2, OATP1 and CYP3A4. However, further studies in patients will be needed to determine the role of miliciclib as modulator (i.e. inducer or inhibitor) of these proteins to fully predict all clinically relevant drug-drug interactions involving miliciclib.

The mild, reversible miliciclib toxicity we observed especially in *Abcb1a/1b<sup>-/-</sup>;Abcg2<sup>-/-</sup>* and *Cyp3a<sup>-/-</sup>* mice is intriguing. Possibly it could relate to some toxicity in the central nervous system (CNS), as it was clearest in the *Abcb1a/1b<sup>-/-</sup>;Abcg2<sup>-/-</sup>* mice, and the observed phenotype would be compatible with CNS toxicity. Importantly, the observed effects could be related to some of the known adverse clinical effects of the drug in humans, namely tremors and ataxia, which were reversible upon drug discontinuation. Neurological effects have been observed in animals as well, including mainly tremors and increased reactivity to external stimuli. The mechanisms responsible for these effects have not been defined, but it has been suggested that the induction of these neurological effects may be influenced by miliciclib inhibiting the neurotrophin/TRKA axis [9]. The increased sensitivity of the *Cyp3a<sup>-/-</sup>* mice could be explained by the nearly twofold increased plasma  $C_{\max}$  (Table 3), which likely similarly increased the brain exposure to miliciclib. However that may be, our data suggest that possible mild toxicity of miliciclib may emerge at plasma and brain concentrations that are not much higher than the clinically relevant (therapeutic) exposure levels in humans, so this is likely a factor that will need to be considered in the clinical application of this drug.

## Conclusions

This study suggests that miliciclib is a weak to moderate transport substrate of ABCB1 and ABCG2, and that its plasma exposure is not likely to be affected by them. Still, ABCB1 and ABCG2 do cooperatively limit the brain penetration of miliciclib, despite it crossing the BBB to a good extent even in wild-type brain. Potentially, therefore, the brain exposure of miliciclib could be further enhanced by the coadministration of

efficacious ABCB1 and ABCG2 inhibitors, and the same might apply for milciclib accumulation in ABCB1- and/or ABCG2-overexpressing tumors. However, the mild, reversible toxicity observed in some knockout strains stipulates caution with measures that can increase brain or plasma concentrations of milciclib. OATP1 marginally (if at all) affects the plasma exposure of milciclib, and CYP3A4 slightly contributes to the milciclib elimination. All together, these results may be considered positive for the therapeutic application of milciclib, since a low risk of affecting its oral plasma exposure by drug-drug interactions via these transporters or CYP3A4 is predicted.

---

*Acknowledgements*

The authors acknowledge Lotte van Andel for the revision of the bioanalytical data generated in this study.

## References

- [1] M.G. Brasca, N. Amboldi, D. Ballinari, A. Cameron, E. Casale, G. Cervi, M. Colombo, F. Colotta, V. Croci, R. D'Alessio, F. Fiorentini, A. Isacchi, C. Mercurio, W. Moretti, A. Panzeri, W. Pastori, P. Pevarello, F. Quartieri, F. Roletto, G. Traquandi, P. Vianello, A. Vulpetti, M. Ciomei, Identification of N,1,4,4-tetramethyl-8-[[4-(4-methylpiperazin-1-yl)phenyl] amino]-4,5-dihydro-1H-pyrazolo[4,3-h]quinazoline-3-carboxamide (PHA-848125), a potent, orally available cyclin dependent kinase inhibitor, *J. Med. Chem.* 52 (2009) 5152–5163. <https://doi.org/10.1021/jm9006559>.
- [2] C. Albanese, R. Alzani, N. Amboldi, N. Avanzi, D. Ballinari, M.G. Brasca, C. Festuccia, F. Fiorentini, G. Locatelli, W. Pastori, V. Patton, F. Roletto, F. Colotta, A. Galvani, A. Isacchi, J. Moll, E. Pesenti, C. Mercurio, M. Ciomei, Dual targeting of CDK and tropomyosin receptor kinase families by the oral inhibitor PHA-848125, an agent with broad-spectrum antitumor efficacy, *Mol. Cancer Ther.* 9 (2010) 2243–2254. <https://doi.org/10.1158/1535-7163.MCT-10-0190>.
- [3] C. Sánchez-Martínez, M.J. Lallena, S.G. Sanfeliciano, A. de Dios, Cyclin dependent kinase (CDK) inhibitors as anticancer drugs: Recent advances (2015–2019), *Bioorganic Med. Chem. Lett.* 29 (2019) 126637. <https://doi.org/10.1016/j.bmcl.2019.126637>.
- [4] I.E. Demir, E. Tieftrunk, S. Schorn, H. Friess, G.O. Ceyhan, Nerve growth factor & TrkA as novel therapeutic targets in cancer, *Biochim. Biophys. Acta - Rev. Cancer.* 1866 (2016) 37–50. <https://doi.org/10.1016/j.bbcan.2016.05.003>.
- [5] C. Ghezzi, A. Wong, B.Y. Chen, B. Ribalet, R. Damoiseaux, P.M. Clark, A high-throughput screen identifies that CDK7 activates glucose consumption in lung cancer cells, *Nat. Commun.* 10 (2019) 1–15. <https://doi.org/10.1038/s41467-019-13334-8>.
- [6] A. Jindal, A. Thadi, K. Shailubhai, Hepatocellular Carcinoma: Etiology and Current and Future Drugs, *J. Clin. Exp. Hepatol.* 9 (2019) 221–232. <https://doi.org/10.1016/j.jceh.2019.01.004>.
- [7] J. Liebl, S.B. Weitensteiner, G. Vereb, L. Takács, R. Fürst, A.M. Vollmar, S. Zahler, Cyclin-dependent kinase 5 regulates endothelial cell migration and angiogenesis, *J. Biol. Chem.* 285 (2010) 35932–35943. <https://doi.org/10.1074/jbc.M110.126177>.
- [8] C. Albanese, R. Alzani, N. Amboldi, A. Degrassi, C. Festuccia, F. Fiorentini, G.L. Gravina, C. Mercurio, W. Pastori, M.G. Brasca, E. Pesenti, A. Galvani, M. Ciomei, Anti-tumour efficacy on glioma models of PHA-848125, a multi-kinase inhibitor able to cross the blood-brain barrier, *Br. J. Pharmacol.* 169 (2013) 156–166. <https://doi.org/10.1111/bph.12112>.
- [9] G.J. Weiss, M. Hidalgo, M.J. Borad, D. Laheru, R. Tibes, R.K. Ramanathan, L. Blydorn, G. Jameson, A. Jimeno, J.D. Isaacs, A. Scaburri, M.A. Pacciarini, F. Fiorentini, M. Ciomei, D.D. Von Hoff, Phase I study of the safety, tolerability and pharmacokinetics of PHA-848125AC, a dual tropomyosin receptor kinase A and cyclin-dependent kinase inhibitor, in patients with advanced solid malignancies, *Invest. New Drugs.* 30 (2012) 2334–2343. <https://doi.org/10.1007/s10637-011-9774-6>.
- [10] S. Aspeslagh, K. Shailubhai, R. Bahleda, A. Gazzah, A. Varga, A. Hollebecque, C. Massard, A. Spreafico, M. Reni, J.C. Soria, Phase I dose-escalation study of miliclib in combination with gemcitabine in patients with refractory solid tumors, *Cancer Chemother. Pharmacol.* 79 (2017) 1257–1265. <https://doi.org/10.1007/s00280-017-3303-z>.
- [11] B. Besse, M.C. Garassino, A. Rajan, S. Novello, J. Mazieres, G.J. Weiss, M. Ciomei, M. Martignoni, A. Petroccione, C. Davite, G. Giaccone, A phase II study of miliclib (PHA-848125AC) in patients (pts) with thymic carcinoma (TC), *J. Clin. Oncol.* 32 (2014) 7526. [https://doi.org/10.1200/jco.2014.32.15\\_suppl.7526](https://doi.org/10.1200/jco.2014.32.15_suppl.7526).
- [12] B. Besse, M.C. Garassino, A. Rajan, S. Novello, J. Mazieres, G.J. Weiss, D.M. Kocs, J.M. Barnett, C. Davite, P. Crivori, G. Giaccone, Efficacy of miliclib (PHA-848125AC), a pan-cyclin d-dependent kinase inhibitor, in two phase II studies with thymic carcinoma (TC) and B3 thymoma (B3T) patients., *J. Clin. Oncol.* 36 (2018) 8519–8519. [https://doi.org/10.1200/jco.2018.36.15\\_suppl.8519](https://doi.org/10.1200/jco.2018.36.15_suppl.8519).

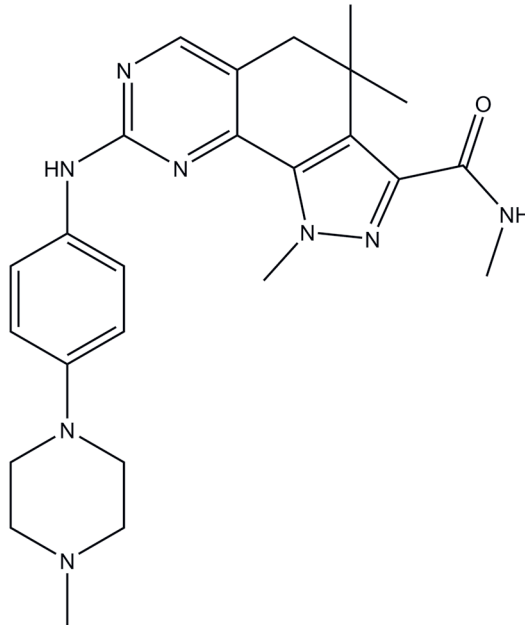
- [13] European Medicines Agency (EMA), Public summary of opinion on orphan designation: milciclib maleate for treatment of malignant thymoma, EMA/COMP/655696/2012. (2013) 1–4. [https://www.ema.europa.eu/en/documents/orphan-designation/eu/3/12/1059-public-summary-opinion-orphan-designation-milciclib-maleate-treatment-malignant-thymoma\\_en.pdf](https://www.ema.europa.eu/en/documents/orphan-designation/eu/3/12/1059-public-summary-opinion-orphan-designation-milciclib-maleate-treatment-malignant-thymoma_en.pdf) (accessed August 14, 2020).
- [14] Clinical Trials.gov: U.S. National Library of Medicine, Identifier NCT03109886, Study of milciclib in patients with unresectable/metastatic hepatocellular carcinoma, (2017). <https://clinicaltrials.gov/ct2/show/NCT03109886> (accessed August 14, 2020).
- [15] A.H. Schinkel, J.W. Jonker, Mammalian drug efflux transporters of the ATP binding cassette (ABC) family: An overview, *Adv. Drug Deliv. Rev.* 64 (2012) 138–153. <https://doi.org/10.1016/j.addr.2012.09.027>.
- [16] G. Szakács, A. Váradi, C. Özvegy-Laczka, B. Sarkadi, The role of ABC transporters in drug absorption, distribution, metabolism, excretion and toxicity (ADME-Tox), *Drug Discov. Today*. 13 (2008) 379–393. <https://doi.org/10.1016/j.drudis.2007.12.010>.
- [17] K.M. Giacomini, S.-M. Huang, D.J. Tweedie, L.Z. Benet, K.L.R. Brouwer, X. Chu, A. Dahlin, R. Evers, V. Fischer, K.M. Hillgren, K.A. Hoffmaster, T. Ishikawa, D. Keppler, R.B. Kim, C.A. Lee, M. Niemi, J.W. Polli, Y. Sugiyama, P.W. Swaan, J.A. Ware, S.H. Wright, S. Wah Yee, M.J. Zamek-Gliszczynski, L. Zhang, Membrane transporters in drug development, *Nat. Rev. Drug Discov.* 9 (2010) 215–236. <https://doi.org/10.1038/nrd3028>.
- [18] J.H. Lin, M. Yamazaki, Clinical Relevance of P-Glycoprotein in Drug Therapy, *Drug Metab. Rev.* 35 (2003) 417–454. <https://doi.org/10.1081/DMR-120026871>.
- [19] K. Natarajan, Y. Xie, M.R. Baer, D.D. Ross, Role of breast cancer resistance protein (BCRP/ABCG2) in cancer drug resistance, *Biochem. Pharmacol.* 83 (2012) 1084–1103. <https://doi.org/10.1016/j.bcp.2012.01.002>.
- [20] D. Kovacsics, I. Patik, C. Özvegy-Laczka, The role of organic anion transporting polypeptides in drug absorption, distribution, excretion and drug-drug interactions, *Expert Opin. Drug Metab. Toxicol.* 13 (2017) 409–424. <https://doi.org/10.1080/17425255.2017.1253679>.
- [21] D. Iusuf, E. Van De Steeg, A.H. Schinkel, Functions of OATP1A and 1B transporters in vivo: insights from mouse models, *Trends Pharmacol. Sci.* 33 (2012) 100–108. <https://doi.org/10.1016/j.tips.2011.10.005>.
- [22] B. Rochat, Role of Cytochrome P450 Activity in the Fate of Anticancer Agents and in Drug Resistance, *Clin. Pharmacokinet.* 44 (2005) 349–366. <https://doi.org/10.2165/00003088-200544040-00002>.
- [23] Tiziana Life Sciences, Phase II study of oral PHA-848125AC in patients with malignant thymoma previously treated with multiple lines of chemotherapy, (2017) 1–101. [https://clinicaltrials.gov/ProvidedDocs/91/NCT01301391/Prot\\_000.pdf](https://clinicaltrials.gov/ProvidedDocs/91/NCT01301391/Prot_000.pdf) (accessed August 2, 2020).
- [24] Food and Drug Administration. Center for Drug Evaluation and Research, Clinical Drug Interaction Studies — Cytochrome P450 Enzyme- and Transporter-Mediated Drug Interactions Guidance for Industry, FDA Guid. Doc. 1 (2020) 1–27. <https://www.fda.gov/media/134581/download> (accessed August 12, 2020).
- [25] E. Bakos, R. Evers, G. Szakacs, G.E. Tusnady, E. Welker, K. Szabo, M. de Haas, L. van Deemter, P. Borst, a Váradi, B. Sarkadi, Functional multidrug resistance protein (MRP1) lacking the N-terminal transmembrane domain, *J. Biol. Chem.* 273 (1998) 32167–32175. <https://doi.org/10.1074/jbc.273.48.32167>.
- [26] R. Evers, M. Kool, L. van Deemter, H. Janssen, J. Calafat, L.C. Oomen, C.C. Paulusma, R.P. Oude Elferink, F. Baas, A.H. Schinkel, P. Borst, Drug export activity of the human canalicular multispecific organic anion transporter in polarized kidney MDCK cells expressing cMOAT (MRP2) cDNA., *J. Clin. Invest.* 101 (1998) 1310–1319. <https://doi.org/10.1172/JCI928>.
- [27] B. Poller, E. Wagenaar, S.C. Tang, A.H. Schinkel, Double-transduced MDCKII cells to study human P-glycoprotein (ABCB1) and breast cancer resistance protein (ABCG2) interplay in drug transport across the blood-brain barrier, *Mol. Pharm.* 8 (2011) 571–582. <https://doi.org/10.1021/mp1003898>.
- [28] J.W. Jonker, Role of Breast Cancer Resistance Protein in the Bioavailability and Fetal Penetration of Topotecan, *J. Natl. Cancer Inst.* 92 (2000) 1651–1656. <https://doi.org/10.1093/jnci/92.20.1651>.



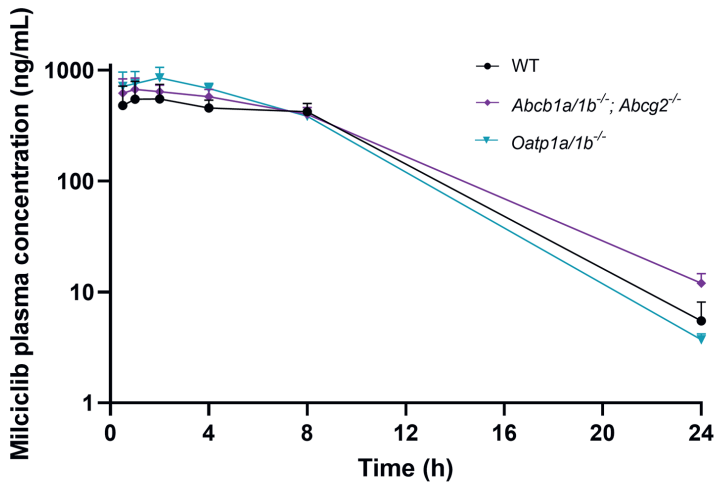
- [29] A.H. Schinkel, U. Mayer, E. Wagenaar, C.A.A.M. Mol, L. Van Deemter, J.J.M. Smit, M.A. Van Der Valk, A.C. Voordouw, H. Spits, O. Van Tellingen, M. Zijlman, W. Fibbe, P. Borst, Normal viability and altered pharmacokinetics in mice lacking *mdr1*-type (drug-transporting) P-glycoproteins, *Proc. Natl. Acad. Sci.* 94 (1997) 4028–4033. <https://doi.org/10.1073/pnas.94.8.4028>.
- [30] J.W. Jonker, M. Buitelaar, E. Wagenaar, M.A. van der Valk, G.L. Scheffer, R.J. Scheper, T. Plosch, F. Kuipers, R.P.J.O. Elferink, H. Rosing, J.H. Beijnen, A.H. Schinkel, The breast cancer resistance protein protects against a major chlorophyll-derived dietary phototoxin and protoporphyria, *Proc. Natl. Acad. Sci.* 99 (2002) 15649–15654. <https://doi.org/10.1073/pnas.202607599>.
- [31] J.W. Jonker, J. Freeman, E. Bolscher, S. Musters, A.J. Alvi, I. Titley, A.H. Schinkel, T.C. Dale, Contribution of the ABC Transporters *Bcrp1* and *Mdr1a/1b* to the Side Population Phenotype in Mammary Gland and Bone Marrow of Mice, *Stem Cells.* 23 (2005) 1059–1065. <https://doi.org/10.1634/stemcells.2005-0150>.
- [32] A.E. Van Herwaarden, E. Wagenaar, C.M.M. Van Der Kruijssen, R.A.B. Van Waterschoot, J.W. Smit, J. Song, M.A. Van Der Valk, O. Van Tellingen, J.W.A. Van Der Hoorn, H. Rosing, J.H. Beijnen, A.H. Schinkel, Knockout of cytochrome P450 3A yields new mouse models for understanding xenobiotic metabolism, *J. Clin. Invest.* 117 (2007) 3583–3592. <https://doi.org/10.1172/JCI33435>.
- [33] R.A.B. Van Waterschoot, J.S. Lagas, E. Wagenaar, C.M.M. Van Der Kruijssen, A.E. Van Herwaarden, J.Y. Song, R.W. Rooswinkel, O. Van Tellingen, H. Rosing, J.H. Beijnen, A.H. Schinkel, Absence of both cytochrome P450 3A and P-glycoprotein dramatically increases docetaxel oral bioavailability and risk of intestinal toxicity, *Cancer Res.* 69 (2009) 8996–9002. <https://doi.org/10.1158/0008-5472.CAN-09-2915>.
- [34] E. Van De Steeg, E. Wagenaar, C.M.M. Van Der Kruijssen, J.E.C. Burggraaff, D.R. De Waart, R.P.J. Oude Elferink, K.E. Kenworthy, A.H. Schinkel, Organic anion transporting polypeptide 1a/1b-knockout mice provide insights into hepatic handling of bilirubin, bile acids, and drugs, *J. Clin. Invest.* 120 (2010) 2942–2952. <https://doi.org/10.1172/JCI42168>.
- [35] A. Martínez-Chávez, M.M. Tibben, J. Broeders, H. Rosing, A.H. Schinkel, J.H. Beijnen, Development and validation of an LC-MS/MS method for the quantitative analysis of milliclib in human and mouse plasma, mouse tissue homogenates and tissue culture medium, *J. Pharm. Biomed. Anal.* 190 (2020) 113516. <https://doi.org/10.1016/j.jpba.2020.113516>.
- [36] Y. Zhang, M. Huo, J. Zhou, S. Xie, PKSolver: An add-in program for pharmacokinetic and pharmacodynamic data analysis in Microsoft Excel, *Comput. Methods Programs Biomed.* 99 (2010) 306–314. <https://doi.org/10.1016/j.cmpb.2010.01.007>.
- [37] T. Burkholder, C. Foltz, E. Karlsson, C.G. Linton, J.M. Smith, Health Evaluation of Experimental Laboratory Mice, *Curr. Protoc. Mouse Biol.* 2 (2012) 145–165. <https://doi.org/10.1002/9780470942390.mo110217>.
- [38] M. de Gooijer, P. Zhang, N. Thota, I. Mayayo-peralta, L. Buil, J.H. Beijnen, O. Van Tellingen, P-glycoprotein and breast cancer resistance protein restrict the brain penetration of the CDK4/6 inhibitor palbociclib, *Invest. New Drugs.* 33 (2015) 1012–1019. <https://doi.org/10.1007/s10637-015-0266-y>.
- [39] S. van Hoppe, R.W. Sparidans, E. Wagenaar, J.H. Beijnen, A.H. Schinkel, Breast cancer resistance protein (BCRP/ABCG2) and P-glycoprotein (P-gp/ABCB1) transport afatinib and restrict its oral availability and brain accumulation, *Pharmacol. Res.* 120 (2017) 43–50. <https://doi.org/10.1016/j.phrs.2017.01.035>.
- [40] W. Li, R.W. Sparidans, Y. Wang, M.C. Lebre, J.H. Beijnen, A.H. Schinkel, P-glycoprotein and breast cancer resistance protein restrict brigatinib brain accumulation and toxicity, and, alongside CYP3A, limit its oral availability, *Pharmacol. Res.* 137 (2018) 47–55. <https://doi.org/10.1016/j.phrs.2018.09.020>.
- [41] H. Kodaira, H. Kusuhara, J. Ushiki, E. Fuse, Y. Sugiyama, Kinetic analysis of the cooperation of P-glycoprotein (P-gp/Abcb1) and breast cancer resistance protein (Bcrp/Abcg2) in limiting the brain and testis penetration of erlotinib, flavopiridol, and mitoxantrone, *J. Pharmacol. Exp. Ther.* 333 (2010) 788–796. <https://doi.org/10.1124/jpet.109.162321>.
- [42] J.C. Kalvass, G.M. Pollack, Kinetic considerations for the quantitative assessment of efflux activity and inhibition: Implications for understanding and predicting the effects of efflux inhibition, *Pharm. Res.* 24 (2007) 265–276. <https://doi.org/10.1007/s11095-006-9135-x>.

- [43] T.J. Raub, G.N. Wishart, P. Kulanthaivel, B.A. Staton, R.T. Ajamie, G.A. Sawada, L.M. Gelbert, H.E. Shannon, C. Sanchez-Martinez, A. De Dios, Brain exposure of two selective dual CDK4 and CDK6 inhibitors and the antitumor activity of CDK4 and CDK6 inhibition in combination with temozolomide in an intracranial glioblastoma xenograft, *Drug Metab. Dispos.* 43 (2015) 1360–1371. <https://doi.org/10.1124/dmd.114.062745>.
- [44] A. Martínez-Chávez, S. van Hoppe, H. Rosing, M.C. Lebre, M. Tibben, J.H. Beijnen, A.H. Schinkel, P-glycoprotein Limits Ribociclib Brain Exposure and CYP3A4 Restricts Its Oral Bioavailability, *Mol. Pharm.* 16 (2019) 3842–3852. <https://doi.org/10.1021/acs.molpharmaceut.9b00475>.
- [45] S. Bolin, A. Borgenvik, C.U. Persson, A. Sundström, J. Qi, J.E. Bradner, W.A. Weiss, Y.J. Cho, H. Weishaupt, F.J. Swartling, Combined BET bromodomain and CDK2 inhibition in MYC-driven medulloblastoma, *Oncogene*. 37 (2018) 2850–2862. <https://doi.org/10.1038/s41388-018-0135-1>.
- [46] J. Wang, T. Yang, G. Xu, H. Liu, C. Ren, W. Xie, M. Wang, Cyclin-dependent kinase 2 promotes tumor proliferation and induces radio resistance in glioblastoma, *Transl. Oncol.* 9 (2016) 548–556. <https://doi.org/10.1016/j.tranon.2016.08.007>.
- [47] H. Gharwan, C. Kim, A. Thomas, A. Berman, S.A. Kim, N. Biassou, S.M. Steinberg, A. Rajan, Thymic epithelial tumors and metastasis to the brain: A case series and systematic review, *Transl. Lung Cancer Res.* 6 (2017) 588–599. <https://doi.org/10.21037/tlcr.2017.08.06>.
- [48] S. Wang, A. Wang, J. Lin, Y. Xie, L. Wu, H. Huang, J. Bian, X. Yang, X. Wan, H. Zhao, J. Huang, Brain metastases from hepatocellular carcinoma: Recent advances and future avenues, *Oncotarget*. 8 (2017) 25814–25829. <https://doi.org/10.18632/oncotarget.15730>.

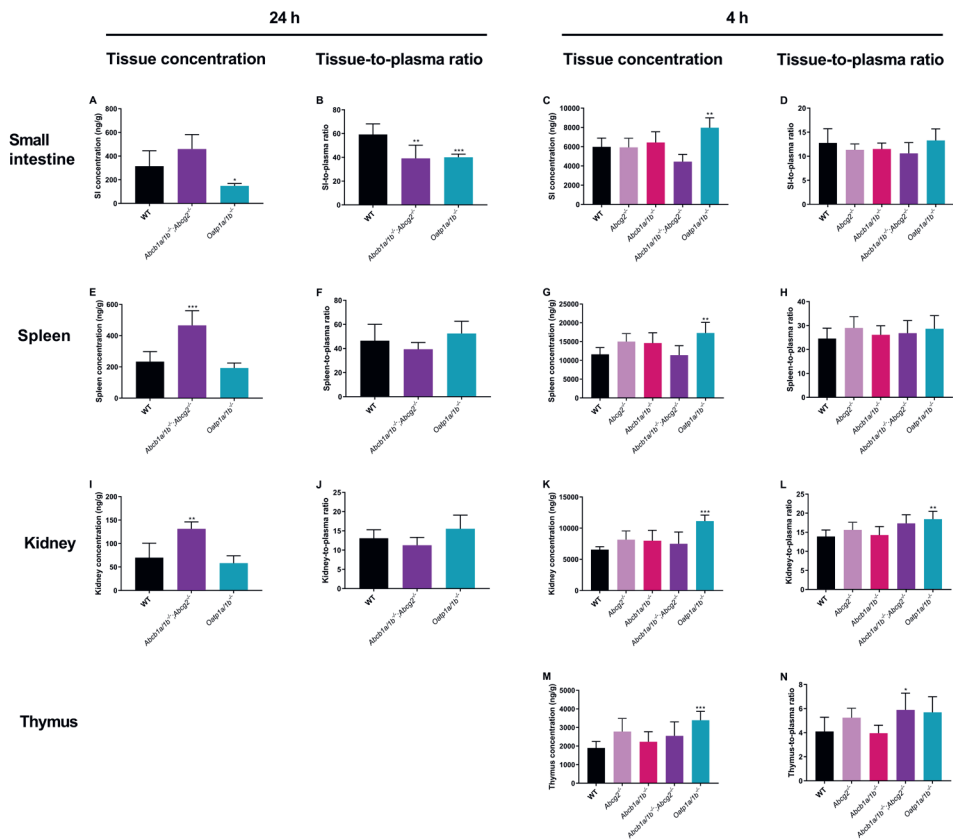
## Supplementary material



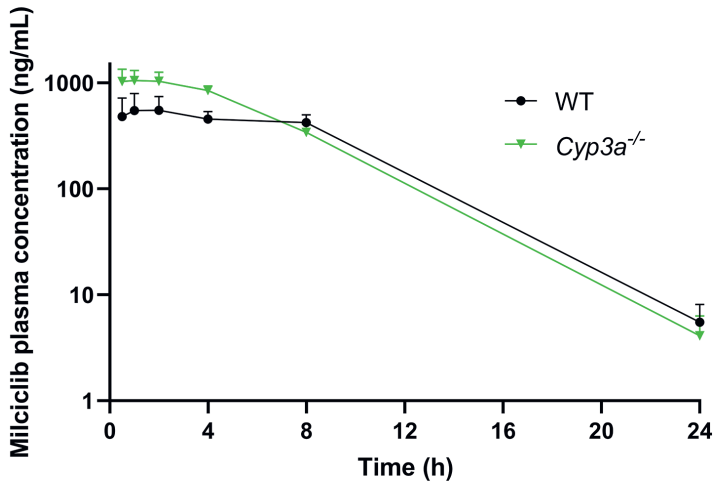
**Supplemental Figure 1.** Chemical structure of miliclib



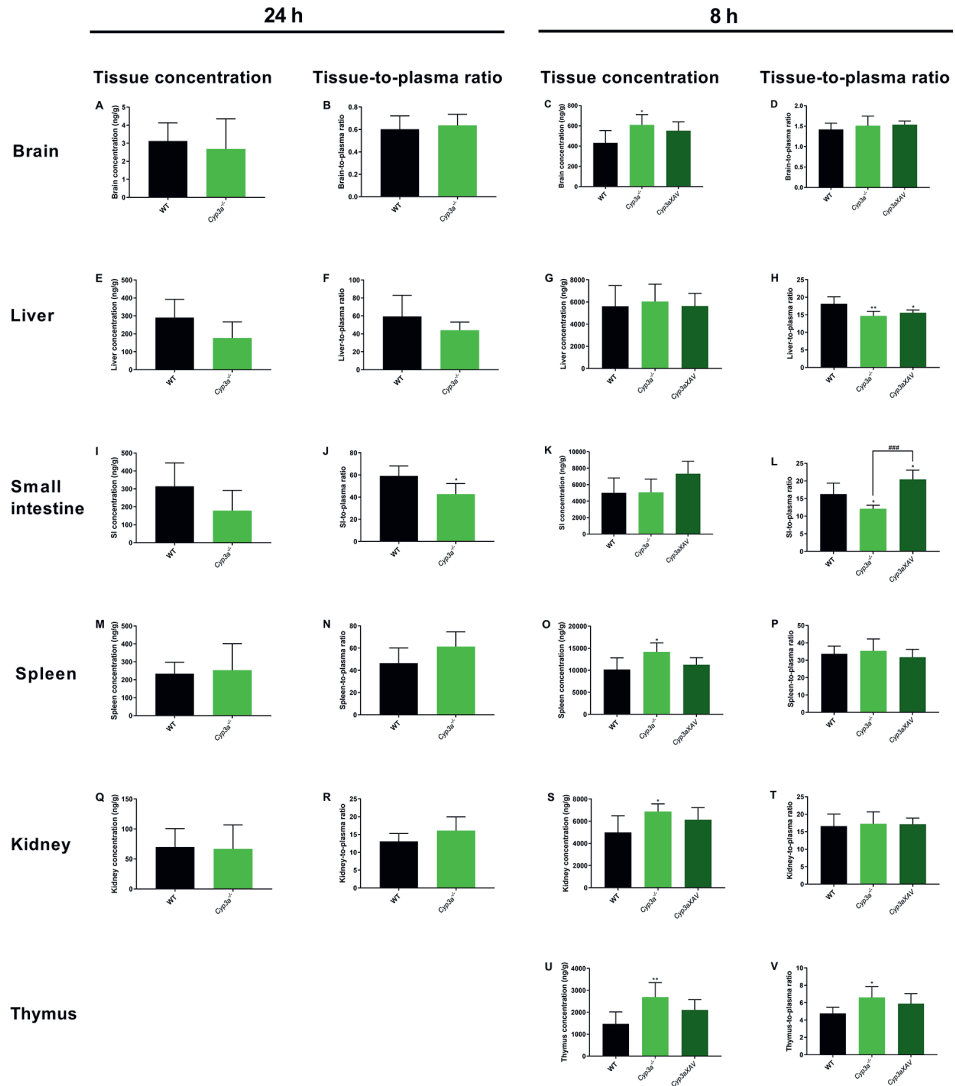
**Supplemental Figure 2.** Semi-log plasma concentration-time curves of miliclib over 24 h in wild-type, *Abcb1a/1b<sup>-/-</sup>; Abcg2<sup>-/-</sup>* and *Oatp1a/1b<sup>-/-</sup>* female mice after oral administration of 10 mg/kg miliclib. Data are presented as mean  $\pm$  SD (n = 6).



**Supplemental Figure 3.** Tissue concentrations (A, C, E, G, I, K, M) and tissue-to-plasma ratios (B, D, F, H, J, L, N) of milliclib in small intestine, spleen, kidney and thymus of wild-type (WT), *Abcb1a/1b*<sup>-/-</sup>; *Abcg2*<sup>-/-</sup>, *Oatp1a/1b*<sup>-/-</sup>, *Abcb1a/1b*<sup>-/-</sup> and *Abcg2*<sup>-/-</sup> female mice at 24 or 4 h after oral administration of 10 mg/kg milliclib. Data are presented as mean ± SD (n = 6). \*,  $P < 0.05$ ; \*\*,  $P < 0.01$ ; \*\*\*,  $P < 0.001$  compared to wild-type mice.



**Supplemental Figure 4.** Semi-log plasma concentration-time curves of miliclib over 24 h in wild-type and *Cyp3a*<sup>-/-</sup> female mice after oral administration of 10 mg/kg miliclib. Data are presented as mean  $\pm$  SD (n = 6).



**Supplemental Figure 5.** Tissue concentrations (A, C, E, G, I, K, M, O, Q, S, U) and tissue-to-plasma ratios (B, D, F, H, J, L, N, P, R, T, V) of milliclib in brain, liver, small intestine, spleen, kidney and thymus of wild-type (WT), *Cyp3a*<sup>-/-</sup> and *Cyp3aXAV* female mice at 24 or 8 h after oral administration of 10 mg/kg milliclib. Data are presented as mean ± SD (n = 6). \*, *P* < 0.05; \*\*, *P* < 0.01 compared to wild-type mice.







## **PART III**

Clinical pharmacokinetics and  
pharmacodynamics of the  
cyclin-dependent kinase inhibitors



# 8

## Clinical pharmacokinetics and pharmacodynamics of the cyclin-dependent kinase 4 and 6 inhibitors palbociclib, ribociclib and abemaciclib

Clinical Pharmacokinetics 2020, 59 (12): 1501-1520

Alejandra Martínez-Chávez\*  
Stefanie L. Groenland\*  
Marloes G.J. van Dongen  
Jos H. Beijnen  
Alfred H. Schinkel  
Alwin D.R. Huitema  
Neeltje Steeghs

\*These authors contributed equally

## Abstract

Palbociclib, ribociclib and abemaciclib are inhibitors of the cyclin-dependent kinases 4 and 6 which have been approved for the treatment of locally advanced or metastatic breast cancer. In this review, we provide an overview of the available clinical pharmacokinetic and pharmacodynamic characteristics of these novel drugs, summarize the results of food-effect and drug-drug interaction studies and highlight exposure-response and exposure-toxicity relationships. All three drugs exhibit a large interindividual variability in exposure (coefficient of variation ranging from 40 – 95% for minimum plasma concentration ( $C_{min}$ )), are extensively metabolized by cytochrome P450 3A4 and have their brain penetration limited by efflux transporters. Abemaciclib has three active metabolites with similar potency that are clinically relevant (i.e. M2, M20, M18), whereas the metabolites of palbociclib and ribociclib are not of clinical significance. Pharmacokinetic exposure increases in a dose-proportional manner for palbociclib, whereas exposure increases under- and over-proportionally with increasing dose for abemaciclib and ribociclib, respectively. High exposure is associated with an increased risk of neutropenia, and for ribociclib also to QTc prolongation. For abemaciclib, a clear exposure-efficacy relationship has been described, while for palbociclib and ribociclib exposure-response analyses remain inconclusive. Future studies are needed to address exposure-efficacy relationships to further improve dosing.

## Introduction

Cyclin-dependent kinase 4 and 6 (CDK4/6) inhibitors have emerged as important targeted therapies in the treatment of patients with advanced breast cancer. CDK4/6 inhibitors act on the cell cycle and prevent G1-to-S-phase progression. In order for cells to proceed past this G1-to-S-phase checkpoint, retinoblastoma protein (Rb) needs to be phosphorylated, which is effectuated by CDK4/6 [1]. Aberrations in this pathway are often involved in carcinogenesis, resulting in persistent cell proliferation [2]. Treatment with CDK4/6 inhibitors prevents phosphorylation of Rb and thereby causes a G1 cell cycle arrest, blocking cell division (Figure 1).

As of today, three CDK4/6 inhibitors are available in the clinic (i.e. palbociclib, ribociclib and abemaciclib), and many more are in (pre)clinical development (Table 1). Although all three CDK4/6 inhibitors are approved for treatment in combination with endocrine therapies (i.e. aromatase inhibitors or fulvestrant), only abemaciclib is registered to use as monotherapy. In general, the efficacy of CDK4/6 inhibitors is strikingly consistent between endocrine partners and clinical settings with respect to improved progression-free survival (PFS), and emerging evidence of overall survival (OS) benefit, but their toxicity differs. The aim of this review is to summarize the available clinical pharmacokinetic and pharmacodynamic data on the currently approved CDK4/6 inhibitors palbociclib, ribociclib and abemaciclib. In addition, we will focus on exposure-response relationships and the potential for pharmacokinetically guided dose individualization.

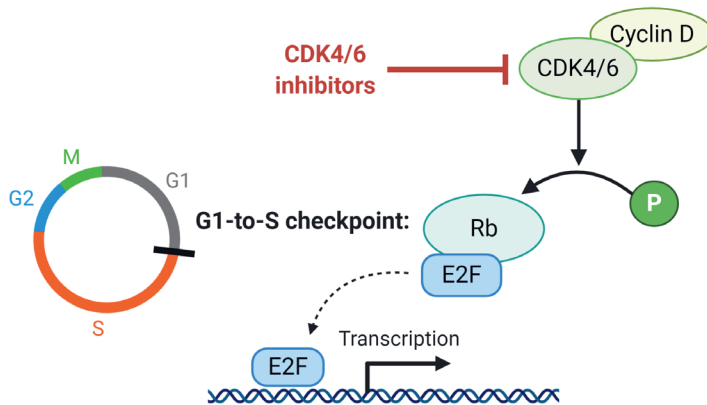


**Figure 1.** Mechanism of action of CDK4/6 inhibitors

For cells to progress from G1 to S phase in the cell cycle, Rb needs to get phosphorylated, which is catalyzed by the complex formed by CDK4/6 and cyclin D. Upon phosphorylation of Rb, the transcription factor E2F is released, ultimately resulting in cells proceeding to S phase. CDK4/6 inhibitors prevent Rb from getting phosphorylated and thereby block cell cycle progression. Created with BioRender.com.

CDK = cyclin-dependent kinases, P = phosphoryl ( $PO_3^-$ ), Rb = retinoblastoma

**Table 1.** Overview of CDK4/6 inhibitors that are approved for clinical use or in clinical development

CDK4/6 inhibitor	Indication	Dose	Year of approval
palbociclib (PD0332991)	BC (HR+ HER2-) <sup>a</sup>	125 mg QD 3/1	2015
ribociclib (LEE011)	BC (HR+ HER2-) <sup>b</sup>	600 mg QD 3/1	2017
abemaciclib (LY2835219)	BC (HR+ HER2-) <sup>b</sup>	150 mg BID 200 mg BID <sup>c</sup>	2018
trifluciclib (G1T28)	SCLC <sup>d</sup> TNBC <sup>e</sup>	240 mg/m <sup>2</sup> <sup>f</sup>	clinical development (phase II)
lerociclib (G1T38)	BC (HR+ HER2-) <sup>g</sup> NSCLC <sup>h</sup>	150 mg BID 200 mg BID <sup>i</sup>	clinical development (phase II)
SHR-6390	BC (HR+ HER2-) <sup>j</sup> BC (HER2+) GC (HER2+) <sup>k</sup>	150 mg QD	clinical development (phase II)
PF-06873600	BC (HR+ HER2-) <sup>b</sup> TNBC ovarian cancer	dose finding ongoing, starting dose not reported	clinical development (phase I/II)
FN-1501	advanced solid tumors	dose finding ongoing, starting at 2.5 mg QD	clinical development (phase I)
BPI-16350	advanced solid tumors	dose finding ongoing, 50 - 500 mg QD	clinical development (phase I)
FCN-437	advanced solid tumors	dose finding ongoing, starting dose not reported, QD 3/1	clinical development (phase I)

All compounds are administered orally, unless indicated otherwise

<sup>a</sup> in combination with an aromatase inhibitor or fulvestrant

<sup>b</sup> in combination with an aromatase inhibitor or fulvestrant, or as monotherapy

<sup>c</sup> 150 mg BID is the recommended dose for combination therapy, 200 mg BID for monotherapy

<sup>d</sup> in combination with topotecan; carboplatin and etoposide; or carboplatin, etoposide and atezolizumab

<sup>e</sup> in combination with gemcitabine and carboplatin

<sup>f</sup> administered intravenously

<sup>g</sup> in combination with fulvestrant

<sup>h</sup> in combination with osimertinib, in patients with EGFR-mutated tumors

<sup>i</sup> not decided yet which dose will be selected for phase III trial

<sup>j</sup> in combination with pyrotinib (EGFR/HER2/HER4 inhibitor)

<sup>k</sup> 3/1 = 3-weeks-on/1-week-off, BC = breast cancer, BID = twice daily, CDK = cyclin dependent kinase, EGFR = epithelial growth factor receptor, GC = gastric cancer, HER = human epithelial growth factor receptor 2, HR = hormone receptor, NSCLC = non-small-cell lung cancer, QD = once daily, SCLC = small cell lung cancer, TNBC = triple negative breast cancer

## Palbociclib

Palbociclib was the first CDK4/6 inhibitor to obtain approval by the Food and Drug Administration (FDA) and European Medicines Agency (EMA) in 2015. In the pivotal PALOMA-2 study, the addition of palbociclib to letrozole as first-line treatment for hormone receptor (HR) positive, human epidermal growth factor receptor 2 (HER2)-negative advanced breast cancer patients resulted in a median progression-free survival (mPFS) of 24.8 months compared with 14.5 months for letrozole alone (HR 0.58 (95% confidence interval (CI): 0.46 – 0.72),  $p < 0.001$ ) [3]. Similarly, the PALOMA-3 study demonstrated that palbociclib and fulvestrant were superior to fulvestrant alone in patients who progressed on  $\geq 1$  prior lines of treatment (mPFS 9.2 vs. 3.8 months, HR 0.42 (95% CI: 0.32 – 0.56),  $p < 0.001$ ) [4].

The approved dose of palbociclib is 125 mg once daily (QD) in a 3-weeks-on/1-week-off dosing schedule. This was also the maximum tolerated dose (MTD), with neutropenia being the only dose-limiting toxicity (DLT) [5].

### Physicochemical properties and formulation

Palbociclib is a synthetic 6-acetyl-8-cyclopentyl-5-methyl-2-(5-piperazin-1-yl-pyridin-2-ylamino)-8*H*-pyrido[2,3-*d*]pyrimidin-7-one, which belongs to the class of pyridopyrimidines (Figure 2) [7]. Palbociclib is a weak base with two  $pK_a$  values of 3.9 and 7.4, and a calculated log octanol-water partition coefficient (cLogP, which is an indicator of lipophilicity) of 2.7 [8,9]. Palbociclib is highly soluble at  $pH < 4$ , but its solubility rapidly decreases at higher  $pH$  [9]. For drugs to be classified as high solubility compounds, their highest approved dose needs to be soluble in  $\leq 250$  mL of aqueous media (i.e.  $\geq 0.5$  mg/mL for palbociclib) over the entire  $pH$  range of 1.0–6.8 [10]. Therefore, palbociclib is considered a low solubility compound. Together with its high permeability, palbociclib is classified as a class II compound, according to the Biopharmaceutics Classification System (BCS) [9]. Initially, palbociclib free base was formulated in capsules, but recently a bioequivalent tablet formulation was approved, containing the free base as well. [11].

*In vitro*, palbociclib bound reversibly to its targets and the half-maximal inhibitory concentrations ( $IC_{50}$ ) were 0.011 and 0.016  $\mu M$  for CDK4 and CDK6, respectively, corresponding to plasma concentrations of 33.5–48.7 ng/mL when corrected for protein binding [12].

### Drug transporters

*In vitro* assays demonstrated that palbociclib is a substrate of the efflux transporters P-glycoprotein (P-gp) and breast cancer resistance protein (BCRP) [13,14]. Although this only marginally affected the oral bioavailability in *in vivo* experiments with P-gp and/or BCRP knock-out mice, it has been demonstrated that the brain penetration was drastically restricted by these transporters [13].

In addition, *in vitro* and *in vivo* studies have shown that palbociclib inhibits the organic cation transporter 2 (OCT2) [15], which is involved in the renal tubular secretion of creatinine. Although this has not been studied in patients treated with palbociclib, inhibition of the OCT2 transporter has been associated with an increase in creatinine levels without affecting glomerular filtration [16].

### Clinical pharmacokinetics

Table 2 provides an overview of selected steady-state pharmacokinetic parameters of palbociclib. The bioavailability of palbociclib is low (46%) [9]. Palbociclib has a large volume of distribution of ~2800 L and the total plasma protein binding is 85.3%, with similar binding to albumin and  $\alpha$ 1-acid glycoprotein [5,9]. Metabolism mainly takes place by cytochrome P450 3A4 (CYP3A4) and sulfotransferase 2A1 (SULT2A1) and results in the formation of many metabolites, of which M22 (i.e. palbociclib glucuronide) is the most abundant (14.8%) and M17 (i.e. a lactam of palbociclib) is pharmacologically active with a similar potency as palbociclib, but accounting for less than 10% of total plasma exposure (Figure 2) [9]. Hepatic metabolism is the main route of elimination, as in the mass-balance study 74.1% of palbociclib was excreted in feces compared with 17.5% in urine, including both unchanged palbociclib and metabolites [9].

### Pharmacokinetics in special populations

#### *Pediatric cancer patients*

As of to date, palbociclib is not approved for the treatment of pediatric cancer and hence no pharmacokinetic data is available in this subgroup [17]. Several phase I-II studies in pediatric patients are currently ongoing [18–22].

#### *Patients with renal impairment*

In a clinical study, subjects with mild (estimated glomerular filtration rate (eGFR) 60–90 mL/min/1.73m<sup>2</sup>), moderate (eGFR 30–60 mL/min/1.73m<sup>2</sup>) and severe (eGFR < 30 mL/min/1.73m<sup>2</sup>) renal impairment showed an increase in palbociclib AUC<sub>0-∞</sub> of 39%, 42% and 31%, respectively, compared with patients with a normal renal function. Similarly, C<sub>max</sub> was 17%, 12% and 15% higher, respectively [23]. In a population pharmacokinetic analysis (n=183, of whom n=73 and n=29 with mild and moderate renal impairment, respectively), creatinine clearance did not significantly affect palbociclib exposure, which is consistent with renal clearance being a minor route of elimination [9]. No data are available for patients requiring hemodialysis, but based on the large fraction of palbociclib bound to plasma proteins (i.e. 85.3%), hemodialysis is expected to have limited effect on palbociclib exposure [9]. In conclusion, no dose adjustments are needed for patients with an eGFR ≥ 15 mL/min/1.73m<sup>2</sup> [23], but it should be kept in mind that exposure is 30–40% higher in patients with renal impairment.

#### *Patients with hepatic impairment*

Palbociclib unbound AUC<sub>0-∞</sub> was 17% lower in subjects with mild hepatic impairment (Child-Pugh class A) and 34% and 77% higher in patients with moderate (Child-Pugh



class B) and severe (Child-Pugh class C) hepatic impairment, respectively, compared with subjects with a normal hepatic function. Unbound  $C_{\max}$  was increased by 7%, 38% and 72%, respectively [23]. These findings are in line with the fact that hepatic clearance is the major route of elimination, and were also supported by population pharmacokinetic analyses [9]. Based on the above, no dose adjustments are needed for patients with mild or moderate hepatic impairment, while a dose reduction from 125 mg (standard dose) to 75 mg QD is recommended for patients with severe hepatic impairment [23]. It has to be noted that interpretation of palbociclib plasma concentrations in this subgroup could be complicated by the increasing fraction unbound with worsening hepatic function, because this might not be reflected in the total concentration, which is usually measured [23]. In addition, caution is warranted when using the Child Pugh score in patients with cancer, as this score has not been developed nor validated for this population [24].

### **Other factors influencing palbociclib pharmacokinetics**

The effect of other intrinsic factors on palbociclib exposure was investigated using a population pharmacokinetic model. Age and body weight were significant covariates on palbociclib clearance, which was higher in younger patients and in patients with a higher body weight (i.e. compared with a typical patient of 61 years and 73.7 kg, clearance was increased by 14.7% and decreased by 8.33% in a 45-year-old and a 97-year-old subject, respectively, while for body weight clearance was decreased by 13.2% at a weight of 55 kg and increased by 14.2% at a weight of 97 kg), although these small differences are not expected to be clinically relevant. Gender had no effect on palbociclib exposure [9].

In a subgroup analysis of the PALOMA-2 study, palbociclib exposure was higher in Japanese and other Asian patients compared to non-Asian patients (geometric mean  $C_{\min}$  95.4 ng/mL and 90.1 ng/mL vs. 61.7 ng/mL), whereas in a similar analysis of the PALOMA-3 study no difference was found [25,26]. In another study (n=25),  $AUC_{0-\infty}$  and  $C_{\max}$  were 30% and 35% higher, respectively, in Japanese subjects [27]. No dose adjustments are recommended based on ethnicity [9].

### **Food effect**

Food-effect studies of capsule and tablet formulations of palbociclib are summarized in Table 3. In a previous pooled analysis it has been demonstrated that palbociclib exposure is substantially lower in a subset of patients (i.e. 13%), possibly due to a decreased absorption caused by an elevated stomach pH. This subgroup is classified as low-liers, defined as  $C_{\max} < 21.4$  ng/mL [9]. In the food-effect study, when the patients who met the low-lier criteria were excluded, 90% CIs were within the bioequivalence margins, implying no food-effect in patients with adequate absorption [28].

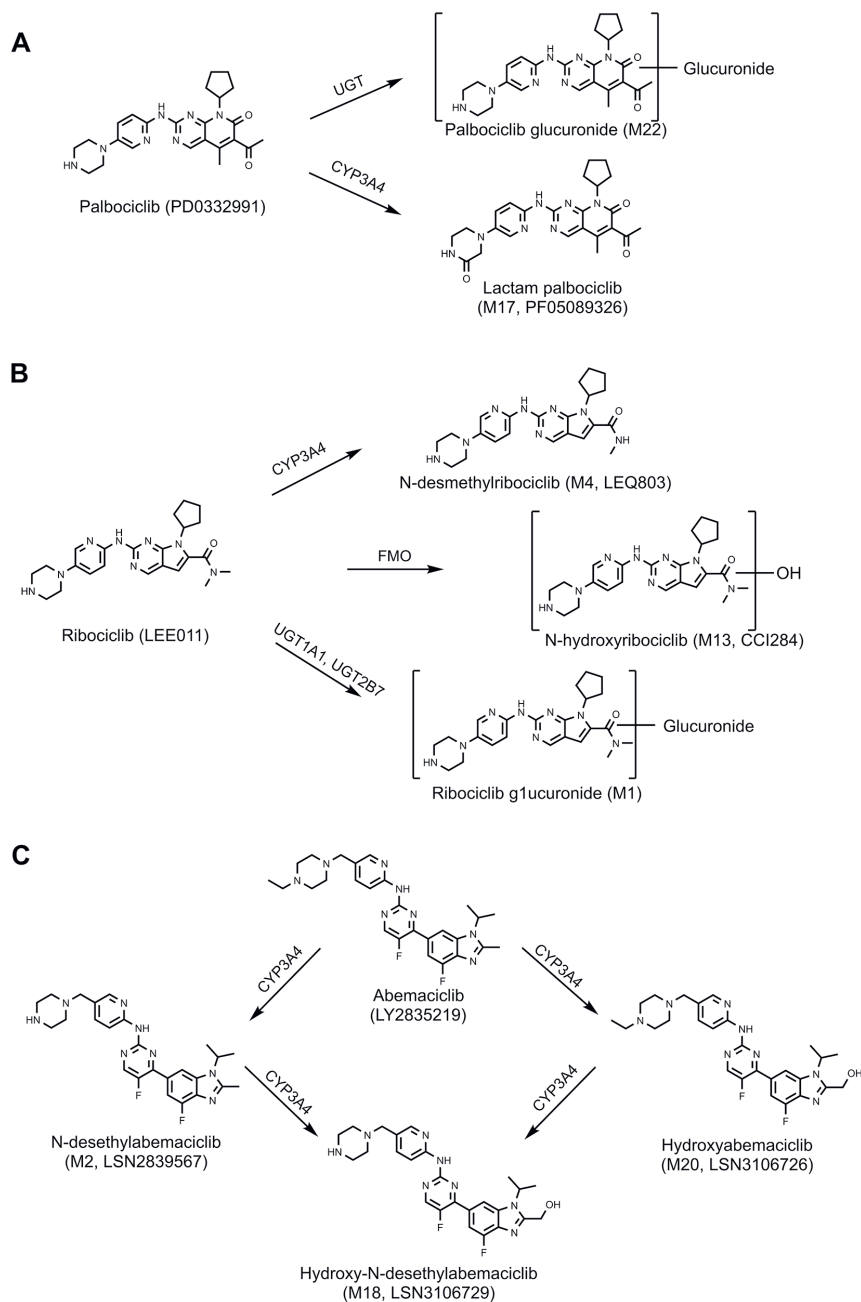


**Figure 2.** Chemical structures of CDK4/6 inhibitors palbociclib (A), ribociclib (B) and abemaciclib (C) and their main metabolites

Chemical structures and metabolism were obtained from FDA and EMA reviews [9,29,30].

UGT = Uridine 5'-diphospho-glucuronosyltransferase, CYP3A4 = cytochrome P450 3A4, FMO = Flavin-containing monooxygenase.

Concomitant intake with food resulted in a reduced interindividual variability, because the small subset of low-liers now leveled up to the exposure of the rest of the population, supporting the recommended ingestion of palbociclib capsules together with a meal [28].

While palbociclib capsules need to be administered with food, the recently approved tablet formulation can be taken with or without food, offering more flexibility to patients. Palbociclib exposure was not significantly altered due to food intake using the tablet formulation, showing to be more robust to pH differences [11].

$AUC_{0-t}$  = area under the plasma-concentration time curve until next dose,  $C_{max}$  = maximum plasma concentration,  $C_{min}$  = minimum plasma concentration, CV = coefficient of variation, NA = not applicable, NR = not reported, SD = standard deviation,  $t_{1/2}$  = terminal elimination half-life,  $t_{max}$  = time to maximum concentration

**Table 2.** Selected steady-state pharmacokinetic parameters of CDK4/6 inhibitors palbociclib, ribociclib and abemaciclib

CDK4/6 inhibitor	Study	N	C <sub>min</sub> (ng/mL)	C <sub>max</sub> (ng/mL)	AUC <sub>0-τ</sub> (ng/mL*h)	t <sub>max</sub> (h)	t <sub>1/2</sub> (h)
Palbociclib	Flaherty <i>et al</i> [5]	13	NR	86 (34%)	NR	4 (1 - 10)	NR
	Flaherty <i>et al</i> [5]	4	47.0 <sup>a</sup> (48%)	97.4 <sup>a</sup> (41%)	1,733 <sup>a</sup> (42%)	5.5 (2.0 - 9.8)	25.9 (29%)
	Mukai <i>et al</i> <sup>c</sup> [25]	142	61.7 <sup>b</sup> (59%)	NR	NR	NR	NR
	Tamura <i>et al</i> [31]	6	88.5 (49%)	185.5 (27%)	2,838 (43%)	4.0 (4.0 - 6.0)	23.2 (33%)
	PALOMA-1, A5481003 [9]	12 (C <sub>min</sub> : 71)	60.8 <sup>b</sup> (42%)	116 <sup>b</sup> (28%)	1,982 <sup>b</sup> (29%)	7.9 (2.2 - 8.2)	28.8 (17%)
	PALOMA-3, A5481023 [27]	218	76.6 <sup>b</sup> (41%)	NR	NR	NR	NR
	Curigliano <i>et al</i> [32]	3	NR	3083 <sup>a</sup> (31%)	38,896 <sup>a,d</sup> (43%)	2 (2 - 2)	NR
Ribociclib	Samant <i>et al</i> [33]	13	NR	1620 <sup>b</sup> (53%)	21,100 <sup>b,d</sup> (57%)	NR	NR
	Samant <i>et al</i> [33]	48	NR	1870 <sup>b</sup> (60%)	23,700 <sup>b,d</sup> (61%)	NR	NR
	Samant <i>et al</i> [33]	36	711 <sup>b</sup> (73%)	NR	NR	NR	NR
	Doi <i>et al</i> <sup>e</sup> [34]	8	NR	3280 <sup>b</sup> (60%)	51,600 <sup>b</sup> (59%)	5.0 (4.0 - 7.6)	53.6 (45%)
	Infante <i>et al</i> [29,35] <sup>h</sup>	64	732 (80%)	2130 (59%) <sup>d</sup>	NR	NR (1 - 5)	32.6 <sup>a</sup>
Abemaciclib	Patnaik <i>et al</i> [36]	72 (150 mg) 52 (200 mg)	169 <sup>b</sup> (95%) 197 <sup>b</sup> (82%)	249 <sup>b</sup> (86%) 298 <sup>b</sup> (72%)	2,390 (90%) <sup>b,d</sup> 3,000 (69%) <sup>b,d</sup>	4 (0 - 10.2) 4 (0 - 10)	22.8 (8.9 - 60.8) <sup>f</sup> 21.3 (11.6 - 63.0) <sup>f</sup>
	Fujiwara <i>et al</i> [37]	2 (150 mg) 5 (200 mg)	1,176, 103 <sup>g</sup> 210 <sup>b</sup> (89%)	1381, 149 <sup>g</sup> 298 <sup>b</sup> (64%)	15,500, 1,460 <sup>g</sup> 3,072 <sup>b</sup> (73%)	4.0 (4.0 - 4.0) 4 (2.1 - 6.0)	21.9 (19.3-24.6) <sup>f</sup> 16.3 (14.2 - 22.6) <sup>f</sup>
	Kim <i>et al</i> [38]	2 (150 mg) 9 (200 mg)	NR	146, 183 <sup>g</sup> 483 <sup>b</sup> (41%)	1,060, 1,600 <sup>g</sup> 3,460 <sup>b</sup> (49%)	4.0 (0 - 7.9) 4.0 (0 - 9.7)	NR
	Kim <i>et al</i> [38]	4 (150 mg) 6 (200 mg)	NR	288 <sup>b</sup> (71%) 304 <sup>b</sup> (66%)	2,060 <sup>b</sup> (66%) 2,100 <sup>b</sup> (58%)	5.5 (4.0 - 8.0) 6.9 (0 - 7.9)	NR
	Kim <i>et al</i> [38]	5 (150 mg) 8 (200 mg)	NR	492 <sup>b</sup> (117%) 227 <sup>b</sup> (17%)	3,460 <sup>b</sup> (125%) 1,380 <sup>b</sup> (144%)	1.0 (0 - 8.0) 5.0 (0 - 8.0)	NR

Reported pharmacokinetic parameters were determined at steady-state, at the approved dose and in patients. Pharmacokinetic parameters are reported as median, unless indicated otherwise. Variability is reported as (CV%) or [90% confidence interval].

<sup>a</sup> arithmetic mean, <sup>b</sup> geometric mean, <sup>c</sup> in non-Asian patients, C<sub>min</sub> in Japanese patients (n=27) was 95.4 ng/mL (31.3%) and C<sub>min</sub> in other Asian patients (n=11) was 90.1 ng/mL (36.0%). <sup>d</sup> based on patient numbers < N. <sup>e</sup> in Japanese patients. <sup>f</sup> after a single dose. <sup>g</sup> individual values are reported if N < 3. <sup>h</sup> C<sub>min</sub> and C<sub>max</sub> values of study X2101 were reported in the FDA review, t<sub>max</sub> and t<sub>1/2</sub> in the paper of Infante *et al*.

## Drug-drug interactions

In Table 4, results of drug-drug interaction studies and recommendations for dose adjustments are shown. Overall, no (clinically relevant) interactions with fulvestrant, goserelin or aromatase inhibitors were found. In contrast, palbociclib exposure was significantly altered by strong CYP3A4 modulators.

No clinical studies have been executed for moderate CYP3A4 inhibitors, but simulations predicted that they would increase palbociclib  $C_{\max}$  and  $AUC_{0-\infty}$  by approximately 23% and 40%, respectively [44]. According to the label, no dose reduction is warranted although these results suggest that a dose reduction from 125 mg (standard dose) to 100 mg QD might be advised. To further substantiate this finding, we are currently performing a clinical study to investigate the effect of the moderate CYP3A4 inhibitor erythromycin on the pharmacokinetics of palbociclib [45]. In addition, relevant interactions between palbociclib and CYP3A4 substrates with a narrow therapeutic index could occur, since palbociclib can weakly inhibit CYP3A4 [46].

As the solubility of palbociclib is pH-dependent, it could be expected that acid-reducing agents would decrease its exposure. Although palbociclib exposure was substantially reduced when administered concomitantly with rabeprazole under fasted conditions, this effect was only modest under fed conditions (Table 4) [47]. Therefore, no dose adjustments are indicated when palbociclib capsules are co-administered with acid-reducing agents, as they have to be administered under fed conditions. Exposure of palbociclib tablets was not affected by acid-reducing agents [11].

## Pharmacokinetic-pharmacodynamic relationships

### *Exposure-response*

Initial exposure-response analyses based on data of the PALOMA-1 study were inconclusive due to limited data ( $n=81$ ). Although a trend for prolonged PFS was observed in patients with an average palbociclib concentration ( $C_{\text{avg}}$ ) above the median of 60 ng/mL (median PFS estimated from Kaplan Meier curves were 17 months vs. 24.5 months,  $p$ -value not reported), multivariable analyses yielded inconsistent results [9].

In the PALOMA-3 study, PFS was similar in patients with  $C_{\text{avg}}$  above and below the median of 78 ng/mL. It has to be noted, though, that exposure in this trial appeared to be higher than in PALOMA-1 (at the same dose, but with fulvestrant instead of aromatase inhibitors). Even in the group with low exposure, median  $C_{\text{avg}}$  was 63 ng/mL, which is higher than the cut-off value used in the PALOMA-1 study. Time-varying  $C_{\text{avg}}$  as a continuous variable was a significant predictor of PFS in univariable analysis, although this did not remain significant in multivariable analysis [27,48].

In the PALOMA-2 study, no exposure-response relationship has been identified [49,50]. As exposure-response analyses have thus far not resulted in a clear answer and optimal

data to perform them were not available, this needs to be further elucidated. Lower thresholds of  $C_{\min}$  may be related to efficacy. Preferably, these additional analyses should include palbociclib plasma concentrations measured at regular intervals throughout treatment and use median  $C_{\min}$  as a measure of exposure. Previously, it has been suggested that individual concentrations could be compared to the mean  $C_{\min}$  of 61 ng/mL of the PALOMA-1 study [51].

#### *Exposure-toxicity*

In phase I studies higher AUC values were related to a greater reduction in absolute neutrophil count and platelet levels, with a wide range in  $EC_{50}$  values (estimated plasma exposure resulting in 50% decrease from baseline) varying from 253–716 ng/mL\*h for neutropenia and 184–1370 ng/mL\*h for thrombocytopenia [5,6].

A semi-mechanistic pharmacokinetic-pharmacodynamic model has been developed to quantify the relationship between palbociclib exposure (i.e. plasma concentration) and neutropenia [52]. In this model, the maximum anti-proliferative effect on neutrophil precursor cells ( $E_{\max}$ ) was notably lower than for cytotoxic drugs (e.g. docetaxel and etoposide), and the reported  $EC_{50}$  value was 40.1 ng/mL.

Interestingly, patients with grade 3 or 4 neutropenia had a significantly longer PFS compared with patients with lower grade or no neutropenia ( $p=0.0046$ ). Multivariable analysis resulted in a hazard ratio of 0.502 (95% CI 0.26–0.98,  $p=0.046$ ). This could be explained by either the hypothesis that tumor cells in patients with neutropenia are more sensitive to palbociclib or an underlying higher exposure in these patients [9]. As higher drug exposure causes more neutropenia and more neutropenia is related to a prolonged PFS, this suggests that an exposure-response relationship exists.

#### **Population pharmacokinetic models**

In a population pharmacokinetic model palbociclib pharmacokinetics was best described by a two-compartment model with first-order absorption [9]. Two additional models have been developed to predict drug-drug interactions with CYP3A4 inhibitors and to quantify the exposure-response relationship for neutropenia [44,52].

**Table 3.** Overview of food-effect on the pharmacokinetics of CDK4/6 inhibitors palbociclib, ribociclib and abemaciclib

CDK4/6 inhibitor	Study	Food-effect	Results	Conclusion
Palbociclib	Ruiz-Garcia <i>et al</i> , n=28, capsules [28]	low fat vs. fasted	↑ AUC <sub>0-∞</sub> 12% <sup>a</sup> ↑ C <sub>max</sub> 28% <sup>a</sup>	Concomitant intake with food resulted in higher exposure, while variability was substantially lower. Therefore, palbociclib capsules should be administered concomitant with food.
		moderate fat vs. fasted	↑ AUC <sub>0-∞</sub> 12% <sup>a</sup> ↑ C <sub>max</sub> 24% <sup>a</sup>	
		high fat vs. fasted	↑ AUC <sub>0-∞</sub> 19% <sup>a</sup> ↑ C <sub>max</sub> 37% <sup>a</sup>	
A5481081, n=44, tablets [11]	moderate fat vs. fasted	↑ AUC <sub>0-∞</sub> 9% <sup>a</sup> ↑ C <sub>max</sub> 10% <sup>a</sup>	No relevant food-effect. Therefore, palbociclib tablets could be administered with or without food.	
	high fat vs. fasted	↑ AUC <sub>0-∞</sub> 22% <sup>a</sup> ↑ C <sub>max</sub> 26% <sup>a</sup>		
Ribociclib	Samant <i>et al</i> [33], n=24, tablets	high fat vs. fasted	↑ AUC <sub>0-∞</sub> 6% <sup>a</sup> ↓ C <sub>max</sub> 0.3% <sup>a</sup>	No relevant food-effect. Therefore, ribociclib can be administered with or without food.
Abemaciclib	CLEE011A211 [29], n=24, capsules	high fat vs. fasted	↓ AUC <sub>0-∞</sub> 0.6% ↑ C <sub>max</sub> 32%	No relevant food-effect. Therefore, ribociclib capsules can be administered with or without food.
		high fat vs. fasted	↑ AUC <sub>0-last</sub> 15% <sup>a</sup> ↑ C <sub>max</sub> 24% ↑ t <sub>max</sub> 2 h	
		standard meal vs. fasted	↑ AUC <sub>0-last</sub> 11% <sup>a</sup> ↑ C <sub>max</sub> 25%	
Turner <i>et al</i> [39,41], n=29, capsules	high fat diet vs. fasted	↑ AUC <sub>0-∞</sub> 26% <sup>a</sup> ↑ C <sub>max</sub> 37% <sup>a</sup>	No relevant food-effect. Therefore, abemaciclib capsules can be administered with or without food.	
	High fat vs. fasted	↑ AUC <sub>0-∞</sub> 13% <sup>a</sup> ↑ C <sub>max</sub> 30% <sup>a</sup>		

All reported studies were randomized crossover studies in healthy volunteers, in which a single dose of the CDK4/6 inhibitor was administered.

<sup>a</sup> Calculated based on AUC<sub>0-∞</sub> and C<sub>max</sub> values

AUC = area under the plasma-concentration time curve, C<sub>max</sub> = maximum plasma concentration, t<sub>max</sub> = time to maximum concentration



**Table 4.** Overview of drug-drug interactions of CDK4/6 inhibitors palbociclib, ribociclib and abemaciclib

CDK4/6 inhibitor	Study	Interacting compound	Results	Conclusion
Palbociclib	Hoffman <i>et al</i> [53], n=12	itraconazole (strong CYP3A4 inhibitor)	↑ AUC <sub>0-∞</sub> 87% ↑ C <sub>max</sub> 34%	clinically relevant interaction, concomitant use with strong CYP3A4 inhibitors should be avoided, otherwise a dose reduction to 75 mg QD is recommended
		rifampicin (strong CYP3A4 and SUL1 inducer)	↓ AUC <sub>0-∞</sub> 85% ↓ C <sub>max</sub> 70%	clinically relevant interaction, concomitant use with strong CYP3A4 inducers should be avoided
		modafinil (moderate CYP3A4 inducer)	↓ AUC <sub>0-∞</sub> 32% ↓ C <sub>max</sub> 11%	no clinically relevant interaction, could thus be used concomitantly with moderate CYP3A4 inducers
Palbociclib	Hoffman <i>et al</i> [46], n=26	midazolam (CYP3A4 substrate)	midazolam: ↑ AUC <sub>0-∞</sub> 61% ↑ C <sub>max</sub> 37%	palbociclib is a moderate CYP3A inhibitor, caution is recommended if administered concomitantly with sensitive CYP3A substrates with narrow therapeutic index
		letrozole on palbociclib	↓ AUC <sub>0-24h</sub> 2% <sup>a</sup> ↓ C <sub>max</sub> 6% <sup>a</sup>	no clinically relevant interaction
Palbociclib	PALOMA-1 [9], n=12, patients	palbociclib on letrozole	↓ AUC <sub>0-24h</sub> 10% <sup>a</sup> ↓ C <sub>max</sub> 9% <sup>a</sup>	
		fulvestrant on palbociclib <sup>b</sup>	↑ C <sub>min</sub> 29% <sup>a</sup>	no clinically relevant interaction
		palbociclib on fulvestrant <sup>c</sup>	↑ C <sub>min</sub> 22% <sup>a</sup>	
Palbociclib	PALOMA-3 [27], n=40, patients	goserelin on palbociclib <sup>d</sup>	↓ C <sub>min</sub> 7% <sup>a</sup>	
		palbociclib on goserelin	↑ C <sub>min</sub> 10% <sup>a</sup>	
		rabeprazole (fasting)	↓ AUC <sub>0-∞</sub> 62% <sup>a</sup> ↓ C <sub>max</sub> 80% <sup>a</sup>	no clinically relevant interaction under fed conditions, could thus be used concomitantly
Palbociclib	Sun <i>et al</i> [47], n=26 (fasting) and n=27 (fed), capsules	rabeprazole (fed)	↓ AUC <sub>0-∞</sub> 13% <sup>a</sup> ↓ C <sub>max</sub> 41% <sup>a</sup>	
		famotidine	↓ AUC <sub>0-∞</sub> 4% <sup>a</sup> ↓ C <sub>max</sub> 5% <sup>a</sup>	
		local antacid	↑ AUC <sub>0-∞</sub> 5-6% <sup>a</sup> ↓ C <sub>max</sub> 4% <sup>a</sup>	



Table 4. Continued

CDK4/6 inhibitor	Study	Interacting compound	Results	Conclusion
Palbociclib	A548T091 [11], n=44, tablets  Yu <i>et al</i> [44], PBPK simulations	rabeprazole	↑ AUC <sub>0-∞</sub> 6% <sup>a</sup> ↓ C <sub>max</sub> 3% <sup>a</sup>	no clinically relevant interaction, could thus be used concomitantly
		diltiazem (moderate CYP3A4 inhibitor)	↑ AUC <sub>0-t</sub> 42% ↑ C <sub>max</sub> 23%	no clinically relevant interactions, no dose adjustments needed
		verapamil (moderate CYP3A4 inhibitor)	↑ AUC <sub>0-t</sub> 38% ↑ C <sub>max</sub> 22%	
		fluoxetine (weak CYP3A4 inhibitor)	↑ AUC <sub>0-t</sub> 3%	
		flvoxamine (weak CYP3A4 inhibitor)	↑ AUC <sub>0-t</sub> 4%	
		efavirenz (moderate CYP3A4 inducer)	↓ AUC <sub>0-t</sub> 38% ↓ C <sub>max</sub> 32%	
Ribociclib	CLEE011A2101 [29,56], n=24	ritonavir (strong CYP3A4 inhibitor)	↑ AUC <sub>0-∞</sub> 220% ↑ C <sub>max</sub> 70%	clinically relevant interaction, concomitant use with strong CYP3A4 inhibitors should be avoided, otherwise a dose reduction to 400 mg QD is recommended
		rifampicin (strong CYP3A4 inducer)	↓ AUC <sub>0-∞</sub> 89% ↓ C <sub>max</sub> 81%	clinically relevant interaction, concomitant use with CYP3A4 inducers should be avoided
	CLEE011A2106 [29,56], n=25, 400 mg <sup>e</sup>	midazolam (CYP3A4 substrate)	midazolam: ↑ AUC 280% ↑ C <sub>max</sub> 110%	ribociclib is a moderate CYP3A4 inhibitor, caution is recommended if administered concomitantly with sensitive CYP3A4 substrates with narrow therapeutic index
		caffeine (CYP1A2 substrate)	caffeine: ↑ AUC 20% ↓ C <sub>max</sub> 10%	ribociclib is a weak CYP1A2 inhibitor, no dose adjustments are needed
	CLEE011E2301, n=15-18 CLEE011X2106, n=11 CLEE011X2101 <sup>b</sup> [29], n=64, patients	letrozole, anastrozole, exemestane	concentrations of monotherapy and combination therapy overlapped	no clinically relevant interaction



Table 4. Continued

CDK4/6 inhibitor	Study	Interacting compound	Results	Conclusion
Ribociclib	Samant <i>et al</i> [33], n=2-48	proton pump inhibitors	$\uparrow/\downarrow$ AUC <sub>0-t</sub> 9-23% <sup>a</sup> $\uparrow/\downarrow$ C <sub>max</sub> 10-23% <sup>a</sup> $\downarrow$ C <sub>min</sub> 17% <sup>a</sup>	no clinically relevant interaction, could thus be used concomitantly
	PBPK simulations [29]	erythromycin (moderate CYP3A4 inhibitor)	$\uparrow$ AUC <sub>0-t</sub> 93% $\uparrow$ C <sub>max</sub> 29%	clinically relevant interaction, no initial dose adjustment needed, but close monitoring for signs of toxicity
		ketoconazole (strong CYP3A4 inhibitor)	$\uparrow$ AUC <sub>0-t</sub> 209% $\uparrow$ C <sub>max</sub> 50%	clinically relevant interaction, concomitant use with strong CYP3A4 inhibitors should be avoided, otherwise a dose reduction to 400 mg QD is recommended
		flvoxamine (weak CYP3A4 inhibitor)	$\uparrow$ AUC <sub>0-t</sub> 2% $\uparrow$ C <sub>max</sub> 1%	no clinically relevant interaction
		carbamazepine (strong CYP3A4 inducer)	$\downarrow$ AUC <sub>0-t</sub> 52% $\downarrow$ C <sub>max</sub> 34%	clinically relevant interaction, concomitant use with CYP3A4 inducers should be avoided
		efavirenz (moderate CYP3A4 inducer)	$\downarrow$ AUC <sub>0-t</sub> 60% $\downarrow$ C <sub>max</sub> 37%	
Abemaciclib	NCT02117648 [57], n=26, patients	clarithromycin (strong CYP3A4 inhibitor)	$\uparrow$ AUC <sub>0-t</sub> 237%/119% <sup>§</sup> $\uparrow$ C <sub>max</sub> 30%/7% <sup>§</sup> $\uparrow$ t <sub>1/2</sub> 120%	clinically relevant interaction, concomitant use with strong CYP3A4 inhibitors should be avoided, otherwise a dose reduction to 100 mg BID is recommended
	NCT02256276 [40], n=24	rifampicin (strong CYP3A4 inducer)	$\downarrow$ AUC <sub>0-t</sub> 95%/77% <sup>§</sup> $\downarrow$ C <sub>max</sub> 92%/45% <sup>§</sup>	clinically relevant interaction, concomitant use with CYP3A4 inducers should be avoided
	Chappell <i>et al</i> [58], n=40	metformin (OCT2, MATE1 and MATE2-k substrate)	metformin: $\uparrow$ AUC <sub>0-t</sub> 37% $\uparrow$ C <sub>max</sub> 22%	abemaciclib inhibits the renal transport proteins OCT2, MATE1 and MATE2-k
	NCT02677844 [59], n=35	loperamide (P-gp substrate)	loperamide: $\uparrow$ AUC <sub>0-t</sub> 13% $\uparrow$ C <sub>max</sub> 35%	no clinically relevant interaction, concomitant use is possible

Table 4. Continued

CDK4/6 inhibitor	Study	Interacting compound	Results	Conclusion	
Abemaciclib	Posada <i>et al</i> [60], PBPK simulations	diltiazem (moderate CYP3A4 inhibitor)	↑ AUC <sub>0-∞</sub> 290%/137% <sup>h</sup> ↑ C <sub>max</sub> 90%	clinically relevant interaction, no initial dose adjustment needed, but close monitoring for signs of toxicity	
		verapamil (moderate CYP3A4 inhibitor)	↑ AUC <sub>0-∞</sub> 127%/62% <sup>h</sup> ↑ C <sub>max</sub> 63%		
		itraconazole (strong CYP3A4 inhibitor)	↑ AUC <sub>0-∞</sub> 611%/278% <sup>h</sup> ↑ C <sub>max</sub> 117%	clinically relevant interaction, concomitant use with strong CYP3A4 inhibitors should be avoided (especially ketoconazole), otherwise a dose reduction to 100 mg BID is recommended	
		ketoconazole (strong CYP3A4 inhibitor)	↑ AUC <sub>0-∞</sub> 1470%/615% <sup>h</sup> ↑ C <sub>max</sub> 146%		
		efavirenz (moderate CYP3A4 inducer)	↓ AUC <sub>0-∞</sub> 69%/52% <sup>h</sup> ↓ C <sub>max</sub> 51%		
		bosentan (moderate CYP3A4 inducer)	↓ AUC <sub>0-∞</sub> 68%/42% <sup>h</sup> ↓ C <sub>max</sub> 60%		
		modafinil (weak CYP3A4 inducer)	↓ AUC <sub>0-∞</sub> 46%/29% <sup>h</sup> ↓ C <sub>max</sub> 34%		

Reported studies were performed in healthy volunteers using a single dose of the CDK 4/6 inhibitor, unless indicated otherwise. <sup>a</sup> calculated based on AUC and C<sub>max</sub> values. <sup>b</sup> no intra-individual comparison, but interindividual comparison with historical data. <sup>c</sup> no intra-individual comparison, but interindividual comparison between treatment and placebo arm. <sup>d</sup> no intra-individual comparison, but interindividual comparison between pre- and postmenopausal patients. <sup>e</sup> simulations predicted that for 600 mg, midazolam C<sub>max</sub> and AUC would increase 140% and 420%, respectively. <sup>f</sup> no intra-individual comparison, but interindividual comparison between patients with and without a proton pump inhibitor. <sup>g</sup> abemaciclib/total active species. <sup>h</sup> abemaciclib/potency-adjusted unbound active species. AUC = area under the plasma-concentration time curve, BID = twice daily, C<sub>max</sub> = maximum plasma concentration, CYP = cytochrome P450, MATE = multidrug and toxin extrusion protein, OCT = organic cation transporter, PBPK = physiologically-based pharmacokinetic, QD = once daily, SULT = sulfoltransferase, t<sub>max</sub> = time to maximum concentration

## Ribociclib

In 2017, ribociclib has been approved by the FDA and EMA based on the results of a preplanned interim analysis of the MONALEESA-2 study [61]. In the second interim analysis of this randomized placebo-controlled phase III trial (n=668) comparing first-line treatment with letrozole with or without ribociclib, mPFS was significantly longer in the ribociclib group compared with the control group (25.3 vs. 16 months, HR 0.57 (95% CI: 0.46 – 0.70),  $p < 0.001$ ) [62]. In 2018, the indication was extended to combination treatment with fulvestrant, based on the MONALEESA-3 study. This study revealed that addition of ribociclib to the treatment of fulvestrant, improved mPFS from 12.8 to 20.5 months (HR 0.60 (95% CI: 0.48 – 0.73),  $p < 0.001$ ) and resulted in a prolonged median OS (40.0 months vs. not reached yet (HR 0.72 (95% CI: 0.57 – 0.92),  $p = 0.005$ ) [63,64].

The approved dose of ribociclib is 600 mg QD in a 3-weeks-on/1-week-off dosing schedule. In the phase I dose escalation study, doses ranging from 50–1200 mg QD were explored [35]. The MTD was established as 900 mg QD, with neutropenia and thrombocytopenia being the most common DLTs [35]. The lower dose level of 600 mg QD was selected for further development, as this resulted in a lower rate of QTc prolongation, and clinical activity was already observed at this dose level [35].

### Physicochemical properties and formulation

Ribociclib is a 7-cyclopentyl-*N,N*-dimethyl-2-[[5-(piperazin-1-yl)pyridine-2-yl]amino]-7*H*-pyrrolo[2,3-*d*]pyrimidine produced by chemical synthesis. It is formulated as a succinate salt in film-coated tablets containing 200 mg of ribociclib free base. Although initially a capsule formulation was used in clinical trials, the equivalence of both dosage forms was demonstrated in a bioequivalence study [65]. Ribociclib is a weak base with two  $pK_a$  values of 5.5 and 8.6, with its succinate salt exhibiting high solubility at  $pH \leq 4.5$  (solubility  $> 2.4$  mg/mL), but it decreases at higher pH. Thus, ribociclib succinate was classified as a low solubility compound [33,65]. The ribociclib Log P was reported to be 1.95, and its estimated effective human permeability ( $hP_{eff}$ ) was  $0.9 \times 10^{-4}$  cm/s. Based on these data, it was categorized in BCS class IV (low solubility, low permeability) [65,66].

*In vitro*,  $IC_{50}$  values for ribociclib were 8 and 39 nM for CDK4 and CDK6, respectively, corresponding to plasma concentrations of 11.6–56.5 ng/mL when corrected for protein binding [29].

### Drug transporters

*In vitro* and *in vivo* studies have demonstrated that ribociclib is a transport substrate of P-gp [67,68]. Interestingly, pharmacokinetic and tissue distribution studies in mouse models showed that this efflux transporter is responsible for limiting the ribociclib penetration into the brain, since the brain-to-plasma concentration ratio increased by at least 23-fold when the P-gp was knocked out or inhibited. Plasma pharmacokinetic

parameters were not significantly affected, except for  $AUC_{0-24h}$ , which increased 2.3-fold in mice lacking the P-gp and BCRP. This increase is likely due to P-gp activity, since ribociclib has not shown noticeable transport by BCRP [67].

Besides interacting as a substrate, ribociclib also inhibited P-gp [68]. Moreover, at clinically relevant concentrations it also inhibited BCRP, OCT2, multidrug and toxin extrusion protein (MATE) 1, and bile salt export pump (BSEP) [15,29,56,68]. In a retrospective study in patients treated with ribociclib, creatinine levels increased 37% compared to baseline, probably due to OCT2 inhibition [69].

### Clinical pharmacokinetics

Selected steady-state pharmacokinetic parameters of ribociclib are displayed in Table 2. Exposure of ribociclib increased over-proportionally with dose in the range of 50–1200 mg, possibly caused by a lower clearance at higher doses [34].

The absolute oral bioavailability has not been determined, but using a physiologically-based pharmacokinetic (PBPK) model it was predicted that 90% of the standard dose of ribociclib (600 mg) would be absorbed mainly in the small intestine [33]. Ribociclib has a moderate human protein binding ( $\pm 70\%$ ), and is equally distributed in plasma and red blood cells. The apparent volume of distribution was estimated at 1090 L, using a population pharmacokinetic analysis [29,56].

Ribociclib is metabolized primarily by CYP3A4 with the formation of the active metabolite M4 (Figure 2). It is also metabolized to a minor extent by flavin-containing monooxygenase (FMO) 3 and FMO1, the last being involved in the formation of the metabolite M13. These two metabolites may be reactive by forming covalent adducts in hepatocytes. M4, M13 and M1 (a secondary glucuronide of ribociclib) were the major circulating metabolites, accounting for, respectively, 8.6%, 9.4% and 7.8% of total radioactivity in a mass balance study. Considering these data, the contribution of the active metabolite M4 to the clinical activity was considered negligible [29,56,70].

Feces was the major route of excretion compared to urine, accounting for, respectively, 69.1% and 22.6% of the dose recovered, where ribociclib was the major entity found in excreta [29,56].

### Pharmacokinetics in special populations

#### *Pediatric cancer patients*

Ribociclib was the first CDK4/6 inhibitor studied in pediatric patients in a phase I clinical trial, where patients with neuroblastoma, rhabdoid tumors or solid tumors with alterations in the cyclin D-CDK4/6-INK4-Rb pathway were included. The MTD and recommended phase II dose (RP2D) were 470 and 350 mg/m<sup>2</sup>, respectively. The RP2D dose was selected based on overall safety and pharmacokinetic considerations, since the exposure at 350 mg/m<sup>2</sup> was equivalent to that observed at 600 mg in adults.

Pharmacokinetic parameters, including  $t_{\max}$ ,  $C_{\max}$ ,  $AUC_{0-\tau}$  and  $t_{1/2}$ , were similar in adults and pediatric patients [71].

#### *Patients with renal impairment*

The effect of renal impairment on the pharmacokinetics of ribociclib was assessed in a population pharmacokinetic analysis, which included patients with normal renal function (n=438), mild renal impairment (n=488) and moderate renal impairment (n=113). In this analysis, mild and moderate renal impairment had no effect on the exposure and clearance of ribociclib, therefore no dose adjustments are recommended for patients with mild or moderate renal impairment [29,56,70].

Furthermore, a clinical trial showed that for patients with severe renal impairment and end stage renal disease (eGFR<15 mL/min/1.73m<sup>2</sup>),  $AUC_{0-\infty}$  increased 281% and 137%, and  $C_{\max}$  168% and 110%, respectively, compared to subjects with normal renal function [72]. Based on these results, a starting dose of 200 mg daily is recommended by the FDA for patients with severe renal impairment, while the EMA recommends a starting dose of 400 mg in these cases [70,73].

#### *Patients with hepatic impairment*

In a clinical study (n=28), mild hepatic impairment had no effect on ribociclib exposure. In contrast, for moderate hepatic impairment,  $AUC_{0-\infty}$  and  $C_{\max}$  increased 28% and 44%, respectively, while for severe hepatic impairment they increased 29 and 32%. A population pharmacokinetic analysis (n=160 with normal hepatic function and n=47 with mild hepatic impairment) further supported that ribociclib exposure was unaffected by mild hepatic impairment. Based on these results, a reduction of the starting dose to 400 mg is recommended for patients with moderate or severe hepatic impairment [29,56].

#### **Other factors influencing ribociclib pharmacokinetics**

The effect of other intrinsic factors on ribociclib pharmacokinetics was evaluated by population pharmacokinetic analyses (n=208). Body weight and age were statistically significant covariates for ribociclib clearance. Based on simulations, it was predicted that a change of body weight from the reference value of 70 kg to 50 or 100 kg would change steady state  $C_{\max}$ ,  $C_{\min}$ , and  $AUC_{0-24h}$  of ribociclib up to 22%, which was considered a small effect relative to the inherent pharmacokinetic variability. Age was predicted to have only a mild effect on exposure. Race and gender were statistically insignificant parameters [29].

Furthermore, a cross-study comparison exhibited that, on average, the exposure of ribociclib in Japanese patients was higher than in Caucasian patients, but the individual values were within the same range. In summary, the effects of body weight, age, gender and race on ribociclib pharmacokinetics were considered not clinically relevant, and therefore, no dose adjustment is required [29][56].

### Food effect

Table 3 summarizes the food-effect studies that have been performed for the capsule and tablet formulation, of which the latter is more relevant since this is the marketed formulation. Since the geometric mean ratios were  $\approx 1$  for  $AUC_{0-\infty}$  and  $C_{max}$ , no effect of food intake was observed on the pharmacokinetics of ribociclib [33].

Additionally, the *in vitro* solubility of ribociclib was evaluated in biorelevant media, including simulated fed (pH 5.0) and fasted (pH 6.5) intestinal fluid, where the maximum dose (600 mg) was dissolved in 250 mL. This suggests that ribociclib absorption is unlikely to be affected by changes in the gastric pH due to food intake, among others. PBPK models also predicted that the exposure of ribociclib was independent of the gastric pH in the range of 1.0–8.0 [33]. Altogether, this information supports that ribociclib can be administered either with or without food [29,56,70].

### Drug-drug interactions

An overview of all drug-drug interaction studies is provided in Table 4. Ribociclib had no (clinically relevant) interactions with fulvestrant and the aromatase inhibitors [29,56,70,73]. Ribociclib is extensively metabolized via CYP3A4, therefore its pharmacokinetics is strongly affected by strong inhibitors or inducers of this enzyme. Ribociclib can reversibly inhibit CYP3A4 and CYP1A2 [68]. Altogether, it is recommended that drugs with narrow therapeutic index that are sensitive substrates of these drug-metabolizing enzymes or transporters which are inhibited by ribociclib (“Drug transporters” section) should be cautiously monitored in concomitant treatments with ribociclib [29,56].

Since ribociclib shows a pH-dependent solubility, drugs that alter the gastric pH could be expected to affect its exposure. However, ribociclib exposure was similar in patients with and without a proton pump inhibitor, and these drugs could thus be administered concomitantly [33].

### Pharmacokinetic-pharmacodynamic relationships

#### *Exposure-response*

Due to very limited data, exposure-response analyses for ribociclib remain inconclusive. In the MONALEESA-2 study only 44 out of 334 patients had progressive disease and available pharmacokinetic data. No indication for an exposure-efficacy relationship was found. Data on confirmed best response were available for 72 patients with pharmacokinetic data, and showed similar ribociclib exposure in responders vs. non-responders. No exposure-response analyses have been performed for the MONALEESA-3 study [29,74]. Future studies should establish exposure-efficacy relationships and identify an optimal threshold concentration.

### *Exposure-toxicity*

Although higher  $C_{\min}$  levels were related to a greater decrease in absolute neutrophil count and platelet count in the phase I study, ribociclib is dosed at the flat ends of these plateauing curves [35]. Pooled data from four clinical studies (n=196) were used to develop a logistic regression model for  $\geq$  grade 2 neutropenia. Although a trend was found for an increased risk of neutropenia at higher ribociclib exposure, this was not statistically significant. For each 100 ng/mL increase in  $C_{\min}$  the odds ratio for  $\geq$  grade 2 neutropenia was 1.05 (95%CI: 0.99–1.11, p=0.087) [29]. In addition, a pharmacokinetic-pharmacodynamic model for neutropenia using data of 1052 patients from six clinical trials showed that the relationship between exposure and neutropenia was not influenced by age, race, or the use of anastrozole, letrozole, tamoxifen or fulvestrant [74].

Furthermore, a relationship between ribociclib exposure and QTc prolongation has been established, which was described by a log-linear mixed effect model. Mean QTc prolongation was 22.87 ms at the mean steady-state  $C_{\max}$  of 2237 ng/mL. No exposure-toxicity relationship could be demonstrated for hepatotoxicity, due to the limited number of grade 3 or 4 events [29].

### **Population pharmacokinetic models**

A population pharmacokinetic model has been developed based on pooled data of 208 patients of whom 4731 pharmacokinetic samples were available. The model was validated using a dataset consisting of 175 pharmacokinetic samples from 93 patients in the MONALEESA-2 study. A two-compartment model with delayed zero-order absorption and linear clearance best fitted the data, with dose and body weight being significant covariates on clearance. Clearance decreased with increasing dose, which is in line with the observed more than dose-proportional increase in exposure [29].

### **Abemaciclib**

Abemaciclib was the third CDK4/6 inhibitor approved by the FDA and EMA in 2018. In the MONARCH-3 study, abemaciclib increased mPFS compared to placebo (14.7 months vs. not reached, HR 0.54 (95% CI: 0.41 – 0.72), p<0.001) in the first-line setting combined with anastrozole or letrozole [75]. In the same way, the MONARCH-2 study demonstrated that abemaciclib was superior to placebo in the second-line setting in combination with fulvestrant [76].

In contrast to palbociclib and ribociclib, abemaciclib is dosed twice daily (BID) and in a continuous dosing schedule. In the dose escalation part of the phase I study, doses up to 275 mg BID have been evaluated with 200 mg BID being identified as MTD [36]. This is the recommended dose for abemaciclib monotherapy, whereas 150 mg BID



is the recommended dose for combination therapy (i.e. with aromatase inhibitors or fulvestrant), because of better tolerability. Although fatigue was the most common DLT, gastro-intestinal and hematological toxicities were also frequently observed [36].

### Physiochemical properties and formulation

Abemaciclib is a synthetic *N*-(5-((4-ethylpiperazin-1-yl)methyl)pyrididin-2-yl)-5-fluoro-4-(4-fluoro-1-isopropyl-2-methyl-1*H*-benzo[*d*]imidazole-6-yl)pyrimidin-2-amine. It is formulated in tablets containing 50, 100, 150 or 200 mg of the free base. Since capsules were used in the pivotal MONARCH-1 and MONARCH-2 trials, bioequivalence between both formulations was tested and confirmed. Abemaciclib is a tribasic compound with  $pK_a$  values of 3.80, 4.48 and 7.95, and a log *P* of 3.36. It is soluble over the pH range of 1.0–6.8 (solubility > 0.8 mg/mL), and classified as a highly soluble drug. Considering that abemaciclib showed a moderate permeability (predicted  $hP_{eff} = 2.46 \times 10^{-4}$  cm/s), it was classified as a BCS class 3 (high solubility, low permeability) drug [60,77].

Abemaciclib is a potent, ATP-competitive, reversible inhibitor of CDK4 and CDK6, with  $IC_{50}$  values of 2 and 10 nM, respectively, corresponding to plasma concentrations of 27.4–136.9 ng/mL after correcting for protein binding [78]. Abemaciclib has three active metabolites with similar potency: *N*-desethylabemaciclib (M2), hydroxyabemaciclib (M20) and hydroxy-*N*-desethylabemaciclib (M18) (Figure 2). Their  $IC_{50}$  values (nM) for CDK4 and CDK6 are 1.2 and 1.3 for M2, 1.5 and 1.9 for M20 and 1.5 and 2.7 for M18 [79,80].

### Drug transporters

Abemaciclib is a substrate of efflux transporters P-gp and BCRP. *In vivo* studies showed that abemaciclib penetration through the blood-brain barrier improved in P-gp deficient mice [14]. The abemaciclib metabolite M2 is also a substrate of P-gp and BCRP, and its exposure increased significantly around 5.3-fold in P-gp/BCRP deficient mice with respect to the wild-type. Also, in this mouse model the brain penetration of both abemaciclib and M2 increased 25- and 4-fold, respectively, compared to the wild-type [81]. Additionally, abemaciclib itself inhibits P-gp and BCRP [57,82].

The renal transporters OCT2, MATE1 and MATE2-K are reversibly inhibited by abemaciclib and its active metabolites M2 and M20 at clinically relevant concentrations [57,58]. *In vitro* studies have shown that OCT2, MATE1 and MATE-K metformin transport is inhibited in the presence of abemaciclib, M2 or M20. The clinical implications of this interaction were also determined (Table 4) [58]. This reversible inhibition of renal transporters has been related to elevated creatinine levels, without renal function being affected [58].

### **Clinical pharmacokinetics**

Abemaciclib pharmacokinetics is summarized in Table 2, and is characterized by a high variability. It showed a relatively modest absolute oral bioavailability of 45% [36,37,39]. Abemaciclib and its active metabolites showed a high protein binding of 96.3% for abemaciclib, 93.4% for M2, 96.8% for M18 and 97.8% for M20. The mean volume of distribution is 750 L [57,83]. Abemaciclib is cleared mainly by hepatic metabolism, primarily by CYP3A4 with the formation of M2, M20 and M18 (Figure 2). The AUC of these metabolites represent 25%, 26% and 13%, respectively, of the total circulating entities in plasma [57]. In a mass balance study, abemaciclib was excreted as metabolites mainly in feces, with 81% of the administered dose recovered in feces, and ≈3% in urine [73, 74].

### **Pharmacokinetics in special populations**

#### *Pediatric Cancer Patients*

Information on abemaciclib pharmacokinetics in the pediatric population is not available hitherto [84]. Currently, two phase I studies are ongoing [70–71].

#### *Patients with renal impairment*

No dedicated study has evaluated the effect of renal impairment on the pharmacokinetics of abemaciclib. However, a population pharmacokinetic analysis, including patients with normal renal function (n=483), mild (n=381) and moderate (n=126) renal impairment, showed no significant differences in abemaciclib exposure. Therefore, no dose adjustment is required in patients with mild or moderate renal impairment. This was expected since the renal clearance of abemaciclib and its active metabolites is minor. The effect of severe renal impairment has not been determined yet [30,57,80,83].

#### *Patients with hepatic impairment*

In a clinical trial, the total exposure of abemaciclib plus M2, M20 and M18 was similar in participants with mild and moderate hepatic impairment, showing an increase of 20% and 10%, respectively, compared to participants with normal hepatic function. In contrast, severe hepatic impairment resulted in a 140% increase in exposure of abemaciclib active entities. Furthermore, the mean plasma half-life of abemaciclib was prolonged ( $t_{1/2}$ =55h vs. 24h in healthy subjects), absorption was slower ( $t_{max}$ =24h vs. 7h in healthy subjects) and protein binding decreased. Consequently, it is recommended to reduce the dose frequency to a once daily administration for patients with severe hepatic impairment (i.e. Child-Pugh class C) [30,57,80,83].

### **Other factors influencing abemaciclib pharmacokinetics**

The influence of intrinsic factors on the abemaciclib pharmacokinetics was evaluated in a population pharmacokinetic analysis (n=994), in which sex, age, race and body weight were found to be insignificant covariates for the abemaciclib exposure [83,87]. As a result, no special dose adjustments are required.

**Food effect**

An overview of food-effect studies for abemaciclib using a capsule or tablet formulation is provided in Table 3. The food-effect study with the tablet formulation is the most relevant since abemaciclib is marketed in this formulation. The exposure of abemaciclib increased with concomitant administration of a high-fat meal, but this was deemed not clinically relevant considering the high inter-subject variability and the fact that changes in exposure were within the abemaciclib therapeutic window [42,43]. Therefore, abemaciclib can be administered with or without food.

**Drug-drug interactions**

Drug-drug interaction studies for abemaciclib are summarized in Table 4. The potential pharmacokinetic interaction between abemaciclib and fulvestrant or aromatase inhibitors was not formally evaluated. However, historical comparisons indicated that these drugs had no clinically relevant effect on the pharmacokinetics of abemaciclib, or vice versa [30,57,83].

Due to the extensive metabolism of abemaciclib via CYP3A4, the exposure of abemaciclib plus its active metabolites M2, M20 and M18 is substantially affected when co-administered with strong CYP3A4 modulators.

Additionally, interactions with abemaciclib as a perpetrator could occur with substrates of transporters inhibited by abemaciclib (i.e. P-gp and renal transporters, Table 4).

**Pharmacokinetic-pharmacodynamic relationships***Exposure-response*

In a preclinical pharmacokinetic-pharmacodynamic model of xenograft tumors,  $C_{\min} \geq 200$  ng/mL has been identified as a potential efficacy threshold. Simulations with this model indicated that a maximum decrease in phosphorylated Rb levels was attained at a dose of 50 mg/kg, corresponding to a  $C_{\min}$  of 200 ng/mL. A limitation of this study is that concentrations of the active metabolites M2 and M20 were not taken into account [88].

In all three MONARCH-studies, exposure-response relationships were demonstrated. Although abemaciclib in the MONARCH-1 study (n=132) could not be linked to objective response rate (ORR) and PFS, simulations with a pharmacokinetic-pharmacodynamic model found a positive relationship between exposure and tumor shrinkage. Also, these simulations suggested that the ORR would be higher at an abemaciclib dose of 200 mg BID compared with 150 mg BID (31% vs. 25%, respectively) [80]. Using a similar approach, higher abemaciclib exposure was related to an increased tumor shrinkage in the MONARCH-2 study (n=477) as well, with the effect being most pronounced in the first months after start of treatment [80]. Finally, in the MONARCH-3 study (n=393) an exposure-response relationship was not only established for tumor size reduction, but also for PFS [79].

In summary, abemaciclib exposure was related to efficacy in several clinical trials. Therefore, it has been suggested that from an efficacy point of view, 200 mg BID would be a better starting dose than 150 mg BID. However, this higher starting dose is not deemed feasible, since 50% of patients needs a dose reduction due to toxicity. Based on the available data, no specific target for TDM can be proposed yet, but the optimal target might probably be somewhere between 169–197 ng/mL (i.e. the median exposure at 150 mg and 200 mg, respectively). Future exposure-response analyses need to identify the optimal threshold for efficacy, which could be performed using data from the MONARCH-studies or from a real-world patient cohort. Preferably, it should also be investigated whether it has additional value to include the concentrations of the active metabolites in this threshold, or that abemaciclib concentrations alone could serve as a proxy.

#### *Exposure-toxicity*

Higher abemaciclib concentrations were related to an increased incidence and severity of neutropenia. Dynamic pharmacokinetic-pharmacodynamic models for neutrophil count have been developed using data of the MONARCH-2 (n=593) and MONARCH-3 (n=477) studies. In these models, higher total  $C_{max}$  of abemaciclib and its active metabolites was related to a greater decrease in neutrophil production rate, and thus an increased risk of neutropenia [79,80].

#### **Population pharmacokinetic models**

In a population pharmacokinetic model based on data obtained from the phase I study (n=224), abemaciclib pharmacokinetics were best described by a linear one-compartment model with time- and dose-dependent bioavailability. Relative bioavailability decreased with an increasing dose, being 10% lower at a dose of 200 mg compared with 150 mg. This could be attributed to a saturable absorption, which is in line with preclinical data [88]. Plasma exposure of abemaciclib also decreased over time with steady-state concentrations being attained after 70 days [87,88].

#### **Discussion**

By providing an overview of the clinical pharmacokinetics and pharmacodynamics of the three licensed CDK4/6 inhibitors palbociclib, ribociclib and abemaciclib, it becomes apparent that they share several characteristics. Similarities include the high interindividual variability in exposure, the predominant metabolism by CYP3A4, the brain penetration being limited by efflux transporters and the exposure-toxicity relationship for neutropenia. On the other hand, there are also substantial differences. First, abemaciclib has a divergent dosing schedule, as it is dosed twice daily and continuously, instead of once daily and intermittently for palbociclib and ribociclib. Second, dose-proportionality of pharmacokinetics varies between compounds.

Palbociclib exposure increases linearly with increasing dose, whereas ribociclib exhibits a more than dose-proportional dose-exposure relationship, and abemaciclib exposure, in contrast, increases less than proportionally with increasing dose, due to the lower fraction absorbed at higher doses. Third, abemaciclib has active and significantly abundant metabolites that should be taken into account when assessing its exposure (i.e. M2, M20 and M18), while this is not the case for palbociclib and ribociclib. Fourth, a clear exposure-efficacy relationship has been described for abemaciclib, while for palbociclib and ribociclib exposure-response analyses remain inconclusive. This might be explained by the applied methodologies and sample sizes that were used in these exposure-response analyses. It is important to further elucidate exposure-response relationship for all three CDK4/6 inhibitors. And finally, ribociclib frequently prolongs the QTc interval, in an exposure-related manner, whereas this, to our current knowledge, has not been reported for palbociclib and abemaciclib. These particular characteristics may support in selecting the most appropriate CDK4/6 inhibitor for individual patients.

Interestingly, the incidence of neutropenia is much lower for abemaciclib than for palbociclib and ribociclib. This is possibly caused by the greater selectivity of abemaciclib for CDK4 compared with CDK6, its twice daily dosing schedule, or the conversion to metabolites with less hematologic toxicity [36,78]. In general, the effect of CDK4/6 inhibitors on neutrophil progenitor cells is cytostatic rather than cytotoxic, and associated with a notably low incidence of febrile neutropenia, in contrast to chemotherapy [52].

Many patients require dose reductions due to neutropenia, which can remain problematic even at the lowest doses according to the label (i.e. 75 mg QD for palbociclib, 200 mg QD for ribociclib and 50 mg BID for abemaciclib). If exposure in these patients is low, switching to an alternative treatment might be preferred, whereas in patients with adequate exposure prolonging the dose interval to every other day (QAD) for palbociclib and ribociclib, or QD for abemaciclib, could be an option, as has previously been described for pazopanib [89]. Alternatively, the time off-treatment could be prolonged (i.e. 2-weeks-on/2-weeks-off treatment, as was allowed in the PALOMA-3 study). From a pharmacological point of view, though, prolonging the dose interval would be more rational.

Although it is known that CDK4/6 inhibitors combined with endocrine therapy provide an effective treatment strategy, it is currently unclear whether CDK4/6 inhibitors can best be added to first- or second-line treatment. This paramount question is currently being addressed in the SONIA study, a nationwide study in The Netherlands that will randomize 1000 patients between first- and second-line treatment with a CDK4/6 inhibitor [90]. In an additional side study, pharmacokinetic samples are collected to further elucidate exposure-response relationships.

The currently approved CDK4/6 inhibitors are predominantly metabolized by CYP3A4. Therefore, increased exposure, and hence an increased risk of toxicity, can be expected in patients harboring mutations as in CYP3A4\*22, as a result of lower levels of functional CYP3A4 and thus a decreased clearance. The reported prevalence of these mutations is up to 10% [91], and it could be argued that this subset of patients may benefit from a lower starting dose. This is currently being investigated in the STAR22 study [92]. Although CDK4/6 inhibitors are currently only approved for the treatment of breast cancer, they are in clinical development for many other indications.

## **Conclusions**

CDK4/6 inhibitors are a new class of promising oral targeted therapies in oncology, with complex pharmacokinetic and pharmacodynamic profiles, which we summarized in this review. Future studies should focus on the further exploration of exposure-response relationships and the potential for pharmacokinetically guided dose individualization.

## References

- [1] J.W. Harbour, R.X. Luo, A. Dei Santi, A.A. Postigo, D.C. Dean, Cdk phosphorylation triggers sequential intramolecular interactions that progressively block Rb functions as cells move through G1, *Cell*. 98 (1999) 859–869. [https://doi.org/10.1016/S0092-8674\(00\)81519-6](https://doi.org/10.1016/S0092-8674(00)81519-6).
- [2] M. Hall, G. Peters, Genetic alterations of cyclins, cyclin-dependent kinases, and cdk inhibitors in human cancer, *Adv. Cancer Res.* 68 (1996) 67–108.
- [3] R.S. Finn, M. Martin, H.S. Rugo, S. Jones, S.-A. Im, K. Gelmon, N. Harbeck, O.N. Lipatov, J.M. Walshe, S. Moulder, E. Gauthier, D.R. Lu, S. Randolph, V. Diéras, D.J. Slamon, Palbociclib and letrozole in advanced breast cancer, *N. Engl. J. Med.* 375 (2016) 1925–1936. <https://doi.org/10.1056/NEJMoa1607303>.
- [4] N.C. Turner, J. Ro, F. André, S. Loi, S. Verma, H. Iwata, N. Harbeck, S. Loibl, C.H. Bartlett, K. Zhang, C. Giorgetti, S. Randolph, M. Koehler, M. Cristofanilli, Palbociclib in hormone-receptor-positive advanced breast cancer, *N. Engl. J. Med.* 373 (2015) 209–219. <https://doi.org/10.1056/NEJMoa1505270>.
- [5] K.T. Flaherty, P.M. LoRusso, A. DeMichele, V.G. Abramson, R. Courtney, S.S. Randolph, M.N. Shaik, K.D. Wilner, P.J. O'Dwyer, G.K. Schwartz, Phase I, dose-escalation trial of the oral cyclin-dependent kinase 4/6 inhibitor PD 0332991, administered using a 21-day schedule in patients with advanced cancer, *Clin. Cancer Res.* 18 (2012) 568–576. <https://doi.org/10.1158/1078-0432.CCR-11-0509>.
- [6] G.K. Schwartz, P.M. LoRusso, M.A. Dickson, S.S. Randolph, M.N. Shaik, K.D. Wilner, R. Courtney, P.J. O'Dwyer, Phase I study of PD 0332991, a cyclin-dependent kinase inhibitor, administered in 3-week cycles (Schedule 2/1), *Br J Cancer.* 104 (2011) 1862–1868. <https://doi.org/10.1038/bjc.2011.177>.
- [7] P.L. Toogood, P.J. Harvey, J.T. Repine, D.J. Sheehan, S.N. VanderWel, H. Zhou, P.R. Keller, D.J. McNamara, D. Sherry, T. Zhu, J. Brodfuehrer, C. Choi, M.R. Barvian, D.W. Fry, Discovery of a potent and selective inhibitor of cyclin-dependent kinase 4/6, *J. Med. Chem.* 48 (2005) 2388–2406. <https://doi.org/10.1021/jm049354h>.
- [8] P. Chen, N. V. Lee, W. Hu, M. Xu, R.A. Ferre, H. Lam, S. Bergqvist, J. Solowiej, W. Diehl, Y.Y.-A. He, X. Yu, A. Nagata, T. VanArsdale, B.W. Murray, Spectrum and degree of CDK drug interactions predicts clinical performance, *Mol. Cancer Ther.* 15 (2016) 2273–2281. <https://doi.org/10.1158/1535-7163.MCT-16-0300>.
- [9] US Food and Drug Administration. Center for Drug Evaluation and Research, Clinical pharmacology and biopharmaceutics review palbociclib, (2014). [https://www.accessdata.fda.gov/drugsatfda\\_docs/nda/2015/207103Orig1s000ClinPharmR.pdf](https://www.accessdata.fda.gov/drugsatfda_docs/nda/2015/207103Orig1s000ClinPharmR.pdf).
- [10] US Food and Drug Administration. Center for Drug Evaluation and Research., Waiver of in vivo bioavailability and bioequivalence studies for immediate-release solid oral dosage forms based on a biopharmaceutics classification system: guidance for industry, (2017). <https://www.fda.gov/media/70963/download>.
- [11] US Food and Drug Administration. Center for Drug Evaluation and Research., Clinical pharmacology review palbociclib, (2019). [https://www.accessdata.fda.gov/drugsatfda\\_docs/nda/2019/212436Orig1s000ClinPharmR.pdf](https://www.accessdata.fda.gov/drugsatfda_docs/nda/2019/212436Orig1s000ClinPharmR.pdf).
- [12] D.W. Fry, P.J. Harvey, P.R. Keller, W.L. Elliott, M.A. Meade, E. Trachet, M. Albassam, X.X. Zheng, W.R. Leopold, N.K. Pryer, P.L. Toogood, Specific inhibition of cyclin-dependent kinase 4/6 by PD 0332991 and associated antitumor activity in human tumor xenografts, *Mol. Cancer Ther.* 3 (2004) 1427–1437.
- [13] M. de Gooijer, P. Zhang, N. Thota, I. Mayayo-peralta, L. Buil, J.H. Beijnen, O. Van Tellingen, P-glycoprotein and breast cancer resistance protein restrict the brain penetration of the CDK4/6 inhibitor palbociclib, *Invest. New Drugs.* 33 (2015) 1012–1019. <https://doi.org/10.1007/s10637-015-0266-y>.
- [14] T.J. Raub, G.N. Wishart, P. Kulanthaivel, B.A. Staton, R.T. Ajamie, G.A. Sawada, L.M. Gelbert, H.E. Shannon, C. Sanchez-Martinez, A. De Dios, Brain exposure of two selective dual CDK4 and CDK6 inhibitors and the antitumor activity of CDK4 and CDK6 inhibition in combination with temozolomide in an

- intracranial glioblastoma xenograft, *Drug Metab. Dispos.* 43 (2015) 1360–1371. <https://doi.org/10.1124/dmd.114.062745>.
- [15] N. Pabla, A.A. Gibson, M. Buege, S.S. Ong, L. Li, S. Hu, G. Du, J.A. Sprowl, A. Vasilyeva, L.J. Janke, E. Schlatter, T. Chen, G. Ciarimboli, A. Sparreboom, Mitigation of acute kidney injury by cell-cycle inhibitors that suppress both CDK4/6 and OCT2 functions, *Proc. Natl. Acad. Sci. U. S. A.* 112 (2015) 5231–5236. <https://doi.org/10.1073/pnas.1424313112>.
- [16] X. Chu, K. Bleasby, G.H. Chan, I. Nunes, R. Evers, The complexities of interpreting reversible elevated serum creatinine levels in drug development: Does a correlation with inhibition of renal transporters exist?, *Drug Metab. Dispos.* 44 (2016) 1498–1509. <https://doi.org/10.1124/dmd.115.067694>.
- [17] J.M. Janssen, T.P.C. Dorlo, N. Steeghs, J.H. Beijnen, L.M. Hanff, N.K.A. van Eijkelenburg, J. van der Lugt, C.M. Zwaan, A.D.R. Huitema, Pharmacokinetic targets for therapeutic drug monitoring of small molecule kinase inhibitors in pediatric oncology, *Clin. Pharmacol. Ther.* 0 (2020) 1–12. <https://doi.org/10.1002/cpt.1808>.
- [18] ClinicalTrials.gov, Palbociclib isethionate in treating younger patients with recurrent, progressive, or refractory central nervous system tumors. <https://clinicaltrials.gov/ct2/show/NCT02255461>.
- [19] ClinicalTrials.gov, Palbociclib and sorafenib, decitabine, or dexamethasone in treating patients with recurrent or refractory leukemia. <https://clinicaltrials.gov/ct2/show/NCT03132454>.
- [20] ClinicalTrials.gov, Study of palbociclib combined with chemotherapy in pediatric patients with recurrent/refractory solid tumors. <https://clinicaltrials.gov/ct2/show/NCT03709680>.
- [21] ClinicalTrials.gov, Palbociclib in combination with chemotherapy in treating children with relapsed acute lymphoblastic leukemia (ALL) or lymphoblastic lymphoma (LL). <https://clinicaltrials.gov/ct2/show/NCT03792256>.
- [22] ClinicalTrials.gov, Palbociclib in treating patients with relapsed or refractory Rb positive advanced solid tumors, non-Hodgkin lymphoma, or histiocytic disorders with activating alterations in cell cycle genes (a pediatric MATCH treatment trial). <https://clinicaltrials.gov/ct2/show/NCT03526250>.
- [23] US Food and Drug Administration. Center for Drug Evaluation and Research., Highlights of prescribing information palbociclib, (2018). [https://www.accessdata.fda.gov/drugsatfda\\_docs/label/2018/207103s0071b1.pdf](https://www.accessdata.fda.gov/drugsatfda_docs/label/2018/207103s0071b1.pdf).
- [24] C. Palmieri, I. Macpherson, Use of the Child-Pugh score in anticancer drug dosing decision making: proceed with caution, *Lancet Oncol.* 20 (2019) e289. [https://doi.org/10.1016/S1470-2045\(19\)30296-7](https://doi.org/10.1016/S1470-2045(19)30296-7).
- [25] H. Mukai, C. Shimizu, N. Masuda, S. Ohtani, S. Ohno, M. Takahashi, Y. Yamamoto, R. Nishimura, N. Sato, S. Ohsumi, H. Iwata, Y. Mori, S. Hashigaki, Y. Muramatsu, T. Nagasawa, Y. Umeyama, D.R. Lu, M. Toi, Palbociclib in combination with letrozole in patients with estrogen receptor–positive, human epidermal growth factor receptor 2–negative advanced breast cancer: PALOMA-2 subgroup analysis of Japanese patients, *Int. J. Clin. Oncol.* 24 (2019) 274–287. <https://doi.org/10.1007/s10147-018-1353-9>.
- [26] N. Masuda, K. Inoue, R. Nakamura, Y. Rai, H. Mukai, S. Ohno, F. Hara, Y. Mori, S. Hashigaki, Y. Muramatsu, T. Nagasawa, Y. Umeyama, X. Huang, H. Iwata, Palbociclib in combination with fulvestrant in patients with hormone receptor-positive, human epidermal growth factor receptor 2-negative advanced breast cancer: PALOMA-3 subgroup analysis of Japanese patients, *Int. J. Clin. Oncol.* 24 (2019) 262–273. <https://doi.org/10.1007/s10147-018-1359-3>.
- [27] US Food and Drug Administration. Center for Drug Evaluation and Research., Clinical pharmacology and biopharmaceutics review palbociclib, (2016). [https://www.accessdata.fda.gov/drugsatfda\\_docs/nda/2016/207103Orig1s002.pdf](https://www.accessdata.fda.gov/drugsatfda_docs/nda/2016/207103Orig1s002.pdf).
- [28] A. Ruiz-Garcia, A. Plotka, M. O’Gorman, D.D. Wang, Effect of food on the bioavailability of palbociclib, *Cancer Chemother. Pharmacol.* 79 (2017) 1–7. <https://doi.org/10.1007/s00280-017-3246-4>.



- [29] US Food and Drug Administration. Center for Drug Evaluation and Research, Clinical pharmacology review ribociclib, (2017). [https://www.accessdata.fda.gov/drugsatfda\\_docs/nda/2017/209092Orig1s000MultidisciplineR.pdf](https://www.accessdata.fda.gov/drugsatfda_docs/nda/2017/209092Orig1s000MultidisciplineR.pdf).
- [30] Committee for Medicinal Products for Human Use (CHMP), Public assessment report abemaciclib, (2018). [https://www.ema.europa.eu/en/documents/assessment-report/verzenios-epar-public-assessment-report\\_en.pdf](https://www.ema.europa.eu/en/documents/assessment-report/verzenios-epar-public-assessment-report_en.pdf).
- [31] K. Tamura, H. Mukai, Y. Naito, K. Yonemori, M. Kodaira, Y. Tanabe, N. Yamamoto, S. Osera, M. Sasaki, Y. Mori, S. Hashigaki, T. Nagasawa, Y. Umeyama, T. Yoshino, Phase I study of palbociclib, a cyclin-dependent kinase 4/6 inhibitor, in Japanese patients, *Cancer Sci.* 107 (2016) 755–763. <https://doi.org/10.1111/cas.12932>.
- [32] G. Curigliano, P. Gómez Pardo, F. Meric-Bernstam, P. Conte, M.P. Lolkema, J.T. Beck, A. Bardia, M. Martínez García, F. Penault-Llorca, S. Dhuria, Z. Tang, N. Solovieff, M. Miller, E. Di Tomaso, S.A. Hurvitz, Ribociclib plus letrozole in early breast cancer: A presurgical, window-of-opportunity study, *Breast.* 28 (2016) 191–198. <https://doi.org/10.1016/j.breast.2016.06.008>.
- [33] T.S. Samant, S. Dhuria, Y. Lu, M. Laisney, S. Yang, A. Grandeury, M. Mueller-zsigmondy, K. Umehara, F. Huth, M. Miller, C. Germa, M. Elmeliegy, Ribociclib bioavailability is not affected by gastric pH changes or food intake : in silico and clinical evaluations, *Clin. Pharmacol. Ther.* 104 (2018) 374–383. <https://doi.org/10.1002/cpt.940>.
- [34] T. Doi, B. Hewes, T. Kakizume, T. Tajima, N. Ishikawa, Y. Yamada, Phase I study of single-agent ribociclib in Japanese patients with advanced solid tumors, *Cancer Sci.* 109 (2018) 193–198. <https://doi.org/10.1111/cas.13428>.
- [35] J.R. Infante, P.A. Cassier, J.F. Gerecitano, P.O. Witteveen, R. Chugh, V. Ribrag, A. Chakraborty, A. Matano, J.R. Dobson, A.S. Crystal, S. Parasuraman, G.I. Shapiro, A phase I study of the cyclin-dependent kinase 4/6 inhibitor ribociclib (LEE011) in patients with advanced solid tumors and lymphomas, *Clin. Cancer Res.* 22 (2016) 5696–5705. <https://doi.org/10.1158/1078-0432.CCR-16-1248>.
- [36] A. Patnaik, L.S. Rosen, S.M. Tolaney, A.W. Tolcher, J.W. Goldman, L. Gandhi, K.P. Papadopoulos, M. Beeram, D.W. Rasco, J.F. Hilton, A. Nasir, R.P. Beckmann, A.E. Schade, A.D. Fulford, T.S. Nguyen, R. Martinez, P. Kulanthaivel, L.Q. Li, M. Frenzel, D.M. Cronier, E.M. Chan, K.T. Flaherty, P.Y. Wen, G.I. Shapiro, Efficacy and safety of Abemaciclib, an inhibitor of CDK4 and CDK6, for patients with breast cancer, non-small cell lung cancer, and other solid tumors, *Cancer Discov.* 6 (2016) 740–753. <https://doi.org/10.1158/2159-8290.CD-16-0095>.
- [37] Y. Fujiwara, K. Tamura, S. Kondo, Y. Tanabe, S. Iwasa, A. Shimomura, S. Kitano, K. Ogasawara, P.K. Turner, J. Mori, H. Asou, E.M. Chan, N. Yamamoto, Phase 1 study of abemaciclib, an inhibitor of CDK 4 and 6, as a single agent for Japanese patients with advanced cancer, *Cancer Chemother. Pharmacol.* 78 (2016) 281–288. <https://doi.org/10.1007/s00280-016-3085-8>.
- [38] E.S. Kim, K. Kelly, L.G. Paz-Ares, P. Garrido, S. Jalal, D. Mahadevan, M. Gutierrez, M. Provencio, E. Schaefer, M. Shaheen, E.L. Johnston, P. Kellie Turner, S.R.P. Kambhampati, R. Beckmann, A. Hossain, W.J. John, J.W. Goldman, Abemaciclib in combination with single-agent options in patients with stage IV non-small cell lung cancer: A phase Ib study, *Clin. Cancer Res.* 24 (2018) 5543–5551. <https://doi.org/10.1158/1078-0432.CCR-18-0651>.
- [39] K. Turner, J. Chappell, P. Kulanthaivel, W.T. Ng, J. Royalty, Food effect on the pharmacokinetics of 200-mg abemaciclib in healthy subject. [abstract]. In: Proceedings of the 107th Annual Meeting of the American Association for Cancer Research; 2016 Apr 16-20; New Orleans, LA. Philadelphia (PA): AACR, *Cancer Res.* 76(14 Supp) (2016) Abstract nr CT152.
- [40] ClinicalTrials.gov, A study of LY2835219 in healthy participants. <https://clinicaltrials.gov/ct2/show/NCT02256267>.
- [41] ClinicalTrials.gov, A study of abemaciclib (LY2835219) in healthy participants with and without food. <https://clinicaltrials.gov/ct2/show/NCT02482935>.

- [42] P. Turner, J. Chappell, A. Aburub, W. Ng, W. Zhang, J. Royalty, P. Kulanthaivel, Abemaciclib tablet formulation is bioequivalent to capsules [abstract]. In: Proceedings of the 2017 San Antonio Breast Cancer Symposium; 2017 Dec 5-9; San Antonio, TX. Philadelphia (PA): AACR, Cancer Res. 78(4 Suppl) (2018) Abstract nr P1-10-14.
- [43] ClinicalTrials.gov, A bioequivalence study comparing abemaciclib capsule and tablet formulations and effect of food on abemaciclib tablet pharmacokinetics in healthy subjects. <https://clinicaltrials.gov/ct2/show/NCT02672423>.
- [44] Y. Yu, C.-M. Loi, J. Hoffman, D. Wang, Physiologically based pharmacokinetic modeling of palbociclib, *J. Clin. Pharmacol.* 57 (2017) 173–184. <https://doi.org/10.1002/jcph.792>.
- [45] Netherlands Trial Register, Effect of moderate CYP3A4 inhibitor erythromycin on the pharmacokinetics of palbociclib. <https://www.trialregister.nl/trial/7549>.
- [46] J.T. Hoffman, A. Plotka, M. O’Gorman, C.-M. Loi, L. Kirkovsky, C. Gallo-Stampino, D. Wang, A phase 1 randomized, open-label, 2-sequence, 2-period crossover study of the effect of multiple doses of palbociclib (PD-0332991) on midazolam pharmacokinetics in healthy women of non-childbearing potential. [abstract]. In: Proceedings of the 105th Annual Meeting, Cancer Res. 74 (2014) Abstract nr CT419. <https://doi.org/10.1158/1538-7445.AM2014-CT419>.
- [47] W. Sun, K.J. Klamerus, L.M. Yuhass, S. Pawlak, A. Plotka, M. O’Gorman, L. Kirkovsky, M. Kosa, D. Wang, Impact of acid-reducing agents on the pharmacokinetics of palbociclib, a weak base with pH-dependent solubility, with different food intake conditions, *Clin. Pharmacol. Drug Dev.* 6 (2017) 614–626. <https://doi.org/10.1002/cpdd.356>.
- [48] W. Sun, Y. Yu, J. Hoffman, N.C. Turner, M. Cristofanilli, D.D. Wang, Palbociclib exposure-response analyses in second-line treatment of hormone-receptor positive advanced breast cancer (ABC), *J. Clin. Oncol.* 35 (2017) 1053–1053.
- [49] US Food and Drug Administration. Center for Drug Evaluation and Research, Clinical pharmacology review palbociclib, 2017. [https://www.accessdata.fda.gov/drugsatfda\\_docs/nda/2019/207103Orig1s004.pdf](https://www.accessdata.fda.gov/drugsatfda_docs/nda/2019/207103Orig1s004.pdf).
- [50] J. Zheng, Y. Yu, C. Durairaj, M. Amantea, V. Dieras, R. Finn, D. Wang, Palbociclib exposure-response analyses in the treatment of hormone-receptor positive (HR+), human epidermal growth factor receptor 2 negative (HER2-) advanced breast cancer (ABC) [abstract]. In: Proceedings of the 2017 San Antonio Breast Cancer Symposium; Cancer Res. 78 (2018) Abstract nr P5-21-21.
- [51] R.B. Verheijen, H. Yu, J.H.M. Schellens, J.H. Beijnen, N. Steeghs, A.D.R. Huitema, Practical recommendations for therapeutic drug monitoring of kinase inhibitors in oncology, *Clin. Pharmacol. Ther.* 102 (2017) 765–776. <https://doi.org/10.1002/cpt.787>.
- [52] W. Sun, P.J. O’Dwyer, R.S. Finn, A. Ruiz-Garcia, G.I. Shapiro, G.K. Schwartz, A. DeMichele, D. Wang, Characterization of neutropenia in advanced cancer patients following palbociclib treatment using a population pharmacokinetic-pharmacodynamic modeling and simulation approach, *J. Clin. Pharmacol.* 57 (2017) 1159–1173. <https://doi.org/10.1002/jcph.902>.
- [53] J.T. Hoffman, C.-M. Loi, A. Plotka, M. O’Gorman, H. Shi, A. Mori, D.D. Wang, A phase I open-label fixed-sequence two-period crossover study of the effect of multiple doses of Itraconazole on palbociclib (PD-0332991) pharmacokinetics in healthy volunteers [abstract]. In Proceedings of the 107th Annual Meeting of the American Association for Cancer Research; 16-20 April 2016, New Orleans (LA). Philadelphia (PA): AACR; Cancer Res. 76 (2016) LB-196. <https://doi.org/10.1158/1538-7445.am2016-lb-196>.
- [54] J.T. Hoffman, A. Plotka, M. O’Gorman, A. Chang, M. Kosa, C.-M. Loi, C. Gallo-Stampino, D.D. Wang, A phase 1 randomized, open-label, fixed-sequence, 2-period study of the effect of multiple doses of rifampin on palbociclib (PD-0332991) pharmacokinetics in healthy volunteers. [abstract]. In: Proceedings of the 106th Annual Meeting of the American Association for Cancer Research, 18-22 Apr 2015; Philadelphia (PA); AACR; Cancer Res. 2015; 75 (15 Suppl.) Abstract nr 4515. <https://doi.org/10.1158/1538-7445.AM2015-4515>.

- [55] J.T. Hoffman, C.-M. Loi, A. Plotka, M. O’Gorman, H. Shi, A. Mori, D.D. Wang, A phase I open-label fixed-sequence two-period crossover study of the effect of multiple doses of modafinil on palbociclib (PD-0332991) pharmacokinetics in healthy volunteers. [abstract]. In: Proceedings of the 107th Annual Meeting of the American Association for Cancer Research; 16-20 April 2016, New Orleans (LA), Philadelphia (PA), AACR; Cancer Res. 76 (2016) LB-198.
- [56] Committee for Medicinal Products for Human Use. European Medicines Agency, European public assessment report ribociclib, (2017). [https://www.ema.europa.eu/en/documents/assessment-report/kisqali-epar-public-assessment-report\\_en.pdf](https://www.ema.europa.eu/en/documents/assessment-report/kisqali-epar-public-assessment-report_en.pdf).
- [57] ClinicalTrials.gov, A study of LY2835219 in participants with cancer. <https://clinicaltrials.gov/ct2/show/results/NCT02117648>.
- [58] J.C. Chappell, P.K. Turner, Y.A. Pak, J. Bacon, A.Y. Chiang, J. Royalty, S.D. Hall, P. Kulanthaivel, J. V. Bonventre, Abemaciclib inhibits renal tubular secretion without changing glomerular filtration rate, Clin. Pharmacol. Ther. 105 (2019) 1187–1195. <https://doi.org/10.1002/cpt.1296>.
- [59] ClinicalTrials.gov, A study of abemaciclib in healthy participants (loperamide). <https://clinicaltrials.gov/ct2/show/results/NCT02677844>.
- [60] M.M. Posada, B.L. Morse, P.K. Turner, P. Kulanthaivel, S.D. Hall, G.L. Dickinson, Predicting clinical effects of CYP3A4 modulators on abemaciclib and active metabolites exposure using physiologically based pharmacokinetic modeling, J. Clin. Pharmacol. 60 (2020) 915–930. <https://doi.org/10.1002/jcph.1584>.
- [61] G.N. Hortobagyi, S.M. Stemmer, H.A. Burris, Y.S. Yap, G.S. Sonke, S. Paluch-Shimon, M. Campone, K.L. Blackwell, F. Andre, E.P. Winer, W. Janni, S. Verma, P. Conte, C.L. Arteaga, D.A. Cameron, K. Petrakova, L.L. Hart, C. Villanueva, A. Chan, E. Jakobsen, A. Nusch, O. Burdaeva, E.M. Grischke, E. Alba, E. Wist, N. Marschner, A.M. Favret, D. Yardley, T. Bachelot, L.M. Tseng, S. Blau, F. Xuan, F. Souami, M. Miller, C. Germa, S. Hirawat, J. O’Shaughnessy, Ribociclib as first-line therapy for HR-positive, advanced breast cancer, N. Engl. J. Med. 375 (2016) 1738–1748. <https://doi.org/10.1056/NEJMoa1609709>.
- [62] G.N. Hortobagyi, S.M. Stemmer, H.A. Burris, Y.S. Yap, G.S. Sonke, S. Paluch-Shimon, M. Campone, K. Petrakova, K.L. Blackwell, E.P. Winer, W. Janni, S. Verma, P. Conte, C.L. Arteaga, D.A. Cameron, S. Mondal, F. Su, M. Miller, M. Elmeliyeg, C. Germa, J. O’Shaughnessy, Updated results from MONALEESA-2, a phase III trial of first-line ribociclib plus letrozole versus placebo plus letrozole in hormone receptor-positive, HER2-negative advanced breast cancer, Ann. Oncol. 29 (2018) 1541–1547. <https://doi.org/10.1093/annonc/mdy155>.
- [63] D.J. Slamon, P. Neven, S. Chia, P.A. Fasching, M. De Laurentiis, S.A. Im, K. Petrakova, G. Val Bianchi, F.J. Esteva, M. Martín, A. Nusch, G.S. Sonke, L. De La Cruz-Merino, J.T. Beck, X. Pivot, G. Vidam, Y. Wang, K.R. Lorenc, M. Miller, T. Taran, G. Jerusalem, Phase III randomized study of ribociclib and fulvestrant in hormone receptor-positive, human epidermal growth factor receptor 2-negative advanced breast cancer: MONALEESA-3, J. Clin. Oncol. 36 (2018) 2465–2472. <https://doi.org/10.1200/JCO.2018.78.9909>.
- [64] D.J. Slamon, P. Neven, S. Chia, P.A. Fasching, M. De Laurentiis, S.A. Im, K. Petrakova, G. V. Bianchi, F.J. Esteva, M. Martín, A. Nusch, G.S. Sonke, L. De La Cruz-Merino, J.T. Beck, X. Pivot, M. Sondhi, Y. Wang, A. Chakravarty, K. Rodriguez-Lorenc, T. Taran, G. Jerusalem, Overall survival with ribociclib plus fulvestrant in advanced breast cancer, N. Engl. J. Med. 382 (2020) 514–524. <https://doi.org/10.1056/NEJMoa1911149>.
- [65] US Food and Drug Administration. Center for Drug Evaluation and Research., Chemistry review ribociclib, (2016). [https://www.accessdata.fda.gov/drugsatfda\\_docs/nda/2017/209092Orig1s000ChemR.pdf](https://www.accessdata.fda.gov/drugsatfda_docs/nda/2017/209092Orig1s000ChemR.pdf).
- [66] A. Mitra, N. Parrott, N. Miller, R. Lloyd, C. Tistaert, T. Heimbach, Y. Ji, F. Kesiosoglou, Prediction of pH-dependent drug-drug interactions for basic drugs using physiologically based biopharmaceutics modeling: industry case studies, J. Pharm. Sci. 109 (2020) 1380–1394. <https://doi.org/10.1016/j.xphs.2019.11.017>.
- [67] A. Martínez-Chávez, S. van Hoppe, H. Rosing, M.C. Lebre, M. Tibben, J.H. Beijnen, A.H. Schinkel, P-glycoprotein limits ribociclib brain exposure and CYP3A4 restricts its oral bioavailability, Mol. Pharm. 16 (2019) 3842–3852. <https://doi.org/10.1021/acs.molpharmaceut.9b00475>.

- [68] A. Sorf, J. Hofman, R. Kučera, F. Staud, M. Ceckova, Ribociclib shows potential for pharmacokinetic drug-drug interactions being a substrate of ABCB1 and potent inhibitor of ABCB1, ABCG2 and CYP450 isoforms in vitro, *Biochem. Pharmacol.* 154 (2018) 10–17. <https://doi.org/10.1016/j.bcp.2018.04.013>.
- [69] B.E. Wilson, K. Mok, B.E. Kiely, R. Nguyen, E. Moylan, Association between ribociclib and changes in creatinine in patients with hormone receptor positive metastatic breast cancer, *Intern. Med. J.* 49 (2019) 1438–1442. <https://doi.org/10.1111/imj.14629>.
- [70] US Food and Drug Administration. Center for Drug Evaluation and Research., Highlights of prescribing information ribociclib, (2019). [https://www.accessdata.fda.gov/drugsatfda\\_docs/label/2020/209092s003lbl.pdf](https://www.accessdata.fda.gov/drugsatfda_docs/label/2020/209092s003lbl.pdf).
- [71] B. Georger, F. Bourdeaut, S.G. DuBois, M. Fischer, T. Cash, J.R. Dobson, A. Marabelle, G.W. Robinson, J.I. Geller, F. Bourdeaut, M. Motta, S. Parasuraman, S. Modak, S.G. Bhansali, S.N. Chi, A. Matano, A.D.J. Pearson, B. Georger, N.G. Gottardo, A phase I study of the CDK4/6 inhibitor ribociclib (LEE011) in pediatric patients with malignant rhabdoid tumors, neuroblastoma, and other solid tumors, *Clin. Cancer Res.* 23 (2017) 2433–2441. <https://doi.org/10.1158/1078-0432.ccr-16-2898>.
- [72] ClinicalTrials.gov, Evaluation of renal function impairment on the pharmacokinetics of LEE011. <https://clinicaltrials.gov/ct2/show/NCT02431481>.
- [73] Committee for Medicinal Products for Human Use. European Medicines Agency, Summary of product characteristics ribociclib, (2017). [https://www.ema.europa.eu/en/documents/product-information/kisqali-epar-product-information\\_en.pdf](https://www.ema.europa.eu/en/documents/product-information/kisqali-epar-product-information_en.pdf).
- [74] US Food and Drug Administration. Center for Drug Evaluation and Research, Clinical pharmacology review ribociclib, (2018). [https://www.accessdata.fda.gov/drugsatfda\\_docs/nda/2019/209092Orig1s001.pdf](https://www.accessdata.fda.gov/drugsatfda_docs/nda/2019/209092Orig1s001.pdf)
- [75] M.P. Goetz, M. Toi, M. Campone, O. Trédan, N. Bourayou, J. Sohn, I.H. Park, S. Paluch-Shimon, J. Huober, S.C. Chen, L. Manso, S. Barriga, O.C. Freedman, G.G. Jaliffe, T. Forrester, M. Frenzel, I.C. Smith, A. Di Leo, MONARCH 3: Abemaciclib as initial therapy for advanced breast cancer, *J. Clin. Oncol.* 35 (2017) 3638–3646. <https://doi.org/10.1200/JCO.2017.75.6155>.
- [76] G.W. Sledge, M. Toi, P. Neven, J. Sohn, K. Inoue, X. Pivot, O. Burdaeva, M. Okera, N. Masuda, P.A. Kaufman, H. Koh, E.M. Grischke, M. Frenzel, Y. Lin, S. Barriga, I.C. Smith, N. Bourayou, A. Llombart-Cussac, MONARCH 2: Abemaciclib in combination with fulvestrant in women with HR+/HER2-advanced breast cancer who had progressed while receiving endocrine therapy, *J. Clin. Oncol.* 35 (2017) 2875–2884. <https://doi.org/10.1200/JCO.2017.73.7585>.
- [77] US Food and Drug Administration. Center for Drug Evaluation and Research., Chemistry review abemaciclib, (2017). [https://www.accessdata.fda.gov/drugsatfda\\_docs/nda/2017/208716Orig1s000ChemR.pdf](https://www.accessdata.fda.gov/drugsatfda_docs/nda/2017/208716Orig1s000ChemR.pdf).
- [78] L.M. Gelbert, S. Cai, X. Lin, C. Sanchez-Martinez, M. Del Prado, M.J. Lallena, R. Torres, R.T. Ajamie, G.N. Wishart, R.S. Flack, B.L. Neubauer, J. Young, E.M. Chan, P. Iversen, D. Cronier, E. Kreklau, A. De Dios, Preclinical characterization of the CDK4/6 inhibitor LY2835219: In-vivo cell cycle-dependent/independent anti-tumor activities alone/in combination with gemcitabine, *Invest. New Drugs.* 32 (2014) 825–837. <https://doi.org/10.1007/s10637-014-0120-7>.
- [79] US Food and Drug Administration. Center for Drug Evaluation and Research., Clinical pharmacology review abemaciclib (in combination with aromatase inhibitors), (2017). [https://www.accessdata.fda.gov/drugsatfda\\_docs/nda/2018/208855Orig1s000MultidisciplineR.pdf](https://www.accessdata.fda.gov/drugsatfda_docs/nda/2018/208855Orig1s000MultidisciplineR.pdf).
- [80] US Food and Drug Administration. Center for Drug Evaluation and Research, Clinical pharmacology review abemaciclib (in combination with fulvestrant), (2017). [https://www.accessdata.fda.gov/drugsatfda\\_docs/nda/2017/208716Orig1s000MultidisciplineR.pdf](https://www.accessdata.fda.gov/drugsatfda_docs/nda/2017/208716Orig1s000MultidisciplineR.pdf).
- [81] A. Martínez-Chávez, M. Tibben, M.C. Lebre, H. Rosing, J.H. Beijnen, A.H. Schinkel, The role of multidrug efflux transporters and CYP3A in the pharmacokinetics and tissue distribution of abemaciclib and its active metabolites [abstract no. 2258]. Proceedings of the 111th Annual Meeting of the American Association for Cancer Research; 2020 June 22–24. Philadelphia (PA): AACR; 2020.

- [82] T. Wu, Z. Chen, K.K.W. To, X. Fang, F. Wang, B. Cheng, L. Fu, Effect of abemaciclib (LY2835219) on enhancement of chemotherapeutic agents in ABCB1 and ABCG2 overexpressing cells in vitro and in vivo, *Biochem. Pharmacol.* 124 (2017) 29–42. <https://doi.org/10.1016/j.bcp.2016.10.015>.
- [83] Committee for Medicinal Products for Human Use. European Medicines Agency, Summary of product characteristics abemaciclib, (2017). [https://www.ema.europa.eu/en/documents/product-information/verzenios-epar-product-information\\_en.pdf](https://www.ema.europa.eu/en/documents/product-information/verzenios-epar-product-information_en.pdf).
- [84] C.C. Mills, E.A. Kolb, V.B. Sampson, Recent advances of cell-cycle inhibitor therapies for pediatric cancer, *Cancer Res.* 77 (2017) 6489–6498. <https://doi.org/10.1158/0008-5472.CAN-17-2066>.
- [85] ClinicalTrials.gov, Abemaciclib in children with DIPG or recurrent/refractory solid tumors (AflacST1501). <https://clinicaltrials.gov/ct2/show/NCT02644460>.
- [86] ClinicalTrials.gov, A study of abemaciclib (LY2835219) in combination with temozolomide and irinotecan and abemaciclib in combination with temozolomide in children and young adult participants with solid tumors. <https://clinicaltrials.gov/ct2/show/NCT04238819>.
- [87] S.C. Tate, A.K. Sykes, P. Kulanthaivel, E.M. Chan, P.K. Turner, D.M. Cronier, A population pharmacokinetic and pharmacodynamic analysis of abemaciclib in a phase I clinical trial in cancer patients, *Clin. Pharmacokinet.* 57 (2018) 335–344. <https://doi.org/10.1007/s40262-017-0559-8>.
- [88] S.C. Tate, S. Cai, R.T. Ajamie, T. Burke, R.P. Beckmann, E.M. Chan, A. De Dios, G.N. Wishart, L.M. Gelbert, D.M. Cronier, Semi-mechanistic pharmacokinetic/pharmacodynamic modeling of the antitumor activity of LY2835219, a new cyclin-dependent kinase 4/6 inhibitor, in mice bearing human tumor xenografts, *Clin. Cancer Res.* 20 (2014) 3763–3774. <https://doi.org/10.1158/1078-0432.CCR-13-2846>.
- [89] S.L. Groenland, D. Katz, A.D.R. Huitema, N. Steeghs, Harnessing soft tissue sarcoma with low-dose pazopanib - A matter of blood levels, *BMC Cancer.* 18 (2018) 1–3. <https://doi.org/10.1186/s12885-018-5043-9>.
- [90] A. Van Ommen-Nijhof, I.R. Konings, C.J.J. Van Zeijl, C.A. Uyl-De Groot, V. Van Der Noort, A. Jager, G.S. Sonke, S.L. De Bakker, H. De Graaf, W. Dercksen, A. Honkoop, A. Imholz, Q. Van Rossum-Schornagel, E. Siemerink, I. Baas, R. Oosterkamp, C. Schröder, J. Kroep, A. Haringhuizen, C.T. Van Driel, F. Erdkamp, P. De Jong, J. Tol, Y. Van De Wouw, J. Heijns, A.M. Van Riel, C. Mandigers, M. Schrieks, Selecting the optimal position of CDK4/6 inhibitors in hormone receptor-positive advanced breast cancer - The SONIA study: Study protocol for a randomized controlled trial, *BMC Cancer.* 18 (2018) 1–7. <https://doi.org/10.1186/s12885-018-4978-1>.
- [91] Y. Zhou, M. Ingelman-Sundberg, V.M. Lauschke, Worldwide distribution of cytochrome P450 alleles: a meta-analysis of population-scale sequencing projects, *Clin. Pharmacol. Ther.* 102 (2017) 688–700. <https://doi.org/10.1002/cpt.690>.
- [92] Netherlands Trial Register, CYP3A4\*22 genotype-guided dosing of TKIs in cancer patients: a new way of personalized therapy. <https://www.trialregister.nl/trial/7514>.



## Conclusions and future perspectives

Specific cyclin-dependent kinase (CDK) inhibitors have emerged as a promising cancer pharmacotherapy, by targeting one of the hallmarks of cancer: uncontrolled cell proliferation. So far, three CDK4/6 inhibitors have been approved for cancer treatment: palbociclib, ribociclib and abemaciclib. In addition, many other promising compounds with several CDK subclass specificities are being investigated in the clinic, including milciclib. In order to contribute to the drug development or to optimize the clinical use of these drugs, this thesis addressed several aspects of the CDK inhibitors. First, it provided reliable and validated bioanalytical methods that can be applied to support preclinical and clinical studies and/or to monitor the therapeutic use of the CDK inhibitors. Second, this thesis delved into the functions of membrane transporters and the drug-metabolizing enzyme CYP3A in the pharmacokinetics and tissue distribution of the CDK inhibitors. In several cases, these proteins were demonstrated to significantly impact the overall exposure and/or the tissue penetration of the investigated drugs. Finally, this thesis summarized the clinical pharmacokinetics and pharmacodynamics of the approved CDK4/6 inhibitors.

Conclusive remarks and perspectives of the investigations of each part are discussed below.

### **Bioanalysis of cyclin-dependent kinase inhibitors**

Bioanalytical methods are critical for providing reliable data and successfully conducting preclinical and clinical studies [1]. Therefore, their suitability for their intended use should be demonstrated with a validation prior its use. According to official guidelines (FDA and EMA), a full validation is required when the study is used for regulatory applications (e.g. pharmacokinetics and bioequivalence studies), while a fit-for-purpose concept can determine the validation level depending on the drug development stage and the intended use of the method [1,2]. The bioanalytical assays described in **Chapters 1-3** contemplate both aspects, a full validation in human plasma was performed, while a partial validation was done for mouse and other matrices. This provides a wide applicability of these bioanalytical methods, including their use in both preclinical and clinical studies.

Liquid chromatography coupled with tandem-mass spectrometry (LC-MS/MS) is currently the technique of choice for quantifying small-molecule drugs in biological matrices (**Chapters 1-3**). This is due to its excellent sensitivity and selectivity, achieved by the combination of chromatographic separation and specific analyte response in the tandem mass spectrometer, which has led to relatively simple sample preparation techniques and rapid analysis times [3]. However, variations in the analyte ionization can occur, leading to a variable analyte response. Apart from sample pre-treatment correction, internal standards normally also correct for response variations of the mass spectrometer; usually the stable isotopically-labeled compounds are the most effective. Stable isotopically-labeled compounds for each analyte were used in **Chapter 1**. In contrast, structural analog compounds were used as internal standards in the methods



described in **Chapters 2–4**, as their appropriate stable isotopically-labeled compounds were not available. In **Chapter 3**, palbociclib was used as internal standard for the quantification of milciclib eluting at almost identical retention times, providing good correction for the MS variation. On the other hand, in **Chapter 2** the stable isotopically labeled abemaciclib was used as internal standard for abemaciclib but also for its active metabolites, where sometimes the internal standard correction was not sufficient for the metabolites, resulting in higher variation and/or bias in their quantification. For this reason, wider acceptance criteria in accuracy and precision were used for the abemaciclib metabolites. It is nevertheless expected that when appropriate stable isotopically-labeled abemaciclib metabolites become available, the accuracy and precision of the method could be improved.

Liquid chromatography with fluorescence detection also provides good selectivity and sensitivity for bioanalysis of drugs. However, only few molecules possess sufficient fluorescent properties to be candidates for fluorescence detection. Irinotecan and its active metabolite SN-38 are analytes with good properties for fluorescence detection (**Chapter 4**). Despite the complexity of the matrices wherein the quantification was done, no interferent compounds were detected and the sensitivity of the fluorescence method was appropriate to measure the wide range of concentrations required by the preclinical study on irinotecan metabolism that this method supported.

Carry-over often occurs specially in analytical methods with a wide calibration range, as in the developed milciclib and abemaciclib methods (**Chapters 2 and 3**). However, efficient strategies pre- and post-analysis were followed to ensure the data integrity during measurements of all study samples.

Preferably, calibration curves and quality control samples should be prepared in the corresponding blank matrix. Preclinical studies often require drug quantification in multiple biomatrices and sometimes blanks of each biomatrix are insufficient [4]. In order to simplify their bioanalysis, the use of human plasma as a surrogate matrix for the quantification of these samples was evaluated (**Chapters 1-4**). In all cases, adequate accuracy and precision was demonstrated, validating the use of human plasma as a surrogate matrix for quantification of mouse samples (**Chapters 1-4**). Finally, bioanalytical methods described in **Chapters 1-3** successfully supported the preclinical studies described in part II of this thesis.

### **The impact of drug transporters and drug-metabolizing enzymes on the pharmacokinetics of the cyclin-dependent kinase inhibitors**

Part II of this thesis demonstrated that ribociclib, milciclib, abemaciclib and its active metabolites (M2, M20 and M18) are transported by ABCB1 and/or ABCG2 efflux transporters, albeit to varying extents. Consequently, the relative impact of these transporters on the pharmacokinetics and tissue distribution of these drugs was found

to differ. These results also suggested that tumors overexpressing ABCB1 and/or ABCG2 may be intrinsically resistant to pharmacotherapies with these CDK inhibitors.

ABCB1 was found to significantly participate in the elimination of ribociclib, ultimately affecting its plasma exposure (**Chapter 5**). Similar effects were observed for the abemaciclib M2 and M18 metabolites, since ABCG2 played only an insignificant role (if any) in limiting the plasma exposure of these compounds, despite efficient *in vitro* transport of these compounds (**Chapter 6**). In contrast, the oral exposure of milciclib, abemaciclib and its M20 metabolite were not significantly affected by ABCB1 and/or ABCG2, although mice lacking these transporters did show a slower elimination of these drugs (**Chapter 6 and 7**).

The most striking findings of these *in vivo* studies were the ability of the ABC transporters to limit the brain penetration of these drugs. ABCB1 dramatically limited the brain penetration of ribociclib (**Chapter 5**), while for milciclib, abemaciclib and its metabolites, ABCB1 was found to cooperate with ABCG2 to restrict the brain accumulation of these drugs (**Chapter 6 and 7**). Having a CDK4/6 or CDK2 inhibitor with decent brain penetration would be relevant for brain cancer treatments, as mechanistic alterations involving these kinases have been detected in some of these malignancies [5–7]. In addition, breast cancer, which is the currently approved indication of abemaciclib and ribociclib, is the second most frequent malignancy that metastasizes to the brain [8].

As was demonstrated in **Chapter 5**, the coadministration of an efficacious ABCB1 and ABCG2 inhibitor like elacridar completely inhibited the efflux activity of the ABC transporters, thus enhancing the ribociclib brain penetration. These results suggest that effective inhibition of ABCB1 and ABCG2 in humans would lead to increased brain exposures of ribociclib, all abemaciclib active compounds and milciclib, and this potentially could also revert any tumor resistance caused by overexpression of ABCB1 and/or ABCG2. However, more work still needs to be done to demonstrate the efficacy of these combined treatment.

CYP3A4 extensively metabolized ribociclib and abemaciclib (**Chapter 5 and 6**), while for milciclib this drug-metabolizing enzyme only had a minor impact (**Chapter 7**). Thus, ribociclib and abemaciclib plasma exposure can be markedly affected by CYP3A4 modulators, while for milciclib the risk of being affected by interactions with other drugs via CYP3A4 is much lower. Additionally, the plasma exposure of ribociclib and abemaciclib is likely to be influenced by genetic polymorphisms in CYP3A4.

### **Clinical pharmacokinetics and pharmacodynamics of the cyclin-dependent kinase inhibitors**

Finally, **Chapter 8** provided an overview of important aspects of the clinical application of the approved CDK4/6 inhibitors. Reviewed literature suggested that the brain penetration of palbociclib is also limited by ABC transporters. Furthermore, several

reviewed studies supported the extensive metabolism of palbociclib, ribociclib and abemaciclib by CYP3A4 and their susceptibility to be affected by CYP3A4 modulators. Therefore, dose adjustments of ribociclib or abemaciclib when concomitantly administered with CYP3A4 modulators are necessary in some cases. A potential advantage of the coadministration of a CYP3A4 inhibitor (e.g. ritonavir) with a lower dose of these anticancer drugs, may result in similar plasma exposure compared to the normal dose. Although rigorous monitoring of the drug levels must be done to assure the efficacy of the treatment, this could ultimately result in reduced treatment costs with these (expensive) CDK4/6 inhibitors. The high interindividual variability in exposure encountered with these drugs may be explained in part by variations in CYP3A4 activity caused by genetic polymorphisms and/or CYP3A4-modulating compounds. Although essential clinical characterization of palbociclib, ribociclib and abemaciclib has already been done, there are still some gaps that must be covered for an optimal characterization and use of these drugs.

In conclusion, the insights into different aspects of the CDK inhibitors provided in this thesis may be useful to optimize the clinical use of abemaciclib, palbociclib and ribociclib. Additionally, this can potentially contribute to the further development and application of these drugs and milciclib. First, by the provided bioanalytical methods in various matrices that can be used in different preclinical or clinical studies, and second by the knowledge generated in our studies that reveal the function of some drug transporters and drug-metabolizing enzymes in the pharmacokinetics and tissue distribution of the studied CDK inhibitors. Ultimately, this information could hopefully lead to CDK treatments with improved efficacy and safety.

## References

- [1] US Food and Drug Administration, Guidance for Industry Bioanalytical Method Validation, (2018) 1–22. <https://www.fda.gov/files/drugs/published/Bioanalytical-Method-Validation-Guidance-for-Industry.pdf>.
- [2] European Medicines Agency, Guideline on bioanalytical method validation, 44 (2012) 1–23. [https://www.ema.europa.eu/documents/scientific-guideline/guideline-bioanalytical-method-validation\\_en.pdf](https://www.ema.europa.eu/documents/scientific-guideline/guideline-bioanalytical-method-validation_en.pdf).
- [3] A. Van Eeckhaut, K. Lanckmans, S. Sarre, I. Smolders, Y. Michotte, Validation of bioanalytical LC-MS/MS assays: Evaluation of matrix effects, *J. Chromatogr. B Anal. Technol. Biomed. Life Sci.* 877 (2009) 2198–2207. <https://doi.org/10.1016/j.jchromb.2009.01.003>.
- [4] Y.-J. Xue, H. Gao, Q.C. Ji, Z. Lam, X. Fang, Z. Lin, M. Hoffman, D. Schulz-Jander, N. Weng, Bioanalysis of drug in tissue: current status and challenges, *Bioanalysis.* 4 (2012) 2637–2653. <https://doi.org/10.4155/bio.12.252>.
- [5] B. O’Leary, R.S. Finn, N.C. Turner, Treating cancer with selective CDK4/6 inhibitors, *Nat. Rev. Clin. Oncol.* 13 (2016) 417–430. <https://doi.org/10.1038/nrclinonc.2016.26>.
- [6] J. Wang, T. Yang, G. Xu, H. Liu, C. Ren, W. Xie, M. Wang, Cyclin-dependent kinase 2 promotes tumor proliferation and induces radio resistance in glioblastoma, *Transl. Oncol.* 9 (2016) 548–556. <https://doi.org/10.1016/j.tranon.2016.08.007>.
- [7] S. Bolin, A. Borgenvik, C.U. Persson, A. Sundström, J. Qi, J.E. Bradner, W.A. Weiss, Y.J. Cho, H. Weishaupt, F.J. Swartling, Combined BET bromodomain and CDK2 inhibition in MYC-driven medulloblastoma, *Oncogene.* 37 (2018) 2850–2862. <https://doi.org/10.1038/s41388-018-0135-1>.
- [8] P.S. Steeg, K.A. Camphausen, Q.R. Smith, Brain metastases as preventive and therapeutic targets, *Nat. Rev. Cancer.* 11 (2011) 352–363. <https://doi.org/10.1038/nrc3053>.





## Summary

Cancer remains a leading global health problem with expected increases in incidence and mortality for the coming years. New cancer therapies have focused on targeted anticancer drugs, which have demonstrated to have higher efficacy and reduced toxicity compared to traditional cytotoxic drugs. The cyclin-dependent kinases (CDKs) have been regarded as promising targets for cancer, since they can control critical checkpoints in the cell cycle when activated by cyclins. To date, three CDK inhibitors selective for CDK4 and CDK6 have been approved: palbociclib, ribociclib and abemaciclib. These drugs are currently used for the treatment of metastatic or advanced breast cancer, and their efficacy for other malignancies is being investigated. In addition, clinical studies of many other CDK inhibitors with different CDK subclass specificity are ongoing.

This thesis addresses several pharmacological aspects of the CDK inhibitors, from bioanalysis (Part I) to preclinical (Part II) and clinical pharmacokinetics (Part III), focusing mainly on the approved CDK4/6 inhibitors: abemaciclib, palbociclib and ribociclib. However, it also examines milciclib, a promising CDK2 inhibitor that is currently clinically investigated for treatment of some malignancies.

### **Part I: Bioanalysis of cyclin-dependent kinase inhibitors**

As reliable bioanalytical methods are pivotal for an appropriate conduction and performance of preclinical and clinical studies of drugs, part I of this thesis focusses on the development and validation of bioanalytical methods for the quantitative analysis of CDK inhibitors. Full method validation was performed according to the U.S. Food and Drug Administration (FDA) and European Medicines Agency (EMA) guidelines. The bioanalytical methods provided in part I were used to support the pre-clinical investigations conducted in part II of this thesis.

**Chapter 1** describes the development and validation of a bioanalytical method for the quantification of three approved CDK inhibitors (abemaciclib, palbociclib and ribociclib) in human and mouse matrices using liquid chromatography-tandem mass spectrometry (LC-MS/MS). This method was fully validated in human plasma and partially validated in mouse plasma and tissue homogenates, including liver, kidney, spleen, brain and small intestine. A fit-for-purpose strategy was followed to evaluate the method performance in the tissue homogenates. This method was linear, accurate and precise for the quantification of abemaciclib, palbociclib and ribociclib in all the biomatrices. The biomatrix stability of the three analytes under several conditions was also examined in this chapter, where palbociclib and ribociclib were found to be unstable in some tissue homogenates, but conditions were modified to increase their storage and processing stability. The applicability of this method was demonstrated in a preclinical pharmacokinetic study of ribociclib, where a new metabolite with the same  $m/z$  transition as the parent drug was detected in mouse samples.



In humans, abemaciclib metabolism leads to the formation of three active metabolites (M2, M20 and M18). Their comparable potency with the parent drug and their relative abundance in human plasma make these metabolites clinically important, as they probably contribute to the overall clinical efficacy and safety of abemaciclib. Therefore, the method presented in **Chapter 2** incorporates the bioanalysis of these metabolites simultaneously with abemaciclib, using an optimized ultra-high performance liquid chromatography-tandem mass spectrometry (UHPLC-MS/MS) method. A full validation of this method in human plasma was performed, whereas in mouse plasma the method was partially validated. This assay was successfully applied in a preclinical pharmacokinetic study, where abemaciclib and its active metabolites were identified and quantified. Inter-species differences between human and mouse samples were encountered, especially in the formation of M20, where isomers of this compound were detected in mouse plasma, but not in human plasma. This was confirmed by high resolution-mass spectrometry (HR-MS) measurements.

In **Chapter 3** a versatile LC-MS/MS assay for milciclib in multiple biomatrices is provided to further support the clinical and preclinical development of milciclib. For this, a wide quantitative concentration range was selected and several biomatrices were included for the method validation, including human and mouse plasma, homogenates of mouse brain, kidney, liver, small intestine, spleen, and tissue culture medium. A full validation in human plasma was performed and a partial validation was done for the other biomatrices. The used sample pre-treatment led to efficient extraction of the analyte, with recoveries between 95–100%. The use of human plasma as a surrogate matrix to quantify milciclib in tissue culture medium and mouse matrices resulted in acceptable accuracy and precision, although tissue culture medium samples required a dilution with human plasma prior the pre-treatment. All performance parameters of the method complied with the acceptance criteria recommended by the guidelines, except for the carry-over, which was slightly above (22.9% of the lower limit of quantification) the recommended percentage (20%). Therefore, additional measures were taken to ensure data integrity. Stability of milciclib in all matrices was additionally evaluated, and in some matrices the analyte was unstable under the tested conditions. Thus, further recommendations on storage and processing were included.

**Chapter 4** reports a rapid bioanalytical method for the simultaneous quantification of irinotecan and SN-38 in mouse plasma and tissue homogenates using High-Performance Liquid Chromatography with Fluorescence detection (HPLC-FL). This method was optimized to specifically support preclinical studies of the metabolism of irinotecan into SN-38 by carboxylesterase enzymes. The selectivity, linearity, accuracy and precision of the method in the concentration range of 7.5 to 1500 ng/mL for irinotecan and from 5 to 1000 ng/mL for SN-38 was demonstrated. Lastly, the applicability of this method in a pharmacokinetic study of irinotecan and SN-38 using *in vivo* mouse models is proven.

## **Part II: The impact of drug transporters and drug-metabolizing enzymes on the pharmacokinetics of the cyclin-dependent kinase inhibitors**

Drug transporters and drug-metabolizing enzymes can influence the disposition of substrate drugs with clinically relevant (pharmacodynamic) consequences. Thus, using *in vitro* and various genetically modified mouse models, part II of this thesis investigates the role of efflux (ABCB1 and ABCG2) and uptake transporters (OATP1) and cytochrome P450 3A (CYP3A) enzymes in the pharmacokinetics and tissue distribution of CDK inhibitors.

**Chapter 5** examines the effects of the efflux transporters ABCB1 and ABCG2 and of CYP3A on the pharmacokinetics of the CDK4/6 inhibitor ribociclib. *In vitro*, ribociclib was avidly transported by human ABCB1. *In vivo*, the ribociclib brain penetration was drastically limited by ABCB1 in the blood–brain barrier, but coadministration of elacridar could fully reverse this process. Our results further suggested that ABCB1 could play an important role in the ribociclib elimination. Moreover, this study showed that human CYP3A4 can extensively metabolize ribociclib and strongly restrict its oral bioavailability. The insights obtained from this study may be useful to further optimize the clinical application of ribociclib, especially for the treatment of (metastatic) brain tumors.

**Chapter 6** investigates whether abemaciclib active metabolites (M2, M20 and M18) are substrates of the efflux transporters ABCB1 and ABCG2. Additionally, this chapter determines the impact of these transporters and of CYP3A on the pharmacokinetics and tissue distribution of abemaciclib and its active metabolites. *In vitro*, abemaciclib was efficiently transported by human ABCB1 and mouse *Abcg2*, and slightly by human ABCG2, and its active metabolites were even better transport substrates of these efflux transporters. ABCB1 and ABCG2 did not affect the plasma exposure of abemaciclib and M20, however, the  $AUC_{0-24h}$  and the  $C_{max}$  of M2 significantly increased in the absence of *Abcb1a/1b* and *Abcg2*, where *Abcb1a/1b* appeared to play a dominant role. In addition, the brain penetration of abemaciclib, M2 and M20 dramatically increased (at least) 25-, 4- and 60-fold, respectively, when both transporters were ablated, and to a lesser extent in single *Abcb1* or *Abcg2*-deficient mice. Similarly, the recovery of abemaciclib and its metabolites was profoundly reduced in *Abcb1a/1b;Abcg2<sup>-/-</sup>* mice, but these effects were also diminished in single knockout mice. Our results show that both *Abcb1a/1b* and *Abcg2* cooperatively limit the brain penetration of abemaciclib and its active metabolites, and also that they participate in the hepatobiliary or direct intestinal elimination of these compounds. Moreover, the human CYP3A4 drastically reduced the abemaciclib plasma  $AUC_{0-24h}$  and the  $C_{max}$  by 7.5- and 5.6-fold, respectively, and it showed to be more active in the formation of M2 and M20 compared to the mouse *Cyp3a*. The insights generated in this study may help to optimize the clinical development of abemaciclib, especially for the treatment of brain malignancies.

**Chapter 7** explores the role of the multidrug efflux and uptake transporters ABCB1, ABCG2, and OATP1A/1B, and the drug-metabolizing enzyme CYP3A in miliciclib disposition. *In vitro*, miliciclib was transported by mouse Abcg2. The plasma exposure of miliciclib was not significantly affected by efflux transporters. The Oatp1a/1b uptake transporter had only a minor impact on the miliciclib plasma  $AUC_{0-24h}$  and  $C_{max}$ . Miliciclib showed good brain penetration even in wild-type mice (brain-to-plasma ratio of 1.2), but this was further increased by 5.2-fold when both Abcb1 and Abcg2 were ablated, and to a lesser extent in single Abcb1- or Abcg2-deficient mice. The miliciclib plasma  $AUC_{0-8h}$  increased 1.9-fold in *Cyp3a*<sup>-/-</sup> mice, but decreased only 1.3-fold upon overexpression of human CYP3A4. Thus, our data indicate that ABCB1 and ABCG2 cooperatively limit miliciclib brain penetration. The low impact of OATP1 and CYP3A could be clinically favorable for miliciclib, reducing the risks of unintended drug-drug interactions or interindividual variation in CYP3A4 activity.

### **Part III: Clinical pharmacokinetics and pharmacodynamics of the cyclin-dependent kinase inhibitors**

Finally, in **Chapter 8**, the clinical pharmacokinetics and pharmacodynamics of the approved CDK4/6 inhibitors (palbociclib, ribociclib and abemaciclib) is reviewed. Here, the pharmacokinetics of these drugs in normal and specific populations is described, as well as some extrinsic factors that affect it, including the food effect and the interaction with other drugs. Similarities among the pharmacokinetics of these drugs included their extensive metabolism by CYP3A4, their brain penetration limited by efflux transporters, and their large interindividual variability in exposure. Furthermore, this chapter highlights the exposure–response and exposure–toxicity relationships. Consistently for all drugs, high exposure is associated with an increased risk of neutropenia, and for ribociclib also to corrected QT prolongation. For abemaciclib, a clear exposure–efficacy relationship has been described, while for palbociclib and ribociclib exposure–response analyses remain inconclusive.

In conclusion, the insights into different aspects of the CDK inhibitors provided in this thesis may be useful to optimize the clinical use of abemaciclib, palbociclib and ribociclib. Additionally, this can potentially contribute to the further development of these drugs and miliciclib. Ultimately, this information hopefully could lead to CDK treatments with improved efficacy and safety.



## Nederlandse samenvatting

Kanker blijft een belangrijk wereldwijd gezondheidsprobleem, met een verwachte verdere toename van incidentie en mortaliteit over de komende jaren. Nieuwe kankertherapieën maken dikwijls gebruik van doelgerichte geneesmiddelen, waarvan is aangetoond dat ze een hogere werkzaamheid en lagere toxiciteit hebben dan traditionele cytotoxische geneesmiddelen. De cycline-afhankelijke kinasen (CDK's) worden beschouwd als veelbelovende doelwitten voor kankerbehandeling, omdat ze kritische stappen in de celcyclus kunnen controleren wanneer ze door cyclinen worden geactiveerd. Tot op heden zijn drie CDK-remmers goedgekeurd die selectief aangrijpen op CDK4 en CDK6: palbociclib, ribociclib en abemaciclib. Deze geneesmiddelen worden momenteel gebruikt voor de behandeling van gemetastaseerde of gevorderde borstkanker, en hun werkzaamheid bij andere typen kanker wordt momenteel onderzocht. Bovendien lopen er klinische onderzoeken naar veel andere CDK-remmers met uiteenlopende specificiteit voor CDK-subklassen.

Dit proefschrift behandelt verschillende farmacologische aspecten van de CDK-remmers, van bioanalyse (Deel I) tot preklinische (Deel II) en klinische farmacokinetiek (Deel III), voornamelijk gericht op de goedgekeurde CDK4/6-remmers: abemaciclib, palbociclib en ribociclib. Het onderzoekt daarnaast ook milciclib, een veelbelovende CDK2-remmer die momenteel klinisch wordt onderzocht voor de behandeling van verschillende maligniteiten.

### **Deel I: Bioanalyse van cycline-afhankelijke kinaseremmers**

Aangezien betrouwbare bioanalytische methoden cruciaal zijn voor een correcte uitvoering en controle van preklinische en klinische geneesmiddelstudies, richt deel I van dit proefschrift zich op de ontwikkeling en validatie van bioanalytische methoden voor de kwantitatieve analyse van CDK-remmers. Volledige validatie van de methode werd uitgevoerd volgens de richtlijnen van de Amerikaanse "Food and Drug Administration" (FDA) en de "European Medicines Agency" (EMA). De bioanalytische methoden in deel I werden gebruikt ter ondersteuning van de preklinische onderzoeken die in deel II van dit proefschrift zijn beschreven.

**Hoofdstuk 1** beschrijft de ontwikkeling en validatie van een bioanalytische methode voor de kwantificering van drie goedgekeurde CDK-remmers (abemaciclib, palbociclib en ribociclib) in humane en muis matrices met behulp van vloeistofchromatografie-tandem massaspectrometrie (LC-MS/MS). Deze methode is volledig gevalideerd in humaan plasma en gedeeltelijk gevalideerd in muisplasma en weefselhomogenaten, waaronder lever, nier, milt, hersenen en dunne darm. Een "fit-for-purpose" strategie werd gevolgd om de prestaties van de methode in de weefselhomogenaten te evalueren. Deze methode was lineair, nauwkeurig en accuraat voor de kwantificering van abemaciclib, palbociclib en ribociclib in alle biomatrices. De stabiliteit in de verschillende biomatrices van de drie analyten onder verschillende omstandigheden werd ook in dit hoofdstuk onderzocht, waarbij palbociclib en ribociclib in sommige

weefselhomogenaten instabiel bleken te zijn, maar de omstandigheden werden aangepast om hun opslag- en verwerkingsstabiliteit te vergroten. De toepasbaarheid van deze methode werd aangetoond in een preklinische farmacokinetische studie van ribociclib, waarbij een nieuwe metaboliet met dezelfde  $m/z$ -transitie als het oorspronkelijke geneesmiddel werd gedetecteerd in muismonsters.

Bij mensen leidt het metabolisme van abemaciclib tot de vorming van drie actieve metabolieten (M2, M20 en M18). Hun vergelijkbare potentie met de moederstof en hun relatief overvloedige aanwezigheid in humaan plasma maken deze metabolieten klinisch relevant, aangezien ze waarschijnlijk bijdragen aan de algehele klinische werkzaamheid en veiligheid van abemaciclib. Daarom omvat de methode gepresenteerd in **Hoofdstuk 2** de bioanalyse van deze metabolieten gelijktijdig met abemaciclib, met behulp van een geoptimaliseerde ultra-high performance vloeistofchromatografie-tandem massaspectrometrie (UHPLC-MS/MS). Een volledige validatie van deze methode in humaan plasma werd uitgevoerd, terwijl in muisplasma de methode gedeeltelijk werd gevalideerd. Deze test werd met succes toegepast in een preklinisch farmacokinetisch onderzoek, waarin abemaciclib en zijn actieve metabolieten werden geïdentificeerd en gekwantificeerd. Inter-species verschillen tussen humane en muismonsters werden aangetroffen, vooral bij de vorming van M20, waar isomeren van deze verbinding werden gedetecteerd in muisplasma, maar niet in humaan plasma. Dit werd bevestigd door metingen met hoge resolutie massaspectrometrie (HR-MS).

In **Hoofdstuk 3** wordt een veelzijdige LC-MS/MS-assay voor milciclib in meerdere biomatrices beschreven om de klinische en preklinische ontwikkeling van milciclib verder te ondersteunen. Hiervoor werd een breed kwantitatief concentratiebereik geselecteerd en werden verschillende biomatrices opgenomen voor de validatie van de methode, waaronder humaan en muisplasma, homogenaten van muishersenen, nieren, lever, dunne darm, milt en weefselweekmedium. Een volledige validatie in humaan plasma werd uitgevoerd en een gedeeltelijke validatie voor de andere biomatrices. De gebruikte monstervoorbewerking leidde tot een efficiënte extractie van de analyt, met recovery's tussen 95-100%. Het gebruik van humaan plasma als surrogaatmatrix om milciclib in weefselweekmedium en muismatrices te kwantificeren, resulteerde in acceptabele nauwkeurigheid en precisie, hoewel monsters van weefselweekmedium vóór de voorbewerking verdunning met humaan plasma vereisten. Alle prestatieparameters van de methode voldeden aan de door de richtlijnen aanbevolen acceptatiecriteria, behalve de carry-over, die iets hoger was (22,9% van de ondergrens van kwantificering) dan het aanbevolen percentage (20%). Daarom werden aanvullende maatregelen genomen om de gegevensintegriteit te waarborgen. De stabiliteit van milciclib in alle matrices werd bovendien geëvalueerd en in sommige matrices was de analyt instabiel onder de geteste omstandigheden. Zo werden verdere aanbevelingen over opslag en verwerking opgenomen.

**Hoofdstuk 4** rapporteert een snelle bioanalytische methode voor de gelijktijdige kwantificering van irinotecan en SN-38 in muisplasma en weefselhomogenaten met behulp van High-Performance vloeistofchromatografie met Fluorescentiedetectie (HPLC-FL). Deze methode is geoptimaliseerd om specifiek preklinische studies van het metabolisme van irinotecan in SN-38 door carboxylesterase-enzymen te ondersteunen. De selectiviteit, lineariteit, nauwkeurigheid en precisie van de methode in het concentratiebereik van 7,5 tot 1500 ng/mL voor irinotecan en van 5 tot 1000 ng/mL voor SN-38 werd aangetoond. Ten slotte is de toepasbaarheid van deze methode in een farmacokinetische studie van irinotecan en SN-38 met behulp *in vivo* muismodellen bewezen.

## **Deel II: De impact van geneesmiddeltransporters en metaboliserende enzymen op de farmacokinetiek van cycline-afhankelijke kinaseremmers**

Geneesmiddeltransporters en geneesmiddel metaboliserende enzymen kunnen de dispositie van substraatgeneesmiddelen beïnvloeden met klinisch relevante (farmacodynamische) gevolgen. Dus, met behulp van *in vitro* studies en verschillende genetisch gemodificeerde muismodellen, onderzoekt deel II van dit proefschrift de rol van efflux- (ABCB1 en ABCG2) en influxtransporters (OATP1) en cytochroom P450 3A (CYP3A) enzymen in de farmacokinetiek en weefseldistributie van CDK-remmers.

**Hoofdstuk 5** onderzoekt de effecten van de efflux-transporters ABCB1 en ABCG2 en van CYP3A op de farmacokinetiek van de CDK4/6 remmer ribociclib. *In vitro* werd ribociclib efficiënt getransporteerd door humaan ABCB1. *In vivo* werd de hersenpenetratie van ribociclib drastisch beperkt door ABCB1 in de bloed-hersenbarrière, maar gelijktijdige toediening van elacridar kon dit proces volledig omkeren. De resultaten suggereerden verder dat ABCB1 een belangrijke rol zou kunnen spelen bij de eliminatie van ribociclib. Bovendien toonde deze studie aan dat humaan CYP3A4 ribociclib uitgebreid kan metaboliseren en de orale biologische beschikbaarheid ervan sterk kan beperken. De inzichten uit deze studie kunnen nuttig zijn om de klinische toepassing van ribociclib verder te optimaliseren, met name voor de behandeling van (uitgezaaide) hersentumoren.

**Hoofdstuk 6** onderzoekt of de actieve metabolieten van abemaciclib (M2, M20 en M18) substraten zijn van de effluxtransporters ABCB1 en ABCG2. Daarnaast bekijkt dit hoofdstuk de impact van deze transporters en van CYP3A op de farmacokinetiek en weefseldistributie van abemaciclib en zijn actieve metabolieten. *In vitro* werd abemaciclib efficiënt getransporteerd door humaan ABCB1 en muis Abcg2, en in geringe mate door humaan ABCG2, en de actieve metabolieten waren zelfs betere transportsubstraten van deze effluxtransporters. ABCB1 en ABCG2 hadden geen invloed op de plasmablootstelling van abemaciclib en M20, maar de  $AUC_{0-24h}$  en de  $C_{max}$  van M2 namen significant toe in de afwezigheid van Abcb1a/1b en Abcg2, waarbij Abcb1a/1b een dominante rol leek te spelen. Bovendien nam de hersenpenetratie van



abemaciclib, M2 en M20 dramatisch toe, respectievelijk (ten minste) 25-, 4- en 60-voudig wanneer beide transporters waren geïnactiveerd, en in mindere mate bij de enkelvoudige *Abcb1*- of *Abcg2*-deficiënte muizen. Ook was de herwinning van abemaciclib en zijn metabolieten vanuit de inhoud van de dunne darm sterk verminderd bij *Abcb1a/1b;Abcg2<sup>-/-</sup>* muizen, en deze effecten waren eveneens minder uitgesproken bij de single knock-out muizen. Onze resultaten laten zien dat *Abcb1a/1b* en *Abcg2* samen de hersenpenetratie van abemaciclib en zijn actieve metabolieten beperken, en ook dat ze deelnemen aan de hepatobiliaire of directe intestinale eliminatie van deze verbindingen. Daarnaast verminderde het humane CYP3A4 de abemaciclib plasma  $AUC_{0-24h}$  en de  $C_{max}$  met respectievelijk 7,5- en 5,6-voud drastisch, en het bleek actiever te zijn in de vorming van M2 en M20 dan het muis *Cyp3a*. De inzichten die in deze studie zijn verkregen kunnen helpen om de klinische ontwikkeling van abemaciclib te optimaliseren, met name voor de behandeling van hersentumoren.

**Hoofdstuk 7** onderzoekt de rol van de multidrug efflux en uptake transporters ABCB1, ABCG2 en OATP1A/1B, en het geneesmiddelmetaboliserende enzym CYP3A in de dispositie van miliclib. *In vitro* werd miliclib getransporteerd door muis *Abcg2*. De plasmablootstelling aan miliclib werd niet significant beïnvloed door effluxtransporters. De *Oatp1a/1b* opnametransporter had slechts een kleine invloed op de miliclib plasma  $AUC_{0-24h}$  en  $C_{max}$ . Miliclib vertoonde een goede hersenpenetratie, zelfs bij wildtype muizen (hersenen-tot-plasmaverhouding van 1,2), maar dit werd verder verhoogd met een factor 5,2 wanneer zowel *Abcb1* als *Abcg2* waren geïnactiveerd, en in mindere mate bij enkelvoudige *Abcb1*- of *Abcg2*-deficiënte muizen. De plasma- $AUC_{0-8h}$  van miliclib nam 1,9-voudig toe in *Cyp3a<sup>-/-</sup>*-muizen, maar nam slechts 1,3-voudig af na overexpressie van humaan CYP3A4. Onze gegevens geven dus aan dat ABCB1 en ABCG2 samen de penetratie van miliclib in de hersenen beperken. De geringe impact van OATP1 en CYP3A zou klinisch gunstig kunnen zijn voor miliclib, aangezien het risico op onbedoelde geneesmiddelinteracties of interindividuele variatie in CYP3A4-activiteit wordt verminderd.

### Deel III: Klinische farmacokinetiek en farmacodynamiek van de cycline-afhankelijke kinaseremmers

Ten slotte wordt in **Hoofdstuk 8** de klinische farmacokinetiek en farmacodynamiek van de goedgekeurde CDK4/6-remmers (palbociclib, ribociclib en abemaciclib) besproken. Hier wordt de farmacokinetiek van deze geneesmiddelen in normale en specifieke populaties beschreven, evenals enkele extrinsieke factoren die hierop van invloed zijn, waaronder het voedsleffect en de interactie met andere geneesmiddelen. Overeenkomsten tussen de farmacokinetiek van deze geneesmiddelen omvatten hun uitgebreide metabolisme door CYP3A4, hun hersenpenetratie beperkt door effluxtransporters en hun grote interindividuele variabiliteit in blootstelling. Verder belicht dit hoofdstuk de blootstelling-respons en blootstelling-toxiciteitsrelaties. Consistent voor al deze geneesmiddelen wordt hoge blootstelling geassocieerd met

een verhoogd risico op neutropenie, en voor ribociclib ook met gecorrigeerde QT-verlenging. Voor abemaciclib is een duidelijke blootstelling-werkzaamheidsrelatie beschreven, terwijl voor palbociclib en ribociclib blootstelling-responsanalyses nog geen uitsluitsel hebben kunnen geven.

Concluderend kunnen de inzichten in verschillende aspecten van de CDK-remmers beschreven in dit proefschrift van nut zijn om het klinische gebruik van abemaciclib, palbociclib en ribociclib te optimaliseren. Bovendien kan dit mogelijk bijdragen aan de verdere ontwikkeling en toepassing van deze geneesmiddelen en milciclib. Uiteindelijk kan deze informatie hopelijk leiden tot CDK-behandelingen met verbeterde werkzaamheid en veiligheid.





Resumen en español

El cáncer continúa siendo un problema de salud mundial, y se espera que su incidencia y mortalidad aumenten en los próximos años. Los nuevos tratamientos contra el cáncer se han enfocado en el desarrollo de fármacos de terapia molecular dirigida, los cuales han demostrado tener una mayor eficacia y una toxicidad reducida comparadas con los fármacos citotóxicos tradicionales. Las quinasas dependientes de ciclina (CDKs) han sido reconocidas como blancos potenciales para tratamientos contra el cáncer, debido a que éstas, cuando son activadas por ciclinas, pueden controlar puntos críticos del ciclo celular. Hasta ahora, tres fármacos que inhiben selectivamente a CDK4 y CDK6 (palbociclib, ribociclib y abemaciclib) han sido aprobados por agencias regulatorias, y actualmente están indicados para el tratamiento de cáncer avanzado o metastásico de mama. Asimismo, otros inhibidores de CDK con diferente especificidad están siendo investigados en estudios clínicos.

Esta tesis aborda varios aspectos farmacológicos de los inhibidores de CDK, incluyendo su bioanálisis (Parte I), farmacocinética preclínica (Parte II) y clínica (Parte III), enfocándose principalmente en los inhibidores de CDK4/6 ya aprobados: abemaciclib, palbociclib y ribociclib. Asimismo, esta tesis también abarca milciclib, un fármaco inhibidor de CDK2 que actualmente se encuentra en investigación clínica para el tratamiento de algunos cánceres.

### **Parte I: bioanálisis de los inhibidores de quinasas dependientes de ciclina**

Debido a que los métodos bioanalíticos son esenciales y críticos para dirigir y realizar apropiadamente estudios preclínicos y clínicos con fármacos, la parte I de esta tesis se enfoca en el desarrollo y validación de métodos bioanalíticos para el análisis cuantitativo de los inhibidores de CDK. La validación de estos métodos se realizó siguiendo las guías de validación de la Administración de Alimentos y Medicamentos (FDA) de Estados Unidos y de la Agencia Europea de Medicamentos (EMA). Los métodos bioanalíticos descritos en la parte I de esta tesis se usaron para dar soporte a los estudios preclínicos realizados en la parte II.

El **capítulo 1** describe el desarrollo y la validación de un método bioanalítico para la cuantificación de los tres inhibidores de CDK4/6 aprobados (abemaciclib, palbociclib y ribociclib) en matrices biológicas humanas y murinas usando cromatografía de líquidos con espectrometría de masas en tándem (LC-MS/MS). Este método fue completamente validado en plasma humano y parcialmente validado en fluidos murinos, incluyendo plasma y tejidos homogeneizados de hígado, riñón, bazo, cerebro e intestino delgado. Para evaluar el desempeño del método en los tejidos homogeneizados, se utilizó una estrategia "fit-for-purpose" fue usada. El método resultó ser lineal, exacto y preciso para la cuantificación de abemaciclib, palbociclib y ribociclib en todas las matrices biológicas. También, en este capítulo se examinó la estabilidad de los tres analitos en todas las matrices biológicas en diferentes condiciones de almacenamiento y de procesamiento, en donde palbociclib y ribociclib

resultaron ser inestables en ciertos tejidos homogeneizados, por lo que las condiciones fueron modificadas con la finalidad de incrementar la estabilidad de almacenamiento y procesamiento de la muestra. La aplicabilidad de este método fue demostrada a través de un estudio de farmacocinética preclínica de ribociclib, en donde se detectó un nuevo metabolito con la misma transición  $m/z$  que el fármaco.

Por otra parte, en humanos, el metabolismo de abemaciclib conlleva a la formación de tres metabolitos activos (M2, M20 y M18), cuya potencia, que es comparable a la de abemaciclib, y abundancia relativa en plasma humano, hacen que estos compuestos sean de importancia clínica, ya que probablemente contribuyen, en general, a la eficacia y seguridad clínicas de abemaciclib. Por consiguiente, el método presentado en el **capítulo 2** incluye el bioanálisis simultáneo de estos metabolitos y abemaciclib, mediante el uso de un método optimizado por cromatografía de líquidos acoplado a espectrometría de masas en tándem (UHPLC-MS/MS). Mientras que para la cuantificación en plasma humano se realizó una validación completa de este método, en plasma murino el método fue parcialmente validado. Este método fue exitosamente aplicado en un estudio de farmacocinética preclínica, en donde se identificaron y cuantificaron abemaciclib y sus metabolitos activos, encontrándose diferencias interespecie entre las matrices humanas y murinas, especialmente en la formación de M20, donde se detectaron isómeros de este compuesto en plasma murino, pero no en plasma humano, lo cual fue confirmado mediante un análisis de espectrometría de masas de alta resolución.

Posteriormente, en el **capítulo 3** se expone un método versátil basado en LC-MS/MS para el análisis cuantitativo de milciclib en múltiples matrices biológicas, con la finalidad de contribuir a su desarrollo clínico y preclínico. Para esto, se seleccionó un rango amplio de concentraciones y el método fue validado en varias matrices biológicas, incluyendo plasma humano y murino, y homogeneizados de cerebro, riñón, hígado, intestino delgado y bazo de ratón, además de medio de cultivo celular. Se realizó una validación completa del método en plasma humano y una validación parcial en las otras matrices biológicas. El pretratamiento de la muestra utilizado produjo una extracción eficiente del analito, logrando entre un 95 y 100% de recobro. El uso de plasma humano como matriz sustituta para cuantificar milciclib en medio de cultivo celular y en matrices biológicas de ratón resultó con precisión y exactitud aceptables, aunque para las muestras en medio de cultivo celular fue necesario diluirlas con plasma humano antes del pretratamiento de la muestra. Todos los parámetros de desempeño del método cumplieron con el criterio de aceptación recomendado por las guías de validación, excepto el carry-over, el cual fue ligeramente mayor (22.9% del límite de cuantificación) del límite recomendado (20%), por consiguiente, se tomaron medidas adicionales para asegurar la integridad de los resultados. Adicionalmente, se evaluó la estabilidad de milciclib en todas las matrices biológicas, donde algunas inestabilidades del analito fueron encontradas en algunas matrices bajo ciertas

condiciones, por lo que para muestras en estas matrices se incluyeron recomendaciones específicas para su almacenamiento y procesamiento.

En el **capítulo 4** se reporta un método bioanalítico rápido para la cuantificación simultánea de irinotecan y SN-38 en plasma y tejidos homogeneizados de ratón usando cromatografía de líquidos de alta eficiencia con detector de fluorescencia (HPLC-FL). Este método fue optimizado para aplicarse específicamente en estudios preclínicos sobre la conversión de irinotecan a SN-38 por medio de las enzimas carboxilesterasas. Se demostró la selectividad, linealidad, exactitud y precisión del método en un rango de concentraciones de 7.5 a 1500 ng/mL y de 5 a 1000 ng/mL para irinotecan y SN-38, respectivamente. Finalmente, se mostró la aplicabilidad del método en un estudio farmacocinético de irinotecan y SN-38 usando modelos *in vivo* en ratones.

## **Parte II: Efecto de los transportadores y enzimas metabolizadoras de fármacos en la farmacocinética de los inhibidores de quinasas dependiente de ciclina**

Los transportadores de membrana y las enzimas metabolizadoras de fármacos pueden influir en la disposición en el organismo de fármacos sustrato, y pueden llegar a tener consecuencias farmacodinámicas clínicamente relevantes. Por lo tanto, la parte II de esta tesis investiga la función de los transportadores de eflujo (ABCB1 y ABCG2) e influjo (OATP1) y de la enzima citocromo P450 3A (CYP3A) en la farmacocinética y la distribución en tejidos de los inhibidores de CDK, mediante el uso de modelos *in vitro* e *in vivo*, en este último incluyendo diversos modelos de ratones modificados genéticamente.

Así, el **capítulo 5** examina los efectos de los transportadores de eflujo ABCB1 y ABCG2, y de CYP3A4 en la farmacocinética de ribociclib, un inhibidor de CDK4/6. *In vitro*, ribociclib fue transportado por ABCB1 humano; asimismo, en estudios *in vivo*, la penetración cerebral de ribociclib fue drásticamente limitada por la actividad de ABCB1 en la barrera hematoencefálica, no obstante, la coadministración con elacridar pudo revertir en su totalidad este proceso. Los resultados, además, mostraron que el transportador ABCB1 podría tener un papel importante en la eliminación de ribociclib. Adicionalmente, este estudio demostró que CYP3A4 puede metabolizar extensivamente a ribociclib y restringir biodisponibilidad oral de este fármaco. Los conocimientos generados en este estudio podrían ser útiles para optimizar el uso de ribociclib en la clínica, especialmente para el tratamiento de tumores cerebrales metastásicos.

Por otra parte, el **capítulo 6** investiga si los metabolitos activos de abemaciclib (M2, M20 y M18) son sustratos de los transportadores de eflujo ABCB1 y ABCG2. Además, este capítulo establece el impacto de estos transportadores y de la enzima CYP3A en la farmacocinética y la distribución en tejidos de abemaciclib y de sus metabolitos activos. En estudios *in vitro*, abemaciclib fue transportado eficientemente por ABCB1 humano, Abcb2 murino, y ligeramente por ABCG2 humano, asimismo, los metabolitos



activos de abemaciclib resultaron ser incluso mejores sustratos de estos transportadores. *In vivo*, ABCB1 y ABCG2 no tuvieron efecto en la exposición plasmática de abemaciclib y de su metabolito M20, mientras que el área bajo la curva de 0 a 24 h ( $AUC_{0-24h}$ ) y la concentración plasmática máxima ( $C_{max}$ ) de M2 aumentó significativamente en ausencia de Abcb1a/1b y Abcg2, donde Abcb1a/1b parece tener un papel más dominante. Asimismo, en ausencia de ambos transportadores, la penetración cerebral de abemaciclib, M2 y M20 aumentó al menos 25, 4 y 60 veces, respectivamente, y en menor grado, en ratones deficientes únicamente de un transportador: Abcb1a/1b o Abcg2. De la misma forma, el recobro de abemaciclib y sus metabolitos en el lumen intestinal se redujo en gran medida en ratones *Abcb1a1b;Abcg2<sup>-/-</sup>*, y en menor grado en ratones deficientes de un solo transportador. Estos resultados sugieren que ambos transportadores limitan cooperativamente la penetración cerebral de abemaciclib y sus metabolitos activos, y que, además, participan en su eliminación hepatobiliar o intestinal directa. Por otra parte, la enzima CYP3A4 redujo drásticamente la  $AUC_{0-24h}$  y  $C_{max}$  plasmática alrededor de 7.5 y 5.6 veces, respectivamente, y además demostró ser más activa en la formación de M2 y M20 comparada con la enzima murina Cyp3a. La información generada en este estudio podría ayudar a optimizar el desarrollo clínico de abemaciclib, especialmente en el tratamiento de cánceres cerebrales.

El **capítulo 7** explora la función de los transportadores de eflujo e influjo ABCB1, ABCG2 y OATP1A/1B, y de la enzima metabolizadora de fármacos CYP3A en la disposición de milciclib. En los resultados de este estudio, se encontró que milciclib fue transportado por el Abcg2 murino *in vitro*, no obstante, los niveles plasmáticos de milciclib no se alteraron de forma significativa por los transportadores de eflujo, mientras que los parámetros farmacocinéticos  $AUC_{0-24h}$  y  $C_{max}$  fueron alterados mínimamente por Oatp1a/1b. Por otro lado, milciclib mostró buena penetración cerebral, incluso en los ratones wild-type (relación cerebro/plasma igual a 1.2), la cual incrementó 5.2 veces en ausencia ambos transportadores de eflujo (Abcb1 y Abcg2) y, en menor grado, en ratones deficientes de un sólo transportador. Por último, la  $AUC_{0-24h}$  plasmática de milciclib aumentó 1.9 veces en ratones *Cyp3a<sup>-/-</sup>*, pero únicamente disminuyó 1.3 veces ratones con sobreexpresión de la enzima CYP3A4 humana. En resumen, estos datos indicaron que ABCB1 y ABCG2 limitan cooperativamente la penetración cerebral de milciclib, mientras que los efectos menores de OATP1 y CYP3A4 en la farmacocinética de milciclib podrían ser clínicamente favorables, ya que disminuiría el riesgo de interacciones fármaco-fármaco no deseadas, o de variaciones interindividuales por la actividad de CYP3A4.

### Parte III: Farmacocinética y farmacodinamia clínica de los inhibidores de quinasas dependientes de ciclina

Finalmente, en el **capítulo 8** se resume la farmacocinética y la farmacodinamia clínica de los inhibidores de CDK4/6 aprobados (palbociclib, ribociclib y abemaciclib),

incluyendo su farmacocinética en poblaciones normales y específicas, así como también la influencia de algunos factores extrínsecos, como el efecto de los alimentos y la interacción con otros medicamentos. Algunas similitudes encontradas entre estos inhibidores de CDK4/6 comprendieron el metabolismo extensivo debido a CYP3A4, su penetración cerebral limitada por los transportadores de eflujo, y su gran variabilidad interindividual en niveles plasmáticos. Por otro lado, este capítulo resalta las relaciones exposición-respuesta y exposición-toxicidad de estos fármacos, en las cuales para abemaciclib existe una relación exposición-respuesta evidente, mientras que para palbociclib y ribociclib, los análisis exposición-respuesta permanecen aún inconclusos. En cuanto a la relación exposición-toxicidad, consistentemente para estos tres fármacos, la alta exposición está asociada con un riesgo aumentado de neutropenia, y para ribociclib también con una prolongación del intervalo QT corregido.

En conclusión, los conocimientos aportados en esta tesis sobre los diferentes aspectos de los inhibidores de CDK podrían ser útiles para optimizar y expandir el uso clínico de abemaciclib, palbociclib y ribociclib, y asimismo, contribuir potencialmente al desarrollo clínico de milciclib, esperando que esta información pueda contribuir al desarrollo de tratamientos con inhibidores de CDK más eficaces y seguros.





## **APPENDICES**

List of publications  
Acknowledgements  
Curriculum vitae

## List of publications

**Martínez-Chávez A**, Tibben MM, de Jong KAM, Rosing H, Schinkel AH, Beijnen JH. 'Simultaneous Quantification of Abemaciclib and its Active Metabolites in Human and Mouse Plasma by UHPLC-MS/MS', *Journal of Pharmaceutical and Biomedical Analysis*, (2021) 203, 114225 <https://doi.org/10.1016/j.jpba.2021.114225>

**Martínez-Chávez A**, Broeders J, Lebre MC, Tibben MM, Rosing H, Beijnen JH, Schinkel AH. 'The Role of Drug Efflux and Uptake Transporters ABCB1 (P-Gp), ABCG2 (BCRP) and OATP1A/1B and of CYP3A4 in the Pharmacokinetics of the CDK Inhibitor Milciclib', *European Journal of Pharmaceutical Sciences*, (2021) 190, 113516 <https://doi.org/10.1016/j.ejps.2021.105740>

**Martínez-Chávez A**,\* Groenland SL,\* van Dongen MGJ, Beijnen JH, Schinkel AH, Huitema ADR, Steeghs N. 'Clinical Pharmacokinetics and Pharmacodynamics of the Cyclin-Dependent Kinase 4 and 6 Inhibitors Palbociclib, Ribociclib, and Abemaciclib', *Clinical Pharmacokinetics*, (2020) 59, 1501-1520 <https://doi.org/10.1007/s40262-020-00930-x>

**Martínez-Chávez A**, Tibben MM, Broeders J, Rosing H, Schinkel AH, Beijnen JH. 'Development and Validation of an LC-MS/MS Method for the Quantitative Analysis of Milciclib in Human and Mouse Plasma, Mouse Tissue Homogenates and Tissue Culture Medium', *Journal of Pharmaceutical and Biomedical Analysis*, (2020) 190, 113516 <https://doi.org/10.1016/j.jpba.2020.113516>

**Martínez-Chávez A**, Rosing H, Gan C, Wang Y, Schinkel AH, Beijnen JH. 'Bioanalytical Method for the Simultaneous Quantification of Irinotecan and Its Active Metabolite SN-38 in Mouse Plasma and Tissue Homogenates Using HPLC-Fluorescence', *Journal of Chromatography B: Analytical Technologies in the Biomedical and Life Sciences*, (2020) 1149, 122177 <https://doi.org/10.1016/j.jchromb.2020.122177>

**Martínez-Chávez A**, van Hoppe S, Rosing H, Lebre MC, Tibben MM, Beijnen JH, Schinkel AH. 'P-glycoprotein Limits Ribociclib Brain Exposure and CYP3A4 Restricts Its Oral Bioavailability', *Molecular Pharmaceutics*, (2019) 16, 3842-3852 <https://doi.org/10.1021/acs.molpharmaceut.9b00475>

**Martínez-Chávez A**, Rosing H, Hillebrand M, Tibben MM, Schinkel AH, Beijnen JH. 'Development and Validation of a Bioanalytical Method for the Quantification of the CDK4/6 Inhibitors Abemaciclib, Palbociclib and Ribociclib in Human and Mouse Matrices Using Liquid Chromatography-Tandem Mass Spectrometry', *Analytical and Bioanalytical Chemistry*, (2019) 411, 5531-5345 <https://doi.org/10.1007/s00216-019-01932-w>

Rivero-Cruz B, **Martínez-Chávez A.** 'Development and Validation of a RP-HPLC Method for the Simultaneous Quantification of Flavonoids Markers in Mexican Propolis', *Food Analytical Methods*, (2015) 8, 413–419 <https://doi.org/10.1007/s12161-014-9908-5>

*\*These authors contributed equally*

## **Acknowledgements**

First of all, Alfred and Jos thank you for giving me the opportunity of being part of your groups and for your supervision during these years. It was a fantastic and challenging experience coming to the Netherlands for my PhD studies, which allowed me to grow both: scientifically and personally. Alfred, I am very grateful for all your help and support during the past years, for all the learnings, advices and critical feedback. Jos, I really appreciate that I also got the opportunity to work in the laboratory of the pharmacy, I am really happy I could perform part of my research in the lab. Thank you for being my promotor and for guiding me.

Hilde, thank you for adopting me in the pharmacy lab and supervising me. Although at the beginning my training in the lab seemed challenging and complicated, thanks to your help and support we could successfully do all my projects not only during few months (as it was originally planned), but all my PhD journey. I really enjoyed our meetings and project discussions I learn a lot from your bioanalytical expertise.

I would like to express my gratitude to all co-authors in this thesis, thank you for your contribution to these projects. Without you, this thesis could not be done!

Olaf, thank you for your great advices on troubleshooting, constructive feedback and practical support in these projects.

Many thanks to all the committee members for your time on assessing this thesis.

To all members of Schinkel group during my time at the NKI: Cristina, Stéphanie, Wenlong, Els, Jing, Changpei, Yaogeng, Margarida and Nancy, many thanks for your support, feedback and teamwork, I enjoyed being part of this multicultural team. Stéphanie, thank you for being so friendly, for your support and guidance, especially when I joined the group, I really appreciate the pleasant conversations and funny moments we shared in the office. Cristina, thank you for all your unconditional support and for all the administrative work on these projects. Wenlong, you were my mate during this whole journey, thank you for your help, advices, and the nice discussions we had. Margarida, also thanks for your support, I am glad we share many fun and pleasant moments in this journey. Nancy, thank you for your kindness and unconditional support anytime, it was pleasant sharing the office with an optimistic and sweet person like you.

Beste collega's van het laboratorium van de apotheek: hartelijk dank voor deze jaren van mooie samenwerking en al jullie hulp. Ik ben ontzettend blij dat mijn Nederlandse ervaring compleet was toen ik deel van het team werd. Bedankt ook voor jullie hulp met het oefenen van de Nederlandse taal. Special thanks to Matthijs, for being my lab



coach, for your continuous guidance and support. Michel, Niels and Abadi, thank you for training me in the lab and sharing all your MS expertise. Luc, many thanks for your advices and help with the special columns and troubleshooting.

To all the lab OIOs that I met during this journey, huge thank you for your support and teamwork. Merel and Lotte, thank you for being so friendly and nice when I joined the lab, and together with Jeroen and Maikel, thanks for your useful advices and help. Maaïke, I was lucky to share most part of my PhD trajectory with you, it was great that you and Merel came to my home city, I was delighted. Karen, thank you for collaborating with your expertise for the abemaciclib project. Ignace, thanks for all the hilarious moments and nice chats while preparing our hundreds of samples. Steffie, I really enjoyed writing our review together and our Spanish-Dutch practices, thank you for this, for your support and pleasant meetings!

Jelle and Albert, I am very glad I had the opportunity to supervise you during your Master's internship, it was an awesome experience. Jelle, many thanks for all your effort and input, which allowed to finalize two chapters of this thesis. Albert, it was enjoyable to work with such an enthusiastic person like you, due to the unlucky pandemic circumstances there were many limitations, but I really appreciate what you achieved in these difficult times.

To all my former and current PhD fellows, many thanks for all the experiences shared in the past years, without the super fun moments, OIO weekends, and events, I would not have survived the PhD life.

Also, I would like to thank all colleagues from the Pharmacology Division for the nice atmosphere in H3; Thea, Lara and Hans thank you for taking care of the organization and administrative processes.

Thanks to all the personnel from the animal facility that somehow were involved in these projects and to the animal caretakers from T2 that took care of our mice and assisted during the experiments.

Thank you all for being part of the most challenging experience in my life! I would have never achieved finishing my PhD without you!

Por último, quiero agradecer a mi familia por apoyarme incondicionalmente y creer siempre en mí, por ser mi inspiración y mi motivación; lo más difícil de estos cinco años ha sido estar lejos de ustedes. Mamá y papá, gracias por todos su amor y apoyo en todas las decisiones que he tomado, gracias por darme todo en la vida, pero sobre todo, lo más valioso, por darme salud y educación, que es lo único necesario para lograr todos los sueños. Tita y Tito, gracias por todo su amor, por apoyarme

incondicionalmente y estar siempre para mí, y por darme los mejores consejos de la vida; Tita, gracias también por inspirarme tanta fortaleza y poner el ejemplo siempre, hasta el final, tú me diste la fortaleza para poder terminar con esto, ya me di cuenta que sigues ingeniándotelas desde donde estás para ayudarnos y cuidarnos, gracias por tanto. Ilse y Arturo, gracias por su apoyo y ser mis hermanos. Ilse y Valeria, gracias por estar siempre y alegrarnos la vida. Gracias a todos: mis tías, tíos, primos y primas, gracias por siempre estar ahí.

Alan, gracias por acompañarme en esta aventura, una más de nuestras vidas, probablemente la más difícil de todas, pero aun así logramos nuestro propósito. Sabes que este logro también es tuyo, por ayudarme tanto y estar siempre detrás de todo, por ser mi primer “reviewer”, y coautor en la vida, por motivarme en los momentos más difíciles y estar juntos casi la mitad de nuestras vidas.

## Curriculum vitae

Diana Alejandra Martínez Chávez was born on May 16<sup>th</sup>, 1988 in Mexico City. In 2006, she started her bachelor studies on Pharmaceutical Biological Chemistry at the National Autonomous University of Mexico (UNAM). She completed her study program in 2011 and started her thesis project on new analytical methods for the characterization of natural products. After obtaining her bachelor degree with honors, in 2012 she started her career in the pharmaceutical industry, where she developed and validated analytical methods for the quality control of new generic drugs. In 2013, she started her master studies in Pharmaceutical Sciences at UNAM, under the supervision of Dr. Blanca Rivero Cruz at the Pharmacy Department of the Faculty of Chemistry. Her research project focused on the *in vitro* permeability of active compounds isolated from natural products, in order to determine their category in the biopharmaceutical classification system. In 2015, she obtained her Master's degree with honors, and returned to the pharmaceutical industry to support the analytical method implementation for quality control of drugs. At the same time, she worked at the Faculty of Chemistry (UNAM), teaching drug analysis techniques to bachelor students. In 2016, she was granted a scholarship from the Mexican Council for Science and Technology (CONACyT) for her doctoral studies abroad and started her PhD research at the Netherlands Cancer Institute (NKI) in the group of Dr. Alfred H. Schinkel, and in the Laboratory of the Pharmacy under the supervision of Prof. Dr. Jos H. Beijnen and Dr. Hilde Rosing. Her research focused on bioanalysis, and the role of drug transporters and drug-metabolizing enzymes in the pharmacokinetics of cyclin-dependent kinase inhibitors. Her research resulted in this thesis.





